Thesis Dissertation

Reverse engineering signalling networks in cancer cells

Submitted by
Mathurin Dorel

for the academical degree
Doctor rerum naturalium (Dr. rer. nat.)

submitted to the
Faculty of Life Sciences of Humboldt Universität zu Berlin

President of Humboldt-Universität zu Berlin
Prof. Dr. Peter Frensch

Dean of the faculty of life sciences
Prof. Dr. Dr. Christian Ulrichs

Reviewers :
1. Prof. Dr. Nils Blüthgen
2. Prof. Dr. Johannes Schulte
3. Prof. Dr. Denis Thieffry

Date of the thesis defense: September 26th 2022

Declaration of Authorship

I, Mathurin DOREL, declare that this thesis, titled "Reverse engineering signalling networks in cancer cells", and the work presented in it are my own. I confirm that:

- This work was done wholly or mainly while in candidature for a research degree at this University.
- Where any part of this thesis has previously been submitted for a degree or any other qualification at this University or any other institution, this has been clearly stated.
- Where I have consulted the published work of others, this is always clearly attributed.
- Where I have quoted from the work of others, the source is always given. With the exception of such quotations, this thesis is entirely my own work.
- I have acknowledged all main sources of help.
- Where the thesis is based on work done by myself jointly with others, I have made clear exactly what was done by others and what I have contributed myself.

Date:

Signature:

Abstract

Cancer therapy has seen immense progress over the last century but resistance to drug treatments remains a major obstacle in the war against cancer. Drug resistance can often not be predicted from static measurements but only revealed when cells are perturbed.

In this work I developed the R package STASNet to generate semi-quantitative models of signal transduction from signalling perturbation-response data using Least Square Modular Response Analysis models. These models can be used to analyse how differences in signal transduction relate to drug resistance and can be used to make predictions about resistance mechanisms and optimal treatments. To show how STASNet can accurately quantify the activity of signalling pathways, we used perturbation data from a pair of isogenic colon cancer cell line with and without SHP2 knock-out, a known resistance mechanism in this cancer type. Comparing the models derived from these cell lines showed that MAPK signalling is more affected by SHP2 knock-out than PI3K signalling, confirming the role of SHP2 as a primary MAPK component.

STASNet was then used to investigate resistance to MEK and ALK inhibition in neuroblastoma, a pediatric cancer with a dismal prognosis. A drug screen showed that the MEK inhibitor Selumetinib separated a panel of neuroblastoma cell lines into three sensitive and six resistant cell lines. A multi-omics analysis showed no clear correlation of sensitivity with individual molecular markers. STASNet models trained on perturbation-response data from these cell lines revealed that the strong resistance to Selumetinib was driven by a strong feedback from ERK to MEK or a multi-layered feedback to both MEK and IGF1R. This was confirmed by phosphoproteomics and suggested a therapy targeting MEK in combination with either RAF or IGF1R depending on the type of feedback present in the cell line. The effectiveness of those strategies predicted by the model was confirmed experimentally.

Finally, studying the effect of NF1-KO on signalling revealed that the loss of NF1 hyper-sensitized the MAPK pathway to ligand-induced activation but disrupted the ERK-RAF feedback. This disruption desensitized the cells to ALK inhibition but increased their vulnerability to MEK inhibition. The insights provided by the models developed in this work will thus help to design personalized combinations of inhibitors that could be used as second line therapy after molecularly monitoring the tumor response to the initial treatment.

Zusammenfassung

Obwohl die Krebstherapie im letzten Jahrhundert große Fortschritte gemacht hat, bleibt die Resistenz gegen medikamentöse Behandlungen ein großes Hindernis im Kampf gegen den Krebs. Arzneimittelresistenzen lassen sich oft nicht aus statischen Messungen vorhersagen, sondern zeigen sich erst, wenn Zellen perturbiert werden.

In dieser Arbeit habe ich das R-Paket STASNet entwickelt, das semi-quantitative Modelle der Signaltransduktion aus Signalisierungs-Störungsantwortdaten unter Verwendung von Least Square Modular Response Analysis-Modellen generiert. Diese Modelle können verwendet werden, um zu analysieren, wie Unterschiede in der Signalübertragung mit Arzneimittelresistenzen zusammenhängen, und können verwendet werden, um Vorhersagen über Resistenzmechanismen und optimale Behandlungen zu treffen. Um zu untersuchen, wie gut STASNet die Aktivität von Signalwegen quantifizieren kann, haben wir Perturbationsdaten von einem Paar isogener Darmkrebszelllinien mit und ohne SHP2-Knock-out, einem bekannten Resistenzmechanismus bei dieser Krebsart, verwendet. Der Vergleich der von diesen Zelllinien abgeleiteten Modelle zeigte, dass der SHP2-Knockout stärker den MAPK Signalweg beeinflusst und weniger die PI3K-Signalübertragung, was die Rolle von SHP2 als primäre Komponente des MAPK-Signalwegs bestätigt.

STASNet wurde dann verwendet, um die Resistenz gegen die MEK- und ALK-Hemmung beim Neuroblastom, einem pädiatrischen Krebs mit schlechter Prognose, zu untersuchen. Ein Wirkstoffscreening zeigte, dass der MEK-Inhibitor Selumetinib ein Panel von Neuroblastom-Zelllinien in drei sensitive und sechs resistente Zelllinien trennte. Eine Multi-Omics-Analyse zeigte keine eindeutige Korrelation der Sensitivität mit einzelnen molekularen Markern. STASNet-Modelle zeigten, dass die starke Resistenz gegen Selumetinib durch eine starke Rückkopplung von ERK auf MEK oder eine vielschichtige Rückkopplung sowohl auf MEK als auch auf IGF1R getrieben wurde. Dies wurde durch Phosphoproteomik bestätigt. Aus dem Modell konnte eine kombinatorische Therapie abgeleitet werden, die auf MEK in Kombination mit entweder RAF oder IGF1R abzielt, je nach Art der in der Zelllinie vorhandenen Rückkopplungen. Die Wirksamkeit dieser vom Modell vorhergesagten Strategien wurde experimentell bestätigt.

Schließlich ergab die Untersuchung der Wirkung von NF1-KO auf die Signalübertragung, dass der Verlust von NF1 den MAPK-Weg für die Liganden-induzierte Aktivierung hypersensibilisierte, aber das ERK-RAF-Rückkopplung störte. Diese Unterbrechung desensibilisierte die Zellen gegenüber der ALK-Hemmung, erhöhte jedoch ihre Anfälligkeit gegenüber der MEK-Hemmung. Die Erkenntnisse aus den in dieser Arbeit entwickelten Modellen werden somit dazu beitragen, personalisierte Kombinationen von Inhibitoren zu entwerfen, die als Zweitlinientherapie nach molekularer Untersuchung der Tumorreaktion auf die Erstbehandlung eingesetzt werden könnten.

Contents

Chapter 1

Introduction

It is the great prerogative of Mankind above other Creatures, that we are not only able to behold the works of Nature, or barely to sustain our lives by them, but we have also the power of considering, comparing, altering, assisting, and improving them to various uses

Robert Hooke

A theory of the cell was first proposed by Theodor Schwann in 1839 when he summarised observations of substructures in living organisms initiated by Robert Hooke's observation of cork alveolae (Hooke et al., 2005). This theory stated that all living organisms are composed of cells, which are the most basic unit of life (Schwann, 1838; Tracy, 2020). The initial theory was rapidly updated in lights of new observations, most important of which was the description of cellular division by Barthelemy Dumortier, later formally enunciated by Rudolf Virchow "Omnis cellula e cellula" (Virchow, 1871) [1].

As basic units of more complex structures, cells must communicate and integrate information in order to build and maintain a complex organism or community. As living units, they must also maintain their own homeostasis, which necessitates sensing and modifying their internal state.

The advancements of cellular and molecular biology since the 1950s, when it became possible to manipulate cells outside of living organisms (Roux, 1885; Carrel, 1912; Carrel and Ebeling, 1921; Gey, 1952) and to purify intracellular molecules (Cori et al., 1939; Southern, 1975; Alwine et al., 1977; Towbin et al., 1979), uncovered multiple mechanisms by which mammalian cells perform those essential functions. Conceptually, those functions require the perception of state or perturbations and

[1] "Wo eine Zelle entsteht, da muss eine Zelle vorausgegangen sein (Omnis cellula e cellula), ebenso wie das Thier nur aus dem Thiere, die Pflanze nur aus der Pflanze enstehen kann"

actions to perform in response, with the involvement of an intermediate processing of the sensory information to determine the most adapted actions to perform. Sensing is permitted by many types of intracellular and transmembrane receptors (Cuatrecasas, 1974; Heldin et al., 2016). The actions a eucaryotic cell can perform are varied and range from adjusting metabolic rates to dividing or modifying the extra-cellular matrix (Kjær, 2004; Hopp et al., 2019; Smith et al., 2018; de Klerk and 't Hoen, 2015; Salama et al., 2014; Hartwell and Weinert, 1989). Finally, the processing of the various information provided by multiple receptors is performed by a complex network of interactions between biomolecules. As the knowledge of those interactions expanded, it became more and more complex to understand how a given set of pertubations would affect a cell.

Systems biology emerged from efforts in the 1970s to understand and be able to predict what happens inside a cell using mathematic models and the computation power of computers (Yates, 1973; Ideker et al., 2001). In the decades following the sequencing of the human genome in 2003, many new high-throughput experimental methods were developed to measure different biomolecules under various experimental settings.

In this work, I used data collected with medium to high throughput methods, and the mathematical method of Least Square Modular Response Analysis, to analyse mechanisms of resistance in cancer cell lines. I developped an R package called "STASNet" which implements Least Square Modular Response Analysis along with methods to enhance and compare the resulting models. I then applied it to analyse the flow of information in one set of isogenic colorectal cell lines and two neuroblastoma studies, one with a panel of neuroblastoma cell lines and the other with two sets of isogenic cell lines.

1.1 A Brief History of Cancer Therapy

Cancer is a leading cause of deaths in industrialized XXIst century countries, representing 25% of deaths in Germany and the European Union (Statistisches Bundesamt, 2020; Eurostat, 2016). It is most often a disease of old age, when mistakes in DNA repair and epigenetic maintenance mechanisms lead to somatic cells escaping normal control of proliferation and cell death (Jeggo and Löbrich, 2015; Hanahan and Weinberg, 2011). As a tumor grows, it consumes resources from the organism and replaces the existing tissue without fullfilling its function leading to the death of the organism via vital disfunction or general exhaustion. Over 50 nobel prizes (among ∼900 Nobel laureates) were awarded for contributions in oncology but the war on cancer has not been won yet, still claiming hundreds of thousands of lives every year.

The first proposed treatment of cancer was surgery, where a surgeon removes the mass of deregulated cells (Hajdu, 2012). This approach had limited success alone in

part because of the risks associated with surgery itself at the time but also because removing all cancer cells cannot always be achieved. This is especially the case in advanced tumors where the cells have started to migrate out of the hosting tissue and form secondary tumors called metastasis. Another complication arising is that inflammation caused by the surgery can hasten this metastatic development (Tyzzer, 1913; Baum et al., 2005; Demicheli et al., 2008).

Radiotherapy was added to the therapeutic arsenal after the discovery of X-rays[2] by Röntgen in 1895 (Artico et al., 1997; Birkenhake and Sauer, 1995) when the penetrating power of the radiation enabled the treatment of non resectable tumors. It led to major improvements in skin cancer treatment (65% of complete response) and prolongation of life in the majority of metastatatic cancers. However, radioresistance eventually occured in most tumors. Radiotherapy also triggered the understanding that alterations to DNA caused cancer, which initiated a fruitous search for carcinogens in the 1930s (Cook and Kennaway, 1940). It made prevention a new option in the fight against the disease with about half of all cancers being preventable (Schüz et al., 2015; Hahn et al., 2018; Wild et al., 2019).

At the beginning of the XX$^{\text{th}}$ century, Paul Ehrlich discovered that some cancers were susceptible to specific chemical compounds such as nitrogen mustard and suggested the use of chemotherapy in 1909, which was tried but quickly discontinued due to high toxicity. It was not until clinical trials in 1946 showed clear benefits in survival (Goodman et al., 1946; Jacobson et al., 1946) and the work of Sidney Farber who used new compounds against childhood cancers in the 1950s that chemotherapy truly integrated the therapeutic arsenal against cancer (Farber et al., 1948, 1956; Farber, 1966; Miller, 2006). This led to major improvements in survival by the end of the 1960s, when many previously deadly diagnosis in children became curable (Rosen et al., 1974).

In the 1970s, molecular characterisation of tumors and the discovery of oncogenes, i.e genes that favor carcinogenesis, led to the idea of using this information to stratify patients for treatment (Duesberg and Vogt, 1970; Bister, 2015). It was recognized by the late 1860s that the majority of primary malignant tumors were microscopically distinct (Hajdu, 2012). But it was not until 2001 that the first kinase inhibitor, imatinib targeting the BCR-ABL fusion kinase, got approved after showing a very strong effect in acute myeloid leukemia (Druker et al., 2001). Many targeted therapies have since been approved for various cancer alterations and have helped reduce the mortality of cancer (Goldberg et al., 2004; Amiri-Kordestani et al., 2014; Wong and Ribas, 2016; O'Bryant et al., 2013). Nonetheless many subtypes elope even targeted treatment (Le Rhun et al., 2019) and resistance arises in many cases (Nahta et al., 2006; Ellis and Hicklin, 2008; Rini and Atkins, 2009; Sierra et al., 2010).

[2]Röntgenstrahlen

Targeted therapy has thus been an important step forward both conceptually and practically in the treatment of cancer, and many discoveries remain to be done in this area of cancer therapy.

1.2 The Role of Signalling Networks

Targeted therapies disrupt cancer growth by interfering with the signalling pathways that promote the unchecked proliferation of tumor cells. A signalling pathway is a set of molecular interactions that mediates a signal through the cell. A signal can be of external or internal origin and a cell can respond by transcribing genes, changing reaction rates, or by releasing simple molecules and proteins.

Most Eukaryotic signalling pathways involve kinases, which are proteins that phosphorylate other proteins. Signalling networks have long been seen as "cascades", linear chains of events where a signal travels directly from a receptor to the nucleus (Cahill et al., 1996; Tatin et al., 2006; Pasparakis et al., 2006). However, more detailed analyses of signalling events showed that they form a complex network with crosstalk and feedback loop beyond the linear cascading progression of a signal. The systematic characterisation of protein interactions showed that topological features such as feedbacks and crosstalks are ubiquitous, and mathematical analyses revealed that they provide robustness to signal transduction (Legewie et al., 2008; Nguyen and Kholodenko, 2016).

Signalling pathways have been extensively mapped since the discovery of the first kinase (Fischer and Krebs, 1955; Kuperstein et al., 2015; Fabregat et al., 2018), but knowing the topology is not the same as understanding it. All the more since the topology of signalling networks is dynamic and varies between cell types. Such variations in topology necessitate different therapeutic strategies depending on the tissue of origin of a tumor. One striking example is the failure of BRAF inhibitors in colon cancer treatment (Prahallad et al., 2012) due to a feedback to EGFR (Endothelial Growth Factor Receptor), which contrasts with the effectiveness of the same inhibitors in melanoma where this receptor is not expressed (Chapman et al., 2011).

1.3 Neuroblastoma

Neuroblastoma is the most common solid infant tumour, representing approximately 13 cases per one million children per year (Berthold et al., 2017; Steliarova-Foucher et al., 2017), which corresponds to 8-9% of all childhood tumours in western countries and 22% of tumours before the age of one (Howlader et al., 2015; Kaatsch et al., 2018). Neuroblastoma originates from the progenitors of adrenergic neurons in the neural crest, resulting in about 50% of primary sites located in the adrenal gland, 28% in the abdominal region, 16% in the thoracic region and 4% in the cervical region (Berthold et al., 2017). In 2020, it remained one of the most difficult childhood cancers to cure, and represented 15% of all children cancer deaths (Maris et al., 2007; Johnsen et al., 2018). The 5-year survival rate is >75% overall, with many patients presenting a good clinical outcome requiring minimum medical intervention but it is below 50% for so-called high-risk neuroblastoma, that represents about 40% of patients (De Bernardi et al., 2003; Maris et al., 2007; Kyo et al., 2011; Berthold et al., 2017). Although major progress has been made in the treatment of mostly high-risk stage 4 neuroblastoma patients with the 5-year survival rate going from 4% in 1979, to 31% in 1990 and 47% in 2004 in Germany (Berthold et al., 2017), and the hope to reach 60% this decade with anti-GD2 therapy (Cheung et al., 2012; Park et al., 2016), it remains a major challenge to treat. Toxic treatment side effects lead to 4% of neurblastoma related deaths and the 10- and 15-year survival rates remain poor (Berthold et al., 2017). One of the major cause of the limited treatment success against high-risk neuroblastoma is the relatively low burden of mutations or other chromosomal aberations in primary neuroblastoma. In fact, only two oncogenes, MYCN and ALK, have been clearly identified and for neither of them has it been possible to develop successfull targeted therapy (Tucker et al., 2019).

1.3.1 The MYCN Oncogene

MYCN proto-oncogene, bHLH transcription factor (MYCN) is a transcription factor inducing hundreds of genes that drive cell cycle, metabolism and also telomeres elongation in neural cells (Mac et al., 2000; Bell et al., 2010; Murphy et al., 2011; Peifer et al., 2015; Hsu et al., 2016). Over-expression of MYCN is a central biological marker for high-risk neuroblastoma (Barone et al., 2013), present in only 13% of low and intermediate stages but in 31% of stage 4 neuroblastoma. The association of MYCN amplification with poor prognosis makes it an important marker of the high-risk group and a prime target for neuroblastoma treatment (Maris et al., 2007). Because many decades of development have failed to design a direct inhibitor for MYCN, the current focus lies on indirect approaches (Soucek et al., 2008; Richards et al., 2016). The most popular approaches involve inhibiting complex formation with MAX and using BET family proteins inhibitors to reduce MYCN translation (Barone et al., 2013).

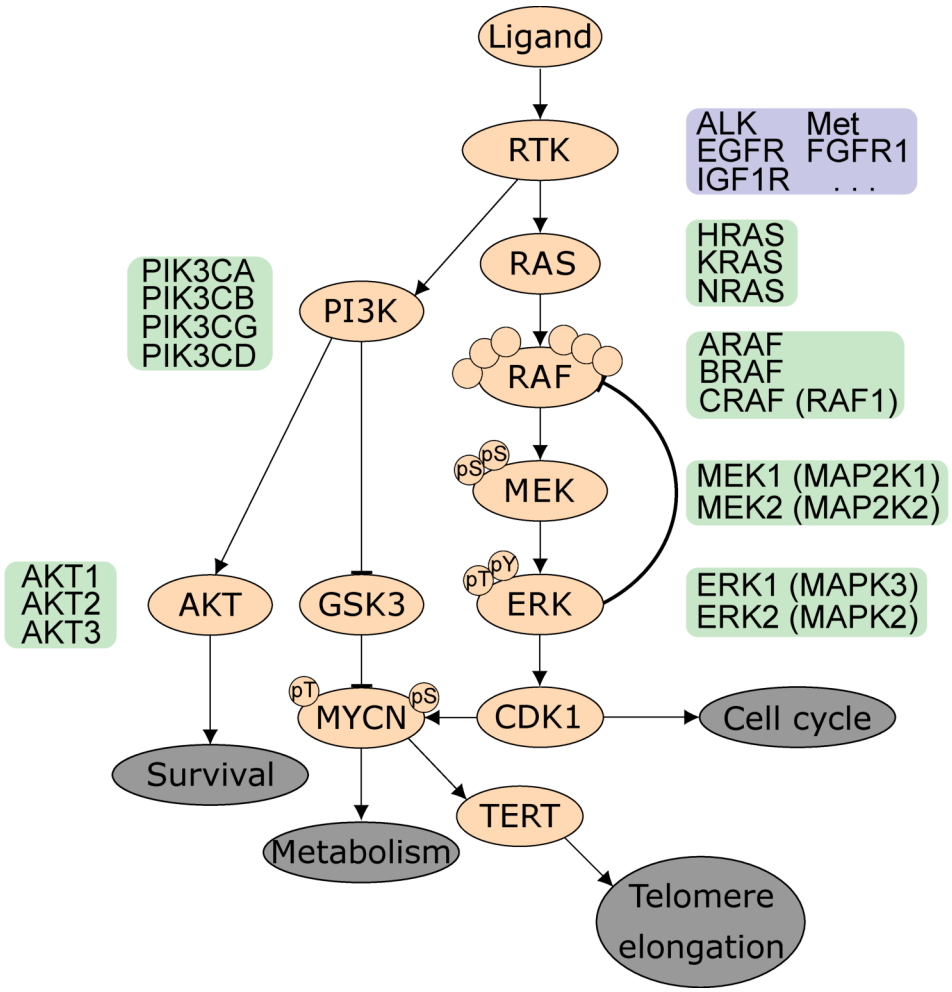

Figure 1.1: Main signalling components in neuroblastoma, Diverse receptors are activated by their specific ligand and activate downstream pathways with varying intensities depending on the receptor itself and on which adaptor proteins are present in the cell. The core of the MAPK pathway consists of RAF activating MEK by dual phosphorylation which exclusively activates ERK by dual phosphorylation. RAF itself is regulated both positively and negatively by multiple phosphorylations coming from upstream and feedback regulators. PI3K is also activated by numerous Receptor Tyrosine Kinase (RTK) and activates the pro-survival AKT while inhibiting the proteolysis promoting GSK3. MYCN is stabilised by the join activation of the MAPK and PI3K pathways. The distinct isoforms in mammals are indicated in green boxes, example family members in blue boxes.

The unmodified MYCN protein has a half-life of 30 minutes but MYCN is also regulated by targeted degradation by the proteasome (Johnsen et al., 2018). Phosphorylation on S62 mediated by activated CDK1 extends MYCN half-life but also primes MYCN for phosphorylation at T58 by GSK3 (Sjostrom et al., 2005; Kenney et al., 2004). The dual phosphorylated MYCN is then ubiquitinated by the E3 ubiquitine ligase FBXW7 and degraded by the proteasome (Welcker et al., 2004). Activation of the PI3K pathway via its inhibition of GSK3 activity increases MYCN stability and drives proliferation in cells expressing MYCN (Kenney et al., 2004; Chesler et al., 2006; Cage et al., 2015). MYCN levels can also be stabilized by AURKA, which in-

hibits FBXW7-mediated ubiquitination of the MYCN:FBXW7 complex (Otto et al., 2009). Finally, the MAPK pathway can also increase MYCN abundance via a specific up-regulation of MYCN translation (Kapeli and Hurlin, 2011).

1.3.2 The ALK Oncogene

Anaplastic Lymphoma Kinase (ALK) is a receptor tyrosine kinase expressed in the nervous system that activates the PI3K/AKT and RAS/MAPK pathways primarily, thus driving cell survival and proliferation when activated (Trigg and Turner, 2018). It is the major driver of familial neuroblastoma which represents 1-2% of all neuroblastoma cases (Mossé et al., 2008) and is altered in 20-43% of relapsed tumors (Eleveld et al., 2015; Martinsson et al., 2011; Bellini et al., 2015; Schleiermacher et al., 2014). ALK alterations at diagnosis include mutations in 8% of all neuroblastoma cases and copy number gain in 17% (Bresler et al., 2014). Gain of ALK copies occurs mainly concurrently with MYCN amplification due to their genomic proximity (13.2 Mb), but it likely has a phenotypic effect as ALK mutation and high copy number gain are mutually exclusive (Bagci et al., 2012; Bresler et al., 2014). R1275, F1174 and F1245 account for 85% of ALK mutations in neuroblastoma (Bresler et al., 2014) and affect the kinase domain of ALK, leading to ligand-independent signalling. These characteristics make ALK an interesting target for treatment of neuroblastoma and several targeted inhibitors (Alam et al., 2019; Tucker et al., 2019). However, rapid resistance to ALK inhibitors means that research is still ongoing for a targeted therapy with long term effects (Tucker et al., 2019; Debruyne et al., 2019; Trigg et al., 2019).

1.3.3 The MAPK Pathway

The mitogen-activated protein kinase (MAPK) pathway activated by ALK consists of a cascade of kinases leading to the activation of ERK1 and ERK2 (Figure 1.1). ERK1 and ERK2 are isoforms that phosphorylate multiple targets in the cytosol and the nucleus linked to metabolism, survival and proliferation (Lavoie et al., 2020). Many receptors other than ALK can activate the MAPK pathway, the main ones in neuroblastoma being the BDNF receptor TrkB and the NGF receptors TrkA and NGFR (Kaplan et al., 1993). Aberrant activation of the MAPK pathway is a major carcinogenic event and leads to tumorigenesis in many cell types with mutations of RAS and RAF isoforoms, the first kinases of the cascade, found in multiple cancer types (Davies et al., 2002; Garnett and Marais, 2004).

Despite MAPK1/3 activation, MEK1/2 inhibition does not block proliferation in ALK-addicted neuroblastoma because those tumors stabilise MYCN via PI3K-AKT-ERK5 signalling (Umapathy et al., 2014, 2017). This might explain why only few MAPK mutations are found in primary neuroblastoma (Eleveld et al., 2015), the MAPK pathway alone being insufficient to drive neuroblastoma progression.

1.3.4 Telomere Maintenance

Telomeres are repeated sequences at the end of linear chromosomes that stabilise this end by escaping DNA repair machinery, via a looped structure and nucleoproteins, and protect the rest of the chromosome from incomplete replication (Greider, 1996). Telomeres are shortened with every chromosomal replication due to incomplete replication of the end of the chromosome (Harley et al., 1990). The loss of telomeres after multiple replication leads to cellular senescence, a state in which a cell stops proliferating (Allsopp et al., 1992; Turner et al., 2019). In cells that are supposed to proliferate, such as embryonic cells or stem cells, telomeres are lengthened by the enzyme telomerase coded by the TET gene. Telomerase expression is repressed in most cells in the adult organism, which is a major break on the uncontrolled proliferation of cells. To escape proliferation induced-senescence there are three mechanisms of telomere maintenance identified in neuroblastoma. TERT expression can be reactived via a 5p15.33 rearrangement placing the expression under an active promoter or driven directly by high levels of MYCN. An alternative lengthening of telomeres mediated by ATRX loss of function also exists and has been found in some neuroblastoma patients (Pickett and Reddel, 2015; Peifer et al., 2015).

1.3.5 MAPK and Telomere Maintenance

Based on a dataset of 418 patients, Ackermann et al. (2018) showed that telomere maintenance and RAS/p53 pathway mutations are the main prognostic factors for neuroblastoma progression. Telomere maintenance alone defines high risk diseases with a 83% 5-year survival but only 44% 5-year event-free survival. Patients with alterations in the RAS/p53 pathways alone without telomere maintenance on the other hand are not at increased risk of death and can be classified as low or intermediate risk. However, an additional RAS/p53 pathway alteration worsens the prognosis in the telomere maintenance context, with only 41% 5-year survival and less than 25% 5-year event-free survival. This very-high-risk group appears to represent about 10% of primary high-risk stage 4 neuroblastoma patients, mostly consisting of MYCN amplified patients with ALK or PTPN11 mutations (Pugh et al., 2013).

Moreover, mutations in the MAPK pathway often occur after relapse (Figure 1.2, Eleveld et al. (2015)) and contribute to resistance to standard-of-care treatments (Hölzel et al., 2010). This makes MAPK inhibition a promising treatment option for neuroblastoma and ALK and MEK inhibitors are already being tested in the clinic (Johnsen et al., 2018).

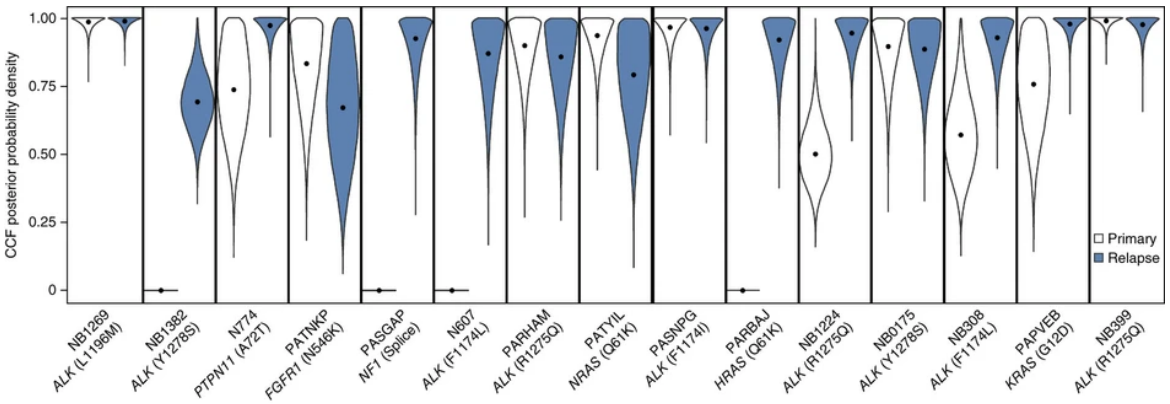

Figure 1.2: Cancer cell fraction (CCF) of RAS-MAPK mutations in primary-relapse pairs of neuroblastoma (from Eleveld et al. (2015)).

1.3.6 Drugs Approved for Neuroblastoma Treatment

Despite these recent important molecular characterisations, a very limited number of drugs is approved for neuroblastoma treatment both in Europe and in the US, none of them being targeted therapies (Table 1.1). They reflect the current strategy of intense cytotoxic chemotherapy treatment coupled with local surgery for primary neuroblastoma and with the tentative addition of immunotherapy for relapsed or refractory neuroblastoma.

Table 1.1: Drugs approved for treatment of neuroblastoma by the European Medicines Agency (EMA) https://www.ema.europa.eu/en/medicines/search_api_aggregation_ema_therapeutic_area_name/Neuroblastoma?sort=field_ema_computed_date_field&order=desc&search_api_views_fulltext=neuroblastoma (consulted 24/05/2021) or by the US Food and Drug Administration (FDA) https://www.cancer.gov/about-cancer/treatment/drugs/neuroblastoma (consulted 24/05/2021)

EMA approved		
Drug	Class	Indication in neuroblastoma
Phelinum (Melphalan hydrochloride)	Cytotoxic, alkylating agent	First line chemotherapy
Qarziba (Dinutuximab)	anti-GD2 antibody	High-risk neuroblastoma patients $>$ 12 months old who had at least partial response to induction chemotherapy or relapsed/refractory disease. Should be used with IL-2 in patients with relapsed/refractory disease.
FDA approved		
Drug	Class	Indication in neuroblastoma
CEM (Carboplatin+ Etoposide+Melphalan)	Cytotoxic, DNA intercalation, topoisomerases II inhibitor and alkylating agents	First line chemotherapy
BuMel (Busulfan+Melphalan)	Cytotoxic, alkylating agents	High risk neuroblastoma as a preparation for a stem cell transplant
Cyclophosphamide	Cytotoxic, alkylating agent	Disseminated neuroblastoma
Unituxin (Dinutuximab)	anti-GD2 antibody	In combination with IL-2 and 13-cis retinoic acid in high-risk neuroblastoma.
Doxorubicin Hydrochloride	Cytotoxic, DNA intercalation and free radicals formation	Metastatic neuroblastoma
Danyelza (Naxitamab)	anti-GD2 antibody	Relapsed or refractory high-risk neuroblastoma with bone marrow metastatis in combination with GM-CSF
Vincristine Sulfate	Cytotoxic, antimitotic alkaloid	First line chemotherapy

1.4 Outline of this thesis

This thesis presents my work on developing an R package to build and analyse Modular Response Analysis (MRA) models, and how I used it to reverse engineer signalling networks in cancer cells. I demonstrated the methodology of the package on a well-studied colorectal cancer test model, then focused on neuroblastoma in the hope of improving the efficiency of targeted therapy for this cancer type.

Chapter 2 introduces Modular Response Analysis, and details the implementation and workflow of the R package STASNet I have developped.

Chapter 3 highlights the extensions I have developped by using STASNet to reverse engineer signalling networks on a dataset of SHP2-knock-out (SHP2-KO) colorectal cell lines. This work has been published in Dorel et al. (2018).

Chapter 4 is dedicated to the analysis of drug resistance in a panel of neuroblastoma cell lines. I used STASNet models to understand the resistance to MEK inhibition in those cell lines. The models are then used to elaborate therapeutic strategies to overcome the resistance. This work has been published in Dorel et al. (2021).

Finally, Chapter 5 is dedicated to my analysis of NF1-knock-out (NF1-KO) neuroblastoma cell lines to understand drug resistance against ALK inhibition and identify emerging vulnerabilites. NF1-KO cell lines, of SH-SY5Y and LAN-5, were generated and characterized by Mareike Bock who then generated perturbation datasets. I used these datasets to build signalling models that helped elucidate how ALK and MEK inhibition affected those cell lines.

Chapter 2

Modular Response Analysis in STASNet

2.1 Modular Response Analysis

Modular Response Analysis (MRA) is a methodology which uses perturbation data to estimate the effects of functional modules on one another. The first formulation was developed by Boris Kholodenko in 2002 (Kholodenko et al., 2002). MRA analyses the steady-state responses to perturbation of the model parameters, which is realised by activation and inhibition of the modules. It relies on the ability to measure the activation state of those modules. Because a such system admits a graphical representation, I will refer to those modules as nodes from now on.
The nodes are linked by an Ordinary Differential Equation (ODE) system, which describes how changes in one node directly affect the others.

$$\dot{x} = f(x, p) \tag{2.1}$$

where x_i in the activity of node i and p is a set of perturbations that can be applied to the system, such that $p_i \neq 0$ means that node i is perturbed.
The derivative $\delta_{ij} = \frac{p_j}{x_i}\frac{\delta x_i}{\delta p_j}$ represents the variation in log space of the node x_i upon variation of the input parameter p_j. We can then for simplicity choose a parametrisation such that $\forall i \neq j, \delta_{ij} = 0$ and $\forall i, \delta_{ii} = 1$. This approach relies on the hypotheses that we use a single concentrations of ligands and inhibitors for stimulation and inhibition, respectively, and that these perturbations affect a single node. Multi-node perturbations can however easily be incorporated as combination of single node perturbations.

When a single parameter is perturbed by an infinitesimal amount, we can express the response of the network at steady-state as :

$$\frac{p_j}{x_i}\frac{dx_i}{dp_j} = \frac{p_j}{x_i}\frac{\delta x_i}{\delta p_j} + \sum_{k \neq i} \frac{x_k}{x_i}\frac{\delta x_i}{\delta x_k}\frac{p_j}{x_k}\frac{dx_k}{dp_j} \tag{2.2}$$

This means that the global response of node x_i to a stimulation of the parameter p_j depends on the direct response to this stimulation plus the response propagated through the other nodes. MRA provides names for the scaled derivatives.

$$R_k^j = \frac{p_j}{x_k}\frac{dx_k}{dp_j} = \frac{d\log(x_k)}{d\log(p_j)} \tag{2.3}$$

are the global response coefficients. They describe the changes of steady-state of the entire network induced by perturbation p_j. They represent log-fold changes of activity of the node x_k at steady-state after the perturbation of node j, i.e. the data that are measured.

$$r_i^k = \begin{cases} \dfrac{x_k}{x_i}\dfrac{\delta x_i}{\delta x_k} \text{ for } k \neq i \\ -1 \text{ otherwise} \end{cases} \tag{2.4}$$

are the local response coefficients. They represent the direct interaction between the nodes. The purpose of MRA is to infer these coefficients which usually cannot be measured directly.
With these notations, equation 2.2 can be expressed as :

$$-\delta_{ij} = -R_i^j + \sum_{k\neq j} r_i^k R_k^j = \sum r_i^k R_k^j \tag{2.5}$$

which can be expressed with the matrix formalism as :

$$rR = -I \tag{2.6}$$

By inverting the R matrix, it can be rewritten as:

$$r = -R^{-1} \tag{2.7}$$

In the original formulation, the local response r was computed by numerically inverting the global response r (Kholodenko et al., 2002). However this formulation strongly limits the usage of MRA as all nodes need to be both measured and perturbed; and it is highly sensitive to noise in the measurements.

To avoid those caveats, a maximum likelihood formulation (ML MRA) was proposed by Prof. Dr. Nils Blüthgen and Dr. Bertram Klinger. Hence, realising that inverting r gives a theoretical expression for the global response R that comparable to the measured response (Klinger et al., 2013). Indeed, knowledge of the network topology allows to build a symbolic expression for the r matrix. This known network built from literature evidence can also be enriched with hypothetic links that might

prove necessary for understanding the dynamic of the network. The symbolic inversion of this r subsequently provides a symbolic expression for R with local response coefficients as variables (Figure 2.1).

$$R = -r^{-1} \tag{2.8}$$

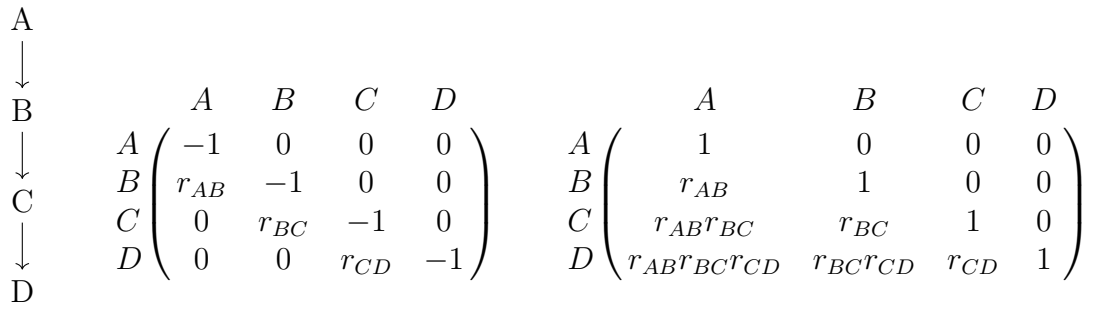

(a) Graph (b) r (c) R

Figure 2.1: Example local and global response matrices on a linear network

ML MRA thus retrieves the local response coefficients using measurements of the variations of activity of the nodes Δx^p, where p is a perturbation, for different sets of perturbations. For each ligand or other drug used, we can define a perturbation vector Δp^j, with entry j being non-zero only if node j is directly perturbed. For a set of perturbations S, we can define the perturbation vector $\Delta p = \sum_{j \in S} \Delta p^j$.

If we assume a linear response of nodes to perturbations, the logarithmic fold change of all the nodes of the network to this perturbation vector can then be calculated by multiplying the global response matrix R by this perturbation vector. Thus, the perturbed response of the network is defined as :

$$\Delta x^p = R \Delta p \tag{2.9}$$

If the hypotheses are satisfied then $R = R^{\text{measured}} - E$ where R^{measured} is the experimentally measured global response and E is the measurement error. This equality provides a set of equations whose solutions are values of r compatible with the data. In the STASNet package, we find this solution using a hill climbing algorithm with random initialisation that tries to minimize the residual function :

$$\mathcal{L} = \left(\sum_{i,j,p} \frac{R_{ij} \Delta p - R^{\text{measured}}_{ij,p}}{\text{s.e.m}_i} \right)^2 \tag{2.10}$$

The *levmar* library (Lourakis, 2005) is used to perform the Levenberg-Marquardt gradient descent (Levenberg and Arsenal, 1943) and the starting points are generated using latin hypercube sampling with the R package *lhs* (Carnell, 2012).

2.2 Managing Different Perturbation Types

A biological network can be perturbed by multiple types of perturbations, which have different impacts on the network and therefore need to be simulated differently.

Stimulation of node j, mostly by the addition of a ligand to a receptor of interest, is directly calculated using Δp^j. It is reflected in the equation as the effect of a change in the activity of this node, which can be read directly into the R matrix.

Inhibition of a node m by small molecules is more complex and two phenomena have to be taken into account: (i) the reduction of the capacity of the inhibited node to relay an upstream signal to downstream nodes, and (ii) the reduction of the basal activity of the node. The first effect is adressed by multiplying the values of the outgoing links in r by an inhibitory term $i_m \in]0, 1[$, yielding in a new local response matrix $\tilde{r}$. The second effect must be specified in a separate perturbation vector, Δp^{inh}, where $\Delta p^{inh}_m \in]-\infty, 0[$ is the log fold reduction of activity of node m induced by the inhibitor. Since i_m represents the proportion of elements still active after the inhibition, those two effects are linked by the relation : $\Delta p^{inh}_m = \log(i_m)$.

Thus, the response of node k to a combined perturbation consisting of a stimulation of node j and an inhibition of node m is :

$$\Delta x_k = (\tilde{r}^{-1})\Delta p_j + (r^{-1})\Delta p^{inh}_m \tag{2.11}$$

where the first term reflects the decreased relay effect of node m and the second its decreased basal activity. Nodes do not always have a basal activity and it should be specified as an input for STASNet. In such a case the second term is set to 0. i_m represents a new parameter because the exact value of the inhibition is *a priori* unknown, and is fitted by the program like any other parameter.

Adapting the inhibition model to the molecular mode of action

The way in which inhibitions are modelled in STASNet supposes that only the activity of the inhibited target is affected, i.e. the inhibitor only affects the catalytic site. There are, however, many inhibitors that are known to have effects on other sites of the kinases, most importantly on the phosphorylation sites. For example, some ATP-competitive AKT inhibitors, such as A443654, are known to induce an AKT hyperphosphorylation (Okuzumi et al., 2009), while others, like MK2206, bind to allosteric sites and prevent phosphorylation by upstream kinases (Hirai et al., 2010). This becomes a problem if a protein in the network is both measured and inhibited.

Those mechanisms can be accounted for by formulating the network differently, without changing the hypotheses of STASNet MRA, in two different ways:

1. One can simply ignore the inhibited kinase readouts when the corresponding inhibitor is used. This has the advantage of not imposing any modifications to the network but the disadvantage of not using data that have been generated.

2. One can add an extra node that will be the target of the inhibition upstream of the measured nodes. This has the advantage of using all the data points but the disadvantage of adding an extra parameter to be fitted that is not guaranteed to be identifiable. In the aformentioned MK2206 example, the second solution would amount to introducing the MK2206_site and replacing PI3K→AKT with PI3K→MK2206_site→AKT.

2.3 Derivation of Confidence Intervals for STASNet Model Parameters

In order to derive a confidence interval for the paths fitted by MRA, STASNet uses profile likelihood (Raue et al., 2009). Profile likelihood is a computationaly intensive method to provide the exact dependency of likelihood on the model parameters, overcoming altogether the inaccuracies arising from limited development methods (Dovì et al., 1991) and the risks of non-invertible hessians (Gill and King, 2004).

A likelihood profile is the set of values taken by the residual when varying one parameter while letting the others relax. Conceptually, it follows the valley of local minima while removing the degree of freedom corresponding to the parameter being varied. Because our model has less degrees of freedom, most of the time one and more generally n, a higher likelihood is acceptable if the difference from the optimum likelihood conforms to a χ^2 distribution with n degrees of freedom. The confidence interval to a given confidence α for a particular parameter of the set of parameters θ are the most extreme values this parameter can take around the optimum such that $\mathcal{L}(\theta_{\text{fixed } i}) - \mathcal{L}\theta < \chi^2(\alpha, n)$ (Hudson, 1971; Venzon and Moolgavkar, 1988; Porter,

1996). The dependency between the parameters means that fixing one parameter might actually remove more than one degree of freedom, though the complexity of this dependency prevents any accurate determination. Consequently, the true threshold to determine the confidence interval is between the point-wise threshold $\chi^2(\alpha, 1)$ and the family-wise threshold $\chi^2(\alpha, N)$, where N is the total number of parameters of the model (Raue et al., 2009). STASNet reports the most conservative confidence interval $\chi^2(\alpha, 1)$, which is likely the correct confidence interval for most reasonably designed networks, where fixing one path removes a single degree of freedom. It uses these confidence intervals to determine if parameters are identifiables, whether they can be removed (subsection A.2), and whether an extension is significant.

A parameter is identifiable when it is constrained to a neighborhood of the optimum, i.e when its confidence interval is finite on both sides (Ljung and Glad, 1994; Porter, 1996). Non-identifiability can have two sources. It is structurally non-identifiable if the likelihood does not change at all when the parameter is varied. Structural non-identifiability is caused by other parameters perfectly compensating the variations of this parameter. It arises from an overspecification of the model that cannot be determined with the experimental setup. STASNet reparametrises the model to remove most structural non-identifiabilities, fitting not every link of the network but a set of identifiable combinations of links (subsection A.1, Klinger et al. (2013)). A parameter is practically non-identifiable if the changes in likelihood are so small that the point-wise threshold is not reached for several orders of magnitude. Experimental non-identifiability comes from a poor signal-to-noise ratio due to either highly variable measurements or too strong of an inhibition of non-measured nodes such that the signal reduction effect is not numerically identifiable (Raue et al., 2010).

Because the other parameters are allowed to relax during the likelihood profile calculation, we also get a 'compensation profile' for each other parameter. These profiles contain the dependency between parameters and can be studied to solve structural non-identifiabilities (Raue et al., 2010).

In STASNet, the function `profileLikelihood` is used to compute the likelihood and compensation profiles, and the information is added to the model with `addPLinfos`.

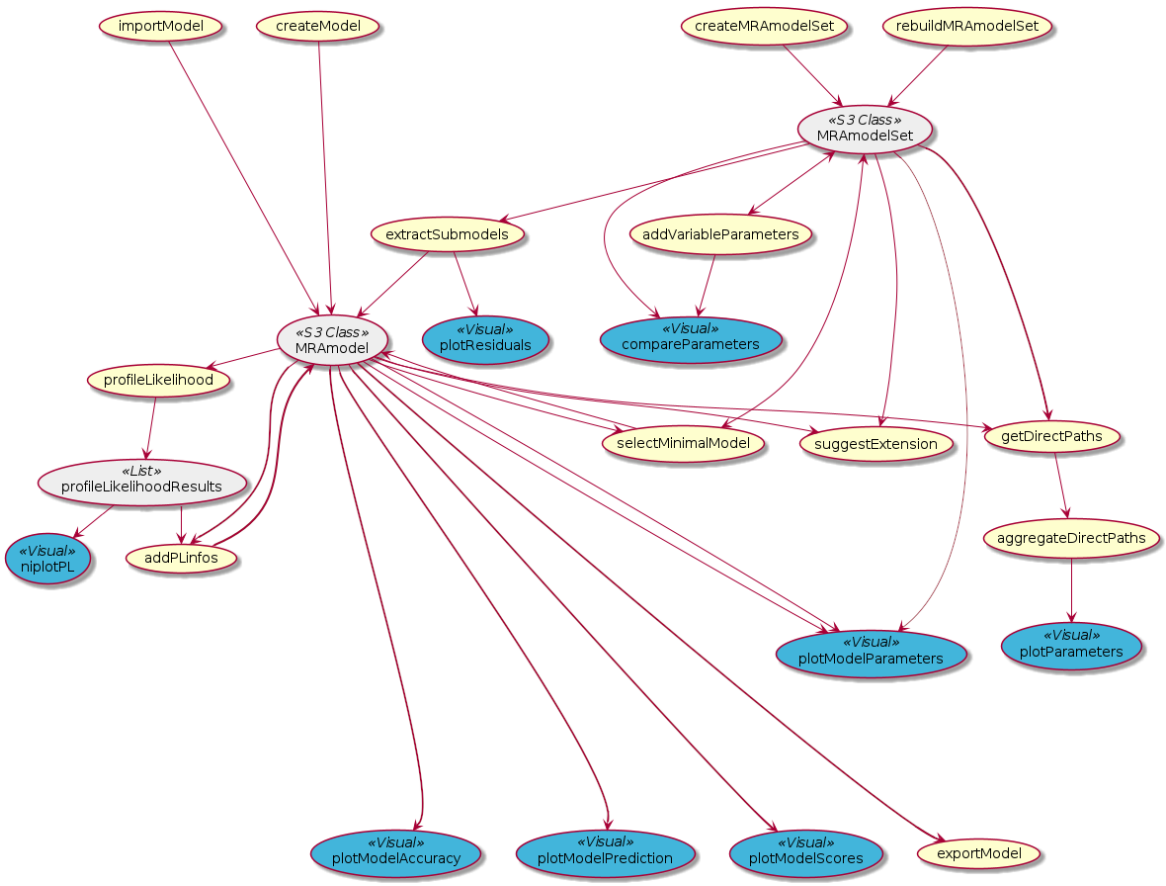

Figure 2.2: Workflow for STASNet showing the relationships between the inputs and outputs of the different functions. R objects are in grey, core STASNet functions are in yellow and functions with a graphical output are in blue.

2.4 STASNet Workflow

An analysis using STASNet involves a precise workflow (Figure 2.2). The core function of STASNet which creates a Maximum Likelihood MRA model is `createModel`, which takes as input a network topology, a list of modules with basal activity and perturbation data, optionally with information on the experimental error (subsection A.3). This returns an object of class *MRAmodel* which can be exported with `exportModel` into a .mra file. The .mra files can be imported with `importModel`, making it easy to share STASNet models. It should be noted that because an *MRAmodel* object uses a C++ pointer, it cannot be cached by R natively. To tackle this problem, and to make STASNet usable in *knit* documents for example, I wrote the helper R package knitHelpersSTASNet where `check*` functions export the outputs of the model to the cache on the first run and then load from the cache on subsequent runs.

The model performance is evaluated with `plotModelAccuracy`, which produces heatmaps and qq-plots to evaluate the agreement between the model prediction and the data. The model can then be refined with `selectMinimalModel`, which automatically removes links that do not significantly improve the fit, and `suggestExtension`,

which systematically tests all possible extensions and reports the best ones to be considered for addition to the model. Dr. Klinger showed in his thesis "Mathematical modelling of molecular networks in cancer cells using modular response analysis" that ML MRA requires strong perturbations with low noise (i.e high signal-to-noise ratio) for an accurate prediction but could reliably detect even non-linear influences. One major limitation, however, remains the loss of precision and sensitivity when trying to predict the topology of larger and denser networks. Prior knowledge about the topology can be easily integrated into ML MRA formulation and drastically improves the predictions, making it a useful tool for the parametrisation and simulation of well studied signalling networks where only a few cell type specific extensions are required. STASNet was built with such prior knowledge in mind and does not provide automatic extension of the network to ensure that biologically relevant links are added. It does however implement an extension exploration routine in the `suggestExtension` function to guide the addition of new links to the model, in coordination with a literature or experimental confirmation. One can then estimate the confidence in the parameters with `profileLikelihood` and add this information to the *MRAmodel* object with `addPLinfos` or visualize it with `niplotPL` which generates separate plots for identifiable and non-identifiable parameters.

Parameters can be compactly compared between models with `compareParameters` or with `plotModelParameters` using extra information provided by the profile likelihood. `plotModelParameters` uses the function `getDirectPaths` to recompute paths from the model parameters with less constraints than imposed for identifiability and optionally merges paths to get the total activation of a pathway. This path recomputation is useful because parameters from STASNet are not always easily interpretable, in particular when some links are at the denominator of a path, and to solve some numerical non-identifiability arising from inhibitions.

2.5 Model Sets

MRA is often used to study isogenic cell lines, which are less noisy models to study the effect of specific alterations on the signalling network. In such a system, only a few variations exist in the signalling networks between those cell lines and they could thus be modelled conjointly. In STASNet, this joined modelling is done via the *MRAmodelSet* interface, which simultaneously fits multiple MRA models with additionnal inter-models constraints that some paths must be equal in all models. Since it is not known *a priori* which paths vary between models, the function `createModelSet` fits the ModelSet with all the paths being shared. Then, the `addVariableParameters` function iteratively allows paths to vary between cell lines, i.e it fits a separate parameter for this path for each cell line. Setting a path to variable between models

significantly improves the fit if the improvement in the residuals passes a χ^2 test with $m-1$ degrees of freedom, where m is the number of models in the ModelSet.

2.6 Discussion

Many approaches have been developed to derive computational models from perturbation-response data. Two major, opposite, trends have dominated. Binarizing the data to use logic approches represents the advantage of a simple model (Morris et al., 2010) but misses more subtle effects that are often important for drug response (Niederdorfer et al., 2020). Alternatively, using dynamic information to fit quantitative models precisely describes what happens in the cell (Raue et al., 2015) but at the cost of necessitating time-resolved data. This quickly becomes expensive and limits the size of the networks that can be fitted. In this chapter, I described the implementation of an approach using an augmented version of Modular Response Analysis (Kholodenko et al., 2002; Klinger et al., 2013), which generates semi-quantitative models from single time point perturbation data at the cost of a limited number of hypotheses on the state of the system. The steady-state assumption is not exactly met in signalling networks, where multiple layers of signal integration take hours or days to be incorporated by the cell. However, a quasi-steady-state assumption is usually valid as biochemical events happen at different time-scales and can thus be approximately separated by a careful choice of time-point. For example, post-translationnal modifications such as phosphorylation happens within minutes, transcription within hours and translation within days. Dr. Klinger already showed in his thesis that ML MRA can retrieve and quantify even non-linear interactions (Klinger and Blüthgen, 2018). STASNet was developped with Dr. Klinger and implements this augmented MRA. It also provides multiple analysis tools to compare and improve models, some of which will be examplified in the following chapters of this thesis.

STASNet proved a convenient R-package to generate ML MRA models from perturbation data and to suggest treatment hypotheses. Few other programs exist to deal with single time point steady state data. CellNOptR (Terfve et al., 2012) can be applied to such data after discretisation or normalisation of the data, which implies to define thresholds and might require external data. Other more precise approaches like CellNOptR variant CNORode (Terfve et al., 2012) or Data2Dynamics (Raue et al., 2015) rely on ODEs and require more data to be parametrised, limiting their application to small networks.

The package is available at https://itbgit.biologie.hu-berlin.de/dorel/STASNet in open source.

Chapter 3

Benchmarking STASNet on isogenenic SHP2-KO colorectal cancer cell lines

After developing STASNet, I wanted to explore the utility of the package to recover signalling alterations and to infer therapeutic strategies. SHP2 alteration is a well-known resistance mechanism in BRAF mutated colon cancer (Prahallad et al., 2015). The intend of this chapter is to demonstrate the possibilities offered by STASNet to fit and refine signalling models to literature networks in a setting where known and well studied alterations are present. *This work was published in Dorel et al. (2018), please refer to the materials and methods section for experimental details.*

3.1 Introduction

3.1.1 SHP/PTPN11 in isogenic cell lines is a good benchmarking example

I decided to study the role of the protein SHP2 encoded by the PTPN11 gene, a phosphatase that is important in receptor tyrosine (RTK) signalling and has been implicated in feedback control of EGFR signalling and drug resistance (Prahallad et al., 2015). Somatic mutations activating PTPN11 activity are the most common cause of the Noonan syndrome, a developmental disorder caused by aberrant activation of the RAS-MAPK pathway. Patients harboring these alterations have a higher risk of developing malignancies (Jongmans et al., 2011; Chan et al., 2008). SHP2 is a phosphatase that binds to tyrosin kinase receptors through adaptors such as GAB1 and participates in the activation of the MAPK cascade by releasing inhibitions on RAS and RAF (Chan et al., 2008; Neel et al., 2003). SHP2 activity is necessary for the activation of the RAS-MAPK pathway (Ruess et al., 2018) but has a more ambigious role for the activation of the PI3K pathway (Figure 3.1), with a possible

negative regulation of GAB1-mediated activation of PI3K in some cell lines (Zhang et al., 2002), or for the JAK/STAT pathway (You et al., 1999).

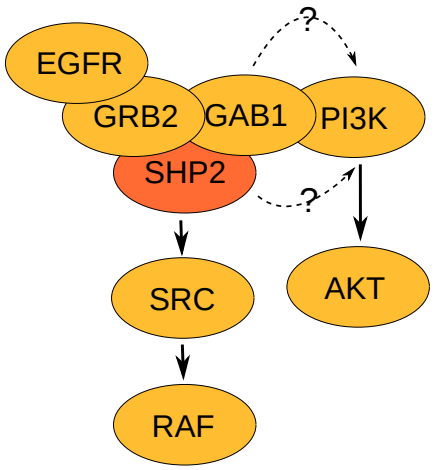

Figure 3.1: Known and postulated role of SHP2/PTPN11 in the transduction of receptor activation to the MAPK and AKT pathways. The activation of the MAPK axis by SHP2 is well established, but its role in the activation of the PI3K axis is more variable.

3.1.2 SHP2-knock-out study design

Our collaborators in the Division of Molecular Carcinogenesis of the Netherlands Cancer Institute (DMC-NCI) generated a PTPN11 CRISPR/Cas9 knock-out (SHP2-KO) in the colorectal cancer cell line Widr. The Widr cell line harbours a $BRAF^{V600E}$ mutation and the PTPN11 KO line was still sensitive to the inhibitor Vemurafenib, which targets this mutation.

In line with previous approaches, the perturbations chosen to train our models used pair-wise combinations of a stimulus and an inhibition (Nelander et al., 2008; Saez-Rodriguez et al., 2009; Morris et al., 2011; Klinger et al., 2013). Specifically, the cells were starved of serum for 24h then pre-inhibited for 60 minutes by AZD6244 or GDC0941, which inhibit MEK1/2 and the PI3K complex respectively. While maintaining the inhibition, the cells were stimulated for 30 minutes with the growth factors EGF, NRG1 and HGF, which stimulated the receptors EGFR, HER2 and Met respectively. The phosphorylation of 7 phosphosites (AKT^{S473}, $MEK1^{S217,S221}$, $p90RSK^{S380}$, $GSK3a/b^{S21/S9}$, $RPS6^{S235/S236}$ and $mTORC^{S2448}$) that are downstream of the stimulated receptors and inhibited kinases were measured simultaneously using the bead-based sandwich ELISA method from Bio-Plex (Figure 3.2). This system grants a high specificity which can be used to quantify phosphosites with a greater dynamic range than a Western blot by 3 to 4 orders of magnitude. *Treatment and measurements were performed by MSc Anja Sieber (CMM) and Dr. Anirudh Prahallad (DMC-NCI).*

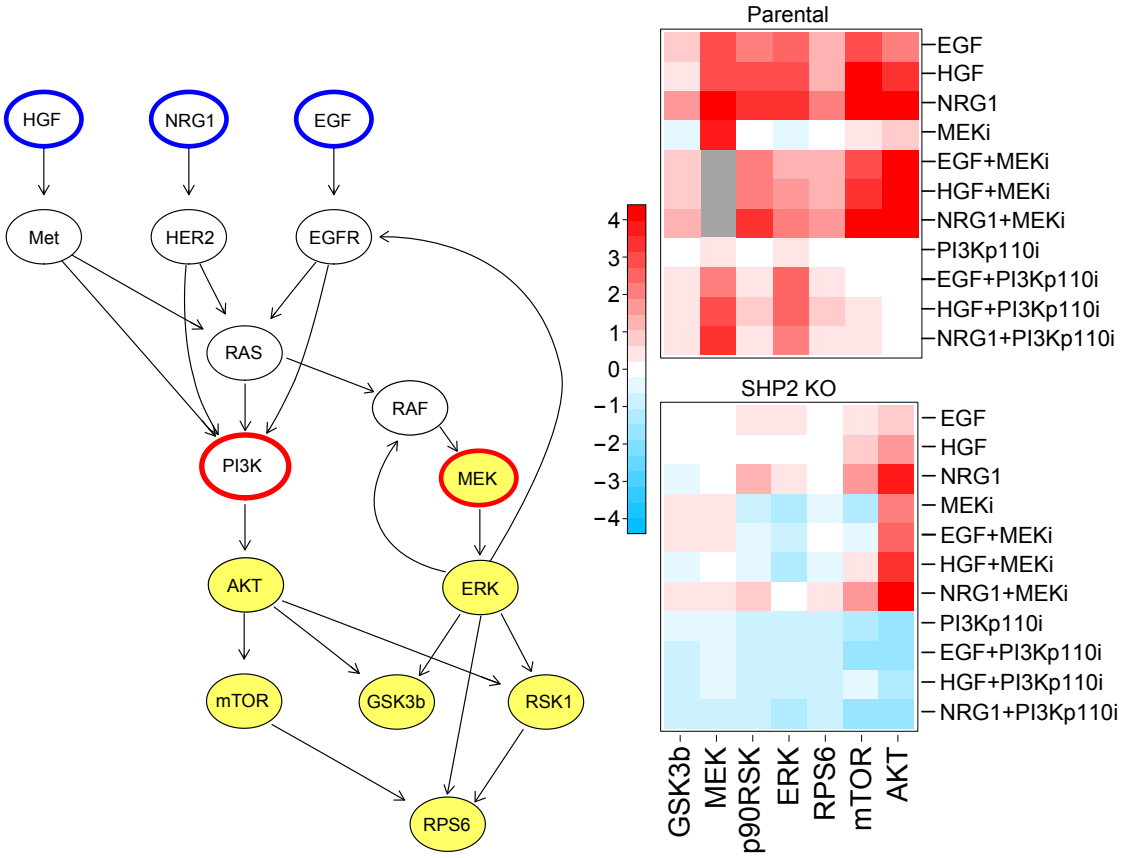

(a) (b)

Figure 3.2: (a) Graphical representation of the perturbation experiment on the literature network. Blue outlines, red outlines and yellow fill represent ligand nodes, stimulated nodes and measured nodes, respectively. (b) Log2-fold-change to, PBS+DMSO control of AKT^{S473}, MEK1^{S217,S221}, p90RSK^{S380}, GSK3a/b$^{S21/S9}$, RPS6$^{S235/S236}$ and mTOR^{S2448} after ligand and drug treatments of the Widr parental and SHP2-KO cell lines. n=2, error bars are standard deviation.

3.2 A simplification of the model resolves structural non identifiabilities

The starting network for the MRA model consisted of the three ligands, their receptors, RAS, PI3K and RAF as unmeasured signalling intermediates, measured pathway components of AKT and MAPK signalling, and lastly pathway targets that include mTOR as an AKT target and GSK3b, p90RSK and RPS6 as common targets of both signalling pathways (Figure 3.2). In addition, I included the well-studied ERK→ RAF and ERK→ EGFR feedback loops in MAPK signalling that are known to play a role in drug resistance (Fritsche-Guenther et al., 2011; Klinger et al., 2013; Poulikakos et al., 2010; Corcoran et al., 2012; Prahallad et al., 2012; Sun et al., 2014). The corresponding model contained 19 parameters that represent either path strength or inhibitor strength. The resulting fit yielded a weighted sum of squared residuals of 51.8, which is compatible with the estimated 55 residual degrees of freedom (74 data points minus 19 parameters).

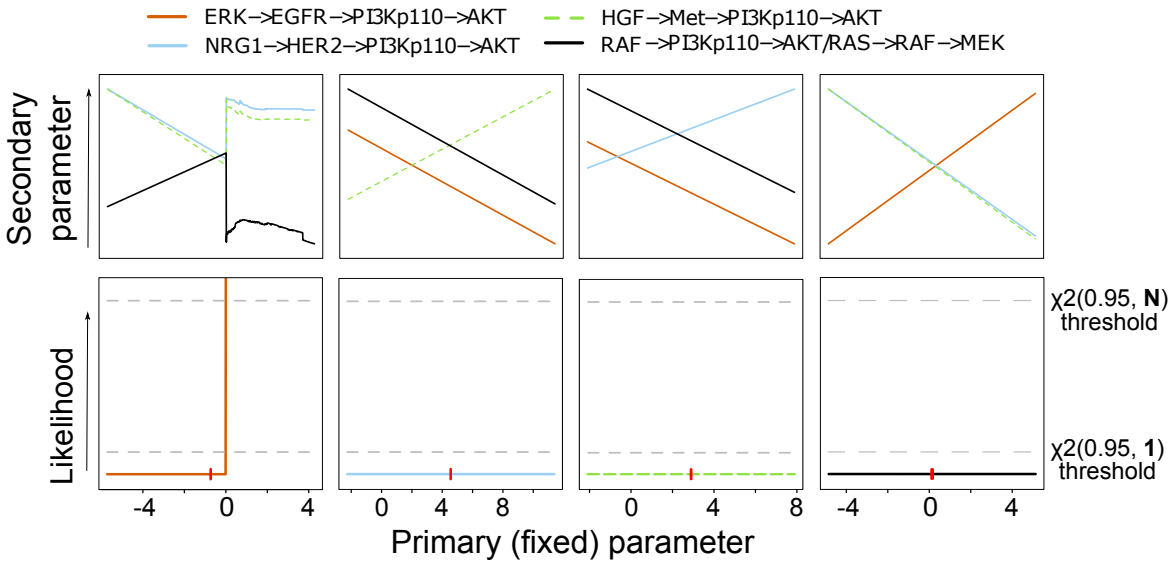

Figure 3.3: Profile likelihood of parameters non-identifiable in the parental model using the literature network. Each parameter is fixed at different values around the optimum, then the model is left to relax and computes the resulting likelihood (bottom row) and other non-identifiable parameter values (top row).

An interesting aspect of the initial network is the different modes of activation of the two pathways: while the MAPK pathway is solely activated through RAS, AKT is activated both in a RAS independent and dependent manner (Hemmings and Restuccia, 2012). However, the relative influence of these two mechanisms could not be estimated independently by our model as no elements of these two paths leading to AKT activation, neither RAS nor relevant receptor adaptor activities, were measured or perturbed. This type of dependance can be detected using profile likelihood (Raue et al., 2009). When plotting the profile likelihoods and the optimized parameters, structural non-identifiabilities are directly visible as flat profile likelihoods, which do

not cross the point-wise confidence interval, and thereby the compensating parameters can be identified as linear compensations (Figure 3.3).

In this case, the model can be reduced by removing one of the links, HER2→PI3K, RAS→ PI3K, Met→PI3K or EGFR→PI3K, without causing changes in the likelihood. As all three models have the same unchanged likelihood, I decided to remove the RAS→PI3K link to separate the PI3K and RAF cascades activation (Figure 3.4c). This allows for a more straight forward interpretation of the parameters and leads to a numerically more stable model. This results in a network model where all links are identifiable. Regardless, one should note that the receptor→PI3K→AKT represents a set of parallel activation pathways, including one via RAS.

3.3 ERK→mTOR regulation improves the Widr model

While the model reproduces the data reasonably well, there were still major qualitative discrepancies for mTOR upon PI3K inhibition. The model predicted no effect when there should have been a significant activation according to the data. To investigate if any additional links can resolve these discrepancies, I used the extension suggestion feature of STASNet. It suggested that adding a link from MEK or downstream of MEK (MEK, ERK, RPS6 or p90RSK) to mTOR would best improve the model fit (Figure 3.4a). Discrimination of these links experimentally would require a different experimental design, where ERK, RPS6 and p90RSK are directly perturbed. A literature search unveiled that mTOR can indeed be activated by ERK, which inhibits the mTOR inhibitory complex protein TSC2 via phosphorylation of the serine residue 664 (Rolfe et al., 2005; Caron et al., 2010). The network was thus updated to include this link, which led to an improved fit of the mTOR readouts (Figure 3.4b with ERK→mTOR).

It is of note that the $mTOR^{S2448}$ phosphorylation, used here as a proxy of mTOR complex 1 (mTORC1) activation, is mediated by p70S6K, which is activated by both mTORC1 and ERK. Although such discrimination was not necessary for the purpose of this work, one could discriminate between these two mechanisms of mTORC1 activation via measurements of TSC2 phosphorylation in response to p70S6K inhibition.

from	to	value	residual	adj_pval
RPS6	mTOR	1.25	48.25	2.23E-02
ERK	mTOR	0.24	48.25	2.23E-02
MEK	mTOR	0.21	48.25	2.23E-02
p90RSK	mTOR	1.09	48.25	2.23E-02

(a)

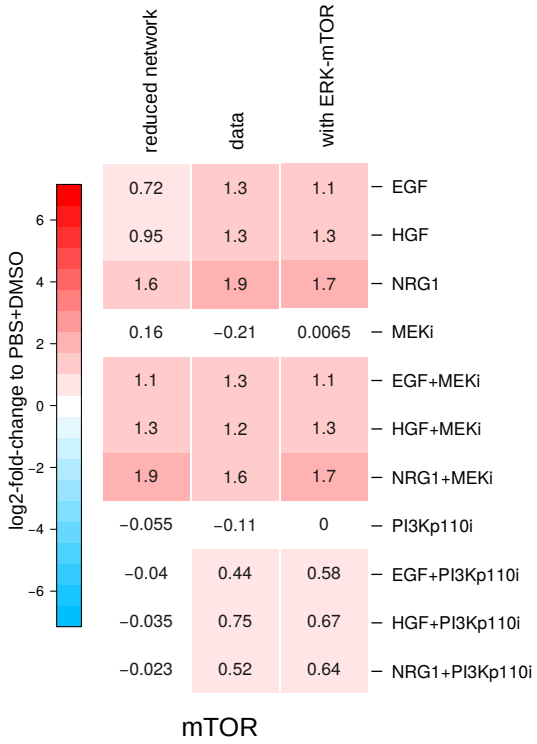

(b)

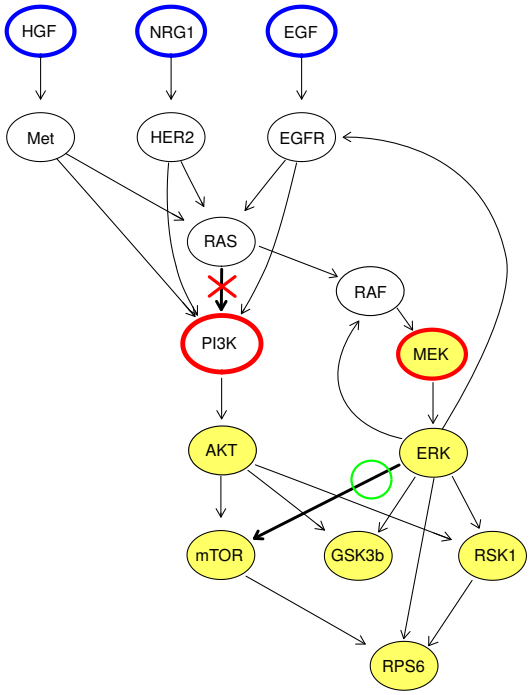

(c)

Figure 3.4: (a) Best extensions of the literature network for the parental Widr model as found with the `suggestExtension` function. (b) Measured and fitted values using a model with or without a link from ERK to mTOR. Values and color indicate log-fold change to PBS+DMSO. (c) Graphical representation of the updates to the literature network. The red cross highlights the suppressed RAS→PI3K link and the green circle highlights the added ERK→mTOR link. Blue outlines, red outlines and yellow fill represent respectively ligand nodes, stimulated nodes and measured nodes.

3.4 The isogenic cell lines highlight differential regulations via PTPN11

Next, I fitted the PTPN11-KO data using the network structure that was adjusted for the parental cell line. Overall, the SHP2 KO cell line seemed less responsive, and it is noteworthy that the inhibitions alone led to a reduction of phosphorylation throughout the network, which was not apparent in the parental cell line (Figure 3.2).

The model using the adjusted parental topology residual of ∼44 was compatible with the 58 residual degrees of freedom. After running a profile likelihood analysis on the SHP2 KO model, I compared it to the parental model for significantly altered parameters (Figure 3.5a). As expected from isogenic cell lines, the parameters did not differ for most paths or the MEK inhibitor parameter. Only four parameters were

significantly different between those two cell lines which correspond to the three paths between the receptors and MAPK signalling and the ERK→ EGFR feedback. These parameters were suppressed in the SHP2 KO compared to the parental. This is in accordance with the known role of SHP2 as an adaptor mediating receptor activation to the RAF/MEK/ERK pathway. The model comparison also highlights that AKT activation by the ligands occurs both with and without SHP2, suggesting that SHP2 is not necessary for the signal transduction between the receptors and PI3K. It does, however, illustrate that SHP2 is implicated in activation of the PI3K as the activation of AKT by EGF is significantly weaker in the SHP2 KO, and a non significant trend can be observed for NRG1 and HGF stimulation suggesting that different receptors rely on SHP2 to varying degrees. Interestingly, the ERK→EGFR→AKT feedback is fully functional in the SHP2 KO, which indicates that ERK regulation of EGFR and other compensatory activations of the PI3K pathway do not depend on SHP2.

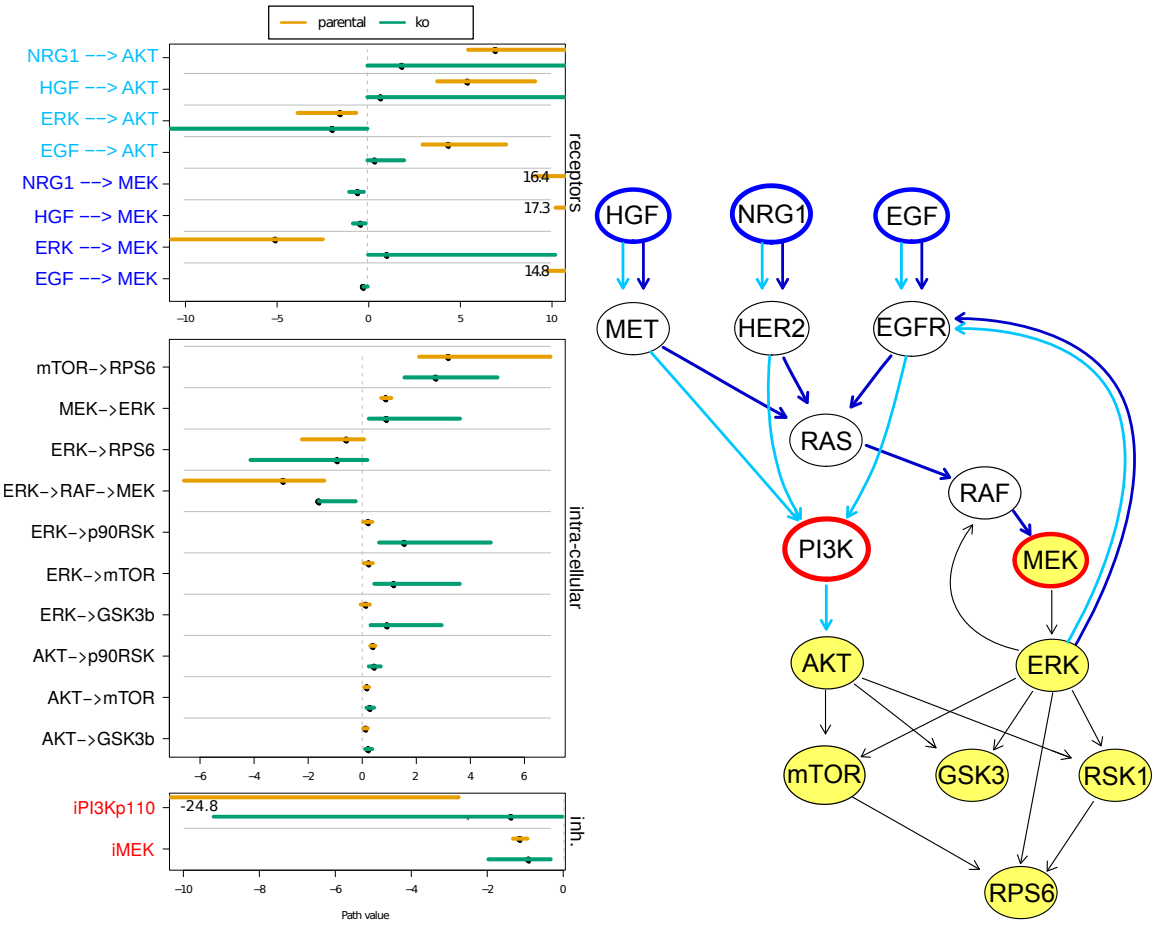

(a) (b)

Figure 3.5: (a) Parameter fitted values (black dot) and confidence interval (colored bars) for the parental Widr and SHP2-KO cell lines in orange and green respectively. Parameters are separated by the class of the path they describe. (b) Graphical representation of the paths significantly different between the parental Widr and the SHP-KO. The paths to AKT and MEK are highlighted in cyan and blue respectively. Inhibited nodes and corresponding parameters are highlighted in red.

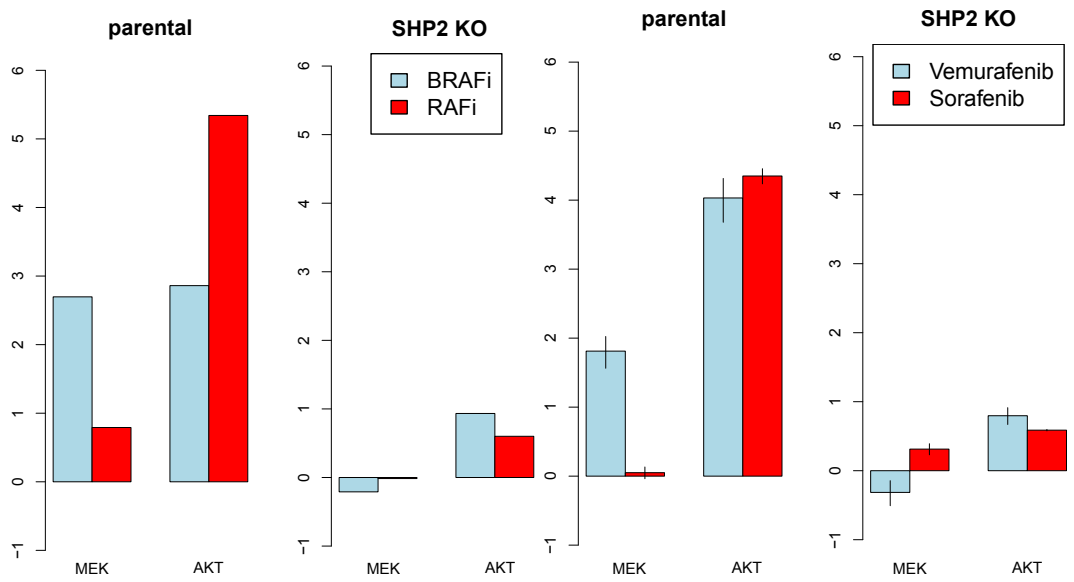

(a) STASNet simulation (b) Experimental measurements

Figure 3.6: Log2-fold-change to EGF+DMSO of pMEK^{S217,S222} and pAKT^{S473} after treatement by EGF with Vemurafenib (BRAF^{V600E} inhibitor) or with Sorafenib (pan-RAF inhibitor).

3.5 SHP2 KO highlights the importance of the receptor feedbacks

Given the differences between the parental and SHP2 KO Widr cell lines, they are likely to exhibit different reponses to inhibitors. In particular, there exist two classes of RAF inhibitors that could act differently in those cell lines depending on their isoform specificity. Inhibitors such as Vemurafenib target specifically mutant BRAF (BRAF^{V600E}, (Bollag et al., 2010)) but might activate other RAF isoforms, whereas inhibitors such as Sorafenib are pan-RAF inhibitors that inhibit all RAF isoforms (Wilhelm et al., 2004). Since receptor feedback plays an important role in inhibitor sensitivity (Friday et al., 2008; Poulikakos et al., 2010; Lito et al., 2012; Corcoran et al., 2012; Prahallad et al., 2012; Sun et al., 2014; Cseh et al., 2014), I hypothesized based on the model observations that those inhibitors would have different effects in the SHP2 KO. In order to simulate different RAF inhibition mechanisms, I augmented the models by including a BRAF^{V600E} node that activates MEK and has no upstream signal, since this mutation desensitizes BRAF from upstream and feedback signals (Friday et al., 2008) (Figure 3.6). Moreover, since RAF is neither stimulated nor inhibited in our initial perturbations, the choice of the inhibitor parameter was free and set to 1 for both classes. This makes our prediction qualitative rather than quantitative as the exact effect of the inhibitions is only suggested.

The aforementioned resistance mechanism to RAF inhibition is mediated via the reactivation of the RAF→MEK→ERK axis, as well as by the activation of the PI3K→AKT axis via the loss of the EGFR feedback. To assess the extent of this

resistance, I simulated the effect of EGF stimulation with RAF inhibition on MEK and AKT phosphorylation. The simulation predicted qualitative differences between the $BRAF^{V600E}$ and pan-RAF inhibitor in the parental Widr cell line (Figure 3.6a). While EGF stimulation activated AKT for both inhibitors, the MEK phosphorylation was preserved only after treatment with the $BRAF^{V600E}$ specific inhibitor. However, the upregulation of MEK phosphorylation is completely blocked in the SHP2 KO, while the increase in AKT phosphorylation is strongly attenuated in comparison to the changes predicted for the parental line (Figure 3.6a). I then sought to confirm the model prediction by measuring AKT and MEK phosphorylation after treating the cells with either Vemurafenib ($BRAF^{V600E}$ inhibitor) or Sorafenib (pan-RAF inhibitor) for 90 minutes and a 30 minutes EGF stimulation (Figure 3.6b). These data confirmed our model predictions.

3.6 Discussion

In this chapter, I used STASNet to model the effect of a SHP2-KO on the PI3K and MAPK signalling pathways. SHP2 is a well-studied protein and I could recover the known role of SHP2 in mediating MAPK signalling by comparing the parameters of the STASNet model for the SHP2-KO cell line to the parameters of the parental cell line. Additionally, the model helped clarify the role of SHP2 in RTK-mediated activation of PI3K/AKT signalling in colon cancer. The corresponding parameters from EGFR, HER2 or Met showed no quantitative difference in the PI3K branch between parental and SHP2-KO, which indicated that PI3K is activated independently of SHP2.

SHP2 has been implicated in the resistance of BRAF mutant colorectal carcinoma, where the mediation of the feedback activation of EGFR leads to the reactivation of MAPK signalling after treatment with BRAF inhibitors (Prahallad et al., 2015). The model confirms the major role of SHP2 in re-activation of MAPK signalling and predicts, with subsequent experimental confirmation, that MEK phosphorylation cannot be recovered in SHP2 knockouts after RAF inhibition. The model also helped investigate the use of a pan-RAF inhibitor to prevent the activation of the MAPK pathway in the parental cell line as an alternative treatment option. As predicted by the model, this option can reduce the parallel activation of the PI3K pathway in the SHP2-KO cell line. These results highlight that STASNet can be used to explore therapeutic vulnerabilities.

Chapter 4

Drug resistance and signalling networks in a panel of neuroblastoma cell lines

In the previous chapter, it was shown that STASNet can be used to investigate disparities in signalling between cell lines. In a next step, I set out to explore unexplored questions regarding signalling. The TerminateNB consortium aimed at characterising neuroblastoma using all omics technologies available to propose news treatment against this aggressive childhood tumor. In this consortium, I contributed by exploring drug sensitivity to targeted therapies in neuroblastoma. *Collaborators in this consortium generated whole proteomics, phosphoproteomics, whole exome sequencing (WES) and RNA sequencing (RNAseq) data.* I analysed these data and generated perturbation and drug sensitivity data for multiple neuroblastoma cell lines. *This work was published in Dorel et al. (2021).*

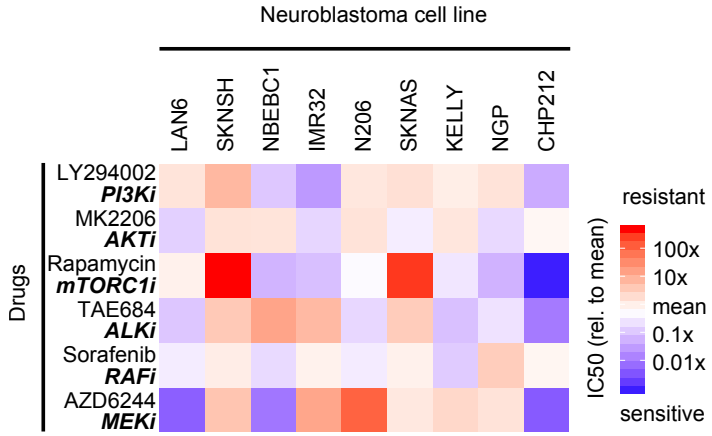

Figure 4.1: Relative IC50 of 9 neuroblastoma cell lines to 6 drugs. Values are log10(IC50) measurements relative to the mean across all cell lines. n=3.

4.1 Drug sensitivity in a panel of very-high-risk neuroblastoma cell lines

I measured the sensitivity to 6 inhibitors targeting the MAPK and PI3K pathways in panel of 9 neuroblastoma cell lines (CHP212, LAN6, NBEBC1, SKNAS, NGP, SKNSH, N206, KELLY and IMR32) (Figure 4.1). The MEK inhibitor AZD6244 and the mTORC1 inhibitor Rapamycin had the most variable effects on the cell lines. AZD6244 was the drug with the most variable sensitivity profile, with six cell lines displaying resistance, i.e with an IC50 value higher than 10μM, and the other 3 being very sensitive, with IC50 values ranging from 10 to 100 nM, Figure 7.1). These IC50 measurements for AZD6244 correlated largely with published drug sensitivity data for the MEK inhibitior Binimetinib (Woodfield et al., 2016). Similarly, Rapamycin measurements were mainly in agreement with previously published data, with the notable exception of SKNAS, which I found to be resistant to Rapamycin while there are reports of sensitivity to sub-nanomolar concentration of the Rapamycin analog Everolimus (Kiessling et al., 2016).

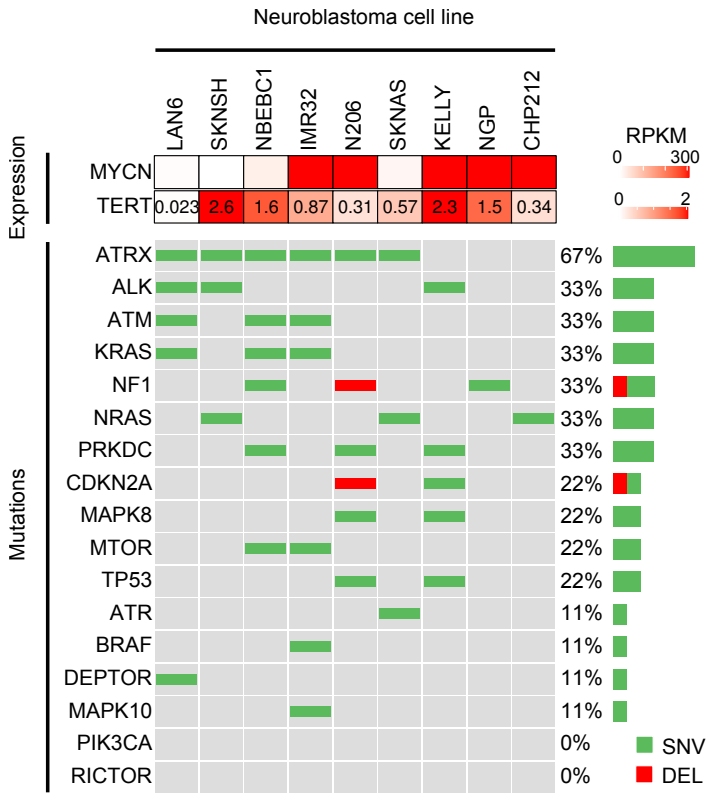

Figure 4.2: (top) Expression of MYCN and TERT mRNA and (bottom) oncoprint of 9 neuroblastoma cell lines for RAS, TP53 and PI3K pathways genes.

The cell line panel analysed here display heterogeneity when considering mutations of individual genes, yet reflects the overall frequency of mutations in high risk tumors (Ackermann et al., 2018) (Figure 4.2). Indeed, all cell lines harbour a mutation in

Table 4.1: Detailed mutations for RAS, TP53 and PI3K pathway genes in 9 neuroblastoma cell lines

Cell line	**Protein change**
CHP212	$NRAS^{Q61K}$
IMR32	$MTOR^{F1888V}$, $MTOR^{R1482C}$, $MAPK10^{I124M}$, $BRAF^{K507E}$, ATM^{I1547M}, $KRAS^{V181M}$, $ATRX^{E1456G}$
KELLY	ALK^{F1174L}, $PRKDC^{V1452L}$, $CDKN2A^{A68T}$, $MAPK8^{A282D}$, $TP53^{P177T}$
LAN6	ALK^{D1091N}, $DEPTOR^{Q239K}$, ATM^{S2218R}, $KRAS^{G12C}$, $ATRX^{E929Q}$
N206	$PRKDC^{V1452L}$, $CDKN2A^{A76Pfs*70}$, $MAPK8^{A282D}$, $TP53^{P177T}$, $NF1^{N664*}$, $ATRX^{E929Q}$, $ATRX^{R907Q}$, $ATRX^{N755K}$
NBEBC1	$MTOR^{W1633*}$, $PRKDC^{C2857R}$, ATM^{C1674Y}, ATM^{T1743K}, ATM^{R2419*}, $KRAS^{G12D}$, $NF1^{P464Q}$, $ATRX^{E2360G}$, $ATRX^{K2359E}$, $ATRX^{G2018W}$, $ATRX^{D2010E}$, $ATRX^{Q1663R}$, $ATRX^{E1460K}$, $ATRX^{E929Q}$, $ATRX^{N862K}$
NGP	$NF1^{E1423*}$
SKNAS	$NRAS^{Q61K}$, ATR^{V2158F}, $ATRX^{E929Q}$
SKNSH	$NRAS^{Q61K}$, ALK^{F1174L}, $ATRX^{E929Q}$

either ALK, BRAF, NF1, NRAS or KRAS, all of which activate the MAPK pathway. IMR32 surprisingly had two mutations in the pathway, with a KRAS mutation probably responsible for MAPK activation and an atypical BRAF mutation being a neutral mutation (Table 4.1). Moreover, p53 pathway genes are mutated in most cell lines, either on ATM, ATR, ATRX, CDKN2A, PRKDC or TP53 itself. Finally, with the exception of LAN6, which to have an alternative lengthening of telomeres (ALT) (Peifer et al., 2015), all of the cell lines express TERT despite only five of the nine cell lines expressing MYCN.

The attempt to correlate inhibitor sensitivity and mutation status yielded no notable correlation for AZD6244 and Rapamycin (Figure 4.3a). Drug sensitivity did not correlate significantly with expression data neither, with an adjusted p-value > 0.95 for the 1000 most variable genes and an ajusted p-value > 0.94 for genes in the Gene Ontology (GO) biological process "signal transduction" (Figure Appendix.9). Looking at specific association, based on the claim of previous reports showing that NF1 expression was linked to sensitivity to MEK inhibitors (Woodfield et al., 2016), only resulted in a weak and non-significant association ($R^2 = 0.34, p = 0.10$, Figure 4.3b), though with a similar trend described previously.

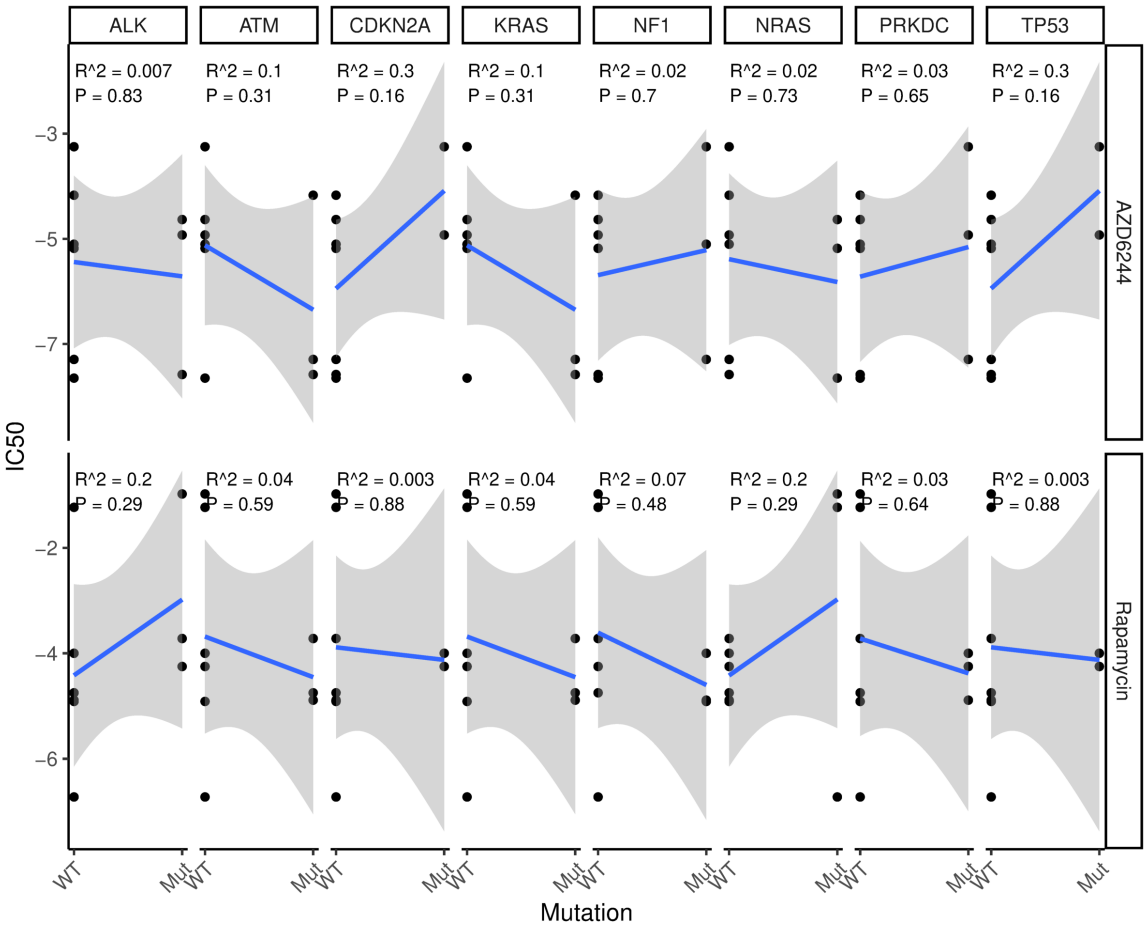

(a)

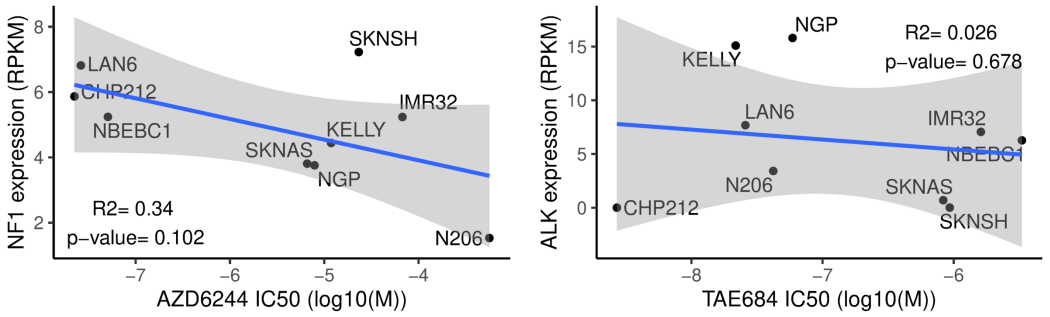

(b)

Figure 4.3: (a) Correlation between AZD6244 and Rapamycin IC50s and mutation status for RAS/P53 pathway genes mutated in 30% to 70% of our panel and (b) correlation between IC50 and gene expression of selected drug-mRNA pairs based on existing literature.

4.2 Using perturbation-response data to investigate the signalling state of cells

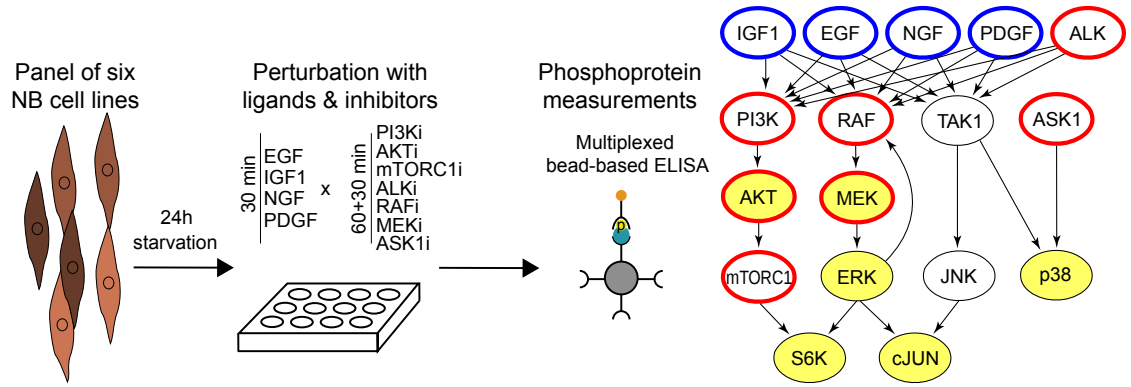

(a) Outline of the perturbation experiments. (b) Graphical representation.

Figure 4.4: Description of the perturbation experiment. (a) A panel of cell lines was treated with growth factors and small molecule inhibitors, and the resulting effect on selected phosphoproteins was measured using multiplexed bead-based ELISAs. (b) Graphical representation of the perturbations; blue and red contour highlight ligand stimulation and kinase inhibition respectively; yellow filling shows measured phosphoproteins.

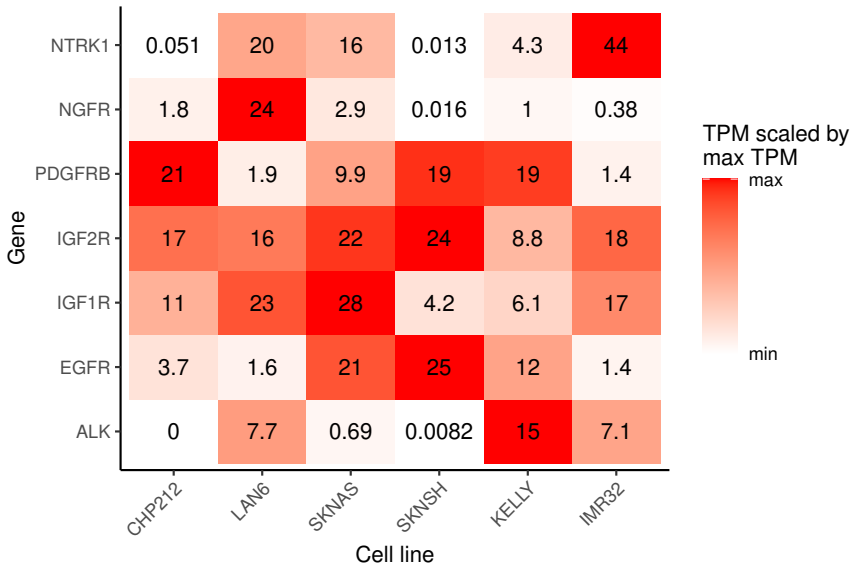

Figure 4.5: Transcript per million reads (TPM) for various receptors in the neuroblastoma cell lines panel. Colors are TPM relative to max TPM across cell lines.

In order to understand the mechanisms underlying resistance to MEK inhibition by AZD6244, I selected six neuroblastoma cell lines covering the whole sensitivity spectrum for perturbation-response analysis. The perturbation experiment consisted of stimulation with growth factors for 30 minutes with growth factors and inhibition with small molecule inhibitors for 90 minutes. The ligands used were selected based on the expression of the corresponding receptors in the cell lines. The heterogeneity

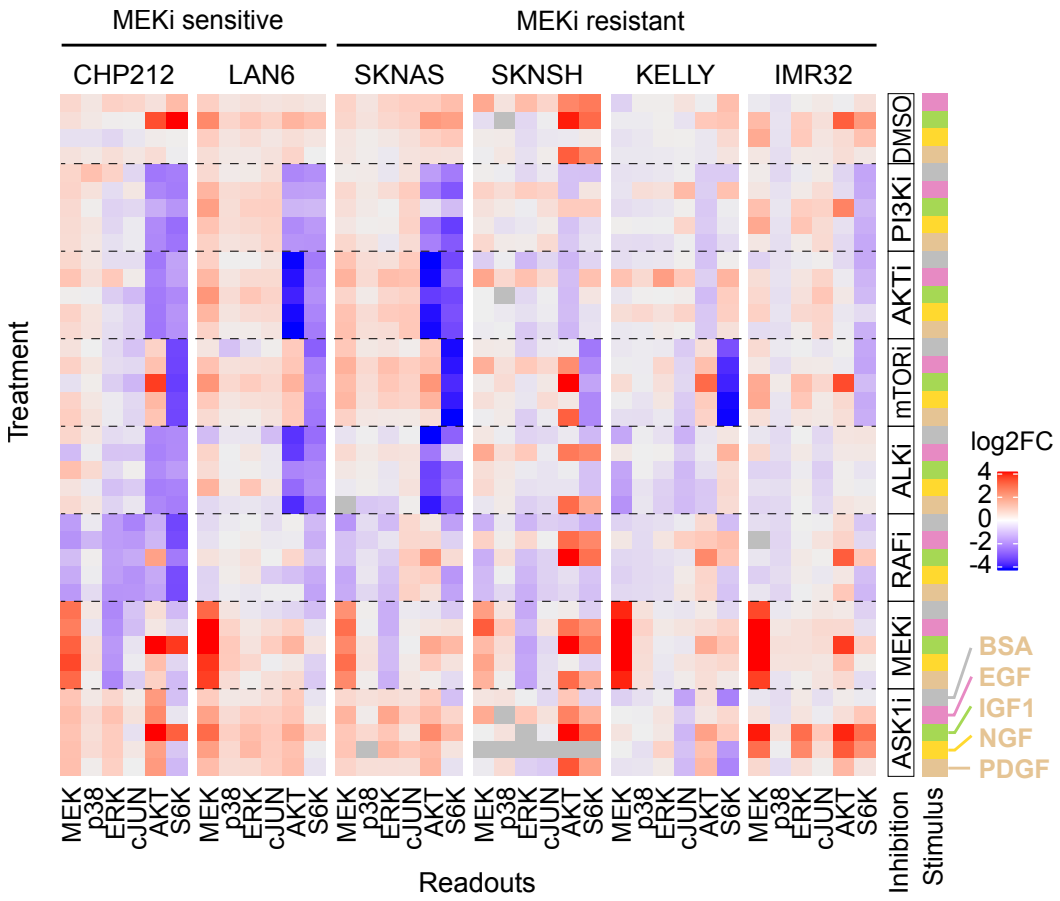

Figure 4.6: Measurements of 6 phosphoproteins in 6 neuroblastoma cell lines in response to combinations of 4 ligands or BSA control with 7 inhibitors or DMSO control. Each measurement is normalised by the BSA+DMSO control of the corresponding cell line and represents at least 2 biological replicates. Readouts are phosphoproteins p-MEK1$^{S217/S221}$, p-p38$^{T180/Y182}$, p-ERK1$^{T202/Y204}$, p-cJUN^{S63}, p-AKT^{S473} and p-S6K^{T389}. Greyed entries are missing data due to insufficient volume or bead count.

of receptor expression displayed in the cell line panel required the use of four distinct ligands in total to ensure that each cell line would be robustly stimulated by at least two ligands (Figure 4.5). The inhibitors were chosen to target key kinases of the pathway upstream of the phosphosites measured as follow: an inhibitor of the p38/cJUN MAP3K ASK1 (GS4997), an AKT inhibitor (MK2206), an mTOR-complex 1 inhibitor (Rapamycin), a clinicaly used MEK inhibitor (AZD6244/Selumetinib), a clinically used Raf/cKIT inhibitor (Sorafenib), an ALK inhibitor (TAE684), and a highly specific PI3K inhibitor (GDC0941). The activity of various signalling pathways was monitored at the phospho-proteins level using the Bio-Plex system (Figure 4.4a). I designed a plex to measure six phosphoproteins from the MAPK and PI3K pathways: p-MEK$^{S217/S221}$, p-p38$^{T180/Y182}$, p-ERK$^{T202/Y204}$, p-AKT^{S473}, p-S6K^{T389} and p-cJUN^{S63}. The phosphorylation of these residues are reliable proxies for the activity of the corresponding kinase (MEK, p38, ERK, AKT and S6K) or the transcription factor cJUN (Figure 4.4b). Overall, 240 data points were measured in duplicate for each cell line (Figure 4.6).

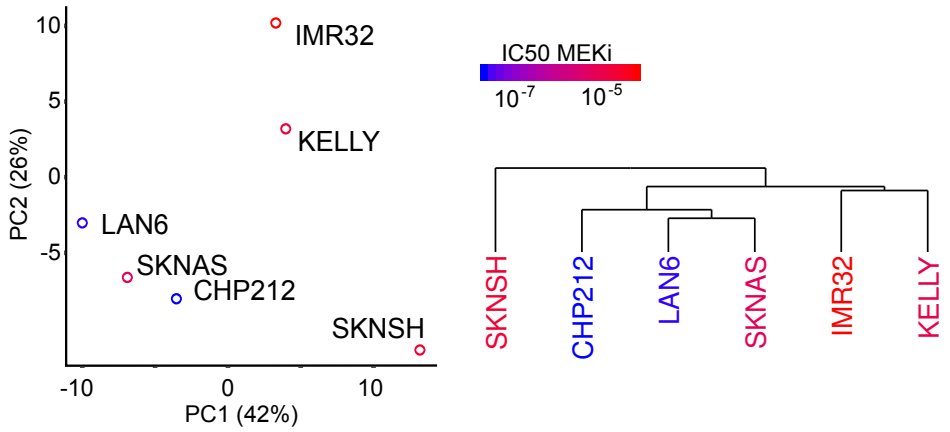

Figure 4.7: Unsupervised classification from the plex data: (LEFT) First two components of a principal component analysis and (RIGHT) hierarchical clustering. Colour scale corresponds to the IC50 for AZD6244 treatment (see also Figure 4.1).

The response to perturbation show similar patterns across different cell lines but important quantitative differences. For instance, S6K phosphorylation was strongly down-regulated by mTORC1 inhibition in all cell lines but the response to inhibition of PI3K and AKT, both kinases upstream of mTORC1, was very cell line specific, ranging from no effect to a 6-fold decrease. Similarly, MEK inhibition led to an increase in MEK phosphorylation in all cell lines but with different intensity, and inhibition of ALK downregulated phospho-MEK in some cell lines (LAN6, KELLY) but not others (CHP212, SKNAS, SKNSH, IMR32). I first performed a principal component analysis on the perturbation dataset to get further insights. This PCA highlighted three groups of cell lines, with 86% of the variance contained in the first three components (Figure 4.7, Figure Appendix.7, Table Appendix.29). The first component (42% of variance) contains the effect of Sorafenib and TAE684 on p-AKT^{S473} and p-S6K^{T389}. The second component (26% of variance) mainly separates IMR32 and KELLY from the others based on the response of p-MEK$^{S217/S221}$ to MEK inhibition. The third component (18% of variance) also separates IMR32 and KELLY, based on the effects of IGF1, GS4997 and Rapamycin on AKT and S6K activation. Hierarchical clustering gave similar results to the PCA, where SKNSH clustered separately, which highlights the very atypical response of this cell line (Figure 4.7). Detailed investigation showed that SKNSH had a very strong response to all ligands, and especially to PDGF, to which the other cell lines were mostly insensitive. This atypical status of SKNSH is also discernable in the mRNA expression, where it is clearly separated from the other cell lines in a PCA with the most variable genes (Figure Appendix.8). Interestingly, CHP212 also appears atypical from the mRNA expression, but it's response to perturbation is quite similar to the one of SKNSH and LAN6. Overall, multivariate analysis by PCA or hierarchical clustering did not separate the cells into groups matching the sensitivity to AZD6244.

4.3 Signalling models highlight differential feedback regulation of MEK

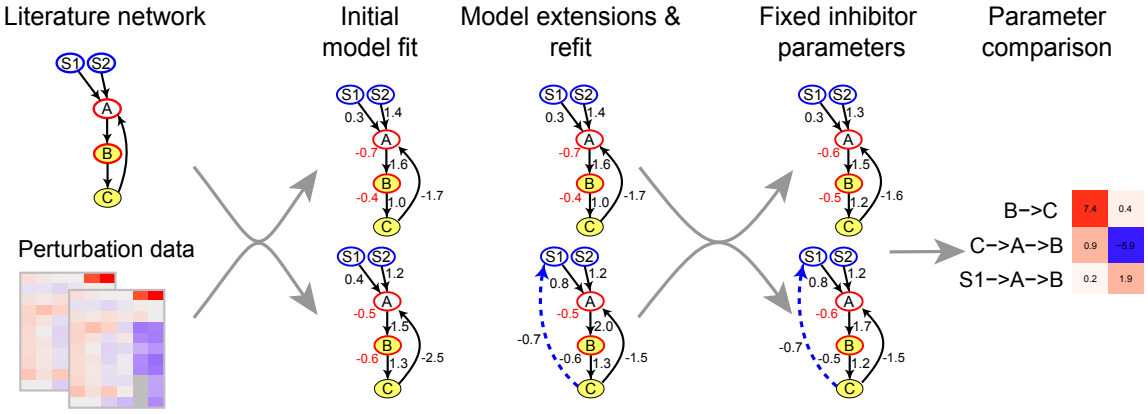

Figure 4.8: Starting from a literature-derived network, an "Initial model fit" is performed for each cell line then extended by successive "Model extensions". Those models with different network structures are then harmonised by using a "Fixed inhibitor parameters" concensus value which enables a direct "Parameter comparison".

In order to understand how the inhibitors where differentially affecting the cells, I used the perturbation data to parametrise cell line specific signalling models using STASNet (section 2.4). As the initial input network for STASNet, I used the MAPK and PI3K/AKT signalling pathway as summarised in KEGG (`https://www.genome.jp/kegg/pathway/hsa/hsa04010.html` and `https://www.genome.jp/kegg-bin/show_pathway?hsa04151`) with intermediate nodes suppressed, the well documented ERK→RAF feedback added and all receptors corresponding to RTK connected with

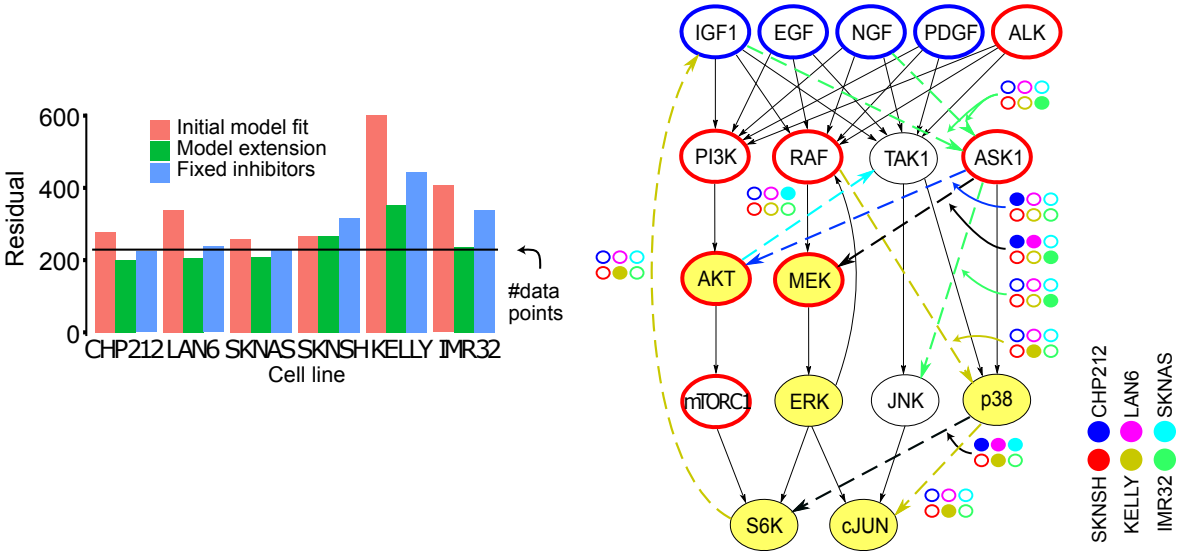

Figure 4.9: Model residuals before and after model extension and harmonisation using fixed inhibitor parameters. and cell-line-specific network extensions (dashed arrows) relative to the literature network. The extended link colour was matched to cell line colour, if present only a particular cell line model, and black otherwise.

every nodes of the next signalling layer (Figure 4.8 first step, Figure 4.4b). The model fit quality was evaluated according to two criteria: the sum of weighted squared residuals should be similar to the number of data points/degrees of freedom and the distribution of residuals for each datapoint should be normally distributed. These initial models using the canonical literature network yielded good fits for CHP212, SKNAS and SKNSH but not for LAN6, KELLY or IMR32 (Figure 4.9 "Initial model fit", Figure Appendix.4).

In order to improve the fit, I performed successive extensions for each cell line independently using the likelihood ratio test framework implemented in STASNet. In this procedure, a link extension is deemed to provide a significant improvement to the fit if the decrease in residuals provided by the link is greater than expected from a χ^2, with the number of degrees of freedom equal to the rank increase (number of independant parameters) induced by the link. This extension procedure found significant improvements for all cell lines, with the most additions for KELLY (4 new links) and IMR32 (3 new links). Only two network extensions (ASK1→MEK and p38→S6K) were significant in more than one cell line. Both correspond to an effect of the ASK1-annotated inhibitor GS4997 on the MEK/ERK pathway and S6K, and have negative strength, which suggests that an antagonism between the p38 MAPK and the MEK/ERK MAPK pathway exists in neuroblastoma cell lines. Such negative crosstalk between these pathways also exists in other cell lines (Finch et al., 2012). The resulting models fitted the data well for all cell lines except KELLY (Figure 4.9 "Model extension", Figure Appendix.5), where further analysis revealed that the ERK readout gave inconsistent results in this cell line.

Because of the inhibition parameters, the paths from inhibited nodes are often structurally non-identifiable, as the three parameters corresponding to upstream path, downstream path and inhibition intensity always appear together in the equations if there is no basal activity. Since the best fit values for the inhibition parameters were similar in all cell lines, I harmonized each inhibitor parameter to the mean value between all cell lines. This consensus fit value for the inhibition parameter is coherent with the fact that the same inhibitor concentration was used in all cell lines. This "fixed inhibitors" procedure resulted in models that stayed in satisfying agreement with the data and provided identifiable path parameters, which allowed for direct comparison between cell lines (Figure 4.9).

I first tried to interpret the strong heterogeneity in ligand-induced pathway activation (Figure 4.10). Only a few receptor expression differences matched the corresponding ligand effect. The response to NGF correlated with the expression of the NTRK1 receptor but not that of the NGFR, suggesting that NTRK1 was responsible for the effect of NGF in these cell lines.

EGFR expression correlated to the activation of the AKT and cJUN pathways by EGF but not of the MEK path, which could be explained by the more direct activation

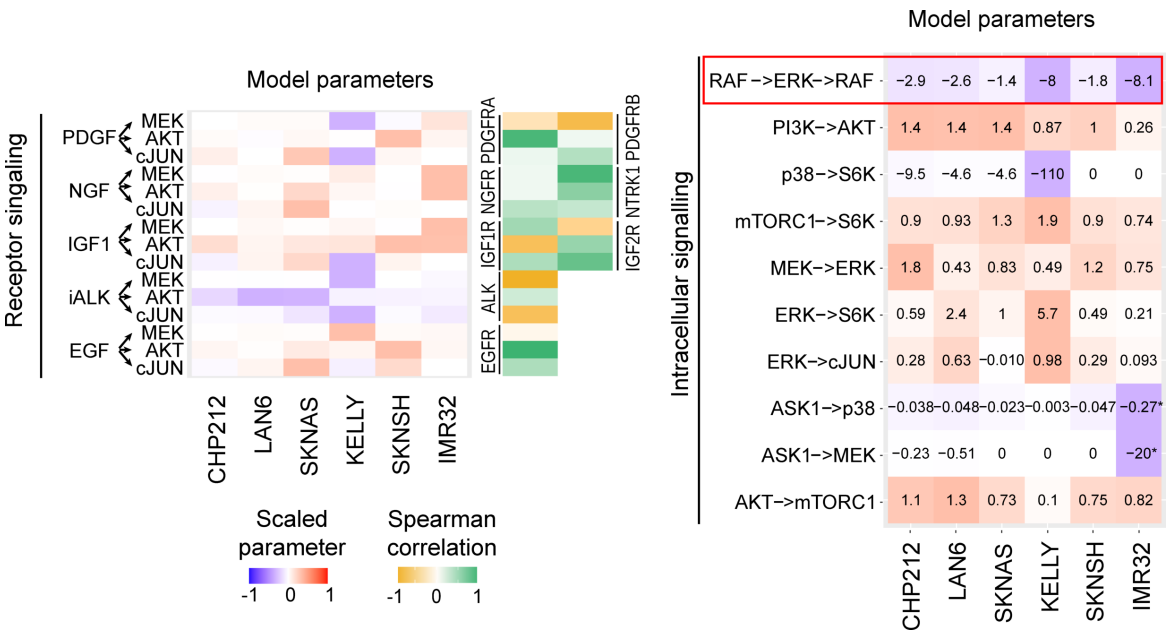

Figure 4.10: (left) Fitted paths and correlation of the receptor-originating paths with the corresponding receptors expression. (right) Model paths between non-receptor perturbed nodes and measured nodes for routes present in at least 2 cell lines. Cells are ordered from left to right from most sensitive to most resistant to the MEK inhibitor AZD6244. Due to the absence of ASK1 basal activity in IMR32 ASK1→p38 and ASK1→MEK represent in this cell line NGF→ASK1→p38 and NGF→ASK1→MEK respectively. The colours correspond to the value of the path scaled by the maximum absolute value of that path between all cell lines.

mechanism of PI3K by the EGFR (chapter 2), while multiple adaptor proteins mediate the activation of the MAPK pathway. Indeed, the expression of GAB2 and SRC is very different between the cell lines and could explain the strong activation of IMR32 and LAN6 by EGF, similar to SKNAS and SKNSH, despite their lower EGFR expression (Figure 4.10, Figure 4.11). Another potential cause for the attenuated activation of MEK/ERK by the receptors is a downstream mutations that already activates the pathway, as the parameter values of the routes from PDGF, EGF, NGF and IGF into MAPK signalling are lower in NRAS mutant cell lines CHP212, SKNAS and SKNSH (Figure 4.10). Conversely, these cell line models display a slightly more inducible PI3K pathway. This observation is in agreement with a recent comparative study of G12V-mutated RAS isoforms in colorectal SW48 cells, where the NRAS mutated cell line showed a weaker coupling of receptors to MEK and a stronger coupling to PI3K than in the parental cell line (Hood et al., 2019). This would suggest that an activation of the MEK/ERK pathway is relayed predominantly by NRAS while the PI3K pathway activation is mediated by other proteins (Yang et al., 2012).

Similarly, the effect of IGF1 on AKT was correlated with the expression of IGF2R, which captures IGF1 and IGF2 without transducing its signal (O'Dell and Day, 1998; Oates et al., 1998; Ghosh et al., 2003), more than with the expression of IGF1R, suggesting that other factors influenced transduction of the IGF1 signal. Overall,

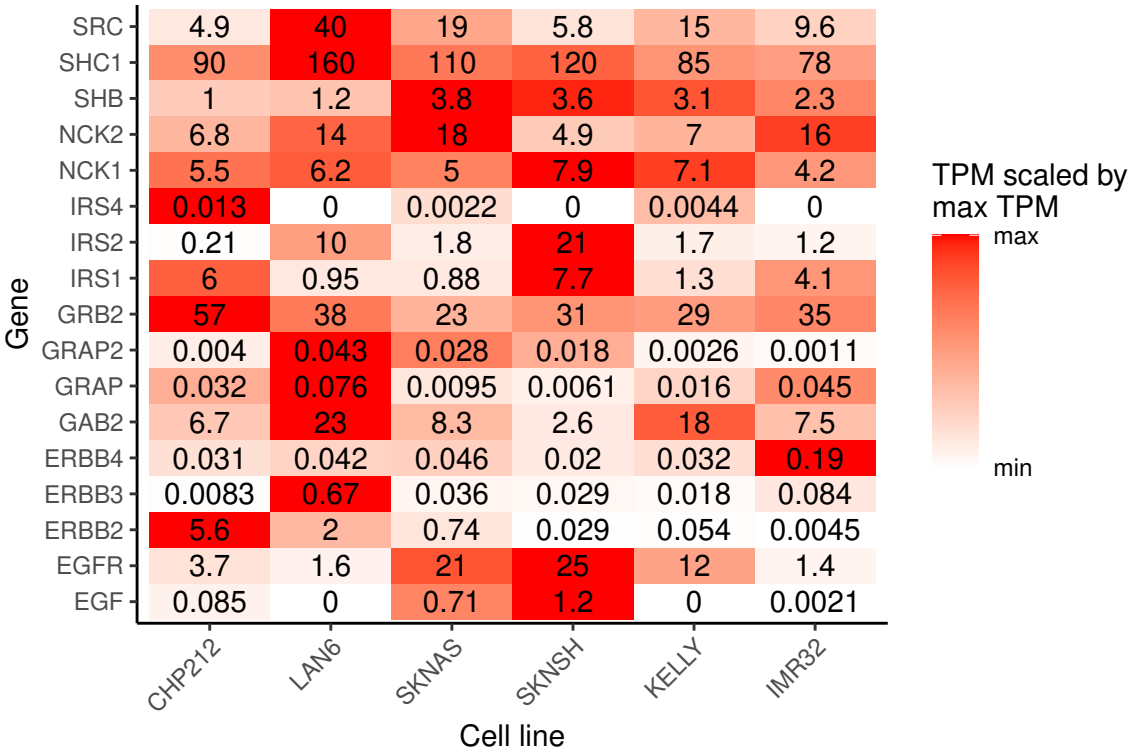

Figure 4.11: Transcript per million reads (TPM) of adaptors and ERRB receptor family genes.

this confirms that expression of receptors and adaptors as well as pathway alterations shape the response of signalling networks to stimulation (Zhang and Samelson, 2000; Bolanos-Garcia, 2005; Cabodi et al., 2010).

Intra-cellular kinase paths show less variability between cell lines, with most paths exhibiting similar values between cell lines (Figure 4.10). The negative feedback in MAPK signalling from ERK to RAF is the most striking exception, exhibiting 3 to 4 times stronger magnitude in KELLY and IMR32 and resulting in a similarly higher phosphorylation level of p-MEK$^{S221/S221}$ after MEK inhibition in these cell lines (Figure 4.12). A strong RAF-mediated feedback is a known resistance mechanism against MEK inhibitors (Friday et al., 2008; Fritsche-Guenther et al., 2011), where relieve of inhibition of upstream components post inhibition can partially reactivate signalling. Since KELLY and IMR32 are highly resistant to AZD6244, this suggests that resistance to MEK inhibition could be mediated by a differential regulation of this feedback.

In the KELLY cell line, the extension procedure added a negative feedback from S6K to IGFR. MAPK signalling is also controlled by receptor-mediated feedbacks which have been reported to mediate drug resistance, most notably to MEK inhibition via reactivation of the MAPK pathway itself and other parallel pathways, by numerous studies (Corcoran et al., 2012; Klinger et al., 2013; Klinger and Blüthgen, 2014; Rozengurt et al., 2014; Lake et al., 2016). Thus, this feedback could explain the

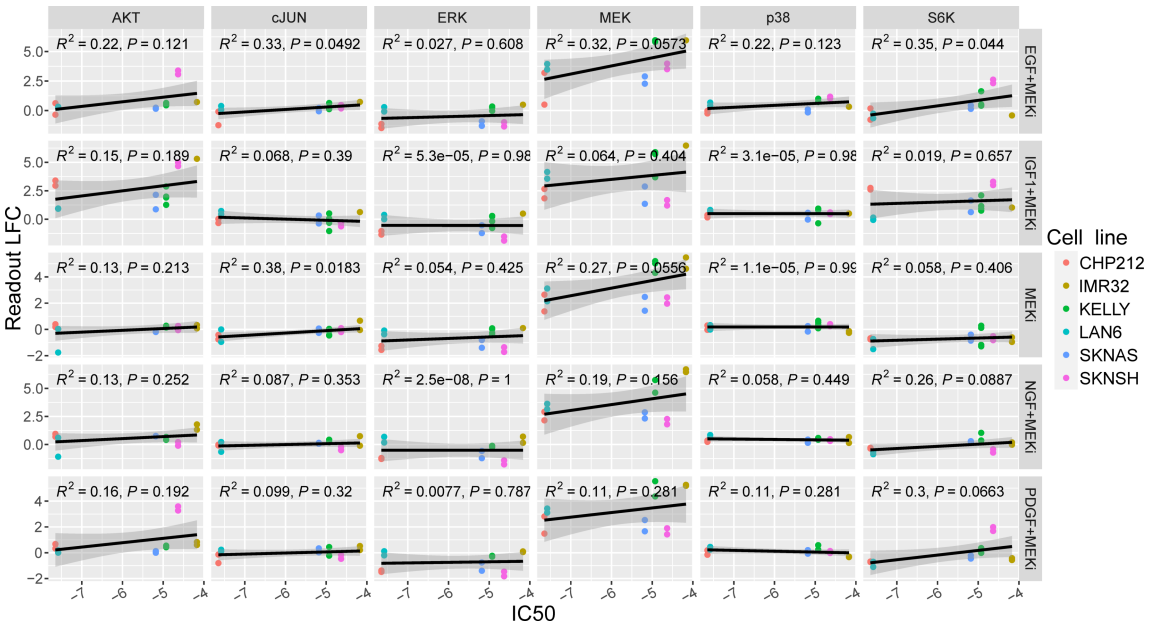

Figure 4.12: AZD6244 IC50 versus responses to perturbations including AZD6244. R^2 and p.value correspond to the linear model shown in black. Points are independent replicates, n=2.

strong upregulation of pMEK following AZD6244 treatment in KELLY (Figure 4.6 and subsection B.6).

In summary, the signalling parameters derived from the perturbation data by our models show that cell lines diverge in receptor expression and feedback regulation, with strong multi-layered feedbacks for some of the resistant cell lines.

4.4 Resistant cell lines display different wiring

We hypothesized that the different relative strength of a multi-layered negative feedback could be the cause of AZD6244 resistance. To test this, I also measured the pMEK response to AZD6244 of N206, the most resistant cell line of the panel. N206 also showed a strong feedback response to AZD6244 (Figure 4.13).

To dissect the feedbacks wiring in more details, I generated perturbation data restricted to the MAPK pathways for those cell lines with a strong feedback response to MEK inhibition: KELLY, IMR32 and N206. I used IGF1 and EGF/NGF stimulations to activate the signalling pathways, blocked MAPK signalling with MEK and RAF inhibitors, and measured the same six phosphoproteins as described earlier (Figure 4.14a, section 4.2).

I used these data to parameterise smaller MRA models with or without S6K→IGF1 feedback (Figure 4.14c). The models which included the IGF receptor-feedback were significantly better for N206 and KELLY ($\chi^2 p < 0.05$) but not for IMR32 (Figure 4.14b). The feedback quantification highlighted interesting variations between KELLY and N206, with the S6K→IGF1→RAF→MEK being stronger in the N206

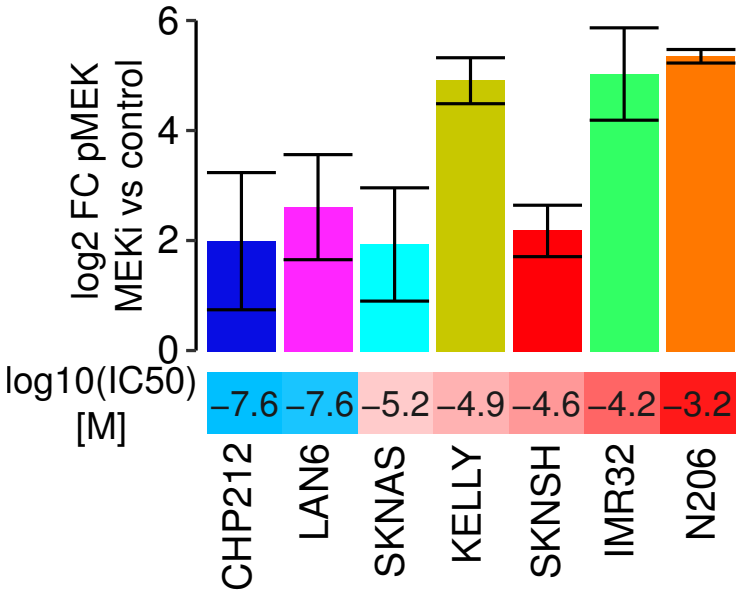

Figure 4.13: pMEK log2-fold change to DMSO after AZD6244 and IC50 to AZD6244 of 7 neuroblastoma cell lines. 95% confidence interval is shown.

model than the ERK→RAF→MEK feedback but the contrary being true in KELLY. This shows that multilayered feedback regulations are modulated differentially between cell lines.

4.5 Breaking feedback-mediated resistance with vertical inhibition

One possible strategy to overcome a multi-layered feedback is to use vertical inhibition, where inhibition of the upstream nodes reactivated by the feedback prevents pathway reactivation (Ricciardi et al., 2012; Rebecca et al., 2014; Woo et al., 2017; Ryan et al., 2020). With the encouraging predictions from the model, I then quantified the growth reduction of IMR32, KELLY and N206 after inhibiting with different dose combinations of inhibitors against MEK (AZD6244), IGFR (AEW541) and RAF (LY300912) (Figure 4.15). In agreement with our model predictions of strong IGFR-mediated feedback in N206 (Figure 4.14b), there was a strong synergistic effect of the combination of MEK and IGFR inhibitions on growth in N206 (Figure 4.15). Conversely, there was little synergy in KELLY, contrary to what the model predicted, and IGFR inhibition had almost no effect on IMR32 growth (Figure 4.15). Even though the model suggested the combination of MEK and RAF inhibition to overcome the strong ERK→RAF feedback in all three cell lines, a synergistic effect could only be observed for N206 and KELLY, whereas IMR32 remained resistant. IMR32 continued to proliferate despite relatively high concentrations of both inhibitors (Figure 4.15). One possible explanation for this observed resistance in IMR32 might be the fact that the dual inhibition by MEKi and RAFi was not effectively inhibiting MEK and

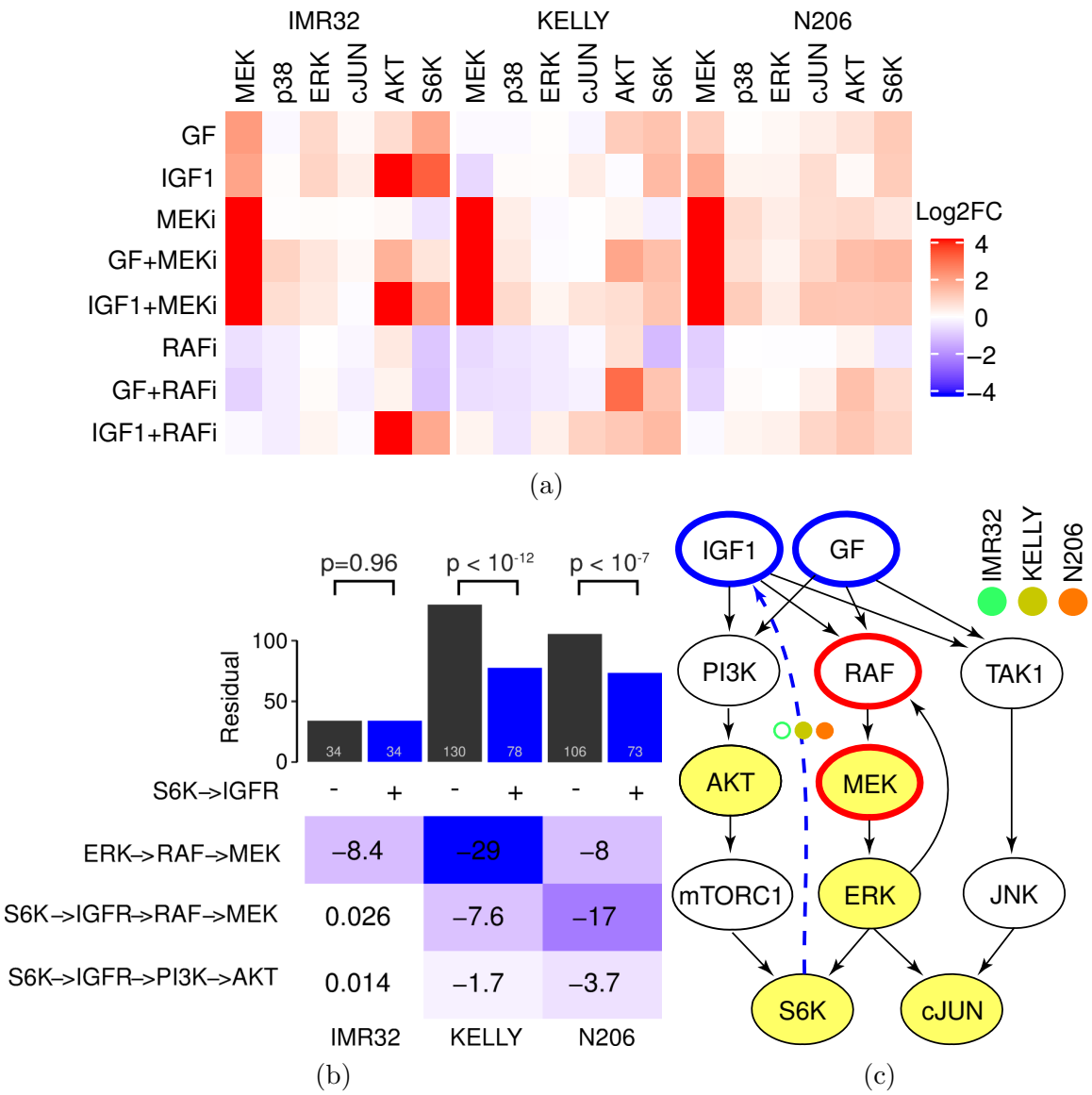

Figure 4.14: Resistant cell lines display different relative feedback strength. (a) Bio-Plex measurements of IMR32, KELLY and N206 response to AZD6244 (MEKi) and Sorafenib (RAFi) under IGF1 or GF (NGF in IMR32, EGF in N206 and KELLY) stimlation. Values are log2-fold relative to PBS+DMSO control. (b) Residual comparison of models with (black) and without (blue) S6K→IGFR feedback and feedback parameters in the model including S6K→IGFR. p-values were computed using a χ^2 test with 1-df. (c) Network representation of the models. Yellow backgrounds indicate measured nodes, red outlines inhibited nodes and blue outlines stimulated nodes. S6K→IGFR is represented as a dotted line with full circle annotation indicating that the addition significantly improved the model.

ERK. To rule out this possibility, I measured the response of KELLY and IMR32 to combinations of AZD6244 (MEKi), SCH772984 (ERKi) and LY300912 (RAFi). Based on the model simulations, the combination of MEK and RAF inhibition was predicted to suppress MAPK signalling much stronger than MEK inhibitor alone or in combination with an ERK inhibitor, with a suppressive effect predicted to be more profound in IMR32 than in KELLY (Figure 4.16). The measurement of pERK and pMEK after treatment with a MEK inhibitor alone and in combination with a RAF

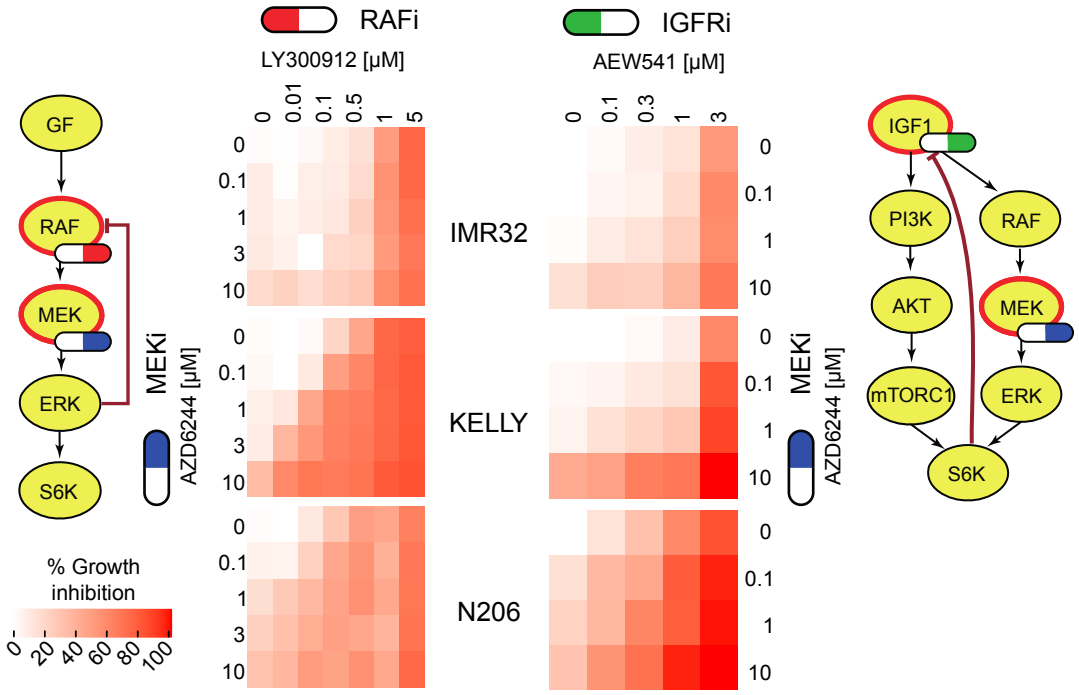

Figure 4.15: Model-inferred targeting strategy of dual inhibition of MEK and LEFT RAF or RIGHT IGFR inhibition and corresponding growth measurements using the specified inhibitors concentration. n=2.

inhibitor or ERK inhibitor showed that MEKi+RAFi treatment indeed reduced ERK phosphorylation in both cell lines more than MEKi alone and suppressed the feedback phosphorylation of MEK. Moreover, this suppression of MEK and ERK phosphorylation was indeed stronger in IMR32 than in KELLY (Figure 4.16). This confirms that the model can accurately predict the response of KELLY and most importantly IMR32 to combinations of perturbations. However, since the growth was least affected by this combination in IMR32, it appears this cell line might no longer depend on ERK signalling for survival and growth.

In the end, two combinations were identified to be effective at low drug concentrations against the MEK-inhibitor resistant cell lines KELLY and N206 respectively: AZD6244 with LY300912 and AZD6244 with AEW541. As both KELLY and N206 display a strong multi-layered feedback, a combination of three inhibitors against IGFR, RAF and MEK might show efficiency in all cell lines, as it targets both layers of the feedback without requiring the identification of the exact relative strength. I thus tested the effect of a combination of the three inhibitors AEW541, AZD6244 and LY300912 together. This combination reduced the viability of both KELLY and N206 at moderate concentration of all three drugs (300nM of AEW541, 50nM of LY300912 and 500nM of AZD6244) making it a potential therapeutic option (Figure 4.17).

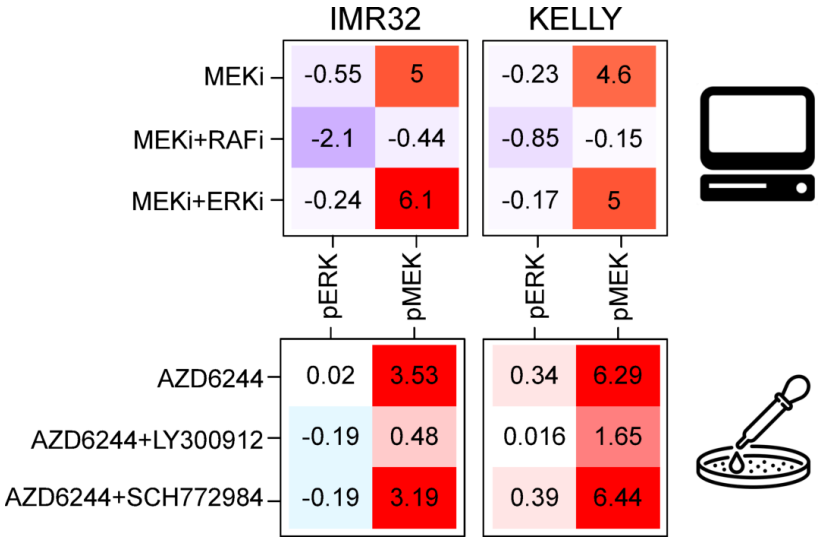

Figure 4.16: TOP: Model predictions of pERK and pMEK activity for MEK inhibition alone and in combination with inhibition of upstream kinase RAF or downstream kinase ERK for KELLY and IMR32. Values are log-fold changes to IGF1 condition. BOTTOM: pERK and pMEK plex measurements in KELLY and IMR32 after 90min treatment of the MEK inhibitor AZD6244 in combination with either DMSO, SCH772984 (ERKi, 10μM) or LY300912 (RAFi, 5μM) in cells grown with 10% FCS. Values are log-fold change to FCS medium condition.

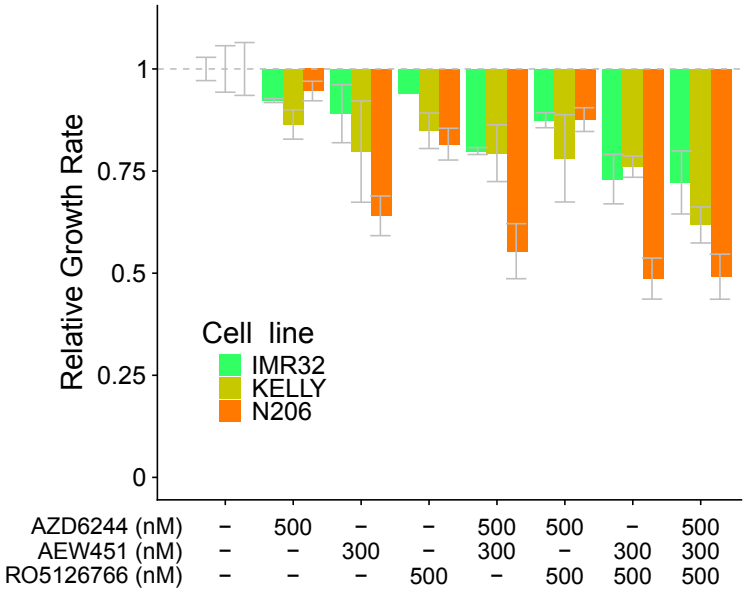

Figure 4.17: Relative growth rate of IMR32, KELLY and N206 cells for selected concentrations of dual and triple inhibitor treatments targeting MEK, RAF and IGFR relative to control measured using the Incucyte Zoom.

4.6 Deep molecular characterisation of the inhibitors combination

I next thought to deciper why IMR32 did not respond to the MEK and RAF inhibition combination and get a more systematic understanding of the effect of the MEK and IGFR combination. I treated the IMR32 and N206 for 4h with IGFR and MEK inhibitors alone or in combination for phospho-proteomics measurements (Figure 4.18) using Tandem Mass Tag mass spectrometry (Gygi et al., 1999; Mertins et al., 2018). *The samples were measured by M.Sc. Tomasso Mari in the group of Prof. Dr. Matthias Selbach (MDC) who also helped with the analysis.* The data were analysed using the *limma* package (Ritchie et al., 2015).

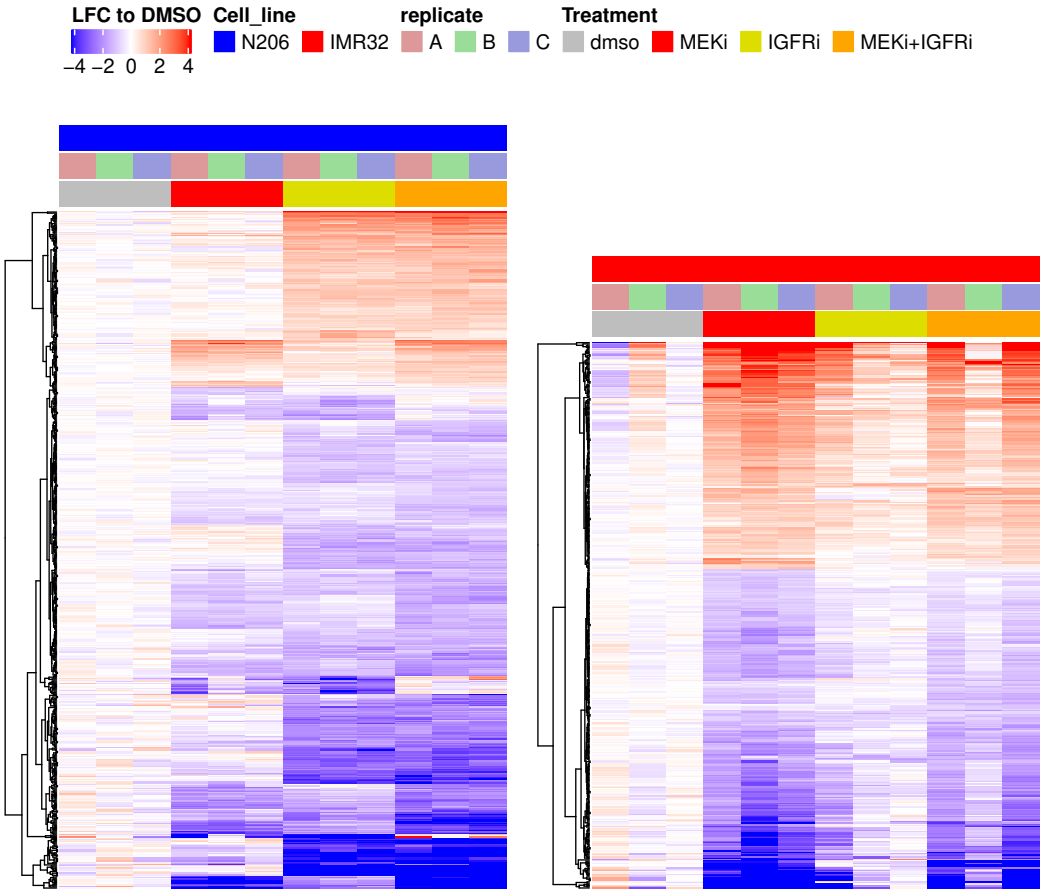

(a) N206 (b) IMR32

Figure 4.18: Heatmaps of phosphosites differentially expressed in each cell line (FDR < 0.05). Values are log-fold change (LFC) to mean DMSO mearusrement. Color annotations indicate the cell line, replicate or treatment corresponding to the sample. n=3.

Although a similar number of phosphosites were disregulated in both cell lines, there were few overlaps between the two cell lines (Figure 4.19a) and they exclusively corresponded to phophopeptides affected by MEK inhibition (Figure Appendix.13). In IMR32, IGFR inhibition had litte effect on the phosphoproteome while the presence of

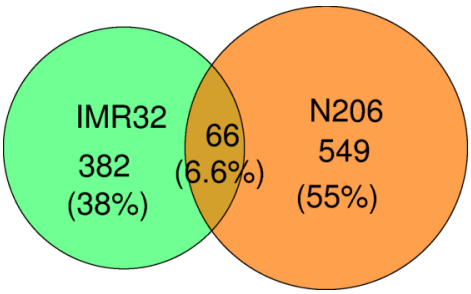

(a) IMR32 vs N206

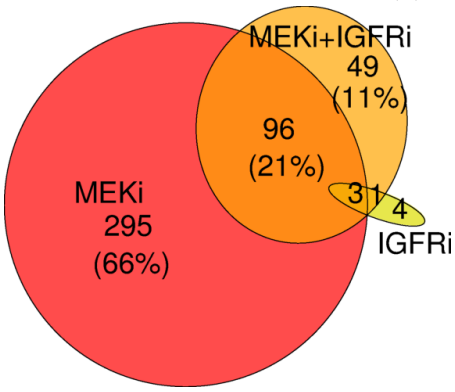

(b) IMR32

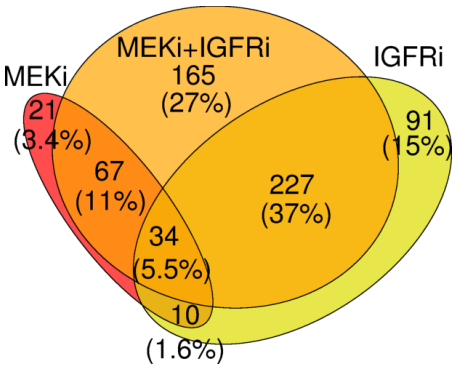

(c) N206

Figure 4.19: Venn diagram showing the overlap of phosphopeptides differentially expressed after IGFR and/or MEK inhibition versus DMSO control in N206 and IMR32 between cell lines for all treatments and between treatments for each cell line. FDR $<$ 0.05.

MEK inhibition, alone or with IGFR inhibitor, provoked extensive changes. Moreover, the effect of MEK inhibition dominated the response in IMR32 with only about a third (49/155) of phosphosites differentially expressed in the MEKi+IGFRi combination being exlusive for the combination (Figure 4.19b). In N206 however, both MEK and IGFR inhibitions induced major changes in the phosphoproteome and the combination had a strong synergistic effect (Figure 4.19c). 25 differentially phosphorylated sites showed a significantly stronger than additive regulation by the combination of MEK and IGFR inhibition in N206, while two sites differed from both individual treatments in IMR32 (Figure 4.20b). Almost half of the phosphosites synergistically affected in N206 are targets of the PI3K/AKT pathway kinases, indicating the blockade of AKT feedback-mediated activation by IGFR inhibition.

I analysed the list of differentially expressed genes using two methods, kinase-substrate enrichment analysis and gene set enrichment analysis.

Gene set enrichment analysis can directly give us phenotypic processes affected by the perturbation, however the current databases only annotate the gene/protein level, which implies loosing the specific information provided by the identity of the altered phosphosite. An enrichment analysis using KEGG pathways showed that MAPK targets are overrepresented in differentially phosphorylated proteins in IMR32. It should be noted here that the enriched pathways have important overlap, and there do

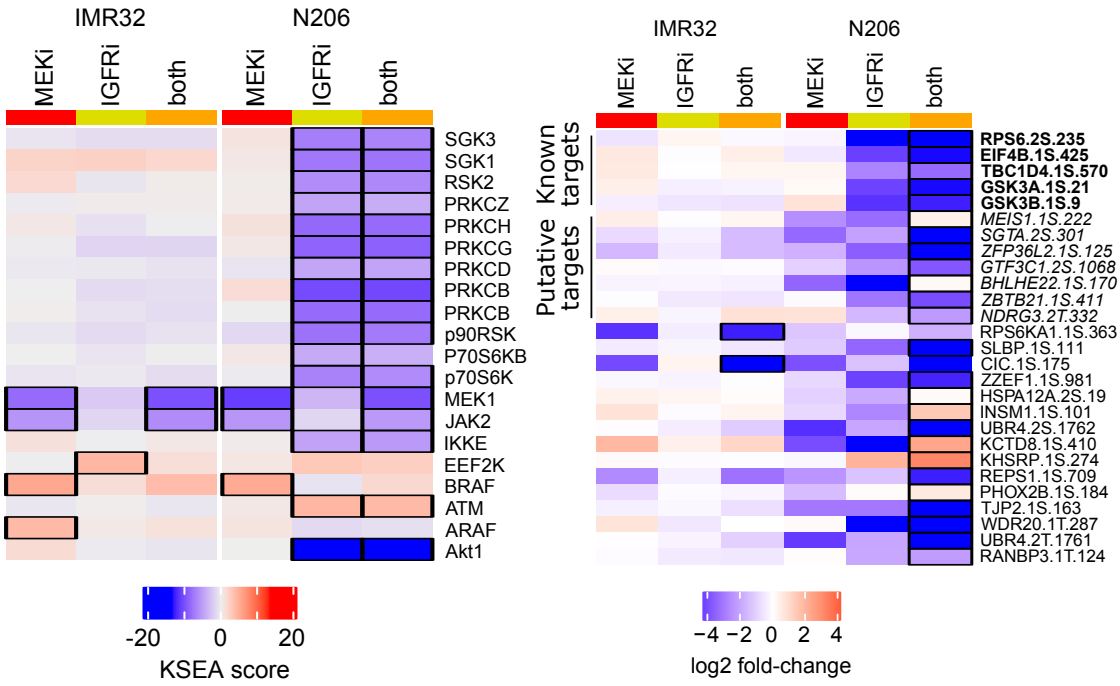

Figure 4.20: (a) Kinases with significant substrate enrichment using PhosphoSitePlus. (b) Phosphosites synergistically altered by MEKi+IGFRi combination compated to the sum of individual inhibitor treatments. AKT, mTOR and p70S6K annotated (bold font) and putative (italic font, top 5 predicted kinase by PhosphoNET Kinase Predictor `www.phosphonet.ca`) are highlighted. Black outline indicates significant conditions, FDR $<$ 0.05.

not provide independant information. In case of IMR32, many processes are enriched uniquely because they contain MAPK genes, which is the only pathway truly affected by MEK inhibition in this cell line (Figure Appendix.14a). Additionally in N206, gene set enrichment analysis revealed that both MEK and IGFR inhibitions affected mTOR and MAPK signalling (Figure Appendix.14b).

Kinase-substrate enrichment analysis (Casado et al., 2013) makes use of the full information of the phosphopeptides to compute kinase activity score, which can then be used to single out kinases with significant changes in their activity in response to the perturbation. It relies on kinase-substrates annotations containing details of which phosphosites are phosphorylated by each kinase and requires prior knowledge to give a phenotypic sense to the result. *Two main sources were suggested by M.Sc. Tommaso Mari for kinase-substrate annotations.*

The *Sugiyama* annotation was derived *in vitro* using phosphoproteomic measurements of phosphatase-treated cell lysates exposed to recombinant kinases (Sugiyama et al., 2019). This approach has the advantage of being able to rapidly test direct phosphorylations. However, it has multiple limitations, which can lead to an incomplete and noisy annotation. E.g the heat inactivation of the phosphatase leads to

denaturation of the proteins, and loss of docking information and substrate specificity. Moreover, the lysates were not fractionned, which loses compartiment specificity information. Those caveats seem to make it a very unreliable annotation. Consequently, using it on the N206-IMR32 phosphoproteomics data failed to pick up MEK1/2 (MAP2K1/2) inhibition after treatment with a MEK inhibitor despite the clear down-phosphorylation of ERK1/2$^{\mathrm{T185/T202+Y187/Y204}}$ (MAPK1/3), it's only validated target (Wu et al., 2015) (Figure Appendix.15).

The other annotation comes from PhosphositePlus (Hornbeck et al., 2015), which is curated from the literature (annotation from March 18th 2021). This approach provides high quality kinase-target pairs but it is biased, with high quality annotation for well studied kinases but missing substrates for kinases that are less thoroughly studied.

Kinase-substrate enrichment analyses using PhosphoSitePlus revealed in both N206 and IMR32 cells a decreased phosphorylation of MEK and JAK targets and an increased phosphorylation of BRAF (N206 and IMR32) and ARAF (IMR32 only) targets in response to MEK inhibition (Figure 4.20a). Overall, this indicates a feedback activation of RAF that fails at completely compensating the interruption of MEK activity by AZD6244. Moreover, the RAF feedback activation is partially removed when an IGFR inhibition is added to the MEK inhibition, whereas other kinase targets seem unaffected. This suggests that RAF reactivation also depends on upstream signals. It furthemore suggests that the strong RAF feedback in IMR32 is mediated via both RAF isoforms ARAF and BRAF, while the weaker feedback in N206 is mediated via BRAF only. While in IMR32 cells IGFR inhibitor treatment had little impact on the kinome, in N206, there was a massive decrease in activity for a range of kinases covering the PI3K/AKT/mTOR pathway (SGK1/3, AKT1, p70S6K, Caron et al. (2010)), MAPK pathway (p90RSK) and many members of the Protein Kinase C Family. The decreases in activity were all upheld in the double treatment. This strong influence of IGFR on central growth and survival pathways likely explains why N206 cells are more susceptible to IGFR inhibition than IMR32. Moreover, the activation of AKT by MEK inhibition supports the IGF1R feedback proposed by the model.

A closer inspection of the phosphorylation of the MAPK pathway components revealed many RAF negative feedback/crosstalk sites downregulated after MEK inhibition (BRAF: T401, S750, T753; RAF1: S29, S642, S259) in both cell lines, while MEK1/2$^{\mathrm{S222/S226}}$ is up-phosphorylated and ERK1/2$^{\mathrm{S204}}$ are down-phosphorylated (Figure 4.21a). An analysis of downstream targets also highlighted that MYCN was heavily affected, with five phosphosites downregulated in N206 after the dual inhibition. This loss of phosphorylation was associated with a loss of MYCN at the protein level, based on Western blots of cells treated for 4h with AEW541 10 μM and/or AZD6244 10 μM or DMSO. *The Western blots were run by M.Sc. Anja Sieber (CMM).*

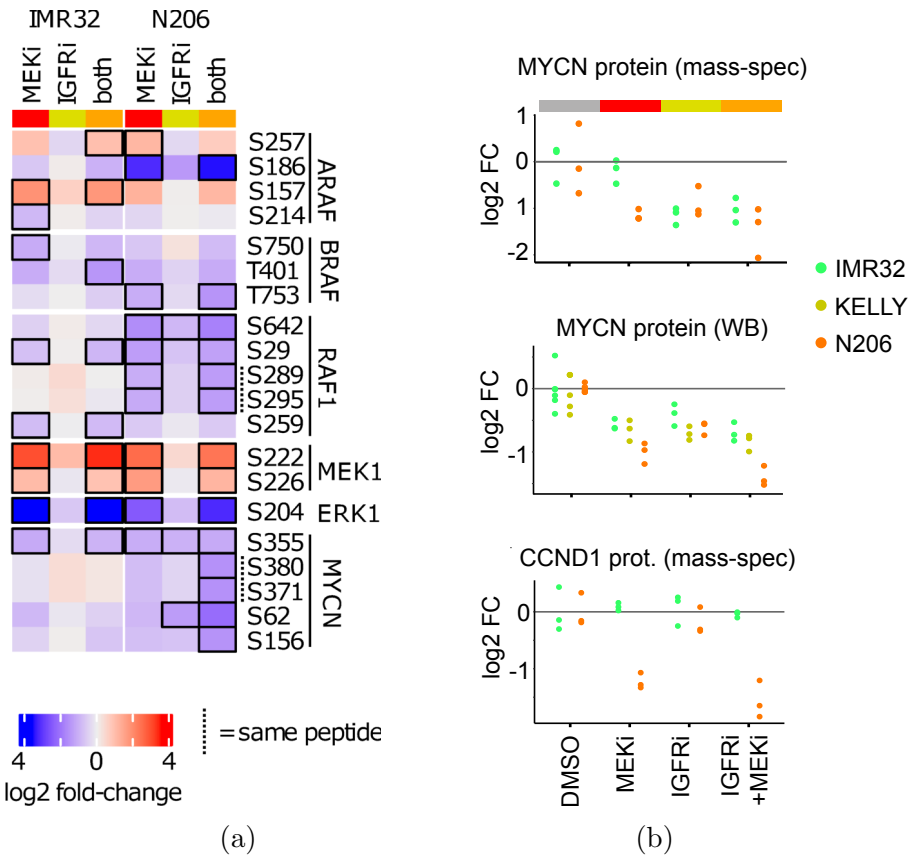

(a) (b)

Figure 4.21: (a) Differentially phosphorylated phosphosites on RAF isoforms, MEK1/2, ERK1/2 and MYCN in IMR32 and N206. (b) Total protein quantification of MYCN and CCND1.

I additionally explored the total proteomics data for other significantly regulated proteins. Only five proteins (PHGDH, DERL1, AMPD3, ARHGEF16 and CCND1) were found to be differentially affected with an FDR $<$ 10% and only in one condition, suggesting that changes in total protein was not detectable at this time scale. Nonetheless, the distribution of p-values was skewed towards low values, suggesting that some proteins were indeed differentially regulated but cannot be picked up with an acceptable false discovery rate (subsection C.6). Of the significant proteins, only PHGDH and CCND1 showed a significant downregulation in the proteomics data after correcting for multiple testing. PHGDH is a metabolic enzyme involved in serine synthesis, and cyclin D1 is essential for cell cycle progression. It is also highly likely that total MYCN is indeed downregulated as a consistent negative fold change is seen in both cell lines after MEKi alone or MEKi+IGFRi treatments. The downregulation of MYCN was also confirmed by Western blot (Figure 4.21b).

Taken together, the proteomics data were coherent with the model that MAPK signalling in N206 is controlled by a dual feedback structure involving RAF and IGFR, whereas it is mainly controlled by a RAF-mediated feedback in IMR32.

4.7 Discussion

In this work, I explored signalling in neuroblastoma cell lines in a quantitative manner and used it to design a combinatorial treatment approach that counteracts various resistance layers. I showed via deep, multi-omics profiling that neuroblastoma cell lines represent high risk neuroblastoma and exhibit a high variability in their response to MEK inhibition. Using carefully designed perturbations, it was possible to characterise the signalling network interacting with the MAPK pathway using STASNet models. These models uncovered multiple layers of feedback mechanisms which provided a strong feedback reactivation in resistant cell lines. They also suggested that the relative strengh of these layers was highly variable between cell lines.

For this dataset, multivariate analysis of the perturbation data alone could not separate cell lines with respect to their drug sensitivity. In contrast, integrating the data with STASNet highlighted that variations of only a few links explained major differences between the cell lines. This integration of the data by the MRA model was therefore key to unveil the feedback loops as potential sources of resistance.

In this work, I showed that two layers of MAPK signalling feedback are present in a number of neuroblastoma cell lines. The first feedback is pathway-intrinsic (from ERK to RAF) and the second is a feedback to the IGF receptor. Interestingly, the relative strengh of these feedback mechanisms from ERK to RAF and IGFR vary between cell lines. In the KELLY cell line, the models unveiled an extremely strong negative feedback from ERK to RAF. This suggested that a combination of MEK and RAF inhibitors would be more potent than a combination of MEK and IGFR inhibitors in this cell line. Indeed, a combination of RAF and MEK inhibitions can overcome a strong intrinsic feedback, similar to what is observed and has been translated to the clinic in melanoma (Czarnecka et al., 2020; Ottaviano et al., 2021). In contrast, in the N206 cell line, both feedback mechanisms have similar strength, suggesting that both combinations might have a significant effect on cell proliferation. Multiple previous lines of work on neuroblastoma point to an important role of IGF1R in tumor progression (El-Badry et al., 1989; Singleton et al., 1996) and suggest IGF1R as a very promising target (Liu et al., 1998; Coulter et al., 2008). This work suggests that the efficiency of IGF1R inhibition could be further enhanced by a combination with MEK inhibition to overcome a feedback to the receptor, similar to what is seen in colorectal cancer (Klinger et al., 2013; Prahallad et al., 2012; Corcoran et al., 2012, 2018). In line with these predictions, the experiments presented here showed that the combination of MEK and RAF inhibitors reduced growth much more than the combination of MEK and IGFR inhibitions in KELLY. In contrast to N206 where both combinations reduce growth. Interestingly, a third resistant cell line, IMR32, showed no response in growth to MEK inhibition in vertical combination with RAF despite the model suggesting a stronger ERK→RAF feedback. However, the cellular ERK signalling was strongly responsive to this combination, which confirmed the prediction of the

model. This highlights that cancer cells might lose ERK-mediated cell cycle control, a case of decoupling of the cellular phenotype from the signalling pathways (Cerezo et al., 2009; Castro et al., 2012). It also suggests that measuring readouts further downstream such as cyclin levels or CDK activation, which are also deregulated in cancer (Keyomarsi and Pardee, 1993; Sung et al., 2014), could improve the prediction of the interaction between signalling and cellular phenotypes (Korkut et al., 2015).

In summary, this work suggests combinations that could make MEK inhibition more sucessful in neuroblastoma, by shedding light on the mechanisms mediating resistance.

Chapter 5

Signalling of NF1-KO neuroblastoma cell lines

In chapter 4 I used STASNet to compare how differences in signalling of a neuroblastoma cell line panel affected drug response. Such system is useful to suggest new therapies with little prior knowledge but requires a large amount of data to overcome the biological noise between unrelated cell lines and provide a good representation of the initial disease. On the contrary, isogenic cells lines, which are derived from a unique cell population, are highly similar and provide in depth knowledge of their genetic differences. Their main constraint is the prelimiinary introduction of genetic alterations which are relevant for the disease of interest in the corresponding system. In this chapter, I discuss the results of using isogenic cell lines to elucidate how the loss of NF1 affects drug resistance in neuroblastoma and demonstrate a use case for the ModelSet feature of STASNet.

The cells lines were generated, characterised and treated by M.Sc. Mareike Bock from the group of Paediatric Haematology of Charité.

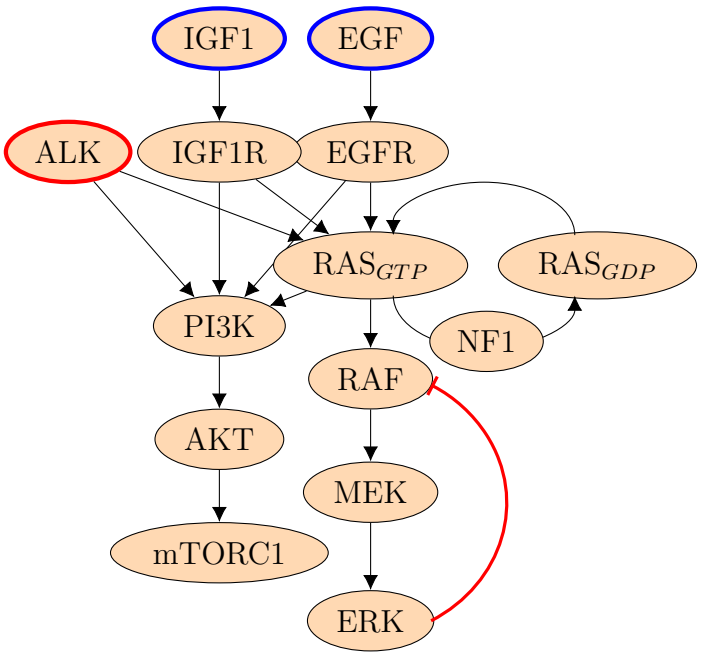

Figure 5.1: Role of NF1 and ALK in MAPK activation. Arrowheads indicate positive influence, flat heads indicate negative influence, and NF1 over the $RAS_{GTP} \rightarrow RAS_{GDP}$ link indicates the catalyses of the GTP hydrolysis by NF1. Nodes with blue contour are ligands, ALK is highlighted with a red contour.

5.1 The NF1 protein

The group of Prof. Dr. Johannes Schulte identified recurrent NF1 inactivating mutations in relapsed neuroblastoma treated with the ALK inhibitor Ceritinib.

NF1 is a GTPase activating protein (GAP) acting on RAS. It deactivates RAS by enhancing the GTPase activity of RAS, switching it from the active GTP-bound state to an inactive GDP-bound state (Figure 5.1, Cichowski and Jacks (2001)). Without NF1 activity, RAS hydrolyses GTP at a slower rate and stays in the active GTP-bound state for longer, leading to a higher activation of the downstream PI3K and RAF pathways.

Since the RAF pathway is activated by ALK, such activation of RAS signalling could explain the resistance to ALK inhibition by decoupling downstream signalling from the receptor. NF1 mutations have also been involved in the resistance of neuroblastoma to retinoic acid-induced differentiation, where the activation of MAPK signalling represses the transcriptional activity of the retinoic acid receptor (Hölzel et al., 2010). NF1 knock-out (NF1 KO) cell lines were thus generated using CRISPR to study the implications of NF1 loss on signalling.

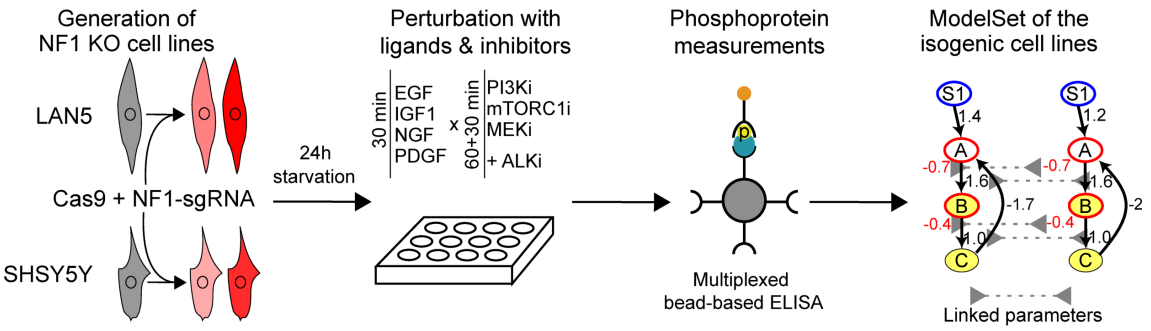

Figure 5.2: Neuroblastoma cell lines with CRISPR knock-outs of NF1 are perturbed with small molecule inhibitors and phosphoproteins measured to generate models highlighting the changes induced by the knock-out.

5.2 Modelling NF1-KO cell lines

Mareike Bock generated isogenic NF1-KO cell lines from the ALK mutant neuroblastoma cell lines LAN5 and SH-SY5Y. For each parental cell line, she selected 2 NF1-KO clones for analysis to be able to single out the specific impact of the NF1 knock-out from potential clonal effects (Figure 5.2).

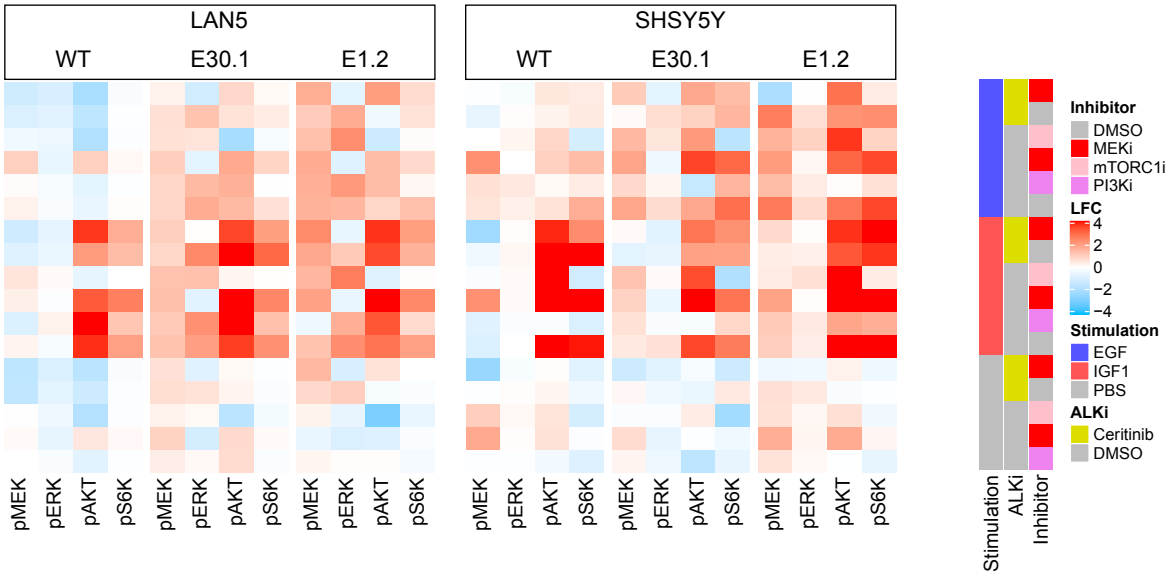

Figure 5.3: Measurements of the 4 phosphoproteins p-MEK$^{S217/S221}$, p-ERK$^{T202/Y204}$, p-AKT^{S473} and p-S6K^{T389} in two sets of isogenic neuroblastoma cell lines derived from LAN5 or SHSY5Y (LAN5 WT and SHSY5Y WT) by knocking-out NF1 (LAN5 E1.2 and LAN5 E30.1, SHSY5Y E1.2 and SHSY5Y E30.2) in response to combinations of 2 ligands or BSA with 3 inhibitors or DMSO and the ALK inhibitor Ceritinib or DMSO. Each measurement is normalised by the BSA+DMSO control of the corresponding cell line. n=3.

We then jointly planned a perturbation panel to tease out the effect of the NF1 knock-out on signalling downstream of RAS. The final set of perturbations consisted of the ligands IGF1, EGF or PBS as a control condition in combination with

the inhibitors Rapamycin (mTORC1), GDC0941 (PI3K), AZD6244 (MEK1/2), Sorafenib (RAF), Ceritinib (ALK) or a DMSO control (Figure 5.3). The cell lines with all combinations of ligands and inhibitors and the levels of pERK1/2$^{T202/Y204}$, pMEK1/2$^{S218/S222}$, pS6K1^{T389} and pAKT^{S473} were measured in triplicates using the MagPix. The data were batch normalised to account for technical variations between replicates (subsection D.1) In both cell line backgrounds, the NF1-KO cell lines exhibited more response to ligands than the parental cell line.

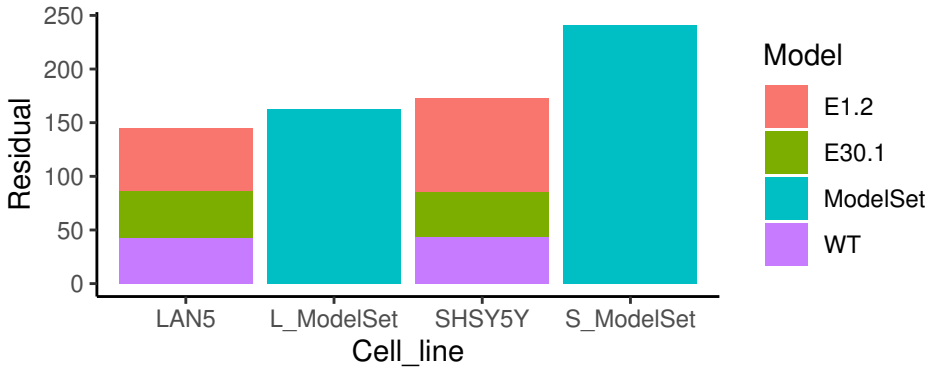

Figure 5.4: Residuals of the NF1-KO single Models and ModelSet for the LAN5 and SH-SY5Y WT and NF1-KO cell lines.

After batch normalisation, I built a model for each cell line separately and checked if any extension of the literature network was necessary to explain the data. Similar to the network introduced in chapter 2, the direct and indirect activation of PI3K by the receptors cannot be deconvoluted. Therefore the RAS→PI3K link was not included in the models. No extension was suggested for any of the cell lines (subsection D.4 and subsection D.2). This led me to the conclusion that the isogenic cell lines were similar enough to be modelled using the ModelSet feature (section 2.5) to robustly highlight the links affected by the loss of NF1.

The ModelSet showed that only a subset of the network parameters varied significantly between isogenic cell lines (Figure 5.5) and the increase in residual is moderate for both LAN5 and SH-SY5Y compared to the sum of residuals from the individual cell line models, which confirmed that the ModelSets robustly identified the important differences between the cell lines (Figure 5.4). In both backgrounds, the EGF→PI3K path was stronger in the NF1-KO cell lines than in the WT. EGF→RAS→RAF→MEK was stronger in LAN5 NF1-KOs than in LAN5 WT. This suggests that the EGF receptor activation of RAS is modulated by NF1, such that the loss of NF1 made the cells more inducible by EGF. Conversely, the inducibility by IGF1 did not differ between cells from the same background suggesting that the activation of RAS and PI3K by the IGF1 receptor is independent or overcomes the inactivation of RAS by NF1. The only exception was SH-SY5Y E30.2 where the IGF1→PI3K link was weaker than in the parental, which suggests a clonal variation rather than a specific effect of the loss of NF1.

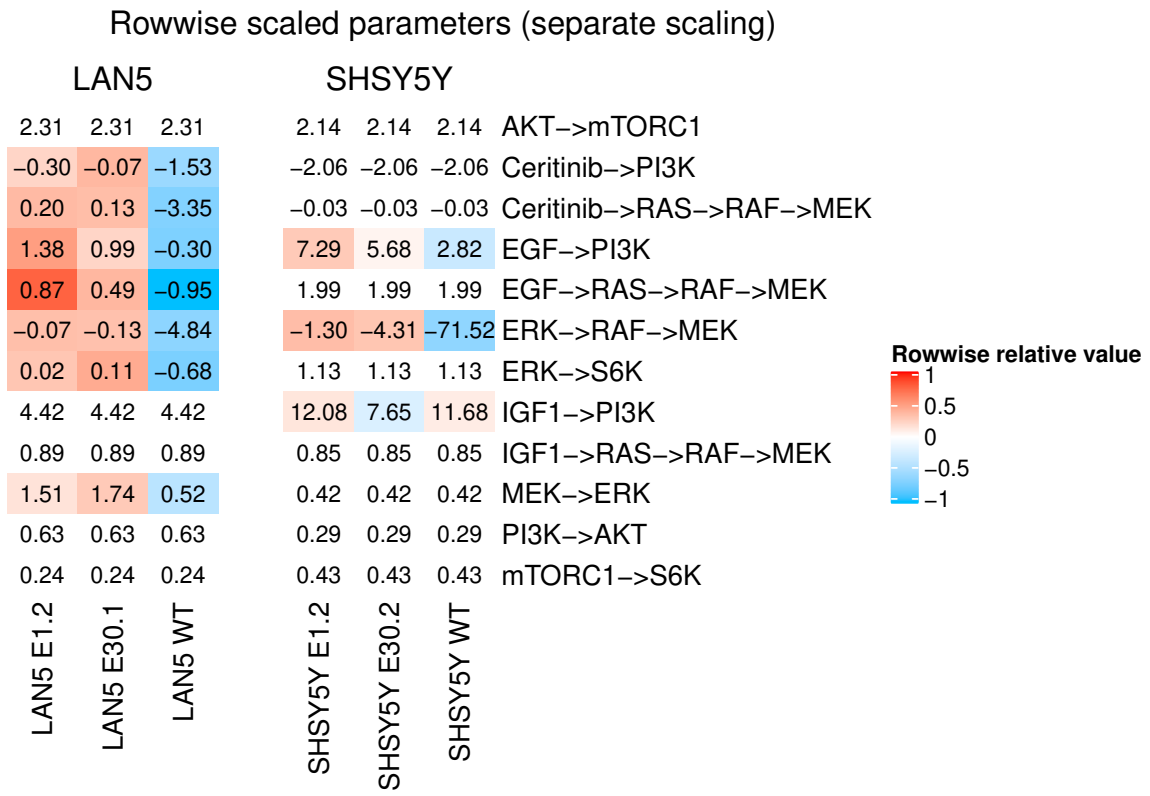

Figure 5.5: Parameters of the MRAmodelSet for each NF1-KO panel of cell lines. The colors reflect the rowwise Z-normalised parameter value for each isogenic panel, red indicates relatively a higher parameter, blue a relatively lower parameter.

More surprinsingly, the ERK→RAF→MEK feedback was attenuated in the NF1 KO clones compared to the parental in both isogenic panels. Such attenuation can be explained by 1) a downregulation of ALK induced activation of MAPK signalling as an adaptation of the network to the increased sensitivity induced by the loss of NF1 to ensure cell survival or 2) a higher basal activation of the MAPK pathway induced by NF1 removal leading to a saturation of the feedback. This attenuation of the feedback could explain the greater sensitivity of the NF1 KO cell lines to MEK inhibition.

5.3 Phosphoproteomics characterisation of NF1 knock-out in SHSY5Y

In order to get additional data that characterises the interaction between ALK and MEK inhibition in NF1-KO, we turned to proteomics. *SHSY5Y isogenic cell lines with or without NF1 deletion were treated by M.Sc. Mareike Bock for 0h, 1h or 6h with Certinib and/or Selumetinib. Proteomic and phosphoproteomic were measured by M.Sc. Tommaso Mari using Tandem Mass Tag mass spectrometry* (section 7.7). I performed differential expression analysis using the R package *limma* (Ritchie et al., 2015).

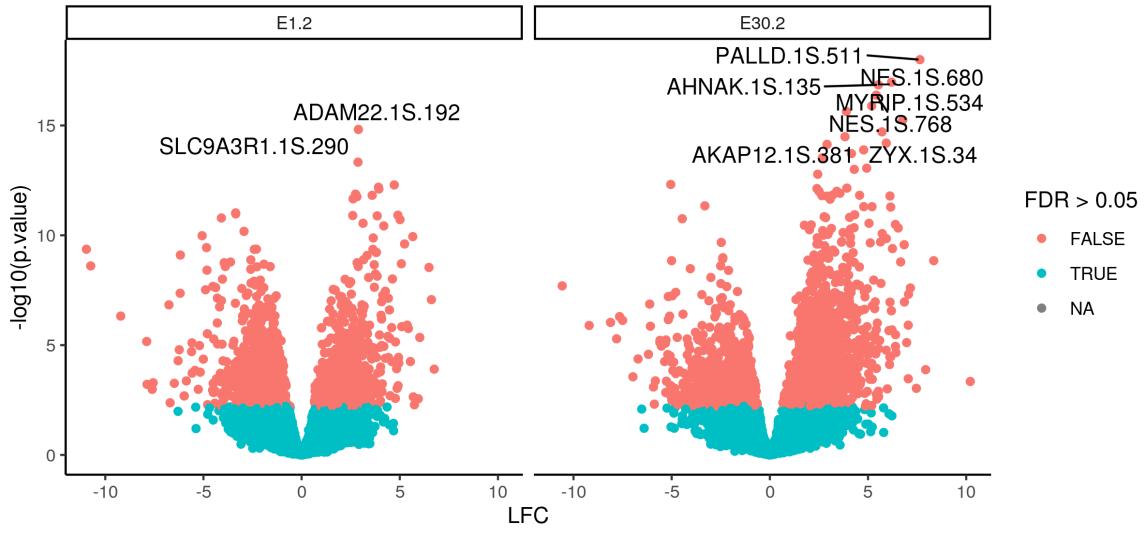

(a)

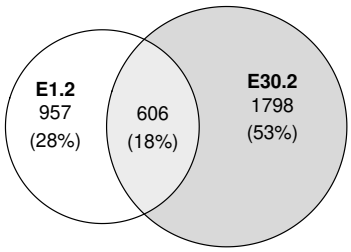

(b)

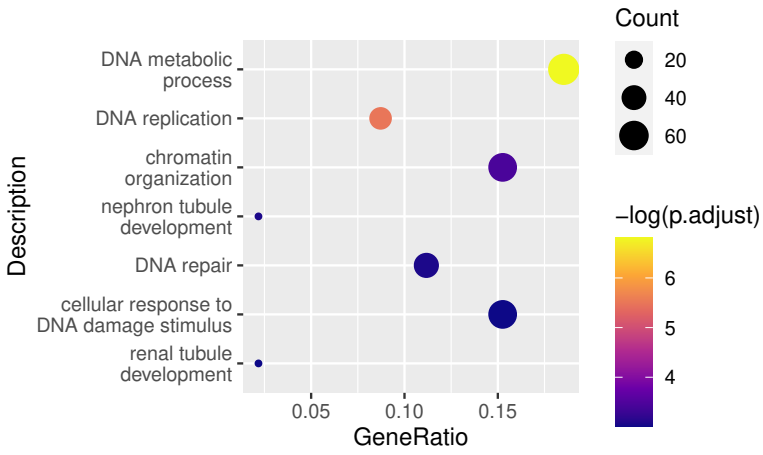

(c)

Figure 5.6: (a) Volcano plot and (b) overlap of differentially phosphorylated peptides between each NF1-KO and the WT cell lines (c) GO Biological Process enrichment for the genes corresponding to the 606 overlapping phosphopeptides. FDR $<$ 0.05.

First, I analysed the effect of NF1 knock-out on the phosphoproteome. 3421 unique phosphosites were differentially phosphorylated in total in NF1-KO cell lines at a false

discovery rate of 5%, with 606 genes overlapping between the clones (Figure 5.6). 'DNA replication' was the only enriched KEGG term using the 606 overlapping phosphopeptides, while a GO analysis also revealed terms linked to DNA repair, replication and metabolic processes (Figure 5.6c). It thus appears that the deletion of NF1 induced DNA damage, likely because of increased proliferation and DNA replication. Investigating terms enriched for each KO cell line showed that RAS target pathways are active in E30.2 (Figure Appendix.29b) while only DNA replication is affected in E1.2 (Figure Appendix.29c).

I then analysed the effect of the treatments independently in each cell line. Every treatment condition including the combination was considered as an independent treatment for a contrast fit versus DMSO (Figure 5.7 and Figure Appendix.28). Using a FDR of 5% resulted in 297 peptides differentially phosphorylated after treatment across all three cell lines (Figure Appendix.28d). The signal-to-noise ratio in this dataset did not seem as good as previous phosphosite studies published on the effect of ALK inhibitors (Emdal et al., 2018; Van Den Eynden et al., 2018), which recovered about a thousand differentially phosphorylated peptides after ALK inhibition alone in ALK-dependent neuroblastoma cell lines. This would explain why less (156) significantly altered phosphosites after ALK inhibition were recovered than reported in these publications with a FDR of 0.05. I thus used a FDR of 0.25 to overcome this lack of power, allowing for more false positives but increasing the sensitivity. This resulted in 466 significant phosphosites (Figure 5.7), 387 of which were significantly altered by the combination treatment. Interestingly, more phosphosites were affected by ALK inhibition in the WT than in the NF-KO (77 vs 11 and 22, Figure 5.8a) while less are affected by MEK inhibition (33 vs 85 and 201, Figure 5.8b).

This matched the drug sensitivity assay results and suggests that the differential effect of these inhibitors on cell proliferation is captured in the phosphoproteomics. An unsupervised clustering of the samples using differentially phosphorylated sites (FDR < 0.25) clustered the replicates of each condition together (Figure 5.7). Interestingly, the 1h and 6h timepoint samples were highly similar for every treatment which indicates that the early effects of the inhibition on the phosphoproteome were maintained for several hours. Crucially, this supports the conclusions derived from the MRA model, which were trained with 90 minutes inhibition data. From the treatment perspective, the data separated in 3 main clusters. Selumetinib treated samples from the parental cell line clustered with DMSO treated samples, which suggests that MEK activity is rather low in the parental cell line despite the ALK mutation. Interestingly Selumetinib treated NF1-KO samples also clustered with the DMSO treated samples of the parental cell line. This suggests that the main phenotype of NF1-KO on the phosphoproteome is an activation of the MEK pathway. Ceritinib treated samples on the other hand were present in the two other clusters. E1.2 Ceritinib samples

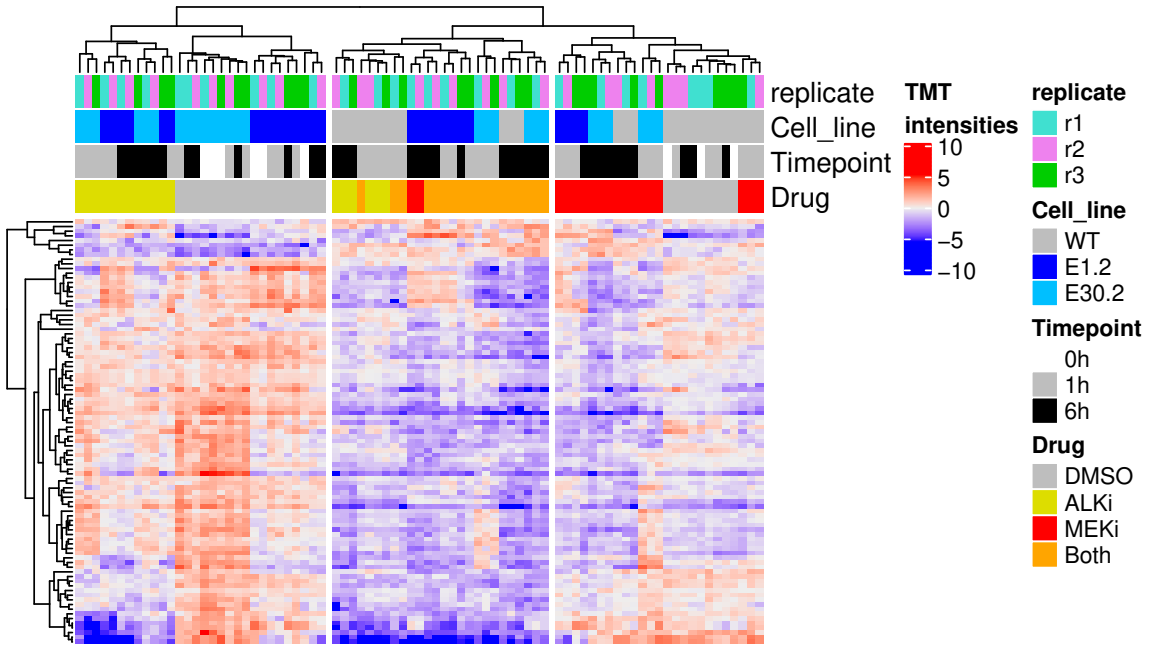

Figure 5.7: Relative abundance of differentially represented phosphosites after treatment with Ceritinib (yellow), Selumetinib (red), or a combination of both (orange) relative to DMSO control (grey) for various durations in the SHSY5Y isogenic panel with (E1.2 and E30.2) or without (WT) NF1 deletion. FDR $<$ 0.05.

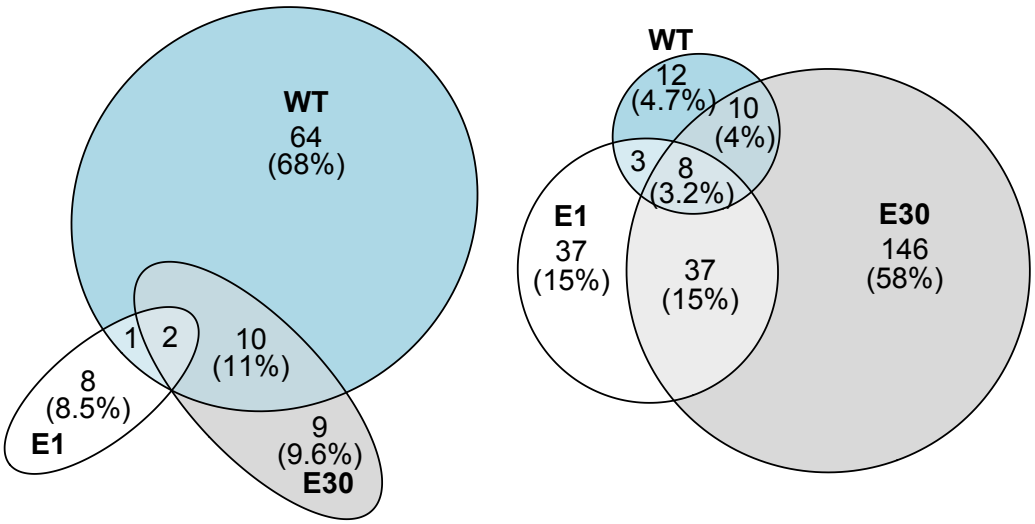

(a) ALKi (b) MEKi

Figure 5.8: Overlap of differentially expressed phosphosites following treatment. FDR $<$ 0.25.

clustered with DMSO treated NF1-KO while WT and E30.2 Ceritinib samples behaved more similarly to combination-treated cells. This suggests that ALK inhibition was sufficient to strongly inhibit WT cells but not E1.2. A closer inspection of the results from the differential expression analysis also reveals that E30.2 only partially reacts to Ceritinib alone, with the addition of MEK inhibition inducing drastic changes (Figure Appendix.28). KEGG enrichment on the phosphosites differentially regulated shows that ALK inhibition particularly affects mTOR signalling targets while MEK inhibition mainly affects MAPK (proteoglycans in cancer and microRNAs in cancer) (Table 5.1). One has to keep in mind that phosphorylated proteins are already enriched for certain pathways, thus only proteins for which a phosphopeptide could be measured was used as the background universe for the enrichment analysis. Enriched terms thus highlight how specific pathways were more affected than the overall signalling of the cell.

Table 5.1: KEGG enriched terms for phosphosites differentially expressed with FDR $<$ 0.25 in any cell line upon treatment with Ceritinib (ALKi) or Selumetinib (MEKi). Enrichment FDR < 0.1, background universe of all measured phosphoproteins.

Perturbation	**Description**	**Gene Ratio**	**p.adjust**
ALKi	mTOR signalling pathway	7/36	0.000095
ALKi	Longevity regulating pathway	4/36	0.00101
MEKi	Proteoglycans in cancer	14/76	0.00106
MEKi	MicroRNAs in cancer	11/76	0.0187
MEKi	Bladder cancer	5/76	0.0339
MEKi	MAPK signalling pathway	11/76	0.0652
MEKi	EGFR inhibitor resistance	6/76	0.0652

I then computed the kinase activity using Kinase Substrate Enrichment Analysis (KSEA, Casado et al. (2013)) and PhosphositePlus (Hornbeck et al., 2015) to get a more refined overview of the pathways affected. Clustering on raw kinase activity separated the cell lines at the first order (Figure 5.9b), so I started by comparing DMSO treated samples (Figure 5.9a). From the DMSO treated samples, it appears that the activity of PRKG, DNAPK and PKCA was increased in the NF1-KO cells. Those proteins responded to DNA damage and suggest a higher oxidative stress in NF1-KO cells (Figure 5.9a). There was also increased activity of the AKT pathway (AKT1, p70S6K, p90RSK), which suggests a pro-survival selection and a decreased activity of CDK1/2/4 pointing towards a slowing down of the cell cycle in NF1-KO. Overall, the kinase activities suggest that an oxidative stress induced by the loss of NF1-KO selected cells with slower proliferation and more active pro-survival signalling.

At a second order, the kinase substrate activity separated treatments (Figure 5.9b). Consistent with the KEGG enrichment (Table 5.1), it appears that AKT1, p70S6K and p90RSK were strongly downregulated after ALK inhibition in all cell lines, which

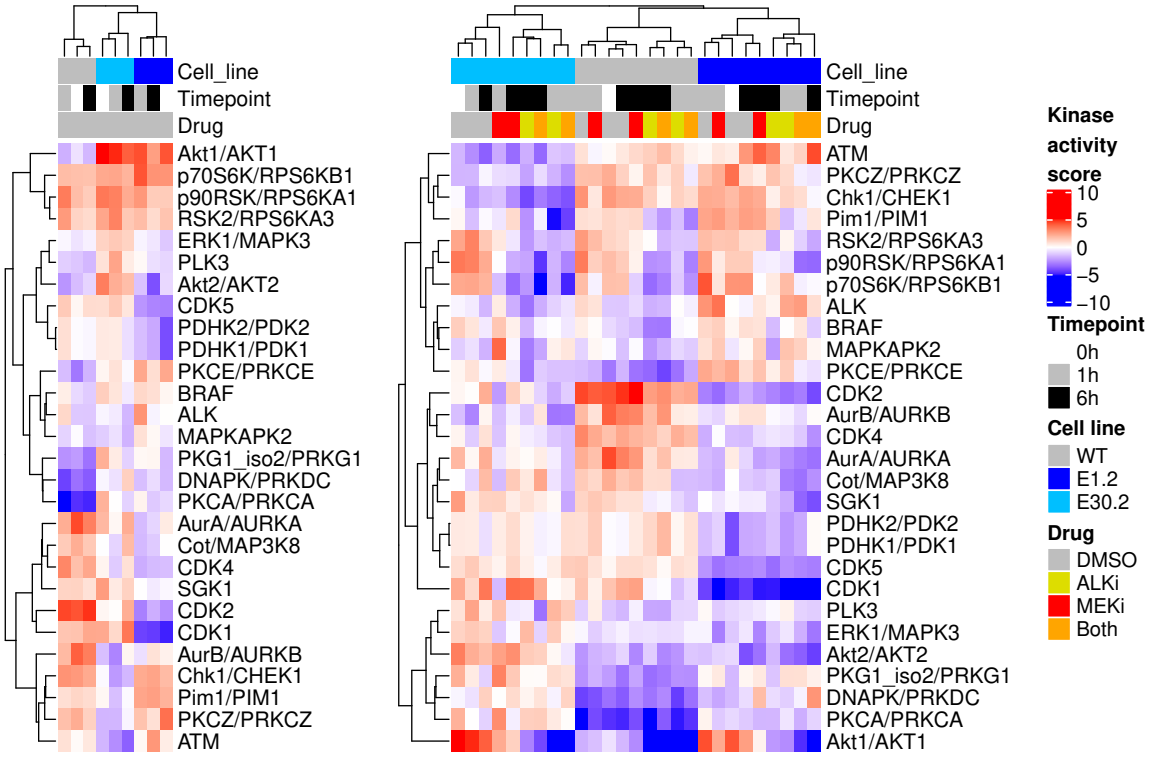

Figure 5.9: Significantly active kinases in (a) DMSO treated or (b) all samples. Statistical significance was assessed with a t-test on the kinase activity score as described in Casado et al. (2013) with $p < 0.05$.

is in line with known literature on ALK signalling to the PI3K/AKT pathway (Slupianek et al., 2001; Schönherr et al., 2012; Claeys et al., 2019). The inhibition of ALK lead to a more profound downregulation of PI3K/AKT signalling in the WT, which could be due to the lower basal activity of the pathway. More surprisingly, the activity of the PI3K/AKT pathway also decreased slightly after MEK inhibition in the NF1-KO, suggesting that some crosstalk takes place in those cells. As expected ALK-substrate-annotated phosphosites were downregulated after ALK inhibition in WT and E30.2, but unexpectedly not in E1.2 (Figure 5.9b). However, this dataset contains few phospho-tyrosines, which are the main substrates of tyrosine kinase receptors such as ALK (Figure Appendix.30a). The only ALK substrates detected were PTPN11.1Y.546 and PTPN11.1Y.584 suggesting that E1.2 might use other adaptors such as SRCIN1 (Cabodi et al., 2010) or VASP to relay ALK activation. Similarly, the activity of different RAF isoforms was not strongly affected by the treatment but only four substrates were present in our data, giving a very partial picture. ERK1/2 substrates coverage was better and showed that ERK activity was decreased by MEK inhibition with a stronger decrease in the NF1-KO, but no effect of ALK inhibition. Finally, CDK2 activity was strongly downregulated by ALK inhibition in the WT cell line only. Overall, the kinase activity showed a clear molecular effect of ALK inhibition

on the PI3K/AKT pathway in all cell lines, and of MEK inhibition on ERK targets in the NF1-KO cell lines. It also suggests that the sensitivity of the WT cell line to ALK inhibition is mediated by the AKT pathway and CDK2, while the sensitivity of the NF1-KO cell lines to MEK inhibition is mediated primarily via ERK1/2. I would thus propose to measure the effect of AKT and CKD2 inhibitors on those cell lines as the NF1-KO cell lines could still depend on these two kinases, in particular AKT.

Interestingly, the ALKi treated parental samples were the only exception to the treatment separation, as they clustered with the samples treated with an effective drug combination. This is consistent with the vulnerability of the parental cell line to ALK inhibition. It seems that this vulnerability is caused by a general reduction of phosphorylation of the pro-survival targets of ERK and AKT that does not happen in the NF1 KO. We now know from the model that the effect of ALK inhibition on the phosphoproteome is reduced in NF1 KO because the loss of NF1 protects the PI3K and MAPK pathways from a reduction in receptor activity (section 5.2).

More puzzling is the fact that under MEKi treatment parental samples seemed very similar to the E30.2 clone sample while this NF1 KO clone is the most sensitive to MEK inhibition. MEK inhibition downregulates many phosphosites affected by ALK inhibition in all cell lines with the notable exception of PI3K/AKT targets, which is coherent with known topology and interactions between the MAPK and PI3K pathways (Rahmouni et al., 2004; Aksamitiene et al., 2012; Sos et al., 2009). Such behaviour is consistent with the fact that ALK is mutated in the parental cell line, as oncogene activation during carcinogenesis tends to create dependencies because of the selective advantage they provide (Reiter et al., 2013; Walker et al., 2018).

In conclusion, this phosphoproteomics dataset sheds light on the dependencies of the SHSY5Y cell line to ALK and highlights how NF1 removal protects the NF1-KO from some of these dependencies.

5.4 Discussion

In this chapter, I used MRA and phosphoproteomics data to investigate the effect of the loss of NF1 on two neuroblastoma cell lines. MRA showed that the deletion of NF1 induced a loss of MAPK feedback strength and an increase in EGF-mediated, but not IGF1-mediated, signalling.

The weaker feedback regulation explains the higher vulnerability of NF1-KO cells to MEK inhibition as it is no longer capable of rescuing the pre-inhibition signalling state.

A deeper characterisation using mass spectrometry phosphoproteomics for one cell line confirmed that those changes led to extensive modifications of the state of the phosphoproteome. Although those phosphoproteomics data had an inferior signal to noise ratio compared to previous phosproteomics studies on similar systems (Emdal

et al., 2018; Van Den Eynden et al., 2018), I could identify key processes affected by MEK and ALK inhibitions such as an increased effect of ALK inhibition on the PI3K/mTOR pathway. The NF1-KO phosphoproteomes also reacted more strongly to MEK inhibiton than the parental's, while the parental cell line was more reactive to ALK inhibition, in agreement with the relative sensitivity of the growth rate measured for these inhibitors. These data also highlighted that a combination of ALK and MEK inhibition had very similar effects in all cell lines, suggesting that such a combination could prevent the emergence of ALK inhibitor resistance via NF1 inactivation.

The pressing question remains whether this combination would be effective against other alterations of the MAPK pathway arising in relapsed neuroblastoma such as SHP2, NRAS or KRAS mutations (Eleveld et al., 2015). Although sensitivity to MEK inhibition has been shown in cell lines harboring those alterations, the addition of an ALK inhibition seems relevant as evidenced by the lack of effect of a MEK inhibitor alone in ALK-mutated neuroblastoma (Umapathy et al., 2017). The data indeed suggest that the inhibition of the PI3K/AKT pathway by ALK inhibition could be crucial to prevent the proliferation of neuroblastoma cells. This also advocates for the investigation of the effect of combinations of MEK inhibitions with PI3K, AKT or mTOR inhibitors, which could recapitulate the effect of ALK inhibition without leaving the opportunity for the cells to develop resistance.

Chapter 6

Conclusion

Signaling networks are mostly similar between cell types but subtle disparities can account for drastic phenotypic differences. For this reason, quantitative analysis is necessary to understand these variations (Yosef et al., 2006). Despite massive advances in high-throughput data generation, targeted perturbations of biological systems remain our most powerful tool to understand their inner workings. While methods such as pathway footprints or molecular signatures (Liberzon et al., 2011; Kanehisa and Goto, 2000; Ashburner et al., 2000; Rydenfelt et al., 2020) can inform us on the active processes in a system of interest, they still fail at accurately predicting actionable pathway dependencies because of the crosstalk between pathways and signalling layers. This crosstalk can induce the activation of repressed pathways after inhibition or simply reactivate the inhibited pathway, making the active pathway an imperfect target for treatment.

In this context, Modular Response Analysis is a useful framework to gather a lot of information from a restricted set of perturbation measurements. MRA models necessitate less data and hypotheses to parameterise compared to ordinary differential equations (Schoeberl et al., 2002; Orton et al., 2005; Sundaramurthy and Gakkhar, 2010; Raue et al., 2015) or similar methods (Oates et al., 2012; Terfve et al., 2015) while providing pertinent quantitative predictions and using more information than Boolean models (Schlatter et al., 2009; Grieco et al., 2013; Gupta et al., 2020; Niederdorfer et al., 2020). The original formulation of MRA (Kholodenko et al., 2002; Andrec et al., 2005) imposed strict conditions on the experimental design, but more modern iterations can deal with incomplete perturbation data via Bayesian or maximum likelihood formulations (Stelniec-Klotz et al., 2012; Klinger et al., 2013; Santra et al., 2013). In this thesis (chapter 2) I developed an R package to reverse engineer signalling networks implementing a Maximum Likelihood Levenberg-Marquart variant of MRA and used it to investigate mechanisms of resistance to targeted inhibition of the MAPK and PI3K pathways with a particular focus on neuroblastoma.

In chapter 3 I explored how STASNet could help to generate pertinent and properly constrained MRA models. This evaluation highlighted the specific case of a single

pathway alteration where MRA can help understand how this alteration influences the flow of information in the signalling network. I also illustrated how biological knowledge can be integrated to quantify the effect of mutations on the reponse to drugs and ligands. Moreover, additionnal features beyond simple Modular Response Analysis make STASNet a capable and relatively accessible tool to analyse signalling networks. The use of prior information at the core of STASNet facilitates the interpretation of the model because it uses biologically plausible networks. The implementation of profile likelihood adds robustness to the interpretation of the parameters while the ModelSet fitting adds another layer of stability when working with isogenic cell lines, using data from multiple similar cell lines to provide a more robust estimation of parameters and highlight differences between cell lines. I also used the ModelSet feature to study why NF1 loss of function mutations leads to relapses after ALK inhibitor therapy in chapter 5. The loss of NF1 induced by CRISPR knockout decreased the RAF feedback strength, making the cells hyper-responsive to ligand stimulation but also more sensitive to MEK inhibition. This is in contrast to the commonly held assumption that loss of NF1 simply activates RAS (Bollag et al., 1996; Nissan et al., 2014) and suggests that upstream inhibition might represent interesting therapeutic options. The identification of actionnable intervention points will require further mechanistic studies.

In chapter 4 I measured drug response and perturbation responses for a panel of neuroblastoma cell lines which were previously characterized thoroughly by members of the TerminateNB consortium. ML MRA unveiled that some cell lines resistant to MEK inhibition displayed strong multilayered feedback mechanisms. Subsequent investigations uncovered a combination of MEK, RAF and IGF1R inhibition with the potential to overcome MEK inhibitor resistance in all neuroblastoma tumors by adressing this multi-layered feedback. This will support the design of clinical trials using combinatorial treatments to prevent or overcome therapy resistance in neuroblastoma. However perturbations are hardly practical for the clinic, where treatment options for cancer patients using scalable diagnostic tools such as sequencing or immuno-staining are required. While no direct diagnostic tool could be found, this work suggests that staining for phospho-MEK after treatment with MEK inhibitors could help to anticipate resistance as it arises in neuroblastoma patients and suggests combinations to overcome them.

As outlined in this work, MRA works best on isogenic systems with few alterations. Cell line panels are a great tool to address the diversity of genotypes and phenotypes encountered in patients. Yet the coupling of genomic and perturbation data is limited by the cost of generating perturbation panels with enough cell lines to cover this diversity and tease out biological effects in a statistically satisfying manner. Although I successfully identified differential feedback strength in a panel of neuroblastoma cell lines as the probable cause for MEK inhibitor resistance, I could not identify the

cause of differential sensitivity to other inhibitors despite their use in the perturbation experiments. Indeed, the signal propagation in signalling pathways implies that minor quantitative changes in the network can lead to many changes in response, not all of which alter the phenotype. Moreover, cell lines show important variations and the relative sensitivity between two cell lines can have multiple origins. In contrast, the few controlled alterations in isogenic panels provide direct causal explanation where MRA can identify the specific interactions in the signaling network affected by these genetic perturbations.

The results in this thesis show that a quantitative understanding of differences in signalling networks is key to understand some resistances and an essential tool to derive effective treatments. STASNet has been and is currently used to study the role of MAPK on stem cell differentiation depending on the number of X chromosomes (Sultana et al. manuscript and thesis in preparation), the role of PI3K/AKT signalling in pancreatic neuroendocrine cell lines (Simon et al, manuscript and thesis in preparation), the changes in signalling networks mediating radioresistance in head and neck cancer cell lines (Tim Rose, Master thesis), the effect of KRAS and NRAS mutations in inducible colon cancer cell lines (Mert Dikmen, Master thesis), the effect of RAS isoforms oncogenic mutations in the colon cancer cell line SW48 (Hood et al., 2019), the cell type specific differences in signalling of intestinal mouse organoids (Brandt et al., 2019), B-cell-receptor signalling in B-cell Lymphoma cell lines (Bertram Klinger, manuscript in preparation), and signalling in human patient-derived colon cancer organoids (Bertram Klinger, manuscript in preparation). Overall, STASNet has proven a versatile toolbox for users less versed in programing and in multiple contexts, and should prove a useful tool to analyse data coming from new perturbation methods.

Recent years have brought tremendous progresses in single cell technology and 3D cell culture, both for cell lines and for organ-like multicellular structures called organoids (Simian and Bissell, 2017; O'Connell and Winter, 2020). Both technologies offer new ways of apprehending signalling networks, where 3D culture systems take into account inter-cellular interactions and single cell technology disentangles the resulting heterogeneity and cell type specificities. While perturbing signalling network in tumour patients will remain extremely challenging as only one treatment after another can be attempted in a changing tumor environment, *ex vivo* cultures such as organoids are an option to provide personnalised signalling analysis, as so called "avatar" (Brandt et al., 2019; Saez-Rodriguez and Blüthgen, 2020; Driehuis et al., 2020). The features of robustness and vulnerability learned from signalling models trained on cell line panels can be used to reduce the set of perturbations required in these avatars to inform a model rapidly and at reduced cost so as to predict efficient treatment options. Additionally, new approches such as CROPseq (Datlinger

et al., 2017) and Perturb-Seq (Dixit et al., 2016) represent important progress compared to individual knock-outs and allow the perturbation of non-druggable targets at high throughput and reasonable cost to study the interaction networks in greater detail. While RNA sequencing gives a good overview of the state of the cell, important cell fate decisions such as apoptosis or cell division are mediated directly via post-translationnal modifications. Methods such as CyTOF (Bendall et al., 2011) or targeted phosphoproteomics (Osinalde et al., 2017) promise to increase the number of signalling readouts at a decreased cost. Combined, these approaches offer rich datasets and STASNet has already been used to study the specificities of the signalling network in the different cells types present in colon cancer organoids (Brandt et al., 2019), forecasting a potential use to study signalling networks closer to the patients. STASNet and other similar tools that disentangle perturbation responses should see increased use as richer and more complex data are generated.

Chapter 7

Materials and methods

7.1 Cell culture

7.1.1 Colorectal cancer cell lines

The Widr and Widr-SHP2-KO cell lines were provided by Anirudh Prahallad (Netherlands Cancer Institute, Amsterdam) and cultured in RPMI Medium 1640 with phenol red (Gibco, Life Technologies), 20 mM L-glutamine (Gibco, Life Technologies), 100 U/ml Penicillin and Streptomycin (Sigma), and 10% FCS (Pan Biotech).

7.1.2 Neuroblastoma cell lines

The neuroblastoma cell lines IMR32, KELLY, CHP212, LAN6, NGP, NBEBC1, SKNAS, SKNSH and N206 were obtained courtesy of Jasmin Wünschel (Deubzer lab, Charité, Berlin) as member of the Terminate-NB consortium. The identity of the cell lines was confirmed with STR profiling Table 7.1 generated by Eurofins Cell Line Authentification Test and matched with the Cellosaurus STR similarity research tool (Robin et al., 2019).

All neuroblastoma cells were grown in DMEM (Gibco, Life Technologies) with 3.5% glucose (Sigma), 5 mM L-glutamin (Gibco, Life Technologies) and 10% FCS (Pan Biotech).

Table 7.1: Top 3 matches from STR profiling of our neuroblastoma cell lines panel.

Accession	Name	Score
IMR32	Query	NA
CVCL_0346 Best	IMR-32	100.00%
CVCL_0346 Worst	IMR-32	93.88%
CVCL_1306	IMR-5	100.00%
KELLY	Query	NA
CVCL_2092 Best	Kelly	100.00%
CVCL_2092 Worst	Kelly	95.24%
CVCL_2338	CCD-1086Sk	66.67%
CHP212	Query	NA
CVCL_1125 Best	CHP-212	100.00%
CVCL_1125 Worst	CHP-212	95.24%
CVCL_Y008	CE146T/VGH	69.23%
LAN6	Query	NA
CVCL_1363	LA-N-6	100.00%
CVCL_1817	Granta-452	81.48%
CVCL_VF96	149RCa	72.00%
NGP	Query	NA
CVCL_HG08	N_N20R1	100.00%
CVCL_2141	NGP	96.55%
CVCL_1809	CAL-78	69.23%
NBEBC1	Query	NA
CVCL_E218	NB-EbC1	98.04%
CVCL_2427	Detroit 510	71.43%
CVCL_2558	LB253	71.43%
SKNAS	Query	NA
CVCL_RR29	SK-N-ASr OXALI4000	92.86%
CVCL_AQ53	SK-N-RA	88.14%
CVCL_1700	SK-N-AS	88.00%
SKNSH	Query	NA
CVCL_0F47	SH-EP1	88.00%
CVCL_0019	SH-SY5Y	75.00%
CVCL_0531	SK-N-SH	75.00%
N206	Query	NA
CVCL_0650	Hs 14.T	83.33%
CVCL_2092 Best	Kelly	73.68%
CVCL_2092 Worst	Kelly	69.09%

7.2 Drug sensitivity

7.2.1 Growth rate measurements

I measured the growth rate using the Incucyte ZOOM (Essen BioScience). The cells were seeded in 24 well plates and imaged every 2-4 hours for 3-5 days depending on their growth rate. The phase confluence was computed for each image using the Basic Analyzer function of the Incucyte ZOOM software (Essen BioScience). Phase confluence data were then exported in csv format and imported in R for analysis using the R package incucyter.

7.2.2 Drug sensitivity computation

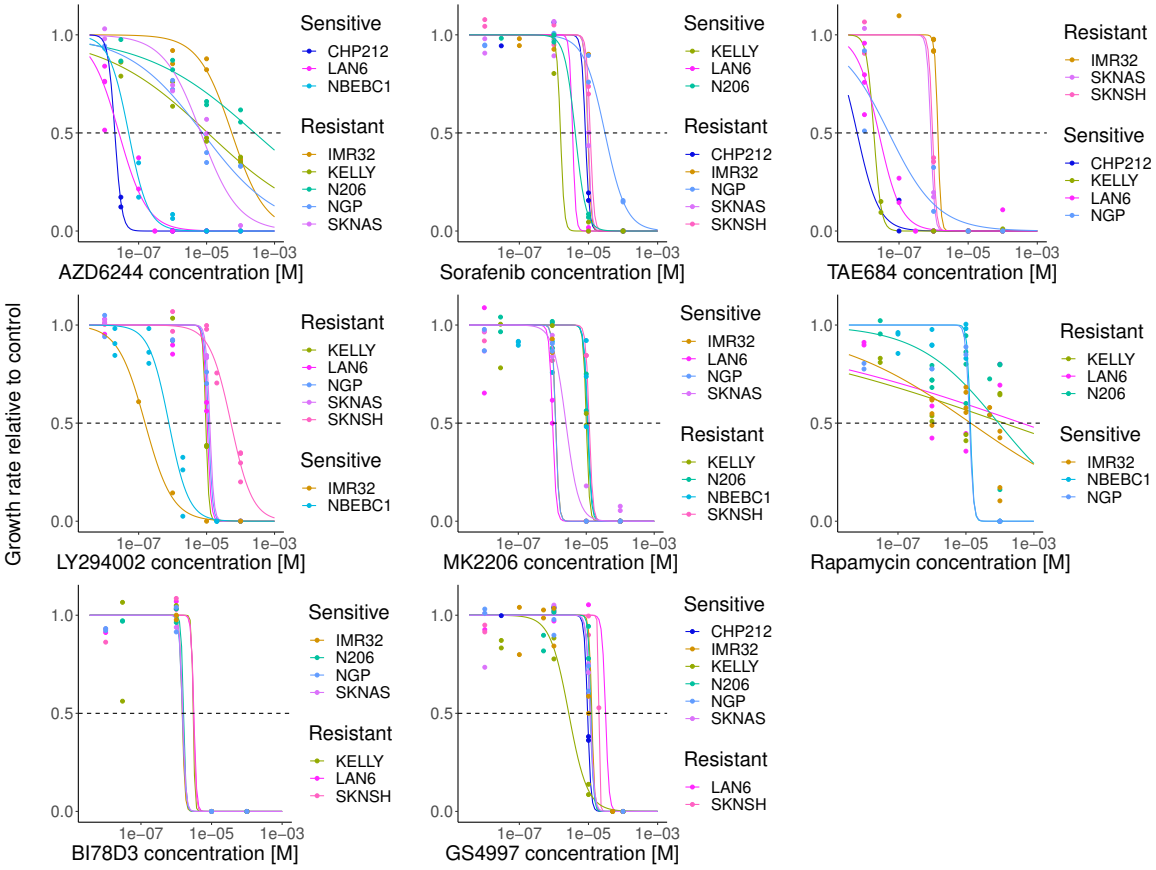

Figure 7.1: Dose-response curve for the viability of 9 neuroblastoma cells lines to the inhibitors. Sensitive or Resistant status was determined using a k-means clustering of the fitted log(IC50) with $k = 2$.

I implemented the R package drugResistance to compute IC50 values from growth data. First, the growth rate of each well is computed by fitting an exponential growth to the data with a threshold at 90% confluence, then normalised to the growth rate of

the control in the same plate. Second, the IC50 value for a given drug d is determined by fitting a logistic function:

$$GR(C^d) = \frac{1}{1 + \exp(-\log(C^d) + IC50^d) \times S^d} \tag{7.1}$$

where C^d is the concentration of drug d, S^d is the slope and $\mathrm{GR}(C^d)$ is the growth rate relative to the control at concentration C^d. The fit was done using the `nlsLM` function from the *minpack.lm* R package, which implements the Levenberg-Marquardt algorithm, with objective function $GR^d(C_i^d) - GR(C)$ where C_i^d is the ith measurement for drug d. In total, I measured the drug response of 9 neuroblastoma cell lines to 8 different drugs Figure 7.1.

7.3 RNA and DNA Sequencing

DNA and RNA were extracted from the human neuroblastoma cell lines, using the NucleoSpin Tissue kit (Macherey-Nagel) according to the manufacturer's protocol by Dr. Michal Nadler-Holly and Dr. Matthias Ziehm (Selbach lab, Max-Delbrück Center for Molecular Medicine, Buch), who also prepared the libraries and sent them for sequencing to the DKFZ. Primary bioinformatics processing (alignment and quality control) was performed by Dr. Joern Toedling, Dr. Eric Blanc and M.Sc. Clemens Messerschmidt (Biofinformatics Core Unit, Berlin Institute of Health, Berlin).

From the DNA, libraries for whole-exome sequencing were prepared using the SureSelect Human All Exon V7 kit (Agilent) and the Illumina TruSeq Exome kit. The libraries were sequenced on Illumina HiSeq 4000 and Illumina NovaSeq 6000 sequencers. The read sequences and base quality scores were demultiplexed and stored in Fastq format using the Illumina bcl2fastq software v2.20. Adapter remnants and low-quality read ends were trimmed off using custom scripts. The quality of the sequence reads was assessed using the FastQC software. Reads were aligned to the human genome, assembly GRCh38, using the bwa mem software version 0..10 (Li, 2013), and duplicate read alignments were removed using samblaster version 0.1.24 (Faust and Hall, 2014). Copy-number alterations were determined using cnvkit version 0.1.24 (Talevich et al., 2016). Single-nucleotide variants (SNVs) were identified using strelka version 2.9.10 (Kim et al., 2018). Afterwards, potential germline variants were filtered out by excluding all SNVs that had also been observed in at least 1% of samples in cohorts of healthy individuals, namely the 1000 Genomes Project (Auton et al., 2015) and the NHLBI GO Exome Sequencing Project (Fu et al., 2013) cohorts.

The RNA from the cell lines was extracted and sequenced in three separate batches. The IMR32, KELLY, SKNAS, LAN6, NBEBC1 cell lines were prepared in triplicate, using a paired-end stranded protocol with 2x75 cycles per fragment and 2 more cell lines (NGP, SKNSH) were prepared in duplicate, using a paired-end stranded protocol

with 2x150 cycles. Two more libraries (CHP212 and N206) were prepared using a paired-end stranded protocol with 2x75 cycles per fragment.

Raw sequencing data were rigorously checked for quality using FastQC. The reads were aligned to the human genome GRCh38 (without patches or haplotypes) and the GENCODE transcript annotation set using the STAR aligner software (Dobin et al., 2013). The read counts per gene were obtained using the featurecounts (Liao et al., 2014) method from the subread software package.

The raw data (RNAseq and WES) are available on ENA under the accession number PRJEB40670.

7.4 Perturbation treatments

For perturbation experiments, cells were grown for 3 days to 80% confluency in medium with 10% FCS, then starved overnight (16 to 24 hours) in medium without FCS. Inhibitors were added to the medium 60 minutes (or 3h30 for the phosphoproteomics) before the ligands and the cells were washed with cold PBS and lysed using BioRad lysis buffer 30 minutes after the addition of ligands (Figure 7.2).

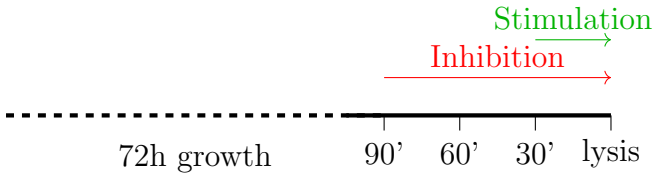

Figure 7.2: Perturbation treatment timeline.

7.5 Bead-based phosphoprotein measurements

I followed the protocol and buffers provided by ProtAtOnce or Bio-Plex for phosphoprotein detection depending on the kit being used. Protein concentration was determined using a BCA Protein Assay (ThermoFischer). Cell lysates were first incubated with magnetic beads coupled to total protein antibodies for at least 90 minutes and washed 2 times. The beads were incubated with the phosphoprotein-specific activin-coupled antibodies for 30 minutes to 1 hour and washed 3 times. Finally the beads were incubated for 15 minutes in streptavidin-phycoerythrin (SAPE), washed twice and resuspended in 120 μL of buffer before being measured using a Bio-Plex MagPix Multiplex Reader.

The MagPIX eXponent software produces lxb files, which follows the Flow Cytometry Standard 3.0 (FCS3) format (Seamer et al., 1997). I imported those data in R using the *lxb* package (Winckler, 2016). I first filtered out beads flagged as invalid by eXponent's preprocessing then removed all beads that have values too close to 0

by removing beads with values $< 0.1 \times$ 5th-percentile(bead_values). Those close to 0 beads are likely beads from former runs stuck in the chamber of the MagPIX whose attached phycoerythrine has been bleached and therefore not a true signal. Finally, I estimated the signal using a boostrap procedure. Assuming a normal distribution of the values, the median is bootstrapped one million time as a more robust estimate for the mean and a confidence interval is estimated taking the 2.5% and 97.5% most extreme bootstrapped values to estimate noise.

7.6 Western Blot

M.Sc. Anja Sieber performed most of the Western Blots from lysates that I provided. Cell lysates were denatured in 4% SDS and 10% Mercaptoethanol, run for 3h at a constant 45 mA in 10% acrylamid gels and blotted for 45 minutes at 400 mA on nitrocellulose. The membranes were stained for total protein using Pierce Reversible Protein Stain (Thermofischer 24580) and blocked for 30 minutes in 1:1 PBS:Odyssey blocking buffer. The primary antibodies were incubated overnight at 4C and the corresponding secondary antibodies during the following day for 2h at room temperature in 1:1 PBST/Odyssey. Total MYCN primary antibody (Santa Cruz sc-53993) was used at a 1:200 dilution.

7.7 Bulk proteomics and phosphoproteomics measurements

All (phospho-)proteomics were measured and preprocessed by Matthias Zhiem and Tommaso Mari (Selbach lab, Max-Delbrück Center for Molecular Medicine, Buch).

They used an adapted version of the TMT workflow (Mertins et al., 2018). Samples were reduced, alkylated and digested with a combination of LysC (Wako) and Trypsin (Promega) using the the single-pot, solid-phase-enhanced sample preparation (Hughes et al., 2019). For each sample, an equal amount of peptide was then chemically labelled with TMTpro reagents (Li et al., 2020). Samples were randomly assigned to one of the first 15 TMT channels, while the 16th channel was composed of a superset of all the samples to allow multi-plex normalisation. Equal amounts of the labelling reactions were combined in two TMT16 plexes, desalted via SepPak columns (Waters) and fractionated via high-pH fractionation (Batth et al., 2014) on a 96 minutes gradient from 3 to 55% acetonitrile in 5 mM ammonium formate, each fraction collected for 1 minute then combined into 24 fractions. From each fraction, an aliquot was used to measure the total proteome while the remaining peptides were combined into 12 fractions and used as input for an immobilised metal affinity chromatography using an Agilent Bravo system. For the total proteome analysis, peptides were on-line fractionated on a multi-step gradient from 0 to 55% acetonitrile in 0.1% formic acid

prior injection in a QExactive HF-x mass spectrometer. Samples were acquired using a data dependent acquisition strategy with MS1 scans from 350 to 1500 m/z at a resolution of 60 000 (measured at 200 m/z), maximum injection time (IT) of 10 ms and an automatic gain control (AGC) target value of 3×10^6. The top 20 most intense precursor ions with charges from +2 to +6 were selected for fragmentation with an isolation window of 0.7 m/z. Fragmentation was done in an HCD cell with a normalised collision energy of 30% and analysed in the detector with a resolution of 45 000 (200 m/z), AGC target value of 10^5, maximum IT of 86 ms. The phosphoproteome analysis used same parameters with the exception of MS2 maximum IT that was set to 240 ms.

The acquired raw files were analysed using MaxQuant v1.6.10.43 (Tyanova et al., 2016), with TMTpro tags manually added as fixed modifications and used for quantitation. The correction factors for purity of isotopic labels was set according to vendor specification and minimum reporter precursor intensity fraction was set to 0.5. The resulting protein groups were filtered for potential protein contaminants, protein groups only identified via peptides decorated with modification or hits in the pseudo-reverse database used for FDR control. The resulting intensities of each sample channel were normalised to the intensity of the 16th reference channel, then median-centered and normalised according to the median-absolute deviation. Identified phosphopeptides were similarly filtered, with the exception of filtering based on modified sites, and normalised using the same strategy.

7.7.1 Differential expression analysis

Finally, I analysed the (phospho-)proteomics data in R. Differentially expressed phosphopeptides were called using the *limma* package (Ritchie et al., 2015) with a false discovery rate of 0.05 on treatment minus control contrasts. Synergies were computed using a contrast fit of the combination minus the sum of single treatments. Kinase substrate activity was implemented in R using the ratio of the mean z-score as described in Casado et al. (2013) and computed for kinase-substrate sets from PhosphoSitePlus (Hornbeck et al., 2015). The normalised intensities and scripts used for the analysis can be found at `https://itbgit.biologie.hu-berlin.de/dorel/phosphoproteomics_tnb_perturbations`.

7.7.2 Gene set enrichment analysis

Gene set enrichment analysis was performed using the proteins corresponding to the enriched phosphopeptides. GO Biological Process and KEGG enrichments were computed using the package clusterProfiler (Yu et al., 2012). The background universe was build from the data, taking all proteins corresponding to phosphopeptides measured in at least one sample.

Chapter 8

Appendix

A Statistical testing and identifiability in STASNet

A.1 Building identifiable parameter combinations

Due to limitations inherent to the experimental system, not all nodes in a network can be measured. Non measurable nodes can also arise because of the aforementioned network adaptations imposed by the exact mode of action of inhibitors. If all links were fitted, this would give rise to structural non-idenfiability, where changes in links upstream of a non-measured node can be perfectly compensated by variation of links downstream of this node and vice versa, this corresponds to a multiplicative non-identifiability (Ljung and Glad, 1994). Those structural non-identifiabilities can be detected in the symbolic global response matrix by the fact that local response parameters from r always appear in combination with others in the measured entries of R. It is possible to fit combination of links, hereafter named paths because they consist in following multiple links through the network, instead of single links. While this is trivial for linear, converging and diverging paths, where unmeasured nodes have one input or one output, this task is more complicated for hubs, nodes with multiple inputs and outputs (see Figure Appendix.1 that will be used as an example), or if networks involve feedbacks. STASNet implements a path reduction approach that permits very detailed networks independent of experimental conditions and guarantees that only structurally identifiable paths will be fitted.

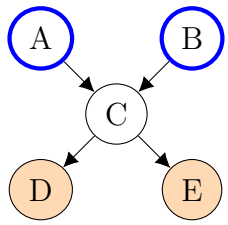

(a) Network structure

$$\mathbf{r}^{-1} = \begin{array}{c} \\ A \\ B \\ C \\ D \\ E \end{array} \begin{array}{c} \begin{array}{ccccc} \boxed{A} & \boxed{B} & C & D & E \end{array} \\ \begin{pmatrix} -1 & 0 & 0 & 0 & 0 \\ 0 & -1 & 0 & 0 & 0 \\ r_{CA} & r_{CB} & -1 & 0 & 0 \\ r_{CA}r_{DC} & r_{CD}r_{DB} & r_{DC} & -1 & 0 \\ r_{CA}r_{EC} & r_{CB}r_{EC} & r_{DE} & 0 & -1 \end{pmatrix} \end{array}$$

(b) Inverted local response matrix

Figure Appendix.1: Example network containing a node with multiple inputs and outputs. Blue frame indicate stimulated nodes and orange background indicates measured nodes. A single stimulation of node A and a combined stimulation of nodes A and B is performed. This experimental setup gives 3 degrees of freedom for a network containing 4 links.

A path R_l corresponds to a product of links in the r^{-1} matrix and can thus be expressed as

$$P_l = \prod_{j,k} (r_{jk})^{a_{jkl}} \qquad \text{(Appendix.1)}$$

with a_{jkl} being the exponent of r_{jk} for path P_l , i.e. the number of times a response coefficient occurs in a path (typically 0 or 1). Taking the logarithm of that equation,

$$\log P_l = \sum_{j,k} a_{jkl} \log r_{jk} \qquad \text{(Appendix.2)}$$

the path equations represent a set of linear equations that can be represented in matrix form,

$$[A, -I] \times (\log r_{11}, r_{12}, \ldots, \log r_{NN}, \log P_1, \ldots, logP_M)^T = 0 \qquad \text{(Appendix.3)}$$

where M is the number of paths, A contains the links multiplicity a_{jkl} and I is the identity matrix. If A is constructed with the combinations of links that are present in matrix R, rank(A) corresponds to the number of identifiable coefficients given the perturbations used and nodes measured.

$$\mathbf{R} = \begin{array}{c} \\ D \\ E \end{array} \begin{pmatrix} \boxed{S_A} & \boxed{S_A + S_B} \\ \boxed{r_{CA}r_{DC}} & \boxed{r_{CA}r_{DC}} + \boxed{r_{CD}r_{DB}} \\ \boxed{r_{CA}r_{EC}} & \boxed{r_{CA}r_{EC}} + \boxed{r_{CB}r_{EC}} \end{pmatrix} = \begin{pmatrix} \boxed{P_1} & \boxed{P_2} + \boxed{P_3} \\ \boxed{P_4} & \boxed{P_5} + \boxed{P_6} \end{pmatrix}$$

Figure Appendix.2: Path derivation for the example network. Blue frames indicate stimulation, orange backgrounds indicate measured nodes and red frames indicate paths.

Applying Gaussian elimination on the rows to $[A, -I]$ yields a matrix of the form

$$G = \left[\begin{array}{c|c} A' & G_1 \\ \hline 0 & G_2 \end{array}\right] \qquad \text{(Appendix.4)}$$

G_2 provides the rules to replace the superfluous paths as combination of the identifiable paths. Indeed they are superfluous because G_2 is also in row echelon form, the leading 1s of each row thus correspond to columns otherwise filled with 0s. The following non-zero entries of the line thus indicate by which combination of non-superfluous paths they can be replaced. Once this replacement is performed the remaining paths, which have no leading entry in G_2, are multiplicatively independent.

In our example P_3, P_5 and P_6 are thus the only paths that are required to calculate the combinations of response coefficients (i.e. that have non-zero entries in the upper-right submatrix G_1). The lower right submatrix, G_2 can now be used to replace the paths that are linearly depending on the other paths. For this example, it follows from the 4^{th} row of G that $\log P_1 = -\log P_3 + \log P_5 + \log P_6$, i.e $P_1 = \dfrac{P_5 P_6}{P_3}$. Similarly

$$G = \begin{array}{c} \\ P_1 \\ P_2 \\ P_3 \\ P_4 \\ P_5 \\ P_6 \end{array} \begin{array}{c} \begin{array}{cccc} r_{CA} & r_{CB} & r_{DC} & r_{EC} \end{array} \\ \left(\begin{array}{cccc|cccccc} 1 & 0 & 1 & 0 & 0 & 0 & -1 & 0 & 1 & 1 \\ 0 & 1 & 1 & 0 & 0 & 0 & 0 & 0 & 1 & 1 \\ 0 & 0 & 1 & -1 & 0 & 0 & 0 & 0 & 0 & 1 \\ \hline 0 & 0 & 0 & 0 & 1 & 0 & 1 & 0 & -1 & -1 \\ 0 & 0 & 0 & 0 & 0 & 1 & 1 & 0 & -1 & -1 \\ 0 & 0 & 0 & 0 & 0 & 0 & 0 & 1 & -1 & 0 \end{array}\right) \end{array} \begin{array}{c} \\ P_1 \\ P_2 \\ P_3 \\ P_4 \\ P_5 \\ P_6 \end{array}$$

Figure Appendix.3: Matrix resulting from of the gaussian elimination of $[A, -I]$ for the network depicted in Figure Appendix.1

the remaining paths can be replaced as $P_2 = \frac{P_5 P_6}{P_3}$ and $P_4 = P_5$. We are left with the following identifiable parametrisation:

$$\mathbf{R} = \begin{array}{c} \\ D \\ E \end{array} \begin{array}{c} \begin{array}{cc} \boxed{S_A} & \boxed{S_A + S_B} \end{array} \\ \begin{pmatrix} \frac{P_5 P_6}{P_3} & \frac{P_5 P_6}{P_3} + P_3 \\ P_5 & P_5 + P_6 \end{pmatrix} \end{array}$$

Note that the initial order of the rows and columns in A is arbitrary. Different orders may lead to different (equivalent) parameterisations of the MRA model. STASNet implements a heuristic to reorder the rows such that the final paths contain mainly products of response coefficients with exponent 1, making it easier to interprete and visualise the paths.

In some cases, no identifiable parametrisation with only positive exponents for the links can be found. STASNet thus also provides a function *getDirectPaths* to convert the set of identifiable paths into a set of paths potentially redundant but only containing positive exponents for the local response coefficients. Those direct paths can then be compared between models with *aggregateDirectPaths* and visualised with *plotParameters*.

A.2 Testing for model reduction

During model reduction, I test whether the reduced model explains the data as well as the complete model using an χ^2-test:

$$\chi^2 = \frac{\text{abs}(RSS_{complete} - RSS_{reduced})}{rank_{complete} - rank_{reduced}} \qquad \text{(Appendix.5)}$$

This compares the gain provided by the link to the estimated noise (which is integrated into RSS). This follows a χ^2-distribution with $df = rank_{complete} - rank_{reduced}$. If the computed χ^2-statistic is inferior to the threshold determined from a χ^2-distribution with the complement to 1 of the type I error ($\sim \chi^2(1-\alpha)$), it means the link does not provide any extra information and it thus not necessary to explain the data.

A.3 Error model

Each measurement $y_{r,i}$ of readout r under perturbation i follows a normal distribution $\mathbb{N}(\bar{y}_{r,i}, \sigma_{r,i})$. We consider that the readout is the main factor of deviation due to protein abundance and specificity of the detection system. All measurements for one readout have the same coefficient of variation CV_r, thus $\sigma_{r,i} \sim \mathrm{CV}_r \times y_{r,i}$.

To compute the residual sum of square, we need the error of the term $y_{r,i} - y^p_{r,i}$, with $y^p_{r,i} = p_{r,i} \times y^0_r$ being the model prediction, $p_{r,i}$ the combination of parameters fitted by the model and y^0_r the value of the readout in the control. y^0_r follows a normal distribution $\mathbb{N}(\bar{y}^0_r, \mathrm{CV}_r \bar{y}^0_r)$. Thus the error $\hat{\sigma}_{r,i}$ of the residual term is:

$$\hat{\sigma}^2_{r,i} = (\mathrm{CV}_r \bar{y}_{r,i})^2 + (p_{r,i}\mathrm{CV}_r \bar{y}^0_r)^2 - 2 \times \mathrm{cor}(y_{r,i}, y^p_{r,i}) \qquad \text{(Appendix.6)}$$

$\mathrm{cor}(y_{r,i}, y^p_{r,i}) \sim 0$ because $y_{r,i}$ and y^0_r are independent measurements. Moreover if the fit is correct, then $\bar{y}_{r,i} \sim p_{r,i}\bar{y}^0_r$. So $\hat{\sigma}_{r,i} \sim \sigma_{r,i}$ and $\sqrt{2}\sigma_{r,i}$ can be used as a relatively good estimator of the error of the terms of the residual sum of square.

Different error models considered

The first error model that was used was $\sigma_{r,i} = \mathit{blank}_r + \mathit{CV}_r \times \mathit{measured\_signal}_{r,i}$ but this error formulation did not account properly for the signification of background noise which the *blank* represents. It was changed to $\sigma_{r,i} = \mathit{CV}_r \times \mathit{measured\_signal}_{r,i}$ with the *blank* introduced as the minimum signal that the model would produce during the fitting procedure ($\mathit{fit}_{r,i} = \max(\mathit{blank}_r, \mathit{prediction}_{r,i})$). However this second implementation presents the problem of giving too much importance to low signals (arising mainly from inhibitions) compared to high signals (arising mainly from stimulations).

Indeed in the simple case of one readout with 2 measurements using the same parameter p (either fit duplicates directly or a simple perturbation vs the same perturbation plus an unrelated other perturbation) the residual is of the form:

$$\chi^2 = (V_1 - py^0)^2/e_1^2 + (V_2 - py^0)^2/e_2^2 \qquad \text{(Appendix.7)}$$

where V_1 and V_2 are values measured after perturbation with respective errors e_1 and e_2 and y^0 is the value measured for the control.

$$\frac{d\chi^2}{dp} = \frac{-y^0 * 2(V_1 - py^0)}{e_1^2} + \frac{-y^0 * 2(V_2 - py^0)}{e_2^2} \qquad \text{(Appendix.8)}$$

$$\frac{d\chi^2}{dp} = 0 \Rightarrow p = \frac{V_1 e_2^2 + V_2 e_1^2}{2y^0(e_1^2 + e_2^2)} \qquad \text{(Appendix.9)}$$

thus the residual (and best fit for the parameter) depends differently on the 2 measurements with the square of the error of the other measurement, giving an overinflated

importance to the lower measurement in the CV model (even corrected) despite having no reason to believe it more than the other. This is linked to the problem of regression.

This proved a problem to correctly fit PDGF stimulation in SK-N-SH as the error of the PDGF+RAFi (which negates the effect of PDGF because of the off-target activity of Sorafenib as a PDGFR inhibitor) was so low that this condition dominated the fit. The same problem was visible for ALKi whose effect was not fitted anywhere else than for IGF1+ALKi where the signal was lower (because TAE684 also targets IGF1R at the concentration used) (Figure 4.6).

Because of the way the C library levmar works, it is not possible to provide an error that depends on the prediction. The computationaly intensive alternative to give a value of 0 for the error and directly compute the residual with an error depending on the prediction was not retained.

The error model was thus corrected to include a minimum value for the error term equal to the mean error of the readout, so as to mitigate the effect of low value and increase the error for readouts with a higher dynamic range.

$$e_{r,i} = \min(\sigma_r, \sigma_{r,i}) \text{ with } \sigma_r = \text{mean}_i(\sigma_{r,i}) \qquad \text{(Appendix.10)}$$

Finally if we suppose that the control data is normally distributed and that the generating process for the data is exponential (i.e the signal is in the fold change), then we expect the perturbed data to be distributed according to a log-normal distribution. An alternative error model is implemented in STASNet (option `data_space='log'`) with a different calculation for the coefficient of variation: $CV = (\exp(\text{sd}(\log x)) - 1)\exp(2 \times \text{mean}(\log x) + \text{sd}(\log x))$.

B Detailed link extension for the TerminateNB neuroblastoma panel

Starting from a linear topology plus the well documented ERK→RAF feedback, the models are refined for each cell line using the results from `suggestExtension`.

To remove non identifiability linked to not measuring all inhibited nodes, we fix the inhibitors to concensus values and refit with this constraint.

B.1 SKNSH fitting summary

Initial linear model SKNSH

SKNSH linear model residual=650 df=33

from	to	value	residual	df	Res_delta	df_delta	pval	adj_pval
IGF1	ALK	-102.51	461.21	34	188.43	1	0	0
p38	TRKA	1	563.99	34	85.65	1	0	0
p38	ALK	3.99e-5	565.93	34	83.71	1	0	0
IL1b	TRKA	7.7e-6	568.51	34	81.13	1	0	0
TAK1	TRKA	3.6e-6	568.51	34	81.13	1	0	0
JNK	TRKA	3.6e-6	568.51	34	81.13	1	0	0
cJUN	TRKA	1	568.51	34	81.13	1	0	0
cJUN	ALK	2.85e-5	570.35	34	79.29	1	0	0
IL1b	ALK	5.64e-5	570.35	34	79.29	1	0	0
TAK1	ALK	2.51e-5	570.35	34	79.29	1	0	0

The first fit is very bad, 3 features need explaining: the low phosphorylation of AKT and S6K upon IGF1+ALKi, the low phosphorylation of AKT and S6K upon PDGF+RAFi and the high phosphorylation of AKT and S6K upon IL1b stimulation. Both low phosphorylation are likely due to offtarget activity of TAE684 on IGFRs (suggested by the IGF1→ALK extension) and Sorafenib and PDGFRs respectively so we change the experimental annotation to take it into account.

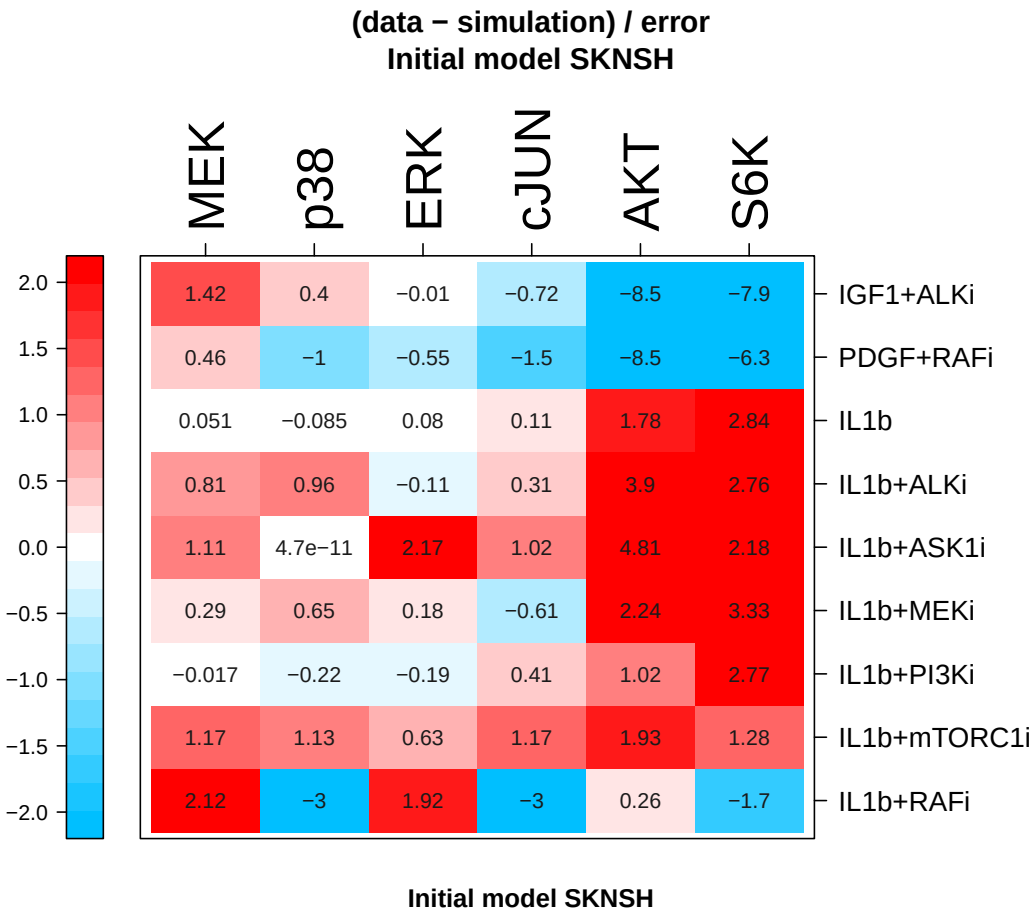

Dual inhibitor effect SKNSH

SKNSH dual inhibition model			residual=343	df=35				
from	to	value	residual	df	Res_delta	df_delta	pval	adj_pval
p38	ALK	8.47e-5	272.81	36	70.42	1	0	0
p38	TRKA	1	273.14	36	70.09	1	0	0
IL1b	ALK	1.7e-4	275.31	36	67.92	1	0	0
TAK1	ALK	4.74e-5	275.31	36	67.92	1	0	0
cJUN	ALK	7.43e-5	275.31	36	67.92	1	0	0
JNK	ALK	5.12e-5	275.31	36	67.92	1	0	0
TAK1	TRKA	0	275.56	36	67.67	1	0	0
JNK	TRKA	0	275.56	36	67.67	1	0	0
IL1b	TRKA	0	275.56	36	67.67	1	0	0
cJUN	TRKA	1	275.56	36	67.67	1	0	0

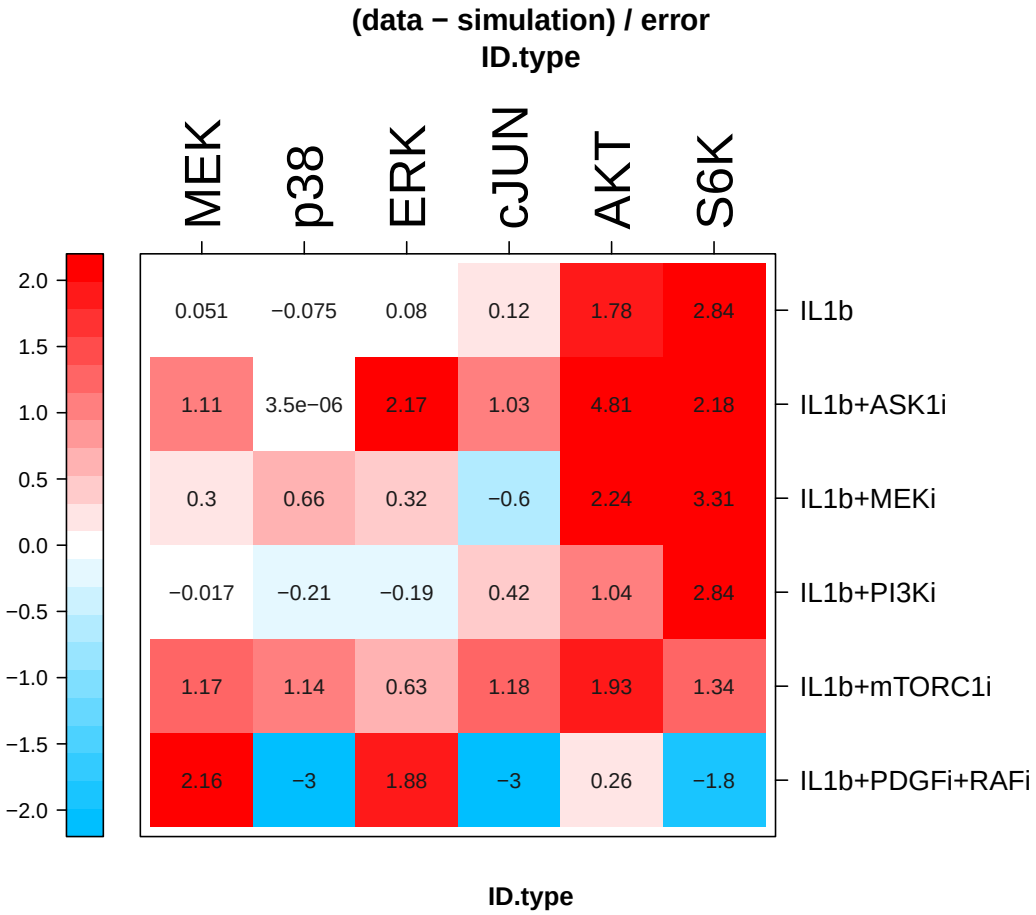

Including the offtarget effects of the inhibitors solved the low phosphorylation problem. To explain the activation of the PI3K pathway by IL1b would require a link from IL1b to this pathway, and IL1b→PI3K was deemed most relevant. The links proposed by the extension would have a similar effect by linking downstream targets of IL1b to activating receptors of the PI3K and MAPK pathways. However the activation of the MAPK1 pathway by IL1b is not supported by the data.

IL1b→PI3K SKNSH

SKNSH IL1b→PI3K model residual=313 df=36

from	to	value	residual	df	Res_delta	df_delta	pval	adj_pval
ERK	JNK	0.35	295.80	37	17.55	1	2.79e-5	6.19e-3
MEK	JNK	0.32	295.80	37	17.55	1	2.79e-5	6.19e-3
ERK	cJUN	0.35	295.80	37	17.55	1	2.79e-5	6.19e-3
MEK	cJUN	0.32	295.80	37	17.55	1	2.79e-5	6.19e-3
ASK1	S6K	2322.85	296.03	37	17.32	1	3.14e-5	6.97e-3
ASK1	mTORC1	2529.21	297.83	37	15.52	1	8.14e-5	0.01
p38	ALK	1.19e-4	302.19	37	11.16	1	8.3e-4	0.18
p38	TRKA	1.0e-5	302.42	37	10.93	1	9.4e-4	0.20
ALK	ERK	96.37	303.06	37	10.29	1	1.3e-3	0.29

SKNSH IL1b→PI3K		model	residual=313	df=36				
from	to	value	residual	df	Res_delta	df_delta	pval	adj_pval
p38	MEK	0.30	303.27	37	10.08	1	1.4e-3	0.33

This extension solved all the remaining major problems.
A significant MEK/ERK→JNK/S6K extension is suggested to solve cJUN downregulation upon Sorafenib treatment.

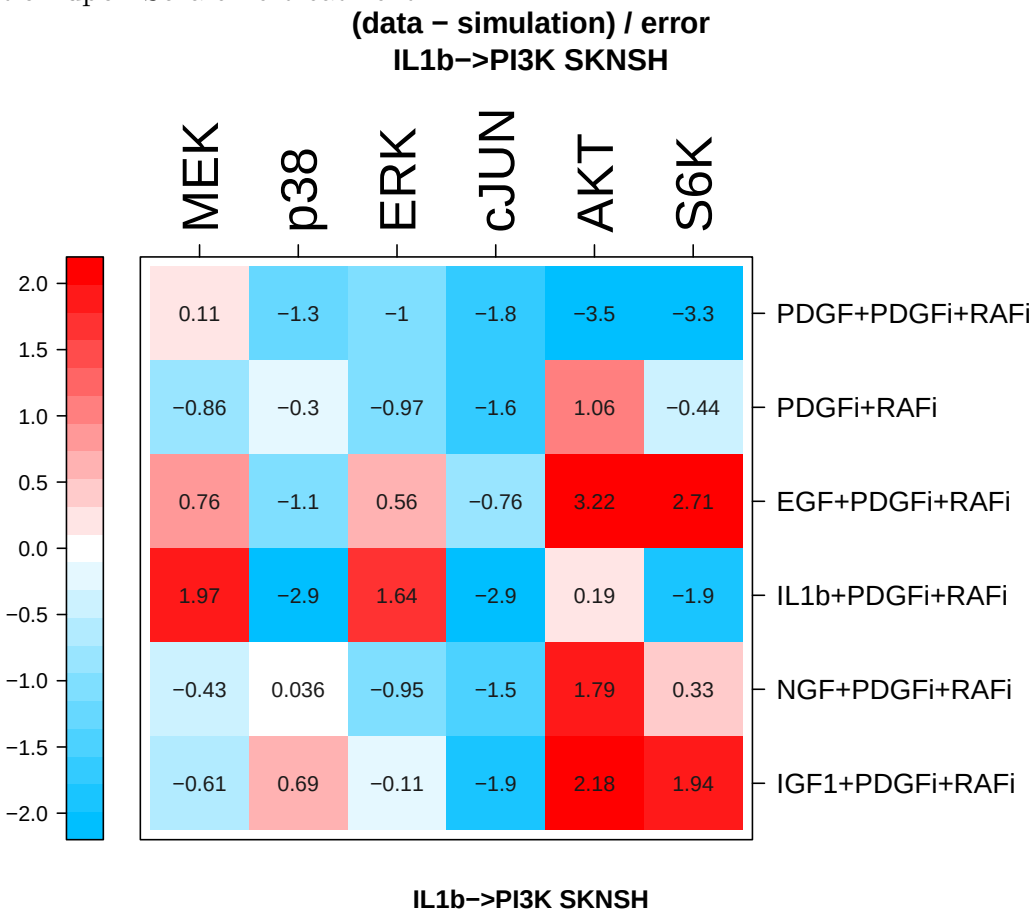

ERK→cJUN SKNSH

SKNSH ERK→cJUN model			residual=267	df=37				
from	to	value	residual	df	Res_delta	df_delta	pval	adj_pval
RAF	ALK	6.80	250.05	38	17.33	1	3.13e-5	6.92e-3
p38	TRKA	1	250.84	38	16.55	1	4.74e-5	0.01
p38	ALK	1.03e-4	251.33	38	16.05	1	6.14e-5	0.01
ASK1	TRKA	1.8e-6	251.37	38	16.01	1	6.28e-5	0.01
ALK	ERK	0.36	252.90	38	14.49	1	1.4e-4	0.03
ASK1	ALK	-2.19e-4	252.96	38	14.43	1	1.45e-4	0.03
cJUN	ALK	6.7e-5	252.98	38	14.41	1	1.46e-4	0.03
cJUN	TRKA	1	253.01	38	14.37	1	1.49e-4	0.03

SKNSH ERK→cJUN model residual=267 df=37

from	to	value	residual	df	Res_delta	df_delta	pval	adj_pval
p38	MEK	0.37	254.22	38	13.16	1	2.85e-4	0.06
p38	RAF	4.7e-6	254.22	38	13.16	1	2.85e-4	0.06

Those effects are seen in all cell lines, so this topology and the dual inhibition actions of TAE684 and Sorafenib are used in all cell lines However here, Sorafenib inhibits p38 and cJUN activation by IL1b which suggests that Sorafenib also inhibits the IL1b receptor.

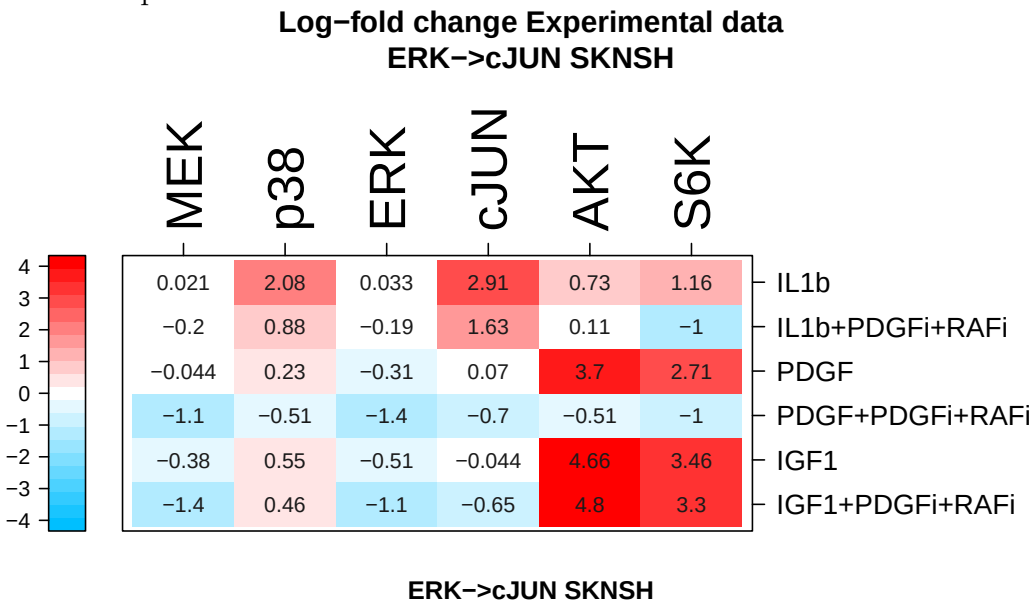

Sorafenib IL1b offtarget SKNSH

SKNSH IL1b offtarget effect model residual=241 df=38

from	to	value	residual	df	Res_delta	df_delta	pval	adj_pval
ASK1	S6K	2952.27	221.82	39	18.79	1	1.46e-5	3.22e-3
ASK1	mTORC1	1867.79	223.66	39	16.95	1	3.83e-5	8.45e-3
ALK	ERK	0.55	226.40	39	14.21	1	1.63e-4	0.03
JNK	S6K	0.04	228.40	39	12.20	1	4.75e-4	0.10
TAK1	S6K	0.04	228.40	39	12.20	1	4.75e-4	0.10
cJUN	S6K	0.20	228.40	39	12.20	1	4.75e-4	0.10
IL1b	S6K	0.44	228.54	39	12.07	1	5.1e-4	0.11
p38	S6K	0.28	228.85	39	11.76	1	6.02e-4	0.13
p38	TRKA	1	229.23	39	11.37	1	7.42e-4	0.16
IGF1	AKT	1.19	229.47	39	11.14	1	8.42e-4	0.18

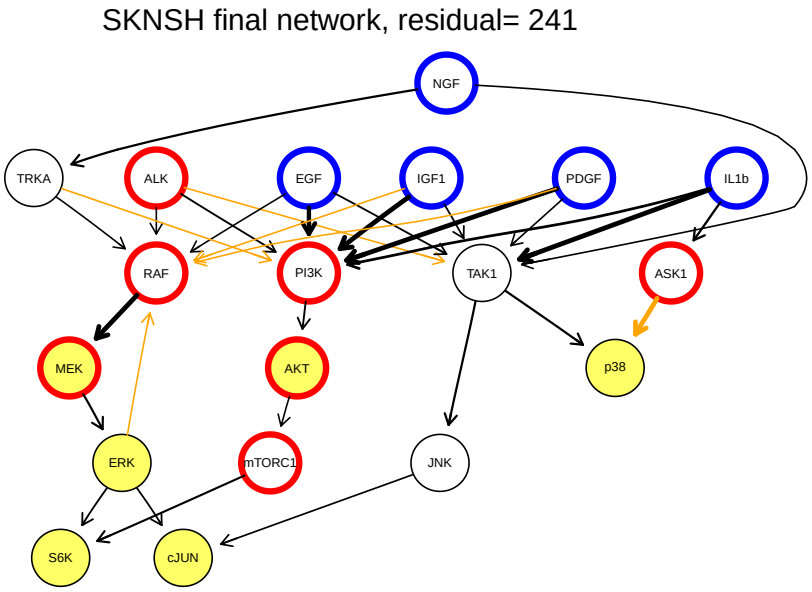

Final model reduction

Only receptor links would be removed so we keep them for inter-models comparison.

Removed Link	New residual	Delta residual	pval
ALK→ TAK1	240.61	0	2.2e-4
TRKA→ RAF	240.62	0	0.05
NGF→ TAK1	240.74	0.13	0.28
NGF→ TRKA	240.94	0.19	0.34
TRKA→ PI3K	240.94	0	0
ALK→ RAF	241.50	0.56	0.55
PDGF→ TAK1	242.05	0.55	0.54
IGF1→ RAF	243.90	1.85	0.83

Completely reduced model: "Best fit: 243.9 , Score= 0.89"

Final SKNSH model with fixed parameters

Fixing the inhibitor parameters is necessary to compare the models between cell lines because they create some non identifiability when non measured nodes are inhibited. The likelihood profiles for the final topology show many non identifiable parameters which become identifiable after fixing the inhibitor parameters. The value for the inhibitor parameters have been chosen after a good model for all cell lines was found and set to the majority value. The final SKNSH model with fixed parameters has a residual of 317.

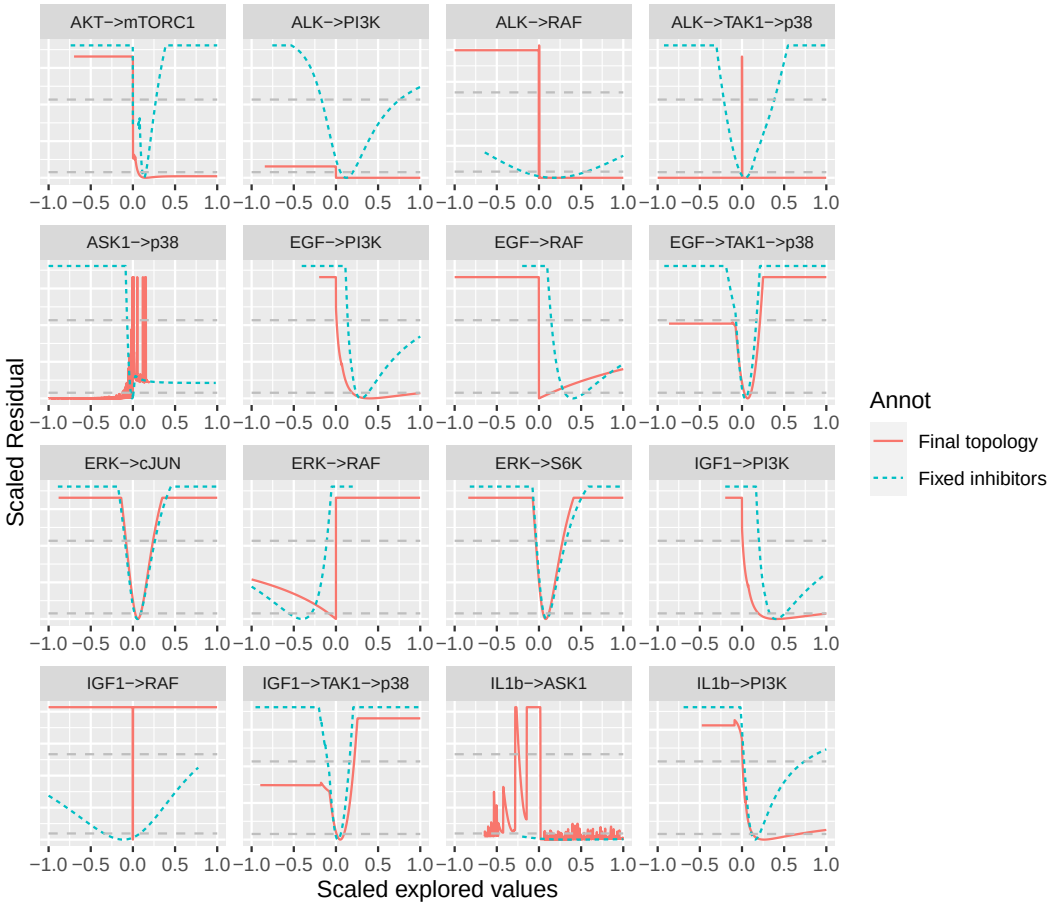

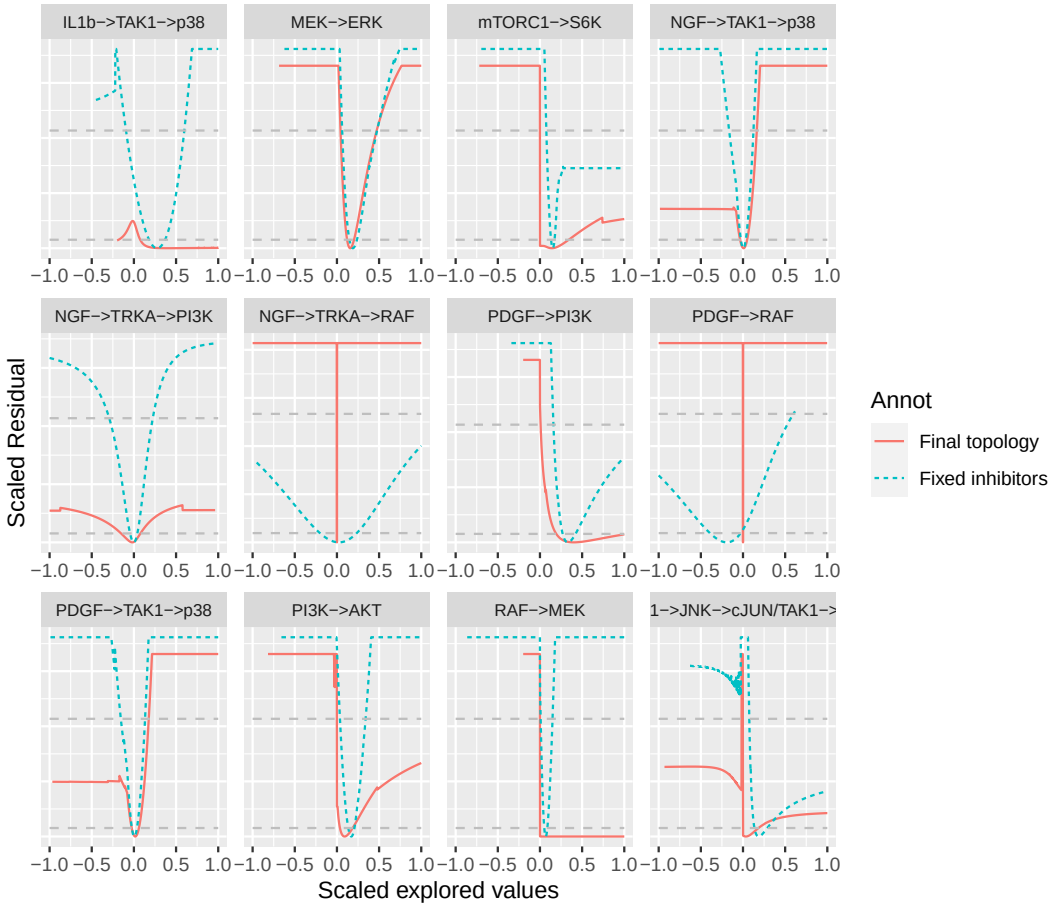

B.2 CHP212 fitting summary

CHP212 was fitted with a PDGF basal activity.

Initial topology CHP212

Initial CHP212 model			residual=278			df=34		
from	to	value	residual	df	Res_delta	df_d	pval	adj_pval
p38	mTORC1	-53.37	253	35	25	1	6e-07	1.4e-4
p38	S6K	-3.34	254	35	24	1	1e-06	2.2e-4
ASK1	S6K	8.80	259	35	19.2	1	1.1e-05	2.7e-3
ASK1	mTORC1	3.68	259	35	19.2	1	1.1e-05	2.7e-3
mTORC1	TAK1	1	259	35	18.9	1	1.3e-05	3.2e-3
S6K	TAK1	-0.06	260	35	18.3	1	1.9e-05	4.5e-3
S6K	RAF	3.55	262	35	16.2	1	5.7e-05	0.01
mTORC1	RAF	0.13	262	35	16.2	1	5.7e-05	0.01
S6K	cJUN	0.13	262	35	15.9	1	6.6e-05	0.01
mTORC1	JNK	7.6e-3	262	35	15.9	1	6.6e-05	0.01

Best extensions are ASK1/p38 → mTORC1/S6K. p38→S6K was choosen because it was found in other cell lines.

p38→S6K effect CHP212

CHP212 p38→ S6K model					residual=254	df=35		
from	to	value	residual	df	Res_delta	df_delta	pval	adj_pval
p38	ALK	0.10	200.9	36	53.14	1	0	0
ASK1	ALK	-5.32	201.0	36	53.04	1	0	0
p38	TRKA	1	204.8	36	49.24	1	0	0
p38	AKT	4.20	212.7	36	41.39	1	0	0
ASK1	PI3K	-101	212.9	36	41.14	1	0	0
ASK1	AKT	-5.89	212.9	36	41.14	1	0	0
p38	PI3K	5.59	212.9	36	41.14	1	0	0
ASK1	TRKA	138	214.0	36	40.10	1	0	0
mTORC1	TAK1	1	235.2	36	18.84	1	1.42e-05	3.37e-3
mTORC1	RAF	4.66	236.7	36	17.40	1	3.03e-05	7.22e-3

ASK1i still had unexplained effects on AKT and MEK that are adressed by the proposed extensions. The links to the receptor are unlikely, making p38/ASK1→AKT the best option.

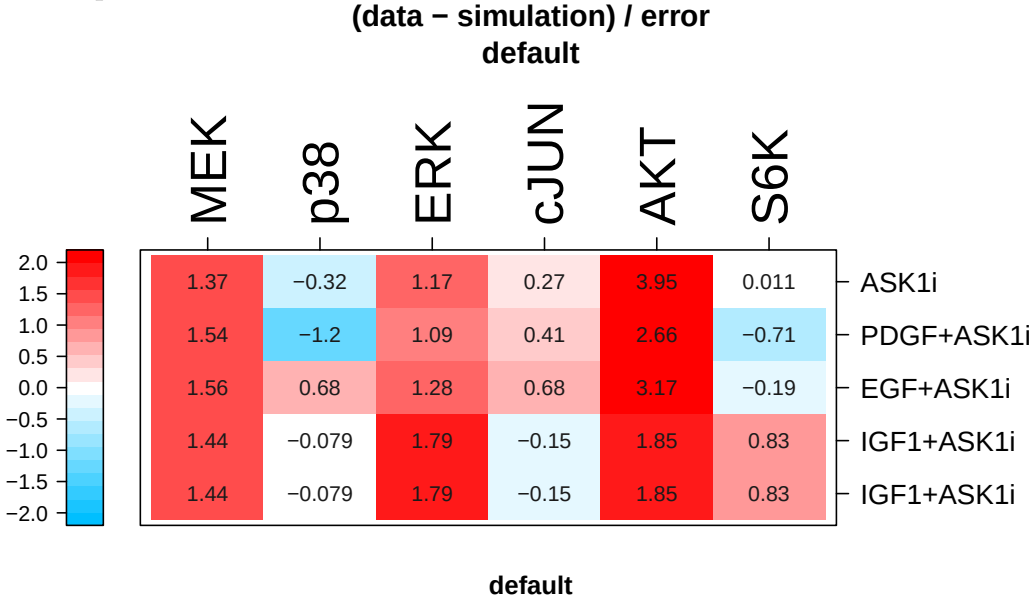

CHP212 ASK1→ AKT model			residual=214			df=36		
from	to	value	residual	df	Res_delta	df_delta	pval	adj_pval

ASK1→AKT effect CHP212

CHP212 ASK1→ AKT model			residual=214			df=36		
from	to	value	residual	df	Res_delta	df_delta	pval	adj_pval
mTORC1	TRKA	1e+0	188	37	25.3	1	5e-07	1.18e-4
mTORC1	RAF	5.3e+0	189	37	24.6	1	7e-07	1.69e-4
mTORC1	MEK	1.7e-1	191	37	22.8	1	1.8e-06	4.27e-4
mTORC1	TAK1	1e+0	192	37	22.1	1	2.6e-06	6.19e-4
S6K	TAK1	-4.6e-2	192	37	21.8	1	3.1e-06	7.32e-4
AKT	ALK	1.5e+0	192	37	21.7	1	3.2e-06	7.55e-4
S6K	TRKA	7.5e+0	196	37	17.7	1	2.5e-05	5.99e-3
S6K	JNK	1.4e-1	196	37	17.5	1	2.8e-05	6.68e-3
S6K	cJUN	1.4e-1	196	37	17.5	1	2.8e-05	6.68e-3
mTORC1	JNK	9.1e-2	197	37	17.0	1	3.8e-05	9.04e-3
mTORC1	cJUN	9.1e-2	197	37	17.0	1	3.8e-05	9.04e-3
cJUN	ERK	5.7e+0	198	37	15.6	1	7.6e-05	0.01
TAK1	ERK	-2.1e+5	198	37	15.5	1	8.3e-05	0.01
JNK	ERK	-1.6e+5	198	37	15.5	1	8.3e-05	0.01
p38	MEK	3.5e+0	199	37	15.0	1	1.1e-04	0.02
ASK1	ALK	-10e+1	199	37	15.0	1	1.1e-04	0.02
p38	ALK	7.0e-4	199	37	15.0	1	1.1e-04	0.02
ASK1	MEK	-7.9e+0	199	37	15.0	1	1.1e-04	0.02
S6K	RAF	2.9e+1	199	37	15.0	1	1.1e-04	0.02

This fit is good. The first extensions suggested would explain the high pMEK upon PI3Ki, AKTi and mTORC1i. However this is likely an overfitting, as the residuals are very low and the signals are not consistent, it would also fail to explain the low pERK upon those same inhibitions. Similarly mTORC1/S6K→TAK1/JNK/cJUN aims at explaining the slight downregulation of cJUN. Overall it appears like the only truly unexplained signal is MEK and ERK upregulation upon ASK1i so ASK1→MEK is selected.

ASK1→MEK effect CHP212

None of the best extensions significantly improve the model. There is however a strong suggestion of a crosstalk from mTORC1/S6K to JNK/cJUN.

CHP212 ASK1→ MEK model			residual=199			df=37		
from	to	value	residual	df	Res_delta	df_delta	pval	adj_pval
S6K	TAK1	-0.04	178.4	38	20.99	1	4.6e-6	1.09e-3
p38	ERK	-81.59	178.4	38	20.97	1	4.7e-6	1.09e-3
mTORC1	TAK1	1	179.1	38	20.33	1	6.5e-6	1.53e-3
S6K	cJUN	0.13	182.1	38	17.32	1	3.16e-5	7.45e-3
S6K	JNK	0.13	182.1	38	17.32	1	3.16e-5	7.45e-3
S6K	TRKA	7.06	183.3	38	16.16	1	5.82e-5	0.01
mTORC1	cJUN	0.08	184.2	38	15.26	1	9.38e-5	0.02
mTORC1	JNK	0.08	184.2	38	15.26	1	9.38e-5	0.02
cJUN	ERK	5.40	185.7	38	13.72	1	2.11e-4	0.04
TAK1	ERK	-276	185.7	38	13.71	1	2.13e-4	0.05

The model is already slightly overfitted, and all new extensions are thus likely overfitting. Three data points (p38 in PI3Ki and EGF+PDGFi+RAFi, and S6K in IGF1+PDGFi+RAFi) exceptionnally badly fitted are likely artefacts since similar perturbations do not show the same effect.

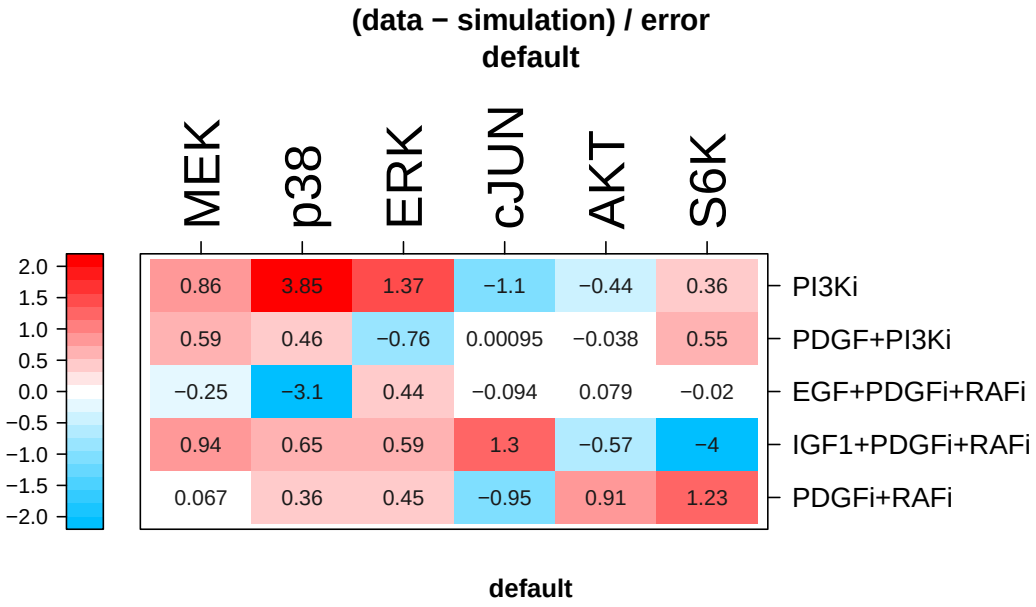

Final model reduction

Removed Link	New residual	Delta residual	pval
EGF→ TAK1	198.63	0.79	0.62
IL1b→ PI3K	198.63	0	3.6e-07
IL1b→ ASK1	198.63	0	0
IL1b→ TAK1	198.63	0	0
ALK→ TAK1	198.89	0.26	0.39

PDGF→ RAF	199.32	0.43	0.49
NGF→ TAK1	200.25	0.93	0.66
IGF1→ RAF	201.53	1.28	0.74
EGF→ RAF	204.94	3.42	0.94

Completely reduced model: "Best fit: 204.95 , Score= 0.69"

Fixed inhibitor model CHP212

The final CHP212 model with fixed parameters has a residual of 223.

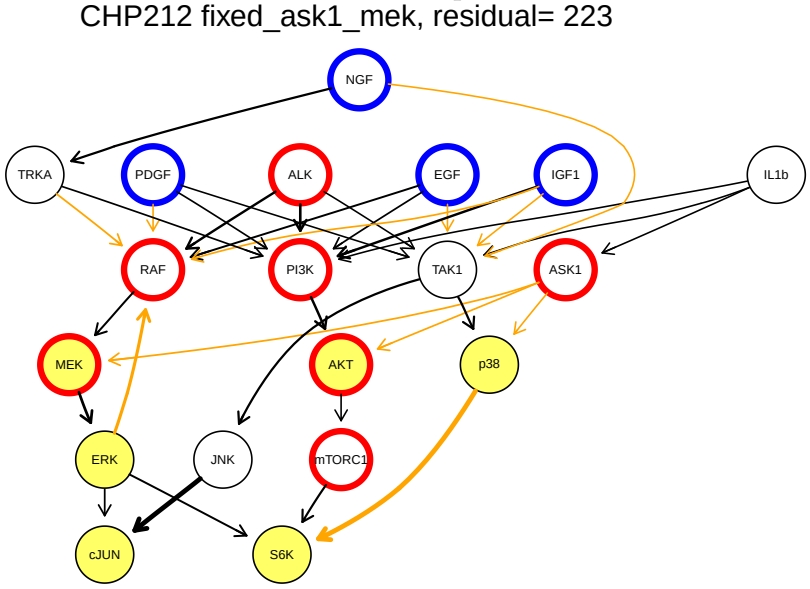

B.3 SKNAS fitting summary

Initial topology SKNAS

SKNAS ERK→ cJUN model residual=259 df=34

from	to	value	residual	df	Res_delta	df_delta	pval	adj_pval
p38	S6K	-2.63	231	35	27.57	1	2e-07	3.62e-5
p38	mTORC1	-2.45	231.54	35	27.02	1	2e-07	4.8e-5
cJUN	S6K	-1.27	235.89	35	22.67	1	1.9e-06	4.59e-4
JNK	S6K	-3.99	235.97	35	22.59	1	2e-06	4.77e-4
TAK1	S6K	-3.62	236.01	35	22.56	1	2e-06	4.86e-4
JNK	mTORC1	-4.38	236.45	35	22.11	1	2.6e-06	6.12e-4
TAK1	mTORC1	-3.34	236.57	35	21.99	1	2.7e-06	6.54e-4
cJUN	mTORC1	-1.07	236.71	35	21.85	1	2.9e-06	7.02e-4
RAF	IL1b	1	237.56	37	21	3	1.05e-04	0.02
cJUN	AKT	-13.07	241.02	35	17.54	1	2.8e-05	6.7e-3

Overall trying to explain the effect of ASK1i on S6K. The best extension p38→S6K makes sense and is used.

p38→S6K effect SKNAS

SKNAS p38→ S6K model residual=230 df=35

from	to	value	residual	df	Res_delta	df_delta	pval	adj_pval
ALK	mTORC1	-5.88	207.4	36	23.06	1	1.6e-6	3.7e-4
ALK	S6K	-5.47	207.4	36	23.02	1	1.6e-6	3.8e-4
AKT	IL1b	1	207.9	38	22.50	3	5.1e-5	0.01
AKT	TAK1	-0.04	208.3	36	22.18	1	2.5e-6	5.9e-4
AKT	ALK	-0.07	209.7	36	20.70	1	5.3e-6	1.3e-3
AKT	cJUN	-0.13	209.7	36	20.69	1	5.4e-6	1.3e-3
AKT	JNK	-0.13	209.9	36	20.58	1	5.7e-6	1.4e-3
S6K	IL1b	1	210.9	38	19.56	3	2.1e-4	0.04
mTORC1	IL1b	1	210.9	38	19.56	3	2.1e-4	0.04
ALK	ASK1	-100	211.6	36	18.83	1	1.4e-5	3.4e-3

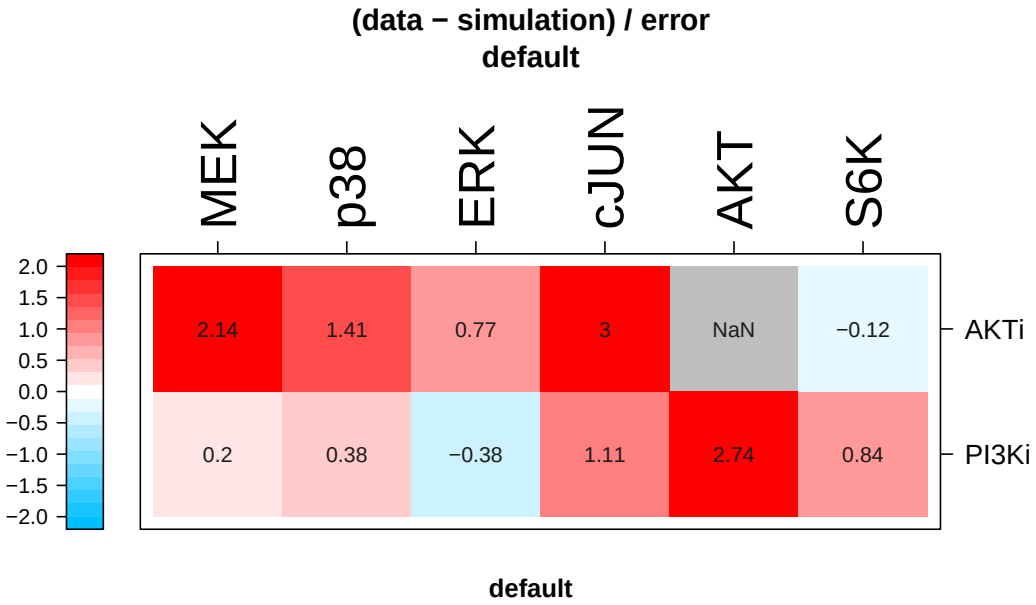

The "shortcut" extensions are ignored. The next best extensions correspond to AKT influencing the TAK1/JNK/cJUN axis. AKT→TAK1 has some literature basis and is thus used.

AKT→TAK1 effect SKNAS

SKNAS AKT→ TAK1 model			residual=208			df=36		
from	to	value	residual	df	Res_delta	df_delta	pval	adj_pval
RAF	IL1b	1	190.25	39	18.02	3	4.33e-4	0.10
RAF	S6K	1.32	190.67	37	17.61	1	2.71e-5	6.42e-3
RAF	mTORC1	1.75	190.77	37	17.50	1	2.87e-5	6.79e-3
RAF	TAK1	-1.26	191.63	37	16.64	1	4.51e-5	0.01
ASK1	TRKA	-0.23	191.73	37	16.55	1	4.74e-5	0.01
IGF1	AKT	1.21	192.04	37	16.23	1	5.6e-5	0.01
p38	TRKA	1	192.32	37	15.96	1	6.47e-5	0.01
ALK	S6K	-12.06	192.72	37	15.55	1	8.03e-5	0.01
ALK	mTORC1	-7.12	192.95	37	15.32	1	9.05e-5	0.02
ALK	cJUN	-6.40	194.69	37	13.58	1	2.27e-4	0.05

The extensions proposed are barely significant and consist in shortcuts. The extension process is stopped at this iteration.

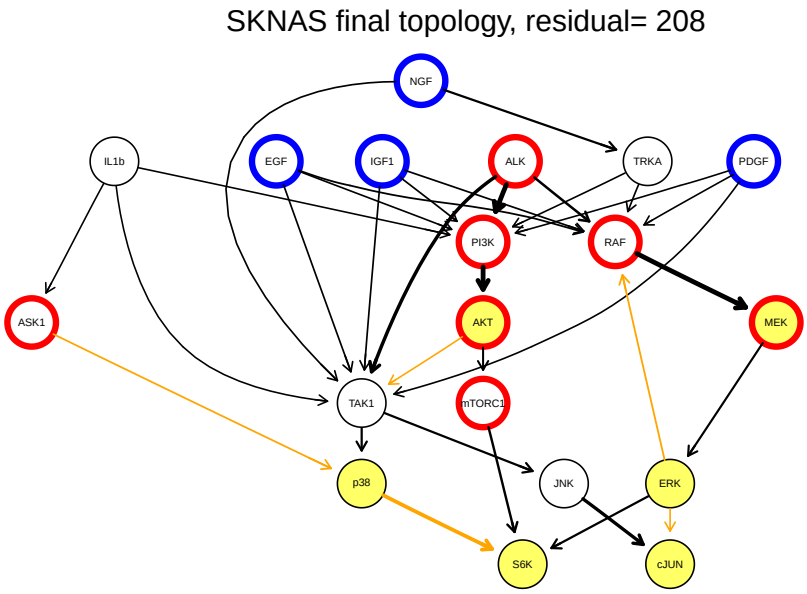

Only receptor links would be removed so we keep them for inter-models comparison. In particular SKNAS all NGF links were removed.

Final model reduction

Removed Link	New residual	Delta residual	pval
IL1b→ ASK1	208.28	0	1.3e-07
IL1b→ TAK1	208.28	0	0
IL1b→ PI3K	208.28	0	0
ERK→ cJUN	208.35	0.07	0.21

Completely reduced model: "Best fit: 208.35 , Score= 0.65"

Final network with fixed parameters SKNAS

The final SKNAS model with fixed parameters has a residual of 229.

B.4 LAN6 fitting summary

The models without PDGF basal activity are selected for their ERK→RAF negative feedback. The difference in residuals with PDGF basal models is low.

Initial topology LAN6

LAN6 ERK→ cJUN model			residual=339			df=37		
from	to	value	residual	df	Res_delta	df_delta	pval	adj_pval
p38	S6K	-4.42	224.9	38	113.80	1	0	0
p38	mTORC1	-0.19	227.0	38	111.70	1	0	0
TAK1	S6K	-4.73	232.2	38	106.60	1	0	0
JNK	S6K	-4.73	232.2	38	106.60	1	0	0
cJUN	S6K	36.31	232.2	38	106.60	1	0	0
TAK1	mTORC1	-0.59	233.1	38	105.60	1	0	0
JNK	mTORC1	-0.59	233.1	38	105.60	1	0	0
cJUN	mTORC1	0.10	233.5	38	105.20	1	0	0
cJUN	TRKA	1	248.4	38	90.35	1	0	0
cJUN	ALK	1.49e-3	249.1	38	89.63	1	0	0

TAK1/JNK/cJUN/p38→mTORC1/S6K extensions greatly improve the model by explaining the effect of ASK1i on S6K.

p38→S6K effect LAN6

LAN6 P38→ S6K model			residual=243		df=34			
from	to	value	residual	df	Res_delta	df_delta	pval	adj_pval
p38	RAF	14.82	205.7	35	37.22	1	e+0	0
ASK1	RAF	-99.95	205.7	35	37.21	1	e+0	0
ASK1	MEK	-99.85	205.7	35	37.18	1	e+0	0
ASK1	ALK	-0.88	218.2	35	24.68	1	7e-07	1.31e-4
p38	ALK	0.56	222.3	35	20.63	1	5.6e-06	1.08e-3
RAF	ERK	0.43	222.5	35	20.42	1	6.2e-06	1.2e-3
cJUN	ALK	0.12	223.6	35	19.29	1	1.12e-05	2.17e-3
ERK	ALK	0.10	223.7	35	19.22	1	1.17e-05	2.26e-3
MEK	ALK	0.04	223.7	35	19.16	1	1.2e-05	2.33e-3
MEK	PI3K	0.12	223.7	35	19.14	1	1.21e-05	2.35e-3

An ASK1/p38→RAF/MEK extension is suggested to explain MEK and ERK up-phosphorylation upon ASK1i. ASK1→MEK is chosen for consistency with other cell lines and biological sense (MAP3K→MAP2K).

ASK1→MEK effect LAN6

LAN6 ASK1→ MEK model residual=206 df=35

from	to	value	residual	df	Res_delta	df_delta	pval	adj_pval
ERK	ALK	0.05	185.9	36	19.78	1	8.7e-6	1.68e-3
MEK	ALK	0.02	185.9	36	19.74	1	8.9e-6	1.71e-3
cJUN	ALK	0.07	186.0	36	19.70	1	9.0e-6	1.74e-3
MEK	PI3K	0.10	186.7	36	18.95	1	1.34e-5	2.58e-3
cJUN	AKT	1.33	186.7	36	18.94	1	1.35e-5	2.59e-3
cJUN	PI3K	0.27	186.7	36	18.94	1	1.35e-5	2.6e-3
ERK	PI3K	0.23	186.7	36	18.92	1	1.36e-5	2.62e-3
ERK	AKT	1.17	186.7	36	18.91	1	1.37e-5	2.63e-3
MEK	AKT	0.54	186.8	36	18.85	1	1.41e-5	2.72e-3
ALK	p38	3.54	190.8	36	14.89	1	1.14e-4	0.02

There are signs of overfitting in the qq-plot and the links proposed do not make any biological sense. They likely represent overadjusting of the remaining badly fitted datapoints. We stop the extension here.

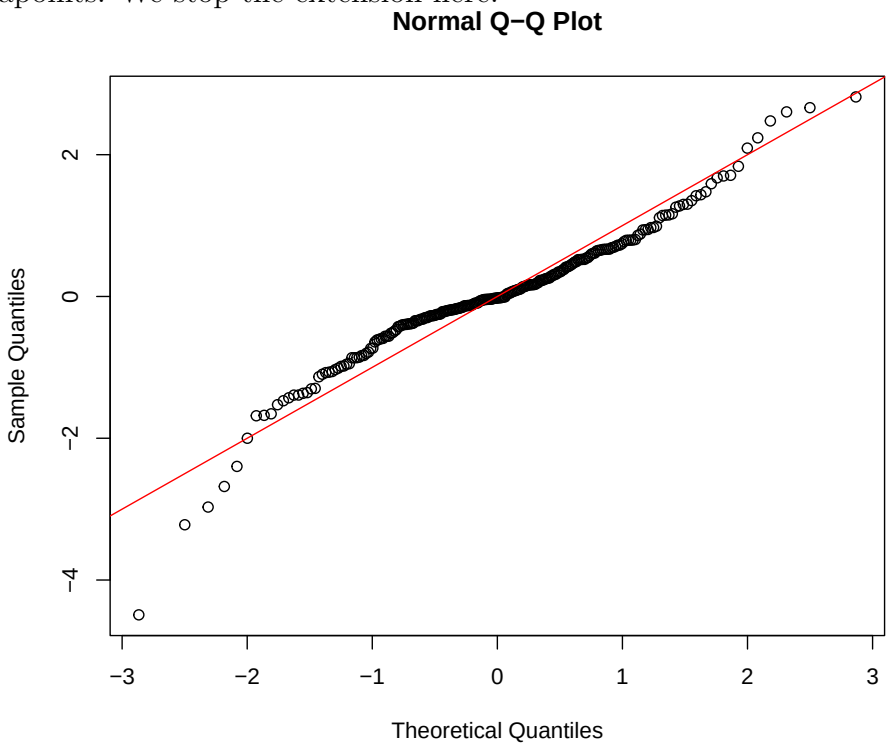

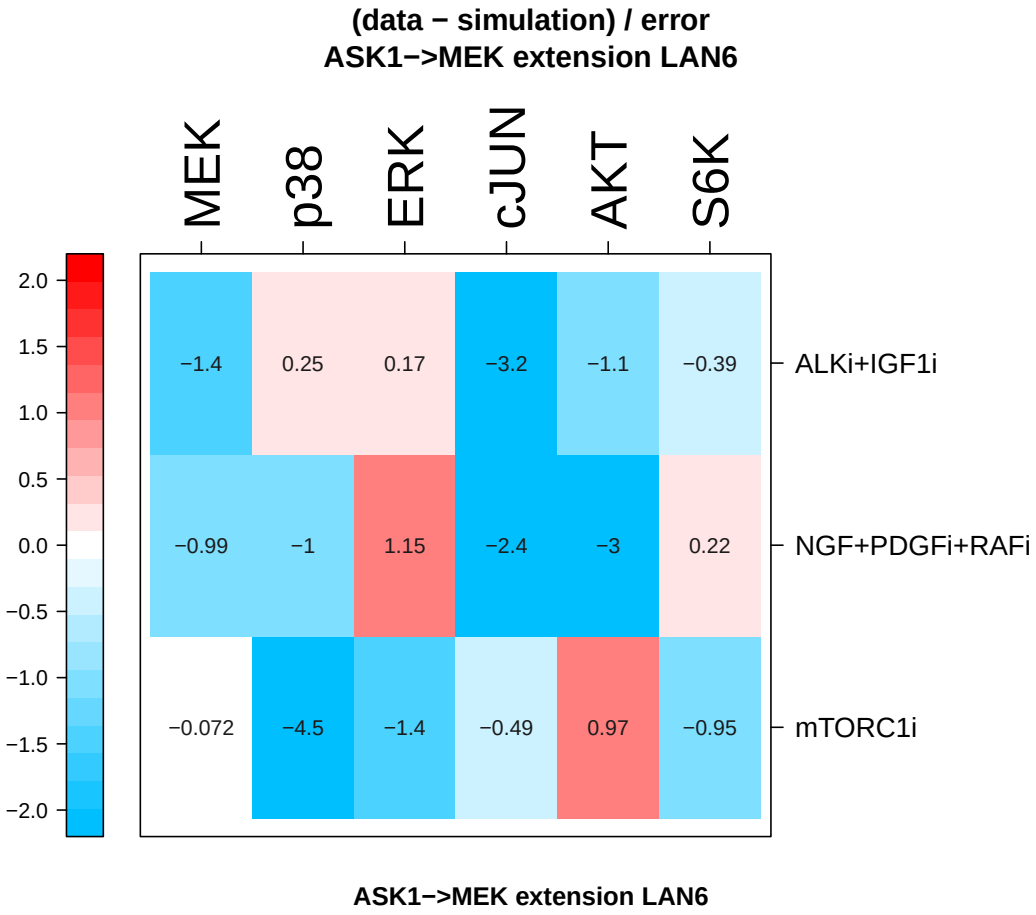

Final model reduction

Removed Link	New residual	Delta residual	pval
NGF→ PI3K	205.68	0.02	0.13
TAK1→ JNK	205.79	0.11	0.26
JNK→ cJUN	205.79	0	0
EGF→ PI3K	206.66	0.87	0.65
PDGF→ PI3K	209.11	2.45	0.88
PDGF→ RAF	211.35	2.24	0.67

Completely reduced model: "Best fit: 211.36 , Score= 0.75"

Final network with fixed parameters LAN6

To remove non identifiability linked to not measuring all inhibited nodes, we fix the inhibitors to concensus values and refit with this constraint.

The final LAN6 model with fixed parameters has a residual of 238.

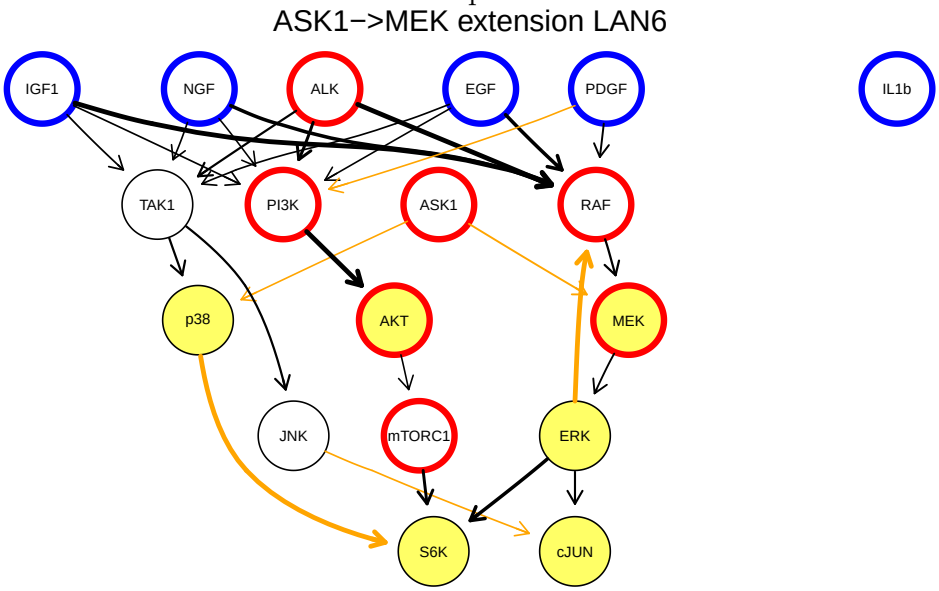

B.5 IMR32 fitting summary

Initial topology IMR32

IMR32 initial model			residual=407	df=34				
from	to	value	residual	df	Res_delta	df_delta	pval	adj_pval
ASK1	TRKA	-29.29	320.18	35	86.31	1	e+0	0e+0
p38	ALK	-32.55	333.77	35	72.72	1	e+0	0e+0
ASK1	MEK	-1.22	345.23	35	61.26	1	e+0	0e+0
ASK1	RAF	-4.98	345.26	35	61.23	1	e+0	0e+0
ASK1	ALK	15.59	362.61	35	43.88	1	e+0	0e+0
ASK1	PI3K	-8.98	369.16	35	37.33	1	e+0	2e-07
ASK1	AKT	-0.31	369.23	35	37.26	1	e+0	2e-07
p38	PI3K	0.15	369.75	35	36.75	1	e+0	3e-07
p38	AKT	-7.68	370.64	35	35.85	1	e+0	5e-07
AKT	ALK	2	380.80	35	25.69	1	4e-07	9.57e-05

The model fits the data for most data, with the notable exception of MEK, ERK, AKT and S6K upon ASK1i treatment. The first extensions suggested ASK1/p38 → RAF/MEK/PI3K/AKT adress exactly this problem. We chose ASK1→MEK as the best, and more biologically coherent than ASK1→RAF.

ASK1→MEK effect IMR32

IMR32 ASK1→ MEK model			residual=342			df=36		
from	to	value	residual	df	Res_delta	df_delta	pval	adj_pval
MEK	ASK1	28.52	249.24	36	92.71	1	e+0	0e+0
ERK	ASK1	25.73	250.40	36	91.54	1	e+0	0e+0
TAK1	ASK1	-9.17	275.41	36	66.54	1	e+0	0e+0
JNK	ASK1	-10.41	275.44	36	66.50	1	0e+0	0e+0
cJUN	ASK1	19.43	276.18	36	65.77	1	e+0	0e+0
p38	ASK1	-100.18	276.66	36	65.29	1	e+0	0e+0
RAF	ASK1	1.80	292.17	36	49.78	1	e+0	0e+0
NGF	ASK1	78.23	314.33	36	27.62	1	1e-07	3.5e-05
TRKA	ASK1	52.04	314.33	36	27.62	1	1e-07	3.5e-05
p38	AKT	-9.40	315.46	36	26.49	1	3e-07	6.29e-05

The ASK1i effect on MEK and ERK is stronger with IGF1 and NGF treatments. This would suggest that those ligands, but not EGF and PDGF, activate ASK1. Moreover, ASK1i alone as no strong effect on MEK and ERK (or any other readouts). To reflect this, we added the links IGF1→ASK1 and NGF→ASK1, and removed ASK1 basal activity.

GS4997 (ASK1i) effect IMR32

IMR32 GS4997 model			residual=236			df=37		
from	to	value	residual	df	Res_delta	df_delta	pval	adj_pval
ASK1	AKT	-1.68	194.41	38	41.40	1	0	0.0e+0
p38	PI3K	0.14	194.41	38	41.40	1	0	0.0e+0
JNK	AKT	-8.2e-3	194.43	38	41.38	1	0	0.0e+0
JNK	PI3K	-2.22e-4	194.61	38	41.20	1	0	0.0e+0
ASK1	PI3K	-0.04	194.62	38	41.20	1	0	0.0e+0
p38	AKT	5.74	194.84	38	40.97	1	0	0.0e+0
p38	ALK	-108.74	198.57	38	37.24	1	0	2.0e-07
cJUN	PI3K	-0.16	203.27	38	32.55	1	0	2.4e-06
cJUN	AKT	-5.83	203.37	38	32.45	1	0	2.5e-06
RAF	AKT	-1.79	205.84	38	29.97	1	0	8.9e-06

This model explains everything except the hyper-activation of AKT by NGF+ ASK1i. The proposed extensions ASK1/p38/JNK → PI3K/AKT would solve this but also overfit the data, with an unexpectedly low residual. Accordingly, we stopped the extensions here.

Final model reduction

Only receptor links would be removed in IMR32 so we keep them for inter-models comparison.

Removed Link	New residual	Delta residual	pval
IL1b→ ASK1	235.82	0	1.3e-07
IL1b→ TAK1	235.82	0	1.3e-07
IL1b→ PI3K	235.82	0	1.3e-07
NGF→ TAK1	236.06	0.24	0.37
IGF1→ TAK1	237.18	1.12	0.71
ASK1→ p38	239.64	2.46	0.88
ALK→ PI3K	242.59	2.95	0.91
EGF→ PI3K	245.53	2.94	0.91

Completely reduced model: "Best fit: 245.54 , Score= 0.66"

Fixed parameters, GS4997 effect IMR32

The final IMR32 model with fixed parameters has a residual of 340.

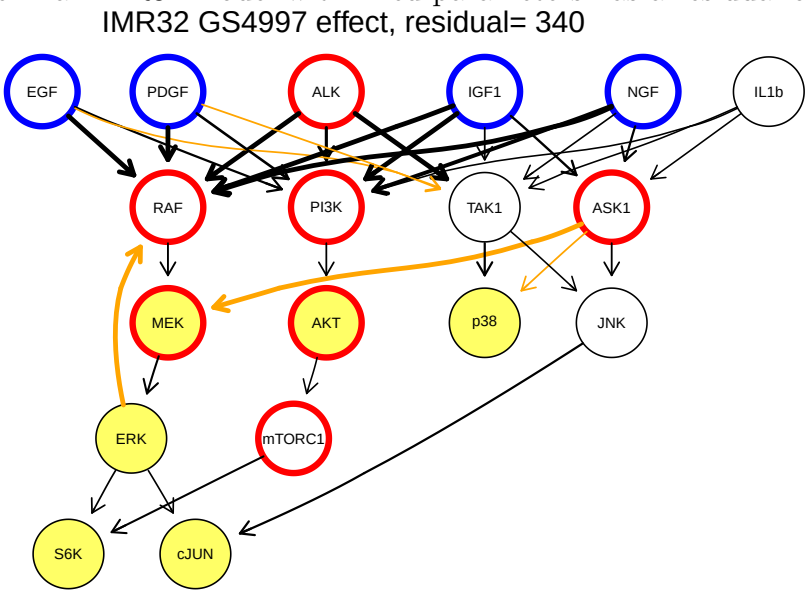

B.6 KELLY fitting summary

Initial model KELLY

KELLY ERK→ cJUN model			residual=602		df=37			
from	to	value	residual	df	Res_delta	df_delta	pval	adj_pval
p38	ALK	1.80	524.20	38	78.08	1	0	0
p38	mTORC1	9.98	525.42	38	76.86	1	0	0
ASK1	TAK1	1.94	526.40	38	75.89	1	0	0
ASK1	JNK	3.03	526.86	38	75.42	1	0	0
p38	cJUN	9.98	527.03	38	75.26	1	0	0
ASK1	cJUN	9.95	527.32	38	74.97	1	0	0
p38	JNK	5.24	527.70	38	74.59	1	0	0
ASK1	ALK	2.32	529.73	38	72.56	1	0	0
p38	TAK1	1	531.31	38	70.97	1	0	0
ASK1	RAF	-10.25	531.50	38	70.78	1	0	0

This initial topology barely explains the behaviour of KELLY and yields a very bad fit. The most striking misfits are the effect of ASK1 on cJUN and S6K. The best extension would be p38→mTORC1, however we chose p38→S6K that makes more sense biologically.

p38→S6K model KELLY

KELLY p38→ S6K model			residual=484		df=38			
from	to	value	residual	df	Res_delta	df_delta	pval	adj_pval
ASK1	cJUN	6722.18	381.48	39	102.33	1	0	0
p38	cJUN	4.46	381.48	39	102.33	1	0	0
p38	JNK	4.46	381.48	39	102.33	1	0	0
ASK1	JNK	6697.83	381.48	39	102.33	1	0	0
ASK1	TAK1	-5423.47	381.48	39	102.33	1	0	0
p38	TAK1	1	381.48	39	102.33	1	0	0
mTORC1	TRKA	1	384.45	39	99.35	1	0	0
p38	TRKA	1	389.11	39	94.70	1	0	0
ASK1	TRKA	1636.37	390.29	39	93.52	1	0	0
S6K	TRKA	-1.29	398.88	39	84.93	1	0	0

This extension greatly improves the fit. As expected ASK1/p38→JNK/cJUN seems necessary to explain the effect of ASK1 on cJUN.

p38→cJUN model KELLY

KELLY p38→ cJUN model		residual=411		df=39				
from	to	value	residual	df	Res_delta	df_delta	pval	adj_pval
S6K	PI3K	-1.58	331.27	40	80.14	1	0	0
S6K	AKT	-0.23	332.04	40	79.38	1	0	0
S6K	TRKA	-3.3e-3	333.14	40	78.27	1	0	0
mTORC1	TRKA	1	347.44	40	63.98	1	0	0
mTORC1	AKT	-0.05	348.23	40	63.18	1	0	0
mTORC1	PI3K	-0.29	348.24	40	63.18	1	0	0
ALK	ERK	-0.04	358.36	40	53.06	1	0	0
EGF	ERK	0.27	359.97	40	51.44	1	0	0
TAK1	ERK	1.06	362.19	40	49.22	1	0	0
JNK	ERK	1.06	362.20	40	49.22	1	0	0

S6K→PI3K/AKT would explain AKT phosphorylation upon mTORC1 inhibition as well as from ASK1 inhibition (via p38→S6K) and has literature support via RICTOR.

S6K→TRKA reflects a possible receptor feedback. The link S6K→IRS1 (an IGFR adaptor) is documented in the literature so we tested it (as S6K→IGF1 to take path identifiability into account)

S6K→IGF1 model KELLY

KELLY S6K→ IGF1 model			residual=327		df=40			
from	to	value	residual	df	Res_delta	df_delta	pval	adj_pval
ALK	ERK	-0.25	301.03	41	25.86	1	0	8.01e-5
EGF	ERK	0.27	303.77	41	23.13	1	1.5e-6	3.31e-4
JNK	ERK	1.20	306.09	41	20.81	1	5.1e-6	1.1e-3
TAK1	ERK	1.20	306.09	41	20.81	1	5.1e-6	1.1e-3
p38	ASK1	-3312	311.12	41	15.77	1	7.13e-5	0.01
mTORC1	p38	1.7e-5	311.90	41	15	1	1.07e-4	0.02
mTORC1	ASK1	1.0e-6	311.94	41	14.96	1	1.09e-4	0.02
S6K	p38	0.03	312.10	41	14.80	1	1.19e-4	0.02
S6K	ASK1	4.3e-6	312.10	41	14.79	1	1.19e-4	0.02
JNK	ASK1	-9.5e-3	312.10	41	14.79	1	1.19e-4	0.02

Final model reduction

Removed Link	New residual	Delta residual	pval
IL1b→ ASK1	332.12	0.08	0.23
IL1b→ PI3K	332.21	0.08	0.23
IGF1→ RAF	332.36	0.15	0.3
IL1b→ TAK1	333.07	0.71	0.6
TRKA→ PI3K	333.81	0.74	0.61
NGF→ TRKA	335.72	1.91	0.83
TRKA→ RAF	335.72	0	8.3e-07
IGF1→ TAK1	337.89	2.16	0.86
ALK→ TAK1	340.21	2.33	0.87
NGF→ TAK1	342.63	2.42	0.88

Completely reduced model: "Best fit: 342.63 , Score= 0.65"

Fixed inhibitor model KELLY (S6K→IGF1)

The error is dominated by the unexplained but probably false signals of very high ERK with EGF+AKTi (but with no other perturbations with AKTi or EGF) and MEK downregulation with EGF alone (while no such effect is seen with EGF+PI3Ki, EGF+ASK1i or EGF+mTORC1i). Removing those 2 datapoints yield a residual compatible with the number of data points.

The final KELLY model with fixed parameters has a residual of 288.

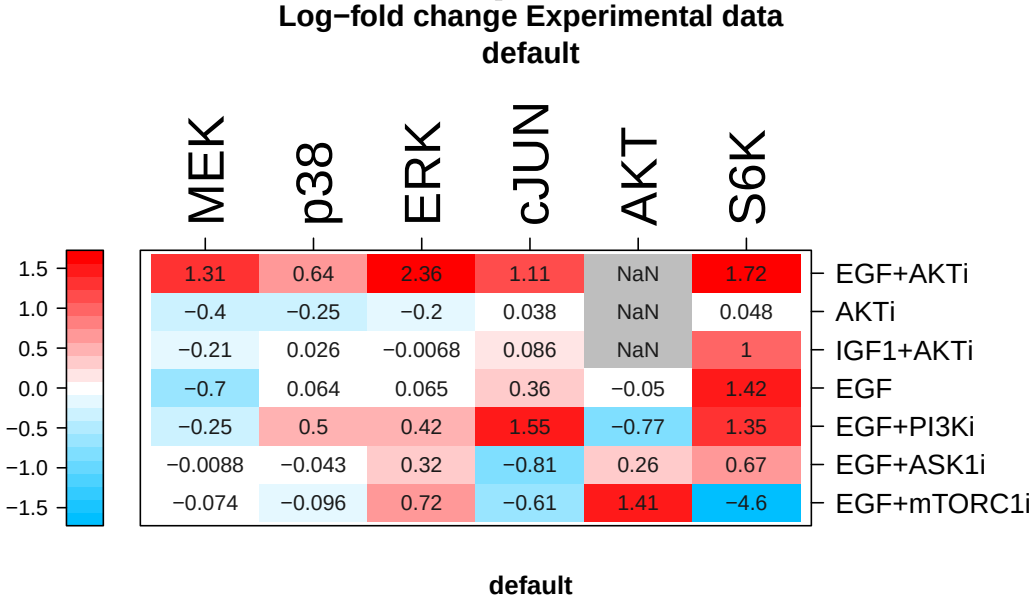

KELLY S6K−>AKT, residual= 372

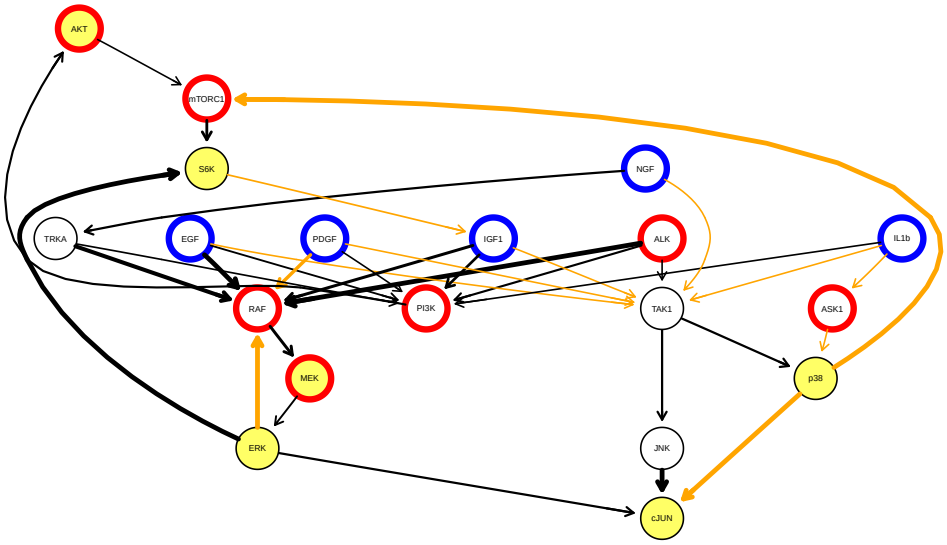

B.7 Models comparison

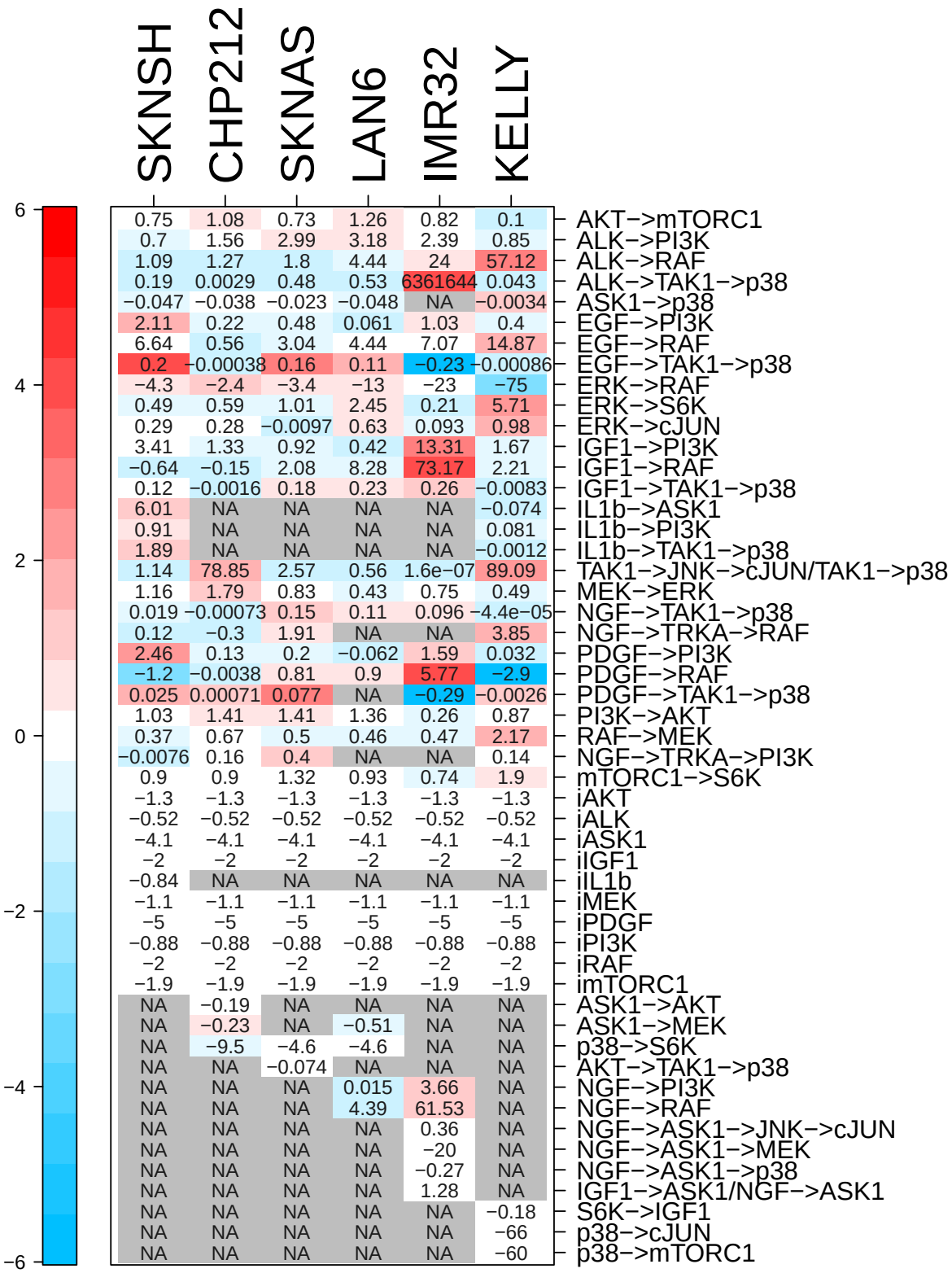

B.8 Evaluation of fit quality with QQ-plots

QQ-plots are a statistical way of evaluating the fit. If the error model and the fit are both correct the residuals should follow a standard normal distribution and deviation from this behaviour are easily visualized on a QQ-plot.

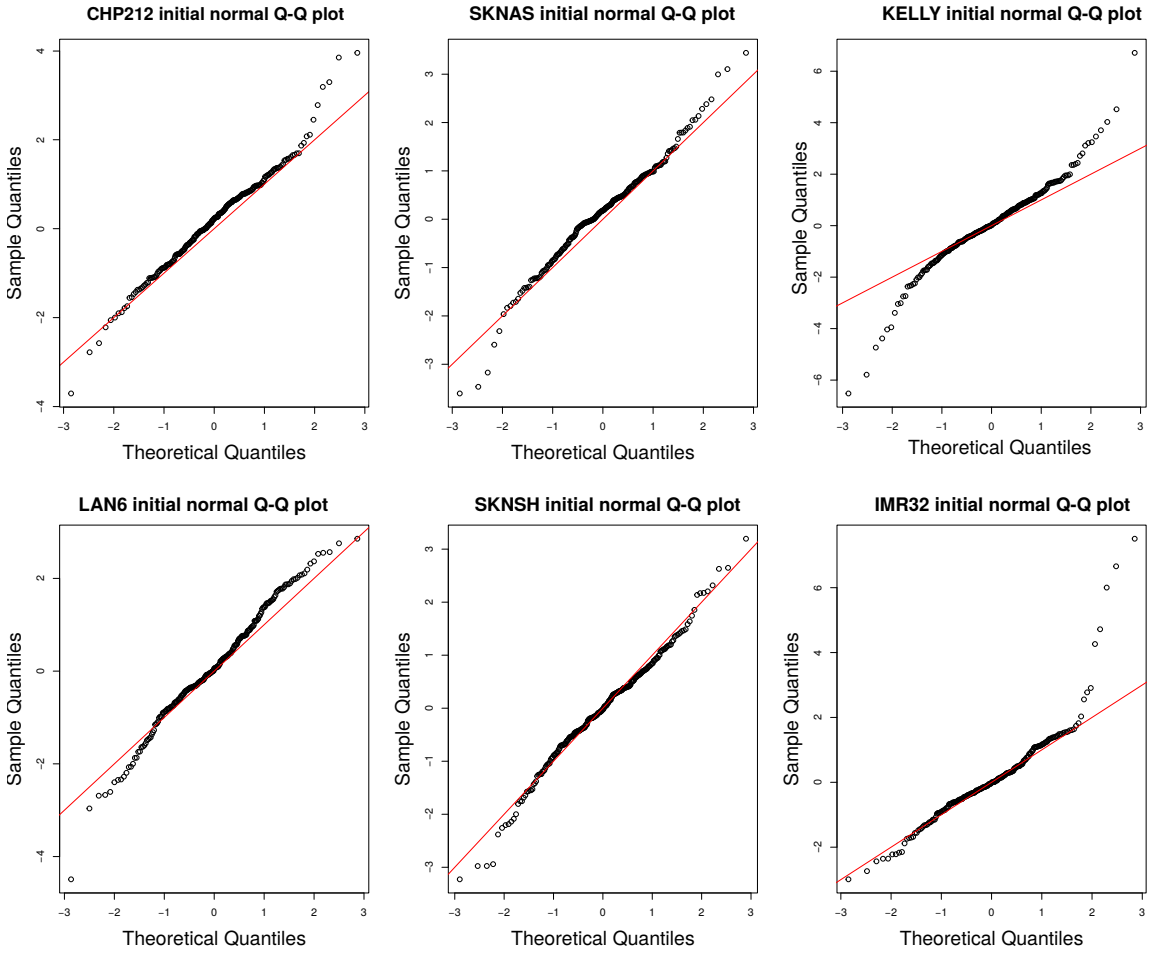

Figure Appendix.4: Quantile-quantile plots of the initial models using the literature topology.

The residuals for the initial models using the literature topology shows important deviations for all cell lines except SKNSH (Figure Appendix.4). After the extension procedure most models show normally distributed residuals, indicating that all the signal was fitted and that the remaining error is due to noise (Figure Appendix.5). Some individual data points remain badly fitted but do no seem to represent any systematic deviation induced by a treatment. They either represent statistically exceptionnally divergent measurements or unexplained mechanism arising in very specific conditions. Deciding which is true would require additionnaly measurements, possibly with different treatments, which I did not perform because of time constraints. Overall the fits are good but some questions remain for some perturbation that could be addressed in future experiments.

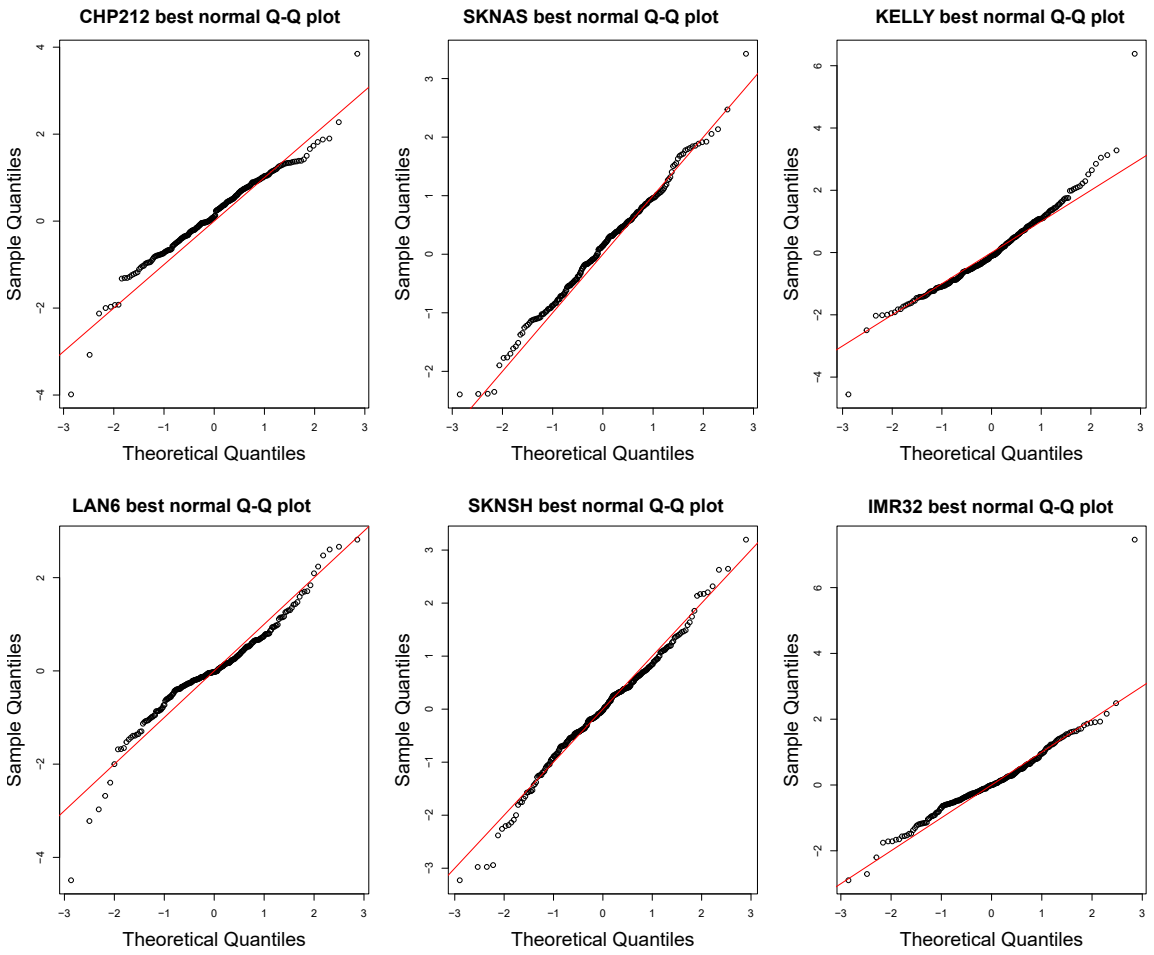

Figure Appendix.5: Quantile-quantile plots of the final models after model extension.

C Additionnal molecular characterisation of the TerminateNB neuroblastoma panel

C.1 Cell lines clustering

A PCA on perturbation response roughly separated the cells according to AZD6244 sensitivity (Figure Appendix.6). The main components of the perturbation data were the clear response of AKT and S6K to receptor stimulation and the consistent feedback-induced hyper-phosphorylation of MEK, occupying the first and third, and second component respectively and representing more than 90% of the variance (Table Appendix.29, Figure Appendix.7).

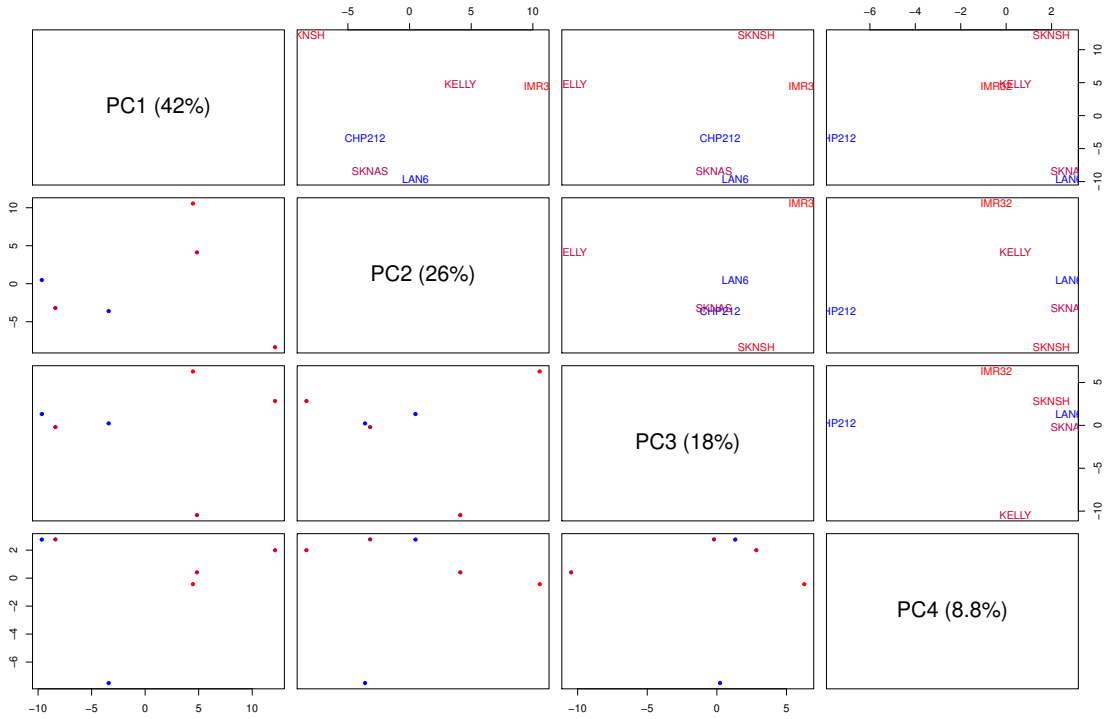

Figure Appendix.6: Pair-plot of the principal components from the perturbation data (Figure 4.6). Components up to the first one explaining less than 10% of the variance are shown.

Table Appendix.29: Main loadings of the first 3 principal components of the perturbation data PCA.

Condition_PC1	**PC1**	**Condition_PC2**	**PC2**	**Condition_PC3**	**PC3**
PDGF+ALKi+ IGF1i AKT	0.31	IGF1+MEKi MEK	0.31	IGF1+ASK1i MEK	-0.24
EGF+ALKi+ IGF1i AKT	0.27	NGF+MEKi MEK	0.27	IGF1+PI3Ki AKT	-0.21
PDGF+ALKi+ IGF1i S6K	0.21	IGF1+ASK1i MEK	0.26	IGF1+mTORC1i S6K	-0.21
EGF+ALKi+ IGF1i S6K	0.21	PDGF+MEKi MEK	0.23	PDGF+ASK1i S6K	-0.21
IGF1+RAFi+ PDGFi AKT	0.20	EGF+MEKi MEK	0.21	PDGF+mTORC1i S6K	-0.21
IGF1+mTORC1i AKT	0.19	MEKi MEK	0.21	NGF+mTORC1i S6K	-0.20
ALKi+IGF1i AKT	0.9	IGF1+PI3Ki AKT	0.15	IGF1 AKT	-0.20
EGF+RAFi+ PDGFi S6K	0.18	ALKi+IGF1i S6K	0.14	EGF+PI3Ki S6K	0.18
IGF1+RAFi+ PDGFi S6K	0.18	EGF+ASK1i AKT	-0.12	EGF+AKTi S6K	0.18
EGF+AKTi S6K	0.17	IGF1+MEKi ERK	0.12	IGF1+MEKi AKT	-0.18

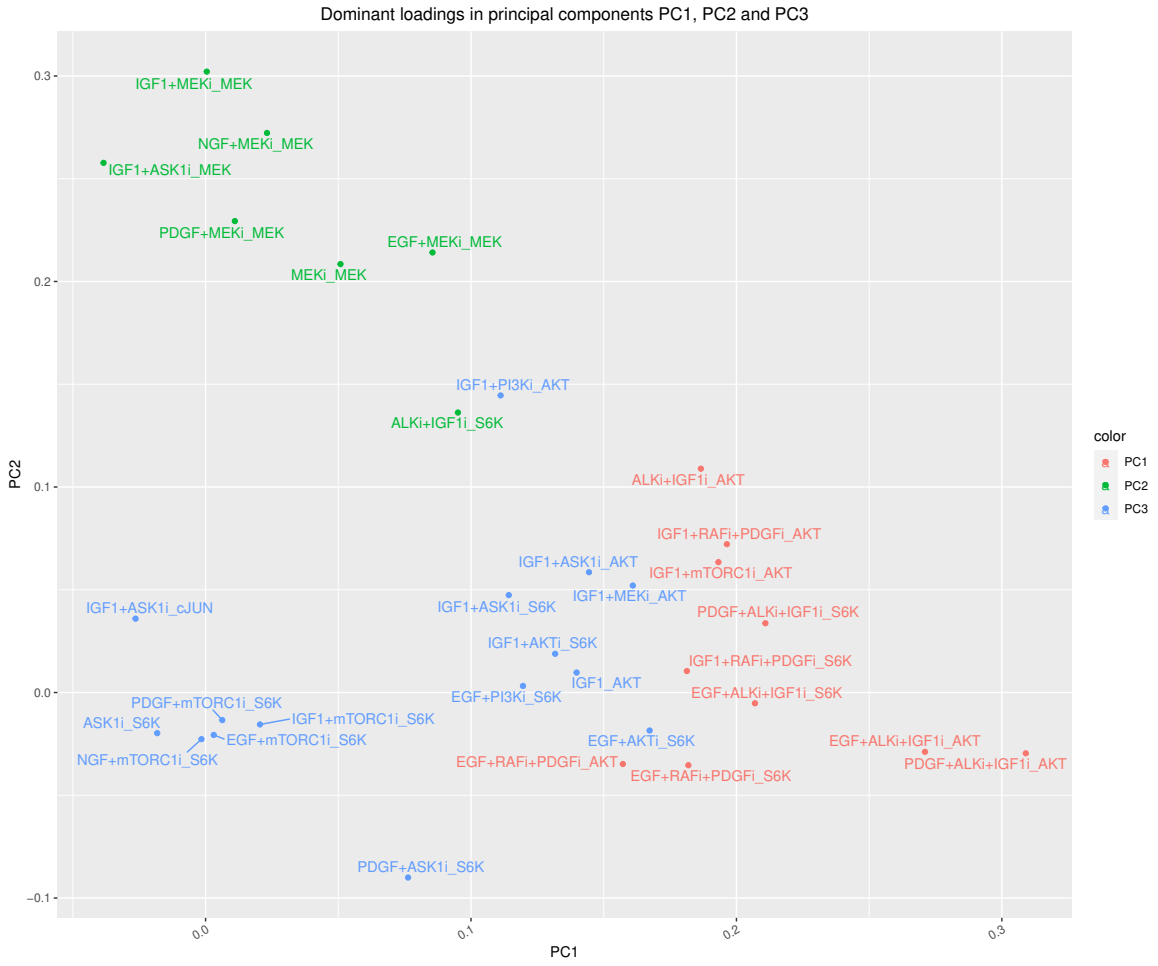

Figure Appendix.7: Main loadings overlap in the first 3 principal components of the perturbation data PCA. Color corresponds to the components for which the condition has the highest absolute weight.

A principal component analysis on the most variables genes differed to a great extend to the one on perturbation data and did not separate the cell lines by drug response (Figure Appendix.8). Since RNA was extracted from non inhibited cells, this highlights that perturbations are essential to reveal the true state of the cell that leads to drug resistance.

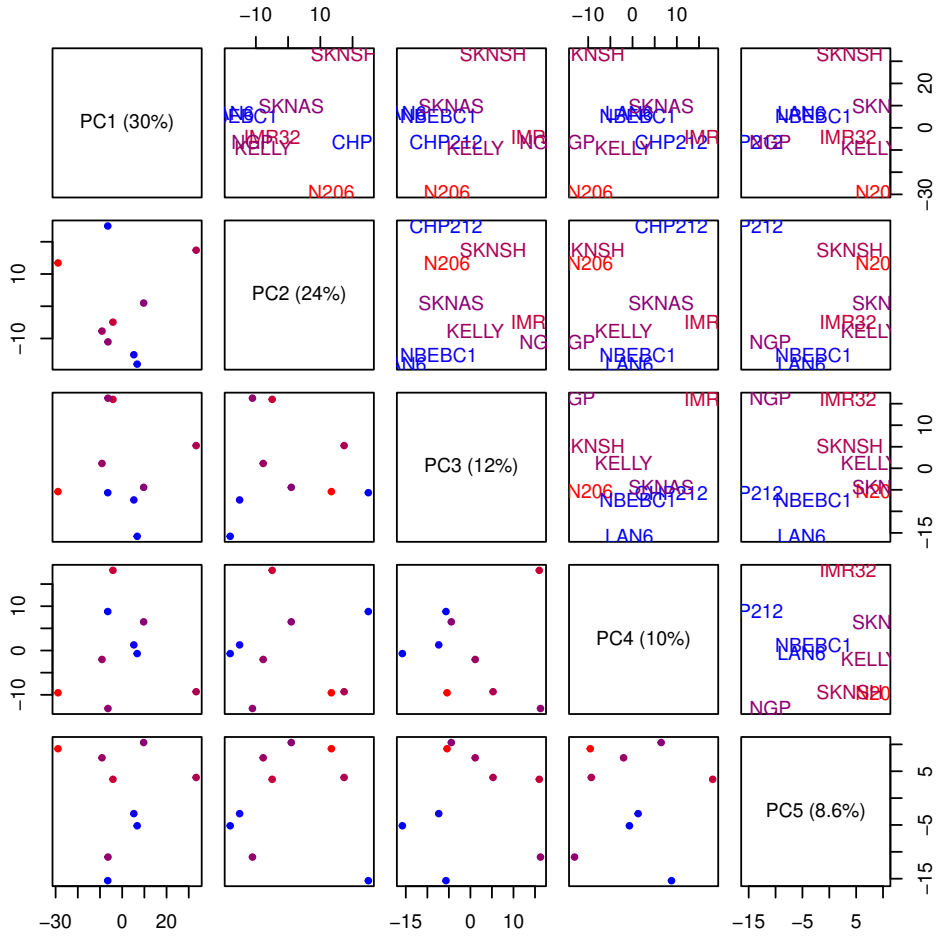

Figure Appendix.8: Principal component analysis on the top 1000 most variable genes. Components up to the first one explaining less than 10% of variance are shown.

C.2 Gene expression and signalling

In the hope of uncovering specific genes involved in drug sensitivity, I correlated the IC50 to mRNA expression (Figure Appendix.9). However because of the small number of cell lines being used, many gene displayed apparent correlations that did not generalise. Consequently the best correlations with IC50 seemed mostly driven by noise than by a biological signal as the correlations were poor and the best one did not appear related to the drug target.

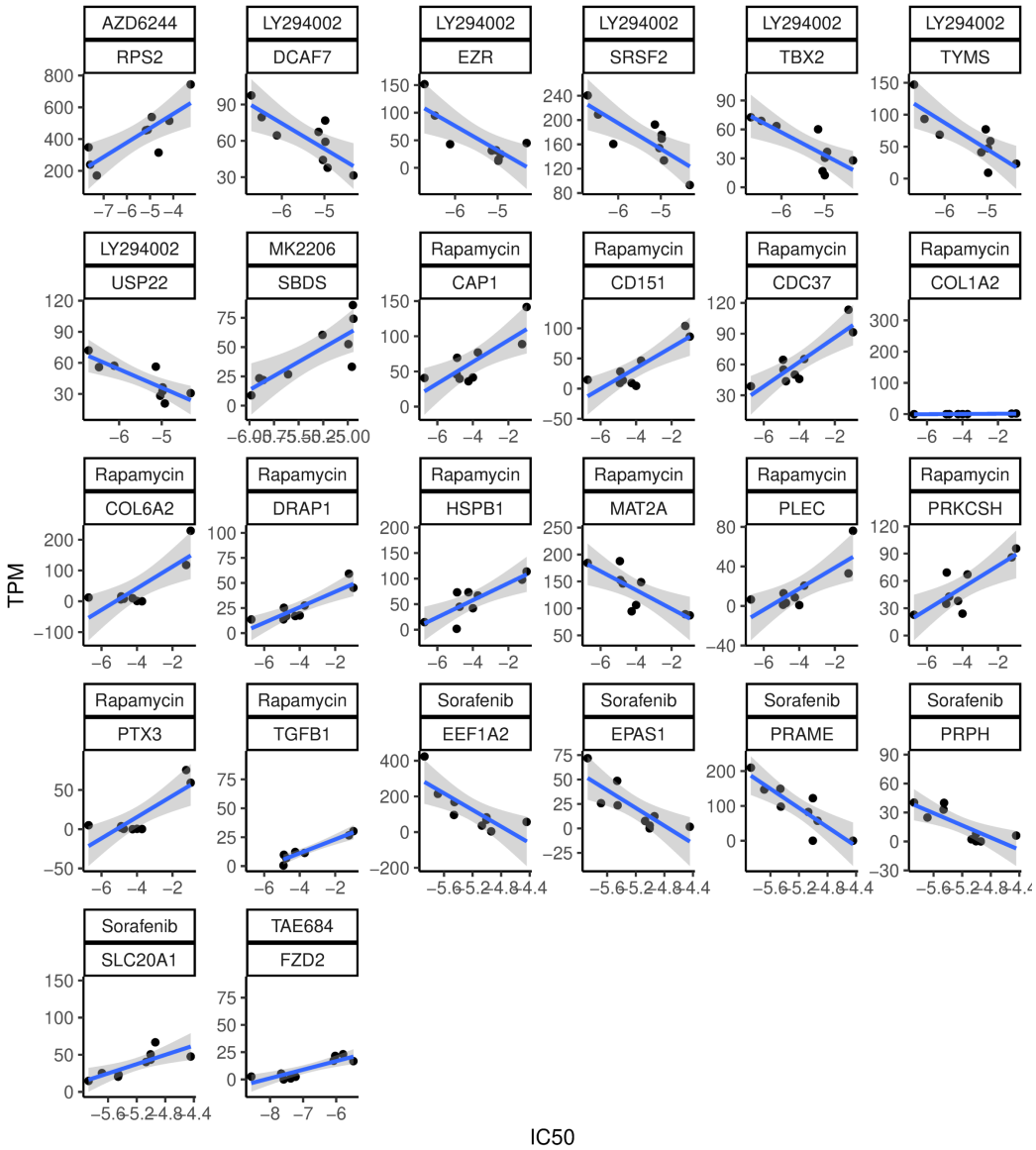

Figure Appendix.9: Top correlations between IC50 and mRNA expression for the 1000 most variable genes (adjusted p> 0.95).

Investigating in more details the relationship between IC50 and the expression of TP53 and RAS pathways genes highlighted two potential interactions: a negative correlation for KRAS expression and the IC50 of the PI3K inhibitor LY294002, and a positive one for HRAS expression and the IC50 to the ALK inhibitor TAE684 (Figure Appendix.11). A negative correlation for KRAS expression and the IC50 of

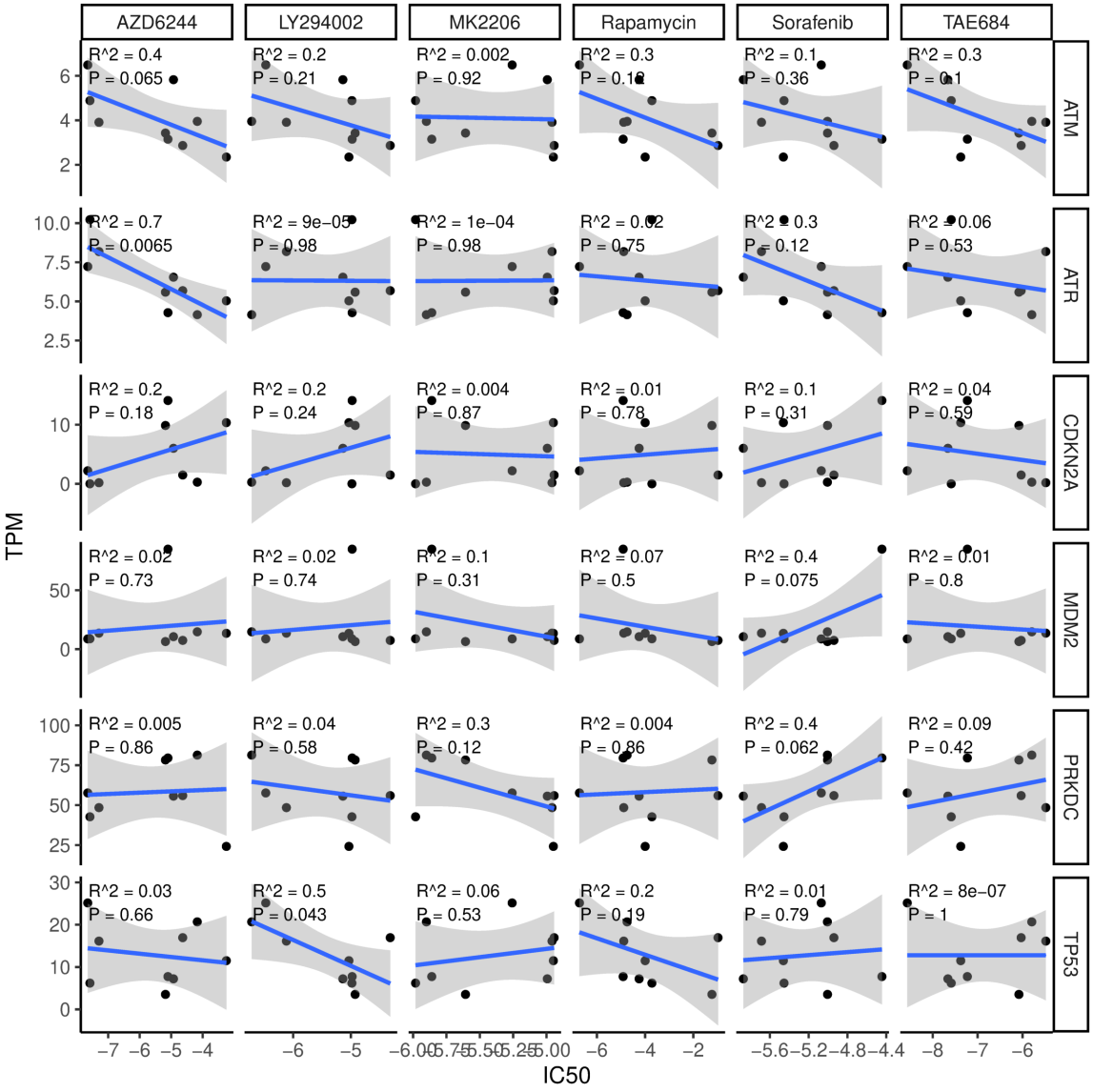

Figure Appendix.10: Correlation between IC50 and gene expression for TP53 pathway genes.

the PI3K inhibitor LY294002 was puzzling as silencing of KRAS inhibits the activation of the PI3K pathway (Zhang et al., 2020) so it could be expected that KRAS expression protects against PI3K inhibition. However it seemed that on the contrary the higher PI3K activaty likely induced by higher KRAS level made the cells more vulnerable to PI3K inhibition. This was not observed for other RAS isoforms, suggesting that KRAS could be the primary activator the PI3K pathway in those cell lines.

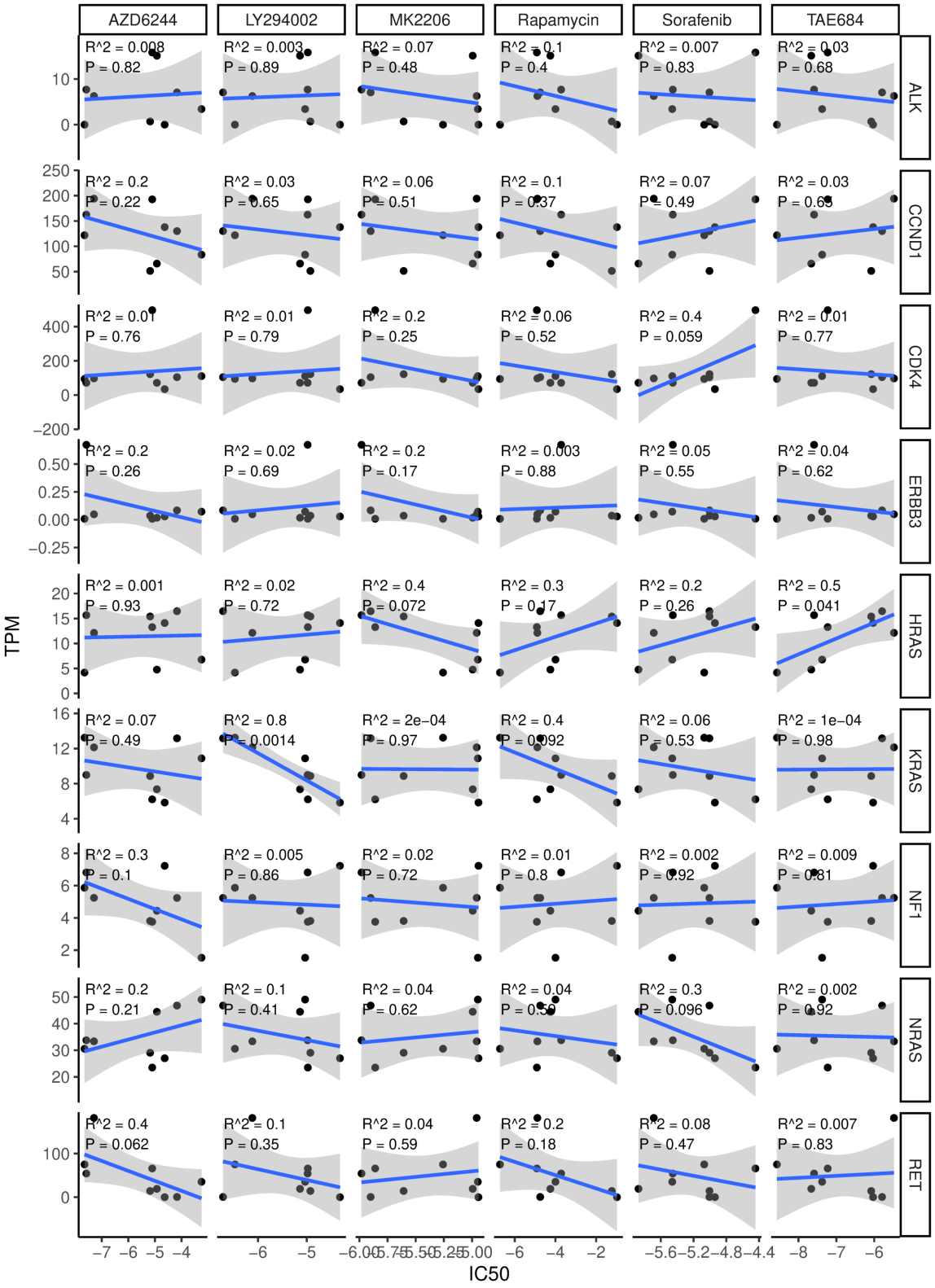

Figure Appendix.11: Correlation between IC50 and gene expression for RAS pathway genes.

Given the highly heterogeneous response of the cell lines to the ligands (Figure 4.6), I also investigated whether this response could be explained with receptor expression by computing the correlation between the fitted path from the ligands to readouts and the expression of biologically plausible receptors for those ligands. Of note, the expression of the receptor ALK anti-correlated with the effect of ALK inhibition on MEK and cJUN suggesting that ALK expression could predict the response of the signalling networks to ALK inhibition. Only 3 path-receptor pairs showed a strong positive correlation. Those results should however be interpreted with caution as only 6 cell lines were perturbed, meaning that no correlation were statistically significant.

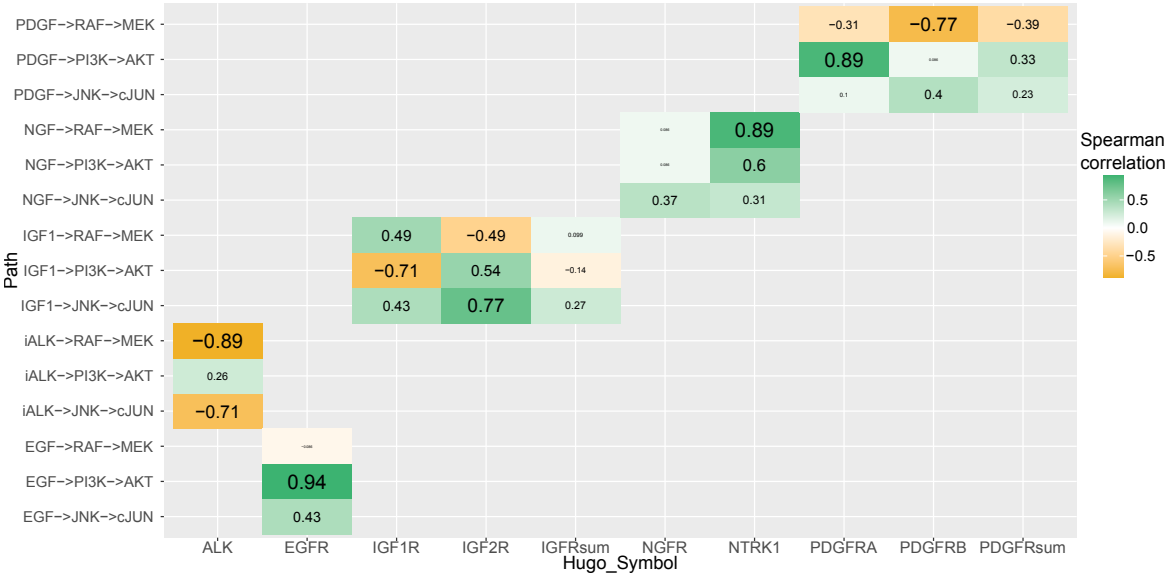

Figure Appendix.12: Spearman correlation between the path value from ligands to readouts fitted in the "Fixed inhibitor" model and the expression of the matching receptor or receptor family. IGFRsum and PDGFRsum are the sum of the isoforms expression for IGFR and PDGFR respectively.

The EGFR expression strongly correlated with the activation of AKT by EGF, and also weakly to the activation of cJUN. Perhaps surprinsingly the activation of MEK by EGF did not correlated with EGFR expression. This can likely be explained by the fact that the recruitement of RAS and RAF by the receptors necessitates adaptors whose expression also vary between the cell lines, as I investigated in chapter 3.

Next, the expression of NTRK1 strongly correlated with the activation of MEK by NGF, which appeared to contradict the observation for the EGFR but could also mean that the NTRK1 adaptors leading to MAPK activation are more stably expressed. This was supported by the fact that NTRK1 expression also correlates with NGF-induced AKT activation, Interestingly, no correlation was observed for the NGFR which strongly suggested that NGF activation was mediated exclusively by NTRK1 in neuroblastoma cell lines, consistent with the relative affinity of those receptors (Ebendal, 1992).

Finally, the activation of AKT by PDGF correlated with PDGFRA expression but not PDGFRB suggesting that this receptor mediated PI3K pathway activation. Surprisingly, the activation of MEK by PDGF anti-correlated with both PDGF receptors expression, again suggesting that adaptors are crucial for some receptor-tyrosine-kinases-mediated activation of the MAPK pathway.

C.3 Phosphoproteomics of the MEKi and IGFRi combination

The few overlapping differentially phosphorylated sites between IMR32 and N206 were all either from MEK inhibition alone or from the combination treatment (Figure Appendix.13). However most sites differentially phosphorylated by the combination of MEKi+IGFRi recapitulated the single drug effect in IMR32 while several phosphosites were synergistically affected by the combination in N206.

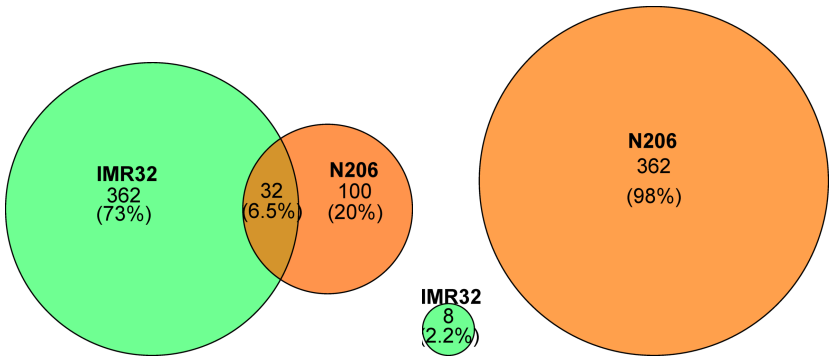

(a) MEKi (b) IGFRi

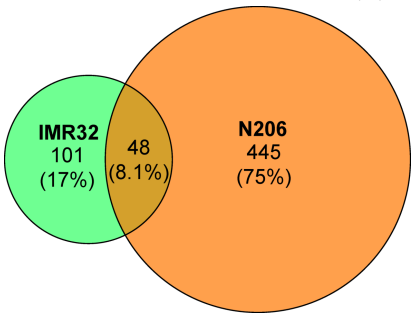

(c) MEKi+IGFRi

Figure Appendix.13: Venn diagram showing the overlap of phosphopeptides differentially expressed after IGFR and/or MEK inhibition versus DMSO control in N206 and IMR32 between cell lines for each treatment. FDR < 0.05.

C.4 Gene set enrichment

Most of the significantly enriched KEGG pathways contained the MAPK and PI3K pathways (Figure Appendix.14).

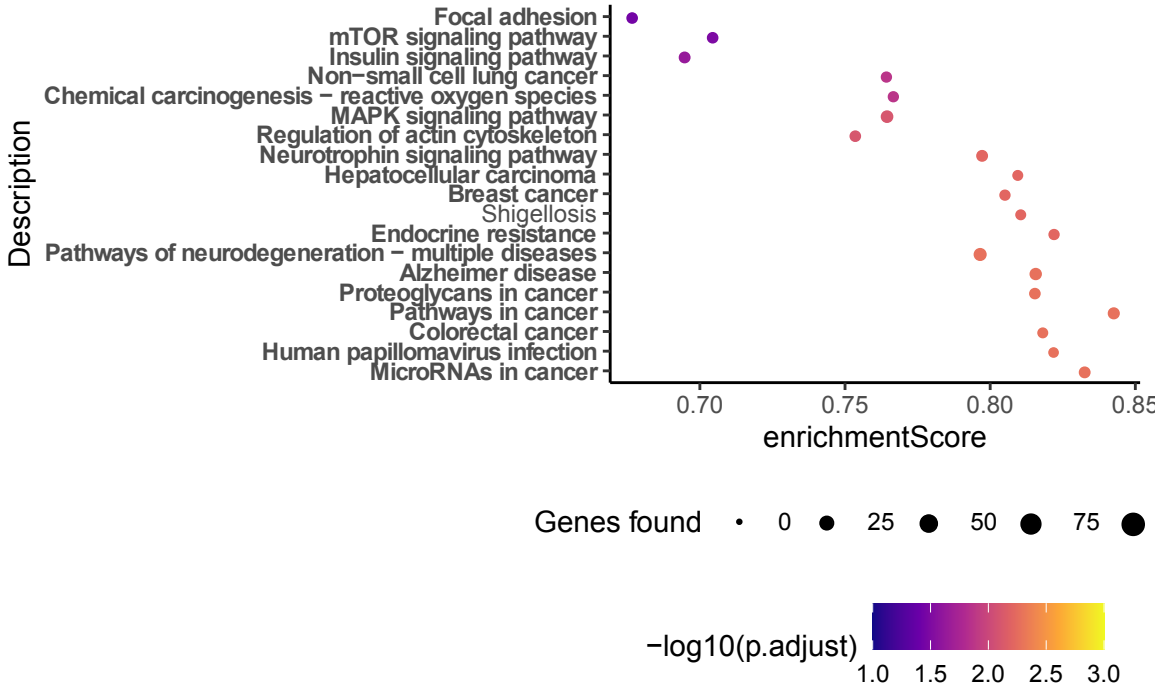

(a) IMR32

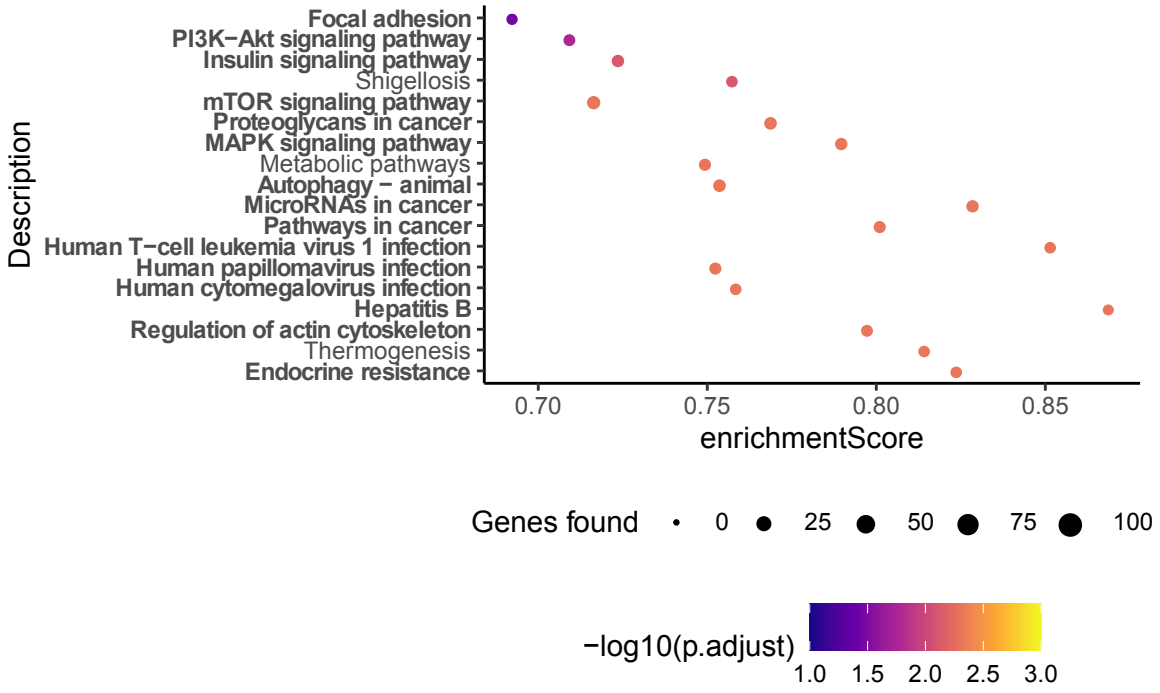

(b) N206

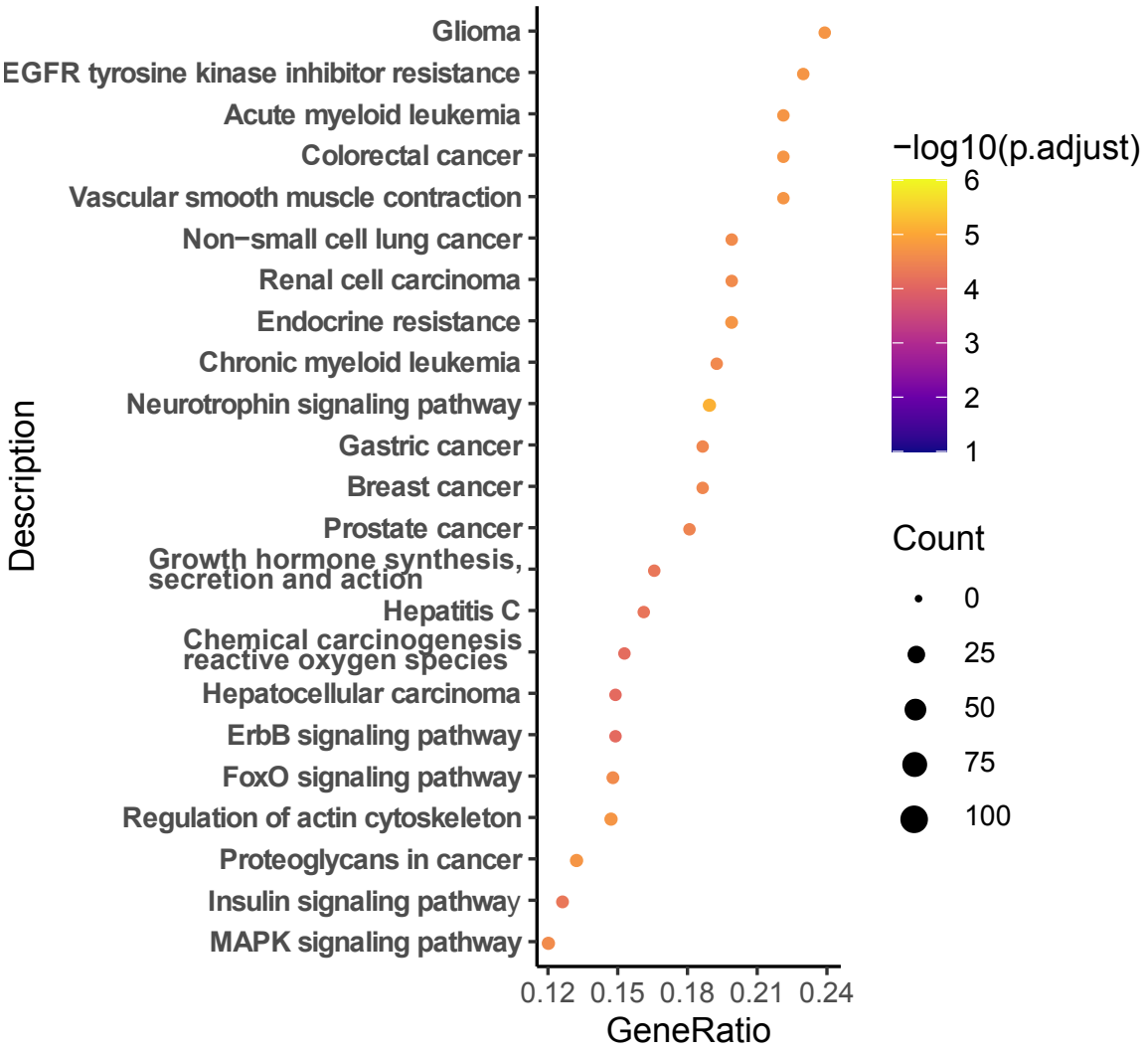

(c) IMR32 and N206

Figure Appendix.14: KEGG pathways enrichment analysis of proteins differentially phosphorylated on at least one site in (a) IMR32, (b) N206 or (c) both cell lines. FDR < 0.05. *Italic* pathway names indicate a shared pathway between IMR32 and N206, **bold** pathway names indicate pathways containing RAF, MEK and ERK. Pathways are o.

As expected from the perturbation data, those two pathways were the most affected by the perturbations, with the PI3K pahtway appearing more affected in N206. However, the fact that pathways related to different ontological processes all end up significantly enriched by this analysis highlighted the need for more refined methods for gene set enrichment that are still to be developped (Pomaznoy et al., 2018; Manjang et al., 2020).

C.5 Evaluation of the Sugiyama kinase-substrates annotation

ERK1/2$^{\text{T185/T202+Y187/Y204}}$ (MAPK1/3) are the only validated target phosphosites of MEK1/2 (Wu et al., 2015). They were profoundly dephosphorylated after MEK inhibition showing that MEK was properly inhibited (Figure Appendix.15b). However, MEK was not picked up as differentially active using the Sugiyama kinase-substrates annotation (Figure Appendix.15a).

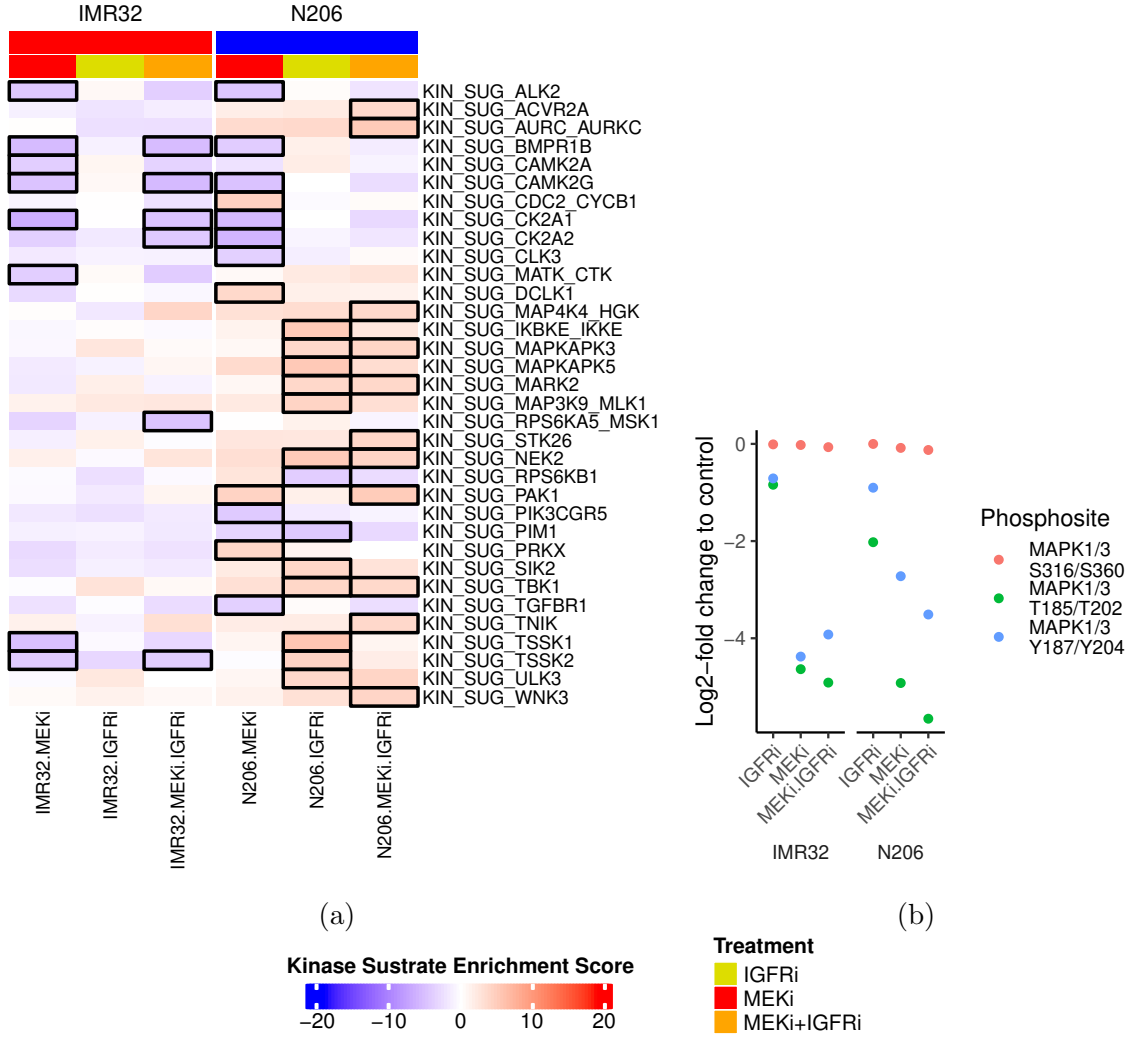

Figure Appendix.15: (a) Kinases with significant substrate enrichment using Sugiyama *et al.* kinase-substrates annotation. Black outline indicates significant conditions, FDR $<$ 0.05. (b) Log2-fold-change to DMSO control of ERK phosphophosites measured by TMT in N206 and IMR32.

Indeed ERK1/2 were not in the substrate list for MAP2K1/2 in this annotation. The annotated target in Sugiyama et al. (2019) of MAP2K1 and MAP2K2 are WAC$^{\text{S373}}$, MAP2K2$^{\text{S125}}$, MAP2K2$^{\text{S129}}$, CHERP$^{\text{S826}}$, TRAFD1$^{\text{S327}}$, PSMA7$^{\text{S150}}$, TPD52L2$^{\text{S21}}$, ZRANB2$^{\text{S310}}$, ZRANB2$^{\text{S305}}$, CPS1$^{\text{S835}}$, FOXK1$^{\text{S445}}$, KHDRBS1$^{\text{S29}}$, FADD$^{\text{S194}}$, INF2$^{\text{S1204}}$, WDR44$^{\text{S561}}$, NCCRP1$^{\text{S31}}$, NCCRP1$^{\text{S33}}$, DCP1A$^{\text{S487}}$, ARGLU1$^{\text{S76}}$, CHMP5$^{\text{S16}}$, SRRM2$^{\text{S1648}}$, SRRM2$^{\text{S2398}}$, MAP3K2$^{\text{S164}}$, EIF4B$^{\text{T205}}$, HSPD1$^{\text{T422}}$, HSPD1$^{\text{T115}}$, PLS3$^{\text{T117}}$, HSP90B1$^{\text{T148}}$, WARS$^{\text{T362}}$, GTF2F1$^{\text{T389}}$,

GTF2F1^{T41}, CAPZB^{T202}, EIF4H^{T100}, FIP1L1^{T420}, GIGYF2^{T382}, FUBP3^{T250}, CHMP5^{T18}, SF3B1^{Y39} and RPS6KA3^{S686}, MAP2K2^{S196}, MAP2K2^{S198}, MAP2K2^{S125}, MAP2K2^{S129}, TOMM70A^{S96}, WDR44^{S561}, STRIP1^{S341}, MEPCE^{S69}, CACTIN^{S108}, CACTIN^{S110}, CCDC86^{S91}, SRRM2^{S1648}, SRRM2^{S876}, CNPY2^{S74}, PPIL3^{T149}, EIF4B^{T205}, AIP^{T48}, HSF1^{T349}, RAF1^{T517}, IPO7^{T968}, TUBB4A^{T35}, SSB^{T120}, HSPD1^{T422}, HSP90B1^{T148}, TGM2^{T368}, WARS^{T362}, GTF2F1^{T41}, PAFAH1B1^{T150}, YAP1^{T110}, PSMD4^{T264}, EIF4H^{T100}, RCN1^{T100}, SF3B4^{T14}, LARP1^{T670}, FNBP4^{T479}, NAP1L4^{T28}, CHMP5^{T18}, RTCB^{T484} respectively. This example highlights problems with both precision, as ERK1/2 were not found, and specificity, as many indirect or non biological targets of MAP2K1/2 were found, in this dataset. For this reason, I considered this annotation improper to determine which kinases were active and chose to rely exclusively on the PhosphositePlus annotation.

C.6 Total proteomics

A total protein measurement was generated in parallel with the phosphoproteomics. The distribution of p-values for the differential expression analysis of the total proteomics following treatment for 4h of IMR32 and N206 cells with AEW541 10 μM and/or AZD6244 10 μM or DMSO displays a heavy skew from a uniform distribution, with many more low p-values than expected by chance. This suggested that some proteins were indeed differentially regulated, however this was not picked up by the false discovery rate approach because the signal-to-noise ratio is insufficient to yield extreme enough p-values. The relative abundancy of p-values < 0.05 suggested that it was not possible to reach an FDR below 30% (Figure Appendix.16). So as to extract protein differentially expressed in both cell lines, I filtered for proteins with $p < 0.05$ in at least 4 of the 6 conditions (2 cell lines $\times$ 3 treatments). 17 proteins fullfilled this criteria: CD97, APEX2, CALD1, CASP7, EIF6, GPATCH2L, HMX1, HSP90AA4P, ID1, JUNB, MRPS34, MT.ATP6, MYCN, PSMA3, SHISA6, TMEM201 and TUBB4A. MYCN was particularly interesting because the corresponding phosphorylated peptides were also downregulated, unlike for the other proteins of this list (Figure Appendix.16). This suggested that the dephosphorylation of MYCN was specifically driven by the inhibitions and could be the cause for its downregulation.

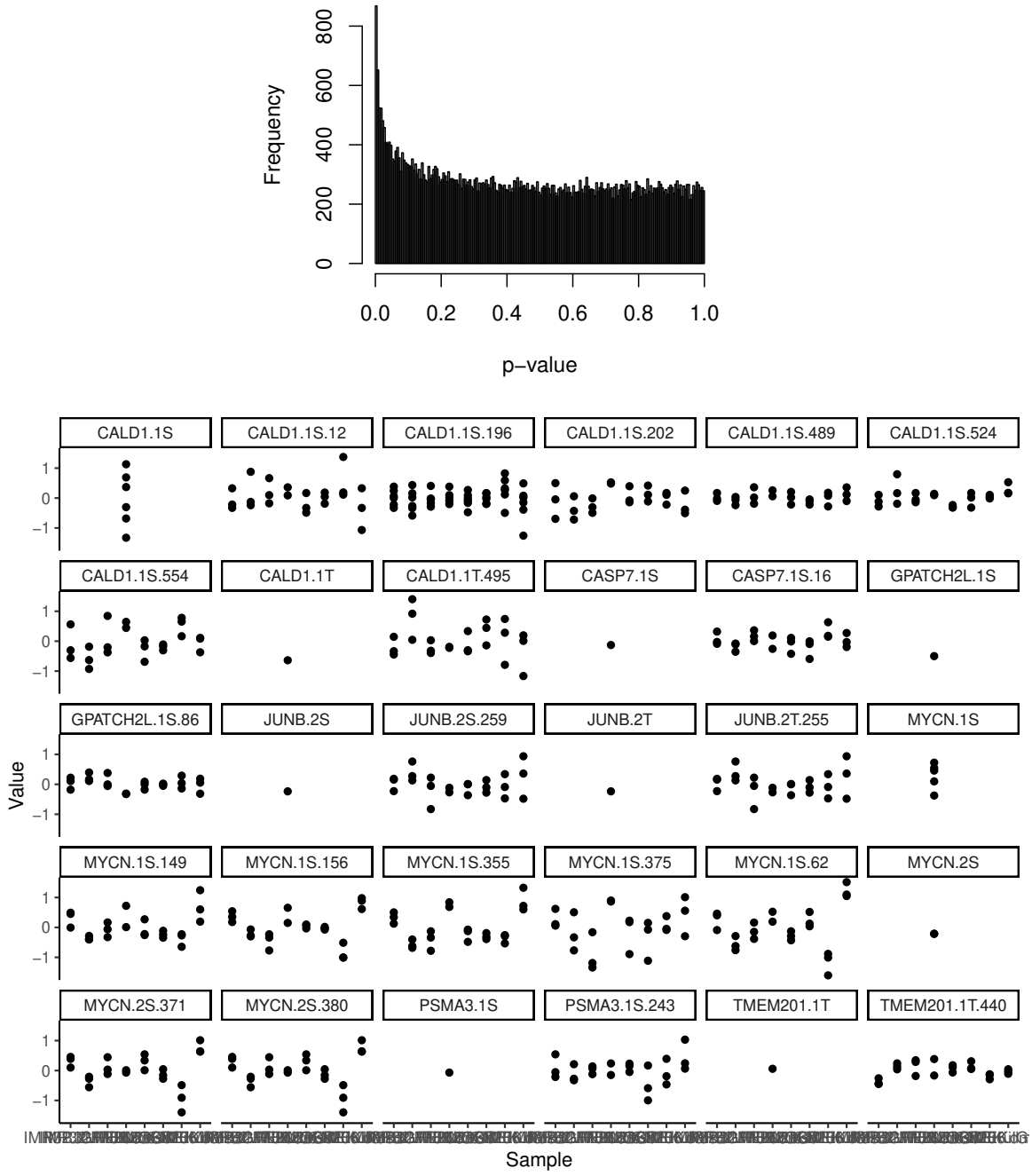

Figure Appendix.16: p-values distribution from the differential expression analysis on total proteomics data of IMR32 and N206. Phosphosites for proteins seeming differentially expressed in 4 out of 6 conditions.

D Supplementary analysis on NF1 KO data

D.1 Batch normalisation of NF1-KO perturbation data

In NF1KO plex panels, an important part of the variance was due to batch effects (Figure Appendix.17). In order to remove this unwanted variation I divided each readout by the mean value in the batch, i.e $M^{\text{norm}}_{t,r} = M_{t,r}/mean(M_{shared_t,r})$ where M is the experimentally measured matrix with treatment in rows and readout in the columns.

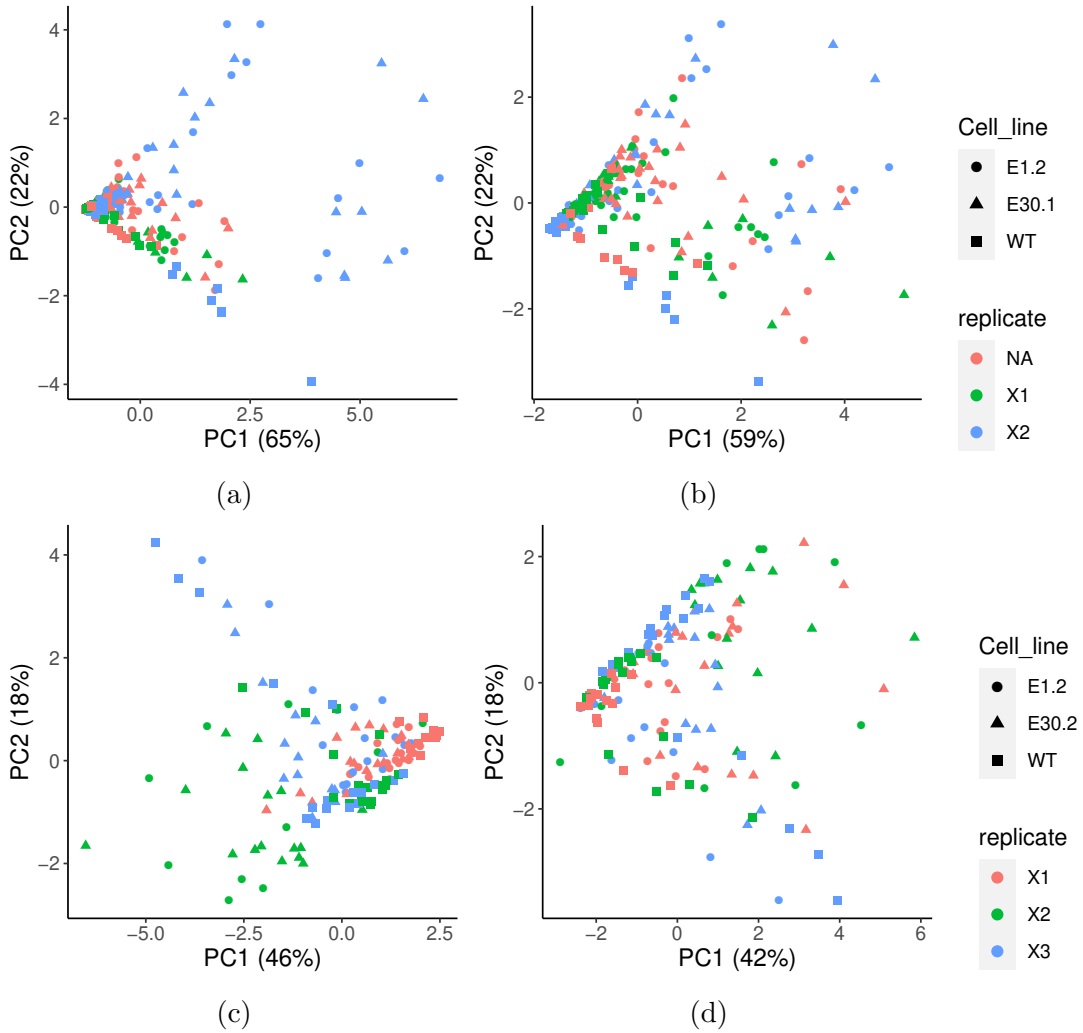

Figure Appendix.17: Plex measurements of LAN5 (top) and SHSY5Y (bottom) before (left) and after (right) batch normalisation.

D.2 LAN5 NF1-KO fitting summary

WT LAN5

```
## [1] "Best fit: 42.249 , Score= 0.8"
```

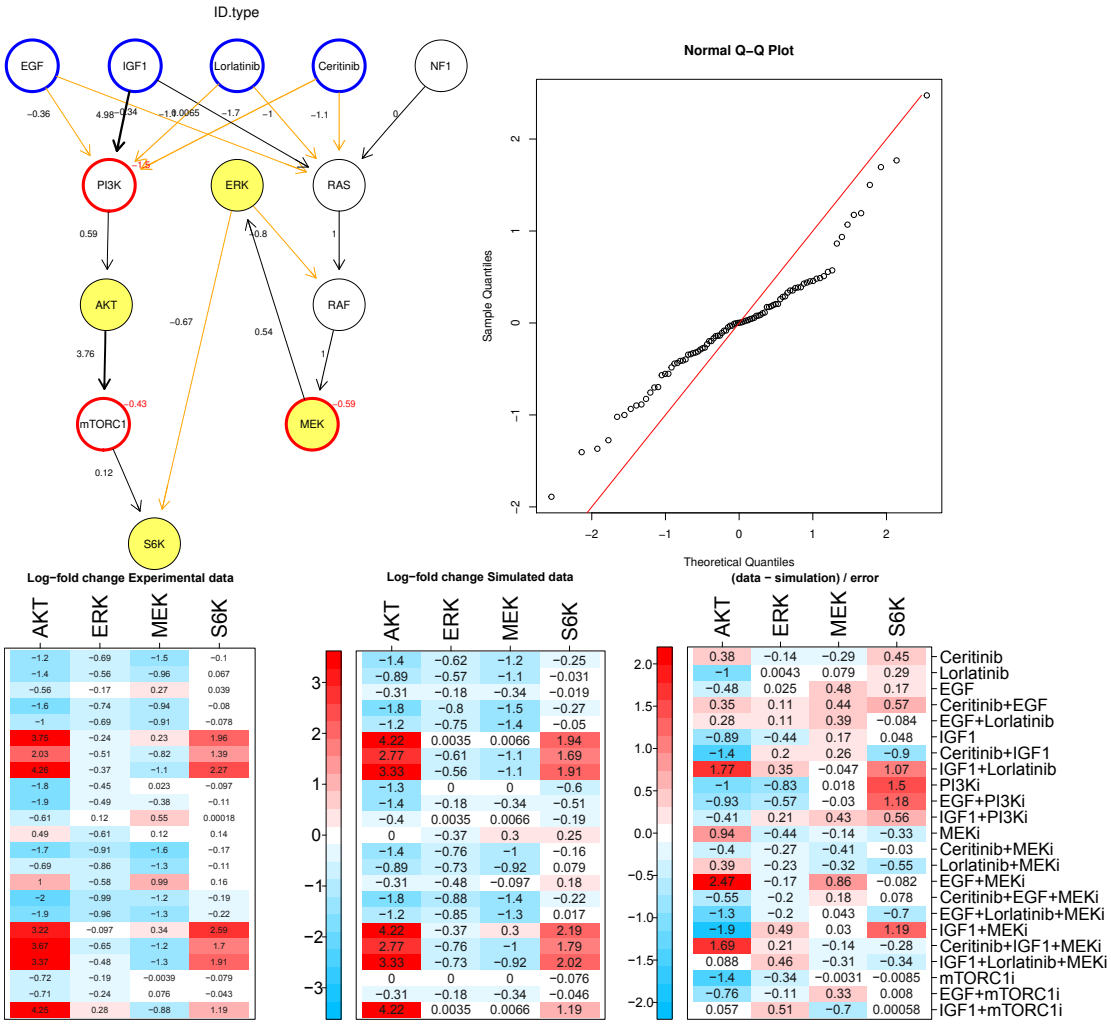

Figure Appendix.18: Graphical representation, qq-plot and direct comparison with the data of the predictions of the WT LAN5 model.

from	to	residual	Res_delta	adj_pval
IGF1	S6K	39.9947651907667	2.25434782676026	1
IGF1	mTORC1	39.9978401962135	2.25127282131351	1
EGF	ERK	40.7131926278426	1.53592038968441	1
AKT	ERK	41.2781393566993	0.970973660827653	1
mTORC1	ERK	41.3978078272604	0.851305190266601	1
mTORC1	RAS	41.4573241423871	0.791788875139872	1

Table Appendix.30: Best extensions for the WT LAN5 model.

E1.2 LAN5

```
## [1] "Best fit: 59.554 , Score= 0.76"
```

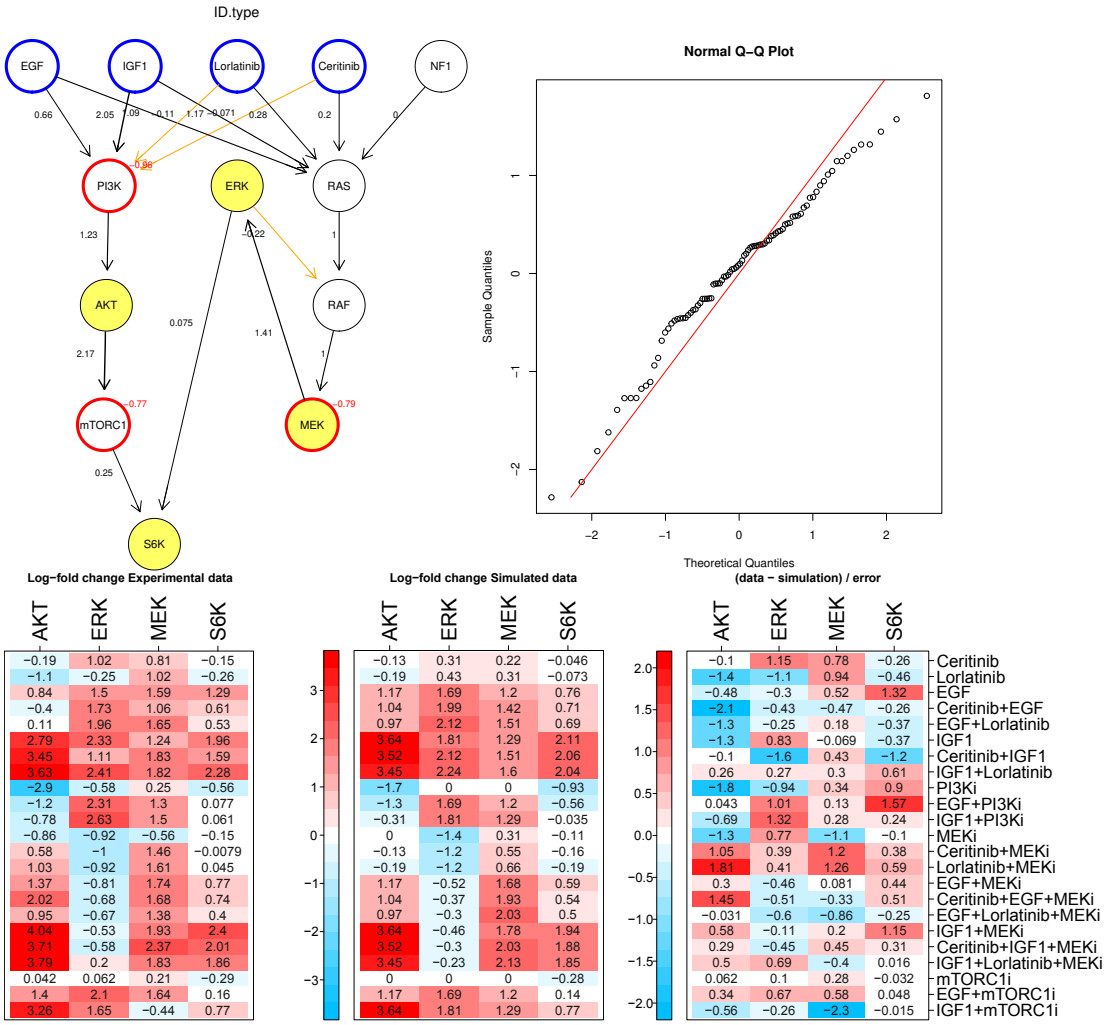

Figure Appendix.19: Graphical representation, qq-plot and direct comparison with the data of the predictions of the E1.2 LAN5 model.

from	to	residual	Res_delta	adj_pval
MEK	PI3K	50.5228874933907	9.03095340038076	0.24
ERK	PI3K	50.5228874933973	9.03095340037416	0.24
ERK	AKT	51.6629035029937	7.89093739077768	0.45
AKT	RAF	57.101630359108	2.45221053466338	1.00
PI3K	NF1	57.1016303591084	2.45221053466298	1.00
AKT	RAS	57.1016303591117	2.45221053465971	1.00

Table Appendix.31: Best extensions for the E1.2 LAN5 model.

E30.1 LAN5

```
## [1] "Best fit: 43.455 , Score= 0.71"
```

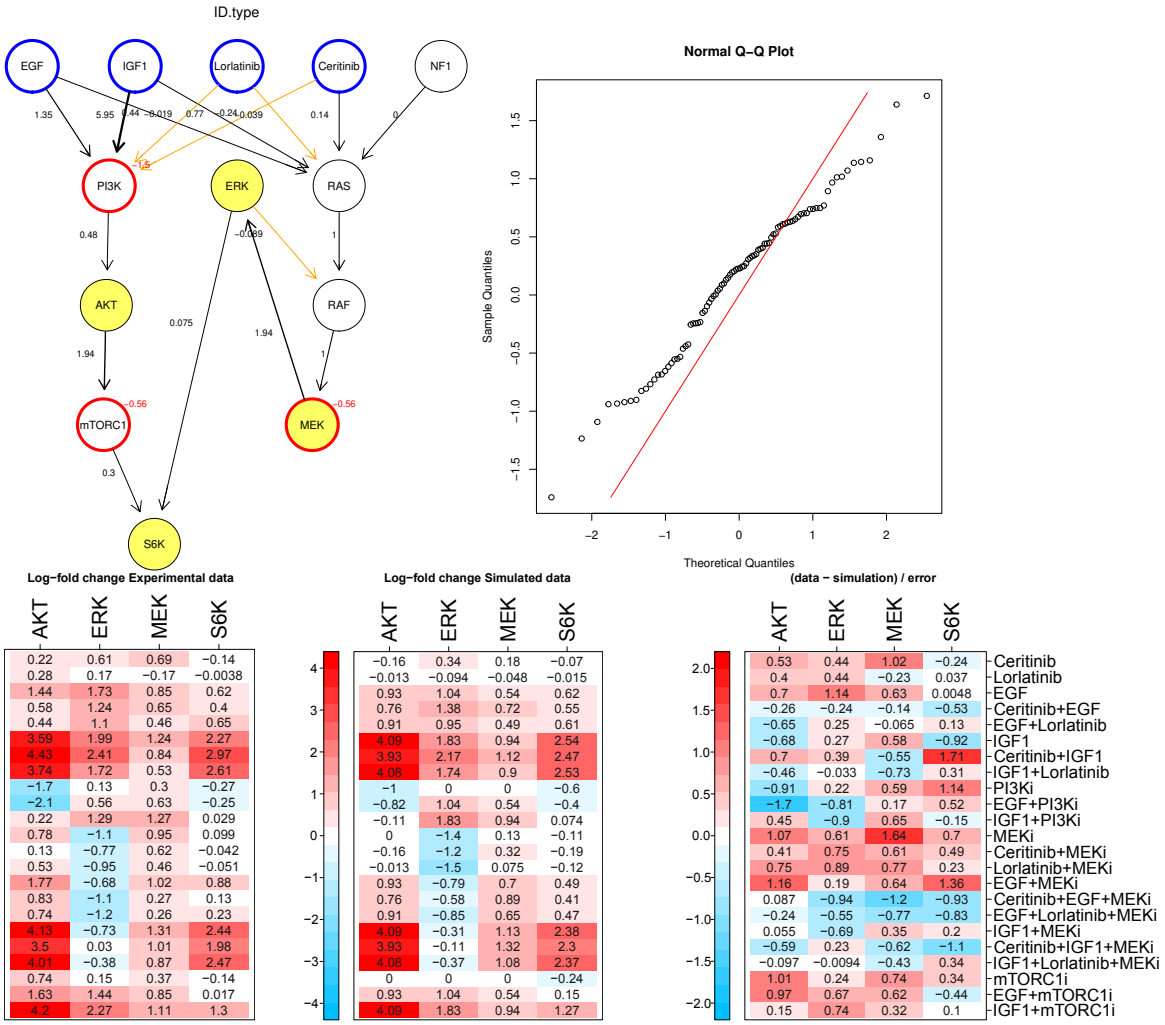

Figure Appendix.20: Graphical representation, qq-plot and direct comparison with the data of the predictions of the E30.1 LAN5 model.

from	to	residual	Res_delta	adj_pval
S6K	PI3K	42.4704029466845	0.984560531308993	1
AKT	ERK	42.5636012064792	0.891362271514268	1
ERK	AKT	42.7420253291673	0.71293814882614	1
ERK	PI3K	42.9019916929389	0.552971785054616	1
MEK	PI3K	42.9019916929825	0.552971785010961	1
mTORC1	PI3K	42.910336330829	0.544627147164533	1

Table Appendix.32: Best extensions for the E30.1 LAN5 model.

D.3 Modelset LAN5 NF1-KO

All LAN5 single cell line models were in good agreement with the data and had the same topology as no extension could significantly improve any of them. This made them suitable for a ModelSet fitting. The LAN5 ModelSet reaches a good agreement with the data for all cell lines (Figure Appendix.22) by relaxing 9 of the 17 parameters.

```
## [1] "Best fit: 162.64 , Score= 0.86"
```

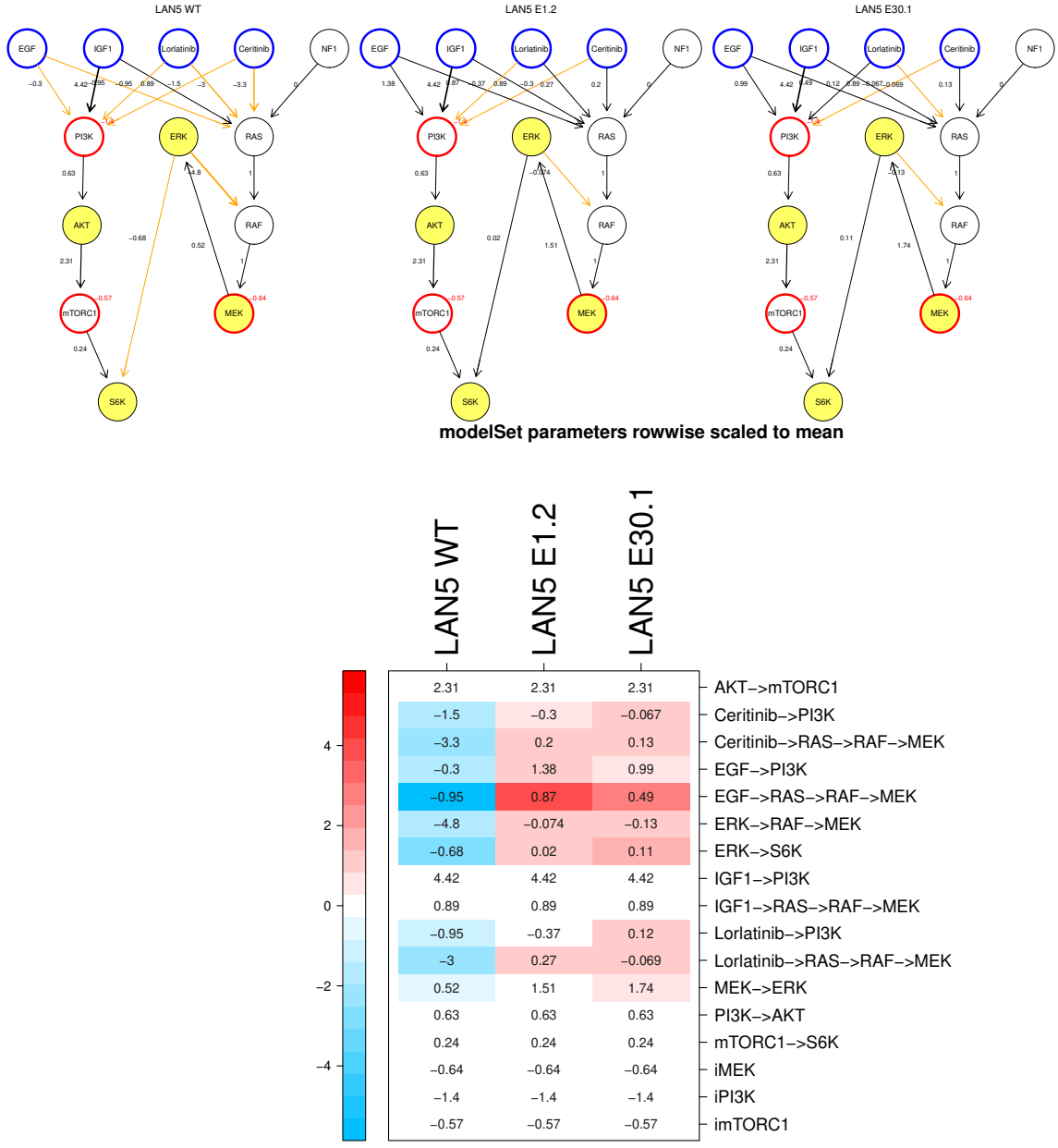

Figure Appendix.21: Graphical representation and paths values of the NF-KO LAN5 ModelSet.

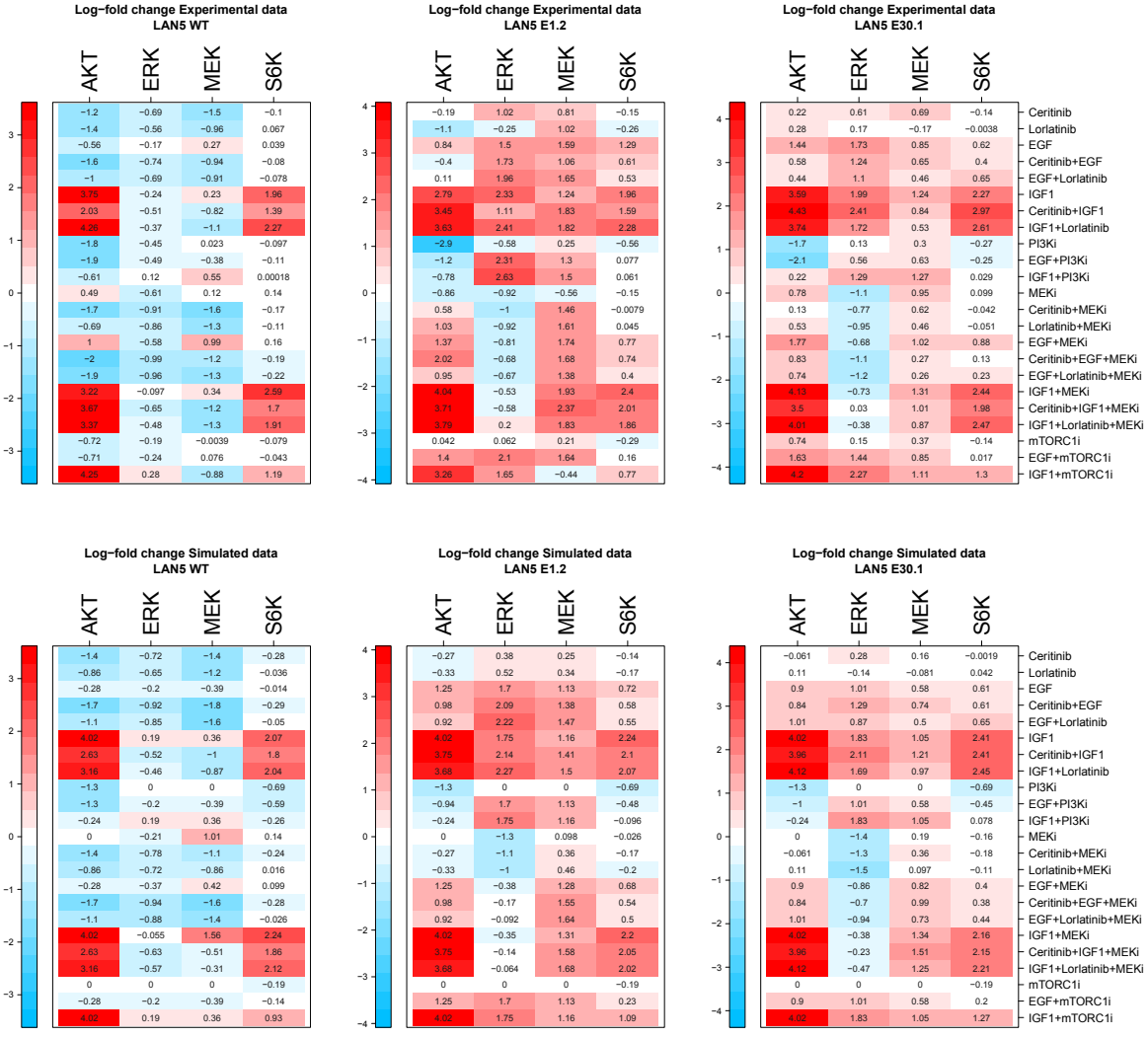

Figure Appendix.22: Direct comparison of the predictions of the NF-KO LAN5 ModelSet.

D.4 SHSY5Y NF1-KO fitting summary

WT

```
## [1] "Best fit: 43.552 , Score= 0.61"
```

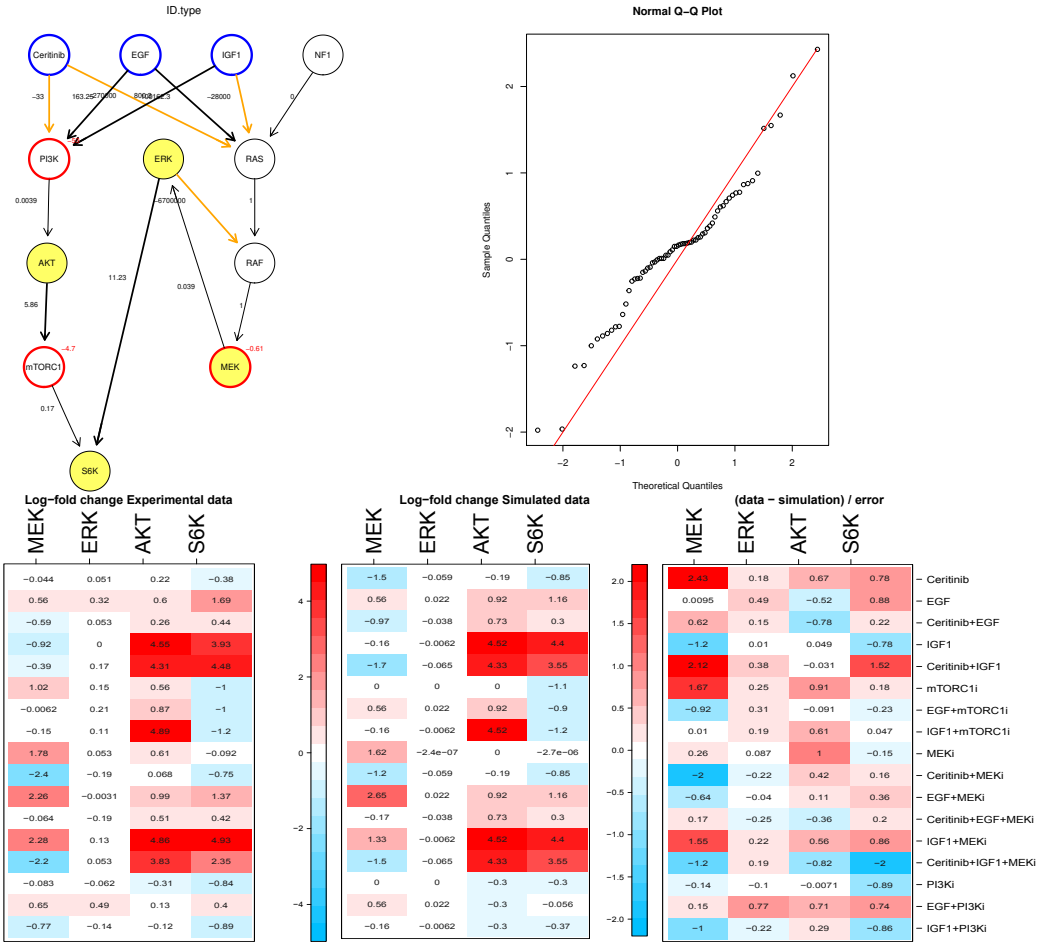

Figure Appendix.23: Graphical representation, qq-plot and direct comparison of the results of the WT SH-SY5Y model.

from	to	residual	Res_delta	adj_pval
EGF	mTORC1	41.4901186733801	2.06226987961616	1
Ceritinib	ERK	41.5787682261239	1.97362032687229	1
Ceritinib	mTORC1	41.7188955696511	1.83349298334509	1
Ceritinib	S6K	41.7189041444509	1.83348440854535	1
EGF	ERK	41.8457048496165	1.70668370337969	1
IGF1	ERK	41.8694358940522	1.68295265894404	1

Table Appendix.33: Best extensions for the WT SH-SY5Y model.

E1.2

The fit for E1.2 SH-SY5Y is overall good, except for the S6K and MEK measurements under Ceritinib+EGF+MEKi treatment. The model cannot explain the downregulation of those readouts conpared to EGF+MEKi. It is unlikely to be an off-target effect of Ceritinib on the EGFR because EGF+Ceritinib is very similar to EGF alone for those readouts.

```
## [1] "Best fit: 87.741 , Score= 0.58"
```

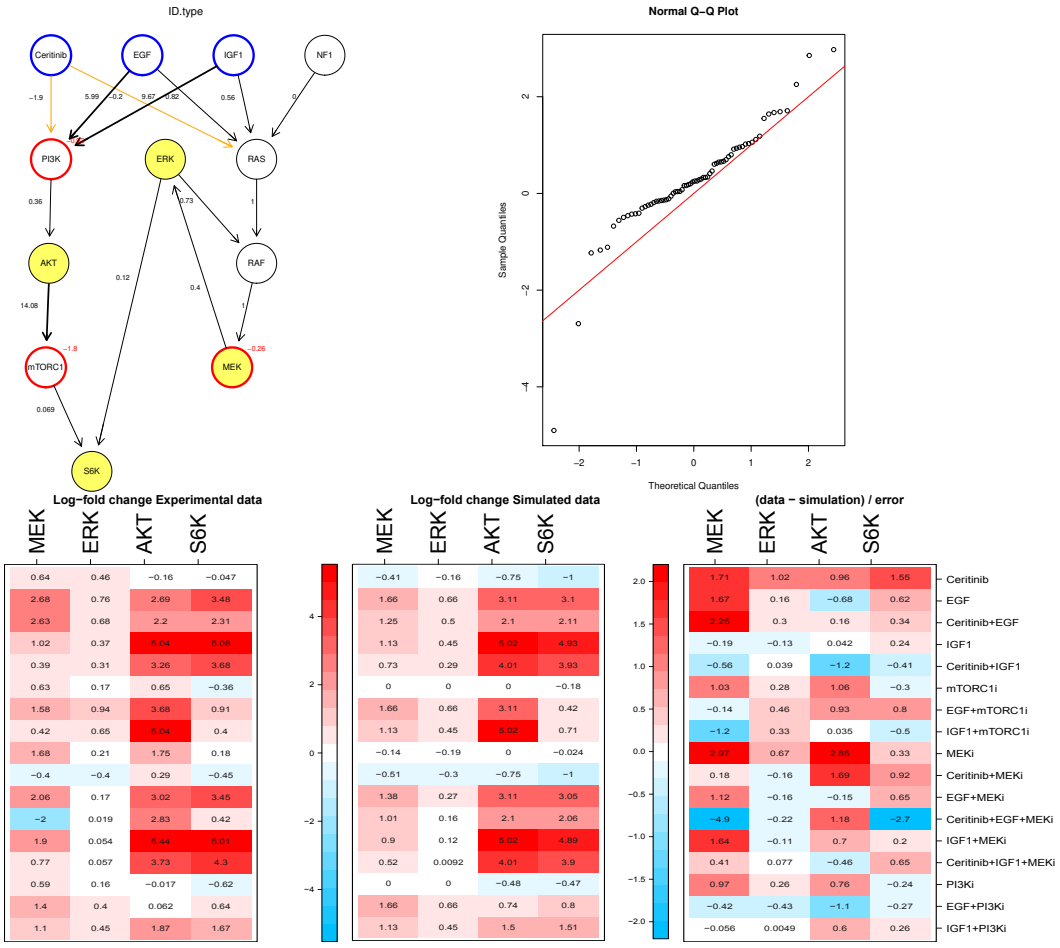

Figure Appendix.24: Graphical representation, qq-plot and direct comparison of the results of the E1.2 SH-SY5Y model.

from	to	residual	Res_delta	adj_pval
MEK	AKT	85.3293241094879	2.41166699229527	1
ERK	AKT	85.32932410949	2.41166699229308	1
MEK	PI3K	86.212943893765	1.52804720801814	1

Table Appendix.34: Best extensions for the E1.2 SH-SY5Y model

E30.2

```
## [1] "Best fit: 41.031 , Score= 0.78"
```

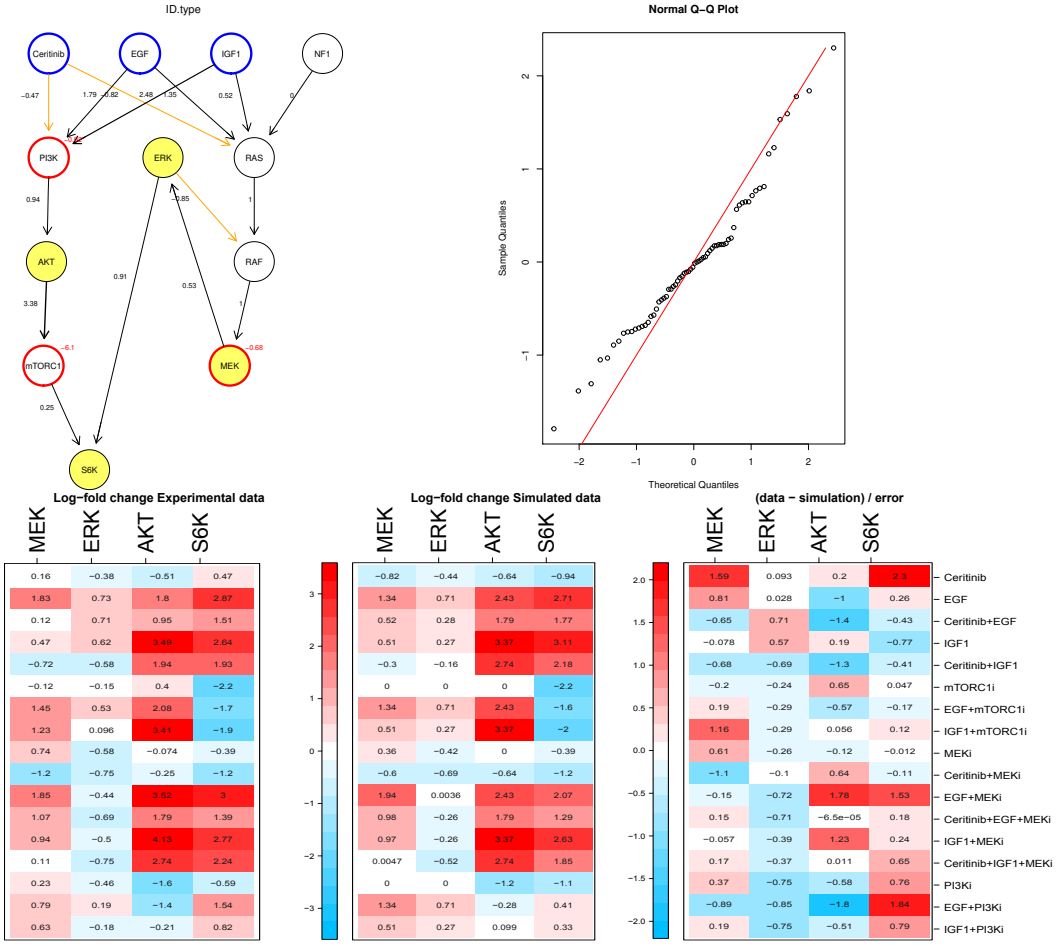

Figure Appendix.25: Graphical representation, qq-plot and direct comparison of the results of the E30.2 SH-SY5Y model.

from	to	residual	Res_delta	adj_pval
MEK	PI3K	32.523326480093	8.50781812265404	0.30
ERK	PI3K	32.5233264801666	8.50781812258045	0.30
MEK	AKT	32.5745371639582	8.45660743878886	0.31
ERK	AKT	32.5745371640485	8.45660743869851	0.31
EGF	mTORC1	34.2701030006243	6.76104160212271	0.78
EGF	S6K	35.2976390518479	5.7335055508991	1.00

Table Appendix.35: Best extensions for the E30.2 SH-SY5Y model

D.5 Modelset SH-SY5Y NF1-KO

All SH-SY5Y single cell line models were overall in good agreement with the data and had the same topology as no extension could significantly improve any of them. This made them suitable for a ModelSet fitting. The SH-SY5Y ModelSet reaches a good agreement with the data for all cell lines (Figure Appendix.27) by relaxing only 3 of the 17 parameters.

```
## [1] "Best fit: 137 , Score= 0.76"
```

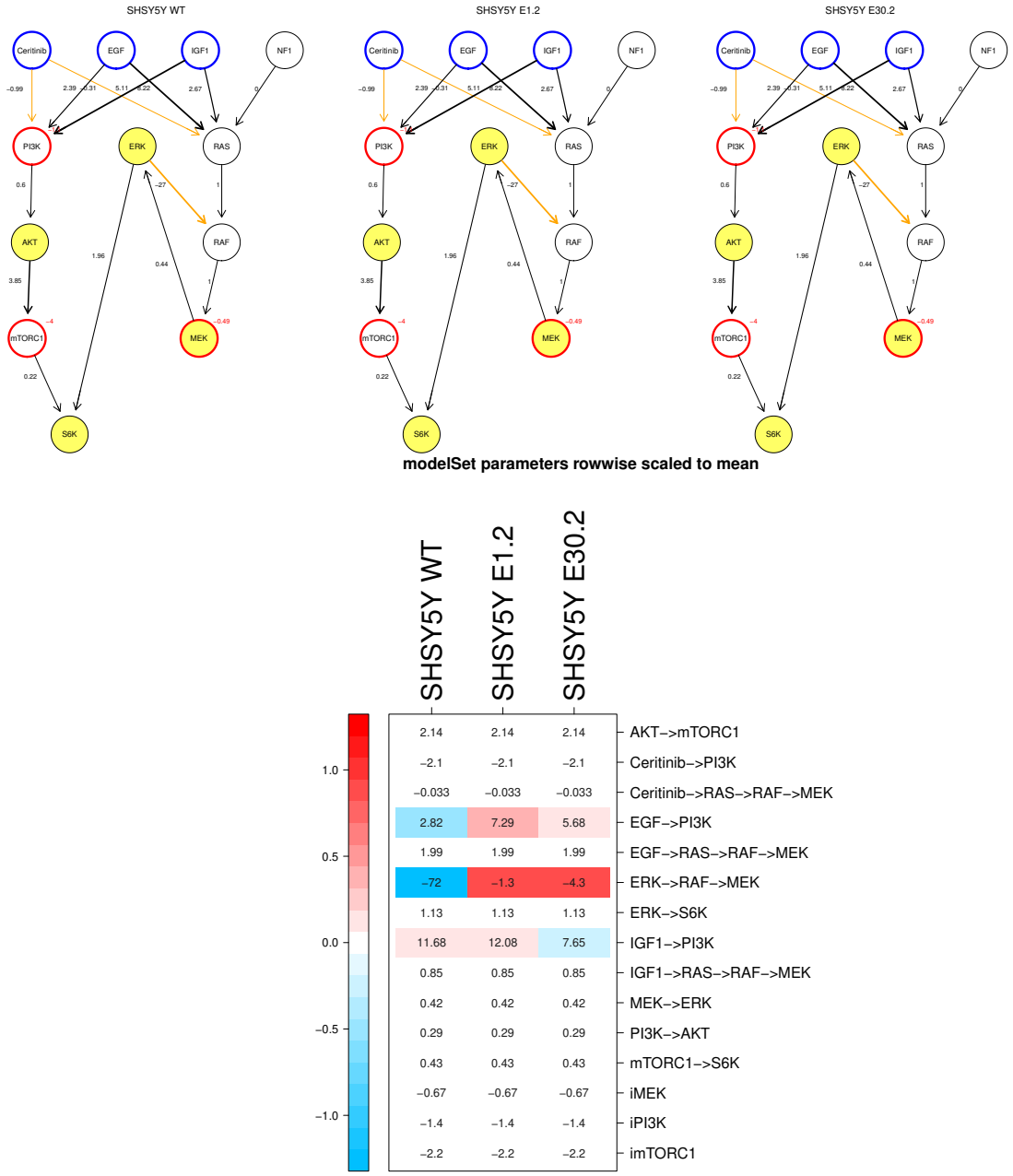

Figure Appendix.26: Graphical representation and parameter values of the SH-SY5Y NF1-KO ModelSet.

Figure Appendix.27: Measurement (top) and prediction (bottom) of the SH-SY5Y NF1-KO ModelSet.

D.6 Differential expression analysis of the NF1-KO phosphoproteomics

To extract the effect of the inhibitors I analysed separately in each cell line the effect of inhibitor treatment after 6h compared to the 6h DMSO control.

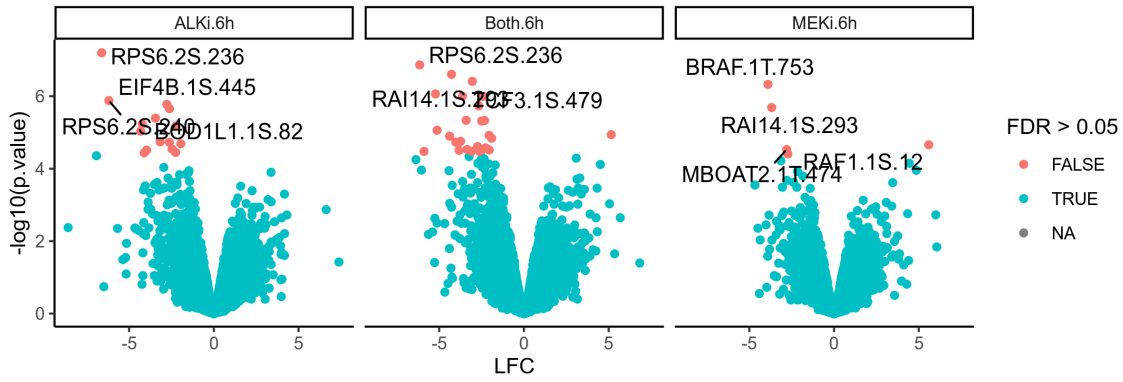

(a) WT

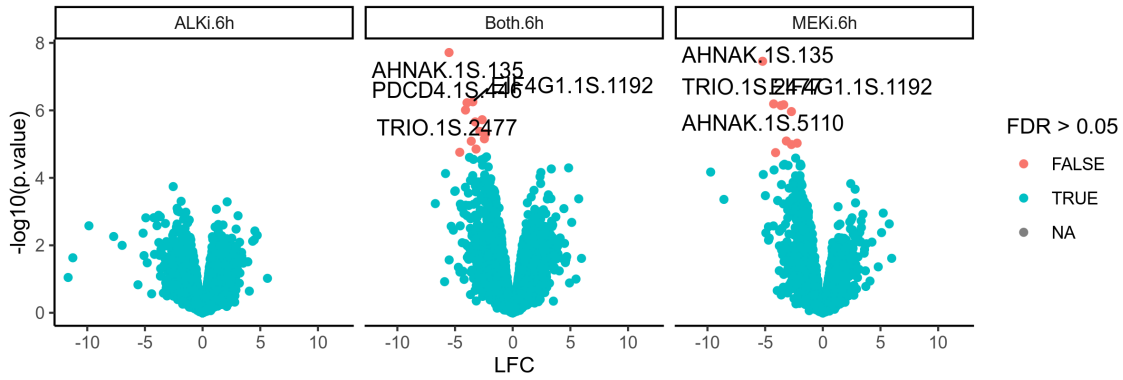

(b) E1.2

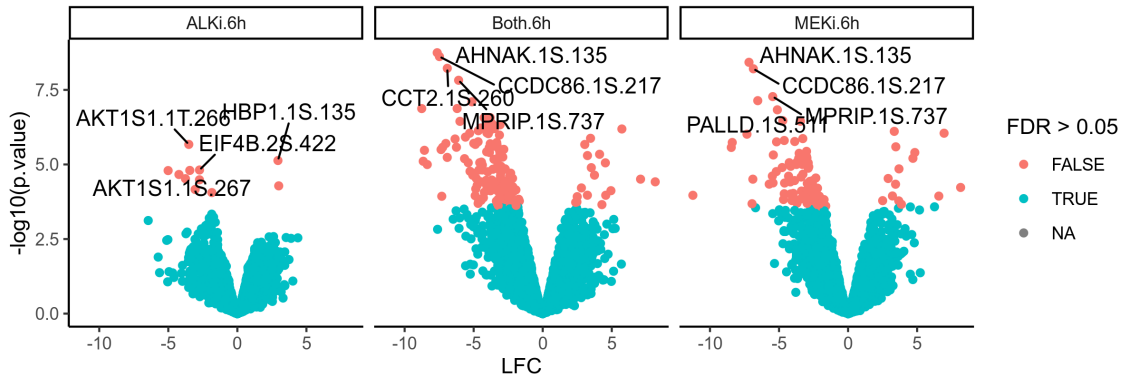

(c) E30.1

D.7 GO Term enrichment in NF1-KO cell lines

I started by performing a GO Biological Process enrichment using the genes corresponding to the phosphopeptides differentially expressed in either SHSY5Y NF1-KO

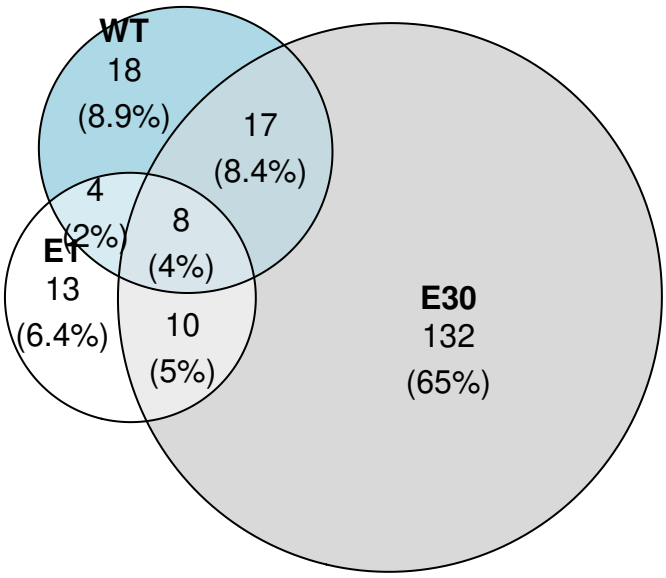

(d)

Figure Appendix.28: (a,b,c) Significantly deregulated phosphosites after treatment with Ceritinib (ALKi) and Selumetinib (MEKi) alone or in combination. (d) Venn diagram of peptides differentially phosphorylated in each SH-SY5Y cell lines after ALKi or MEKi treatment. FDR $<$ 0.05.

compared to the parental cell line (Figure Appendix.29). As expected it revealed mostly terms regulated by small GTPase deactivated by NF1 such as actin-filaments organization (Vallée et al., 2012; Cobleigh et al., 2021) or neuron differenciation (Crespo and León, 2000; Sun et al., 2006). Surprinsingly however the enriched terms were really different between the two clones, with only the two terms 'chromatin organisation' and 'DNA replication' enriched with p-value cutoff of 0.01 in E1.2 (Figure Appendix.29c) while morphogenesis related terms were the most enriched in E30.2 (Figure Appendix.29b).

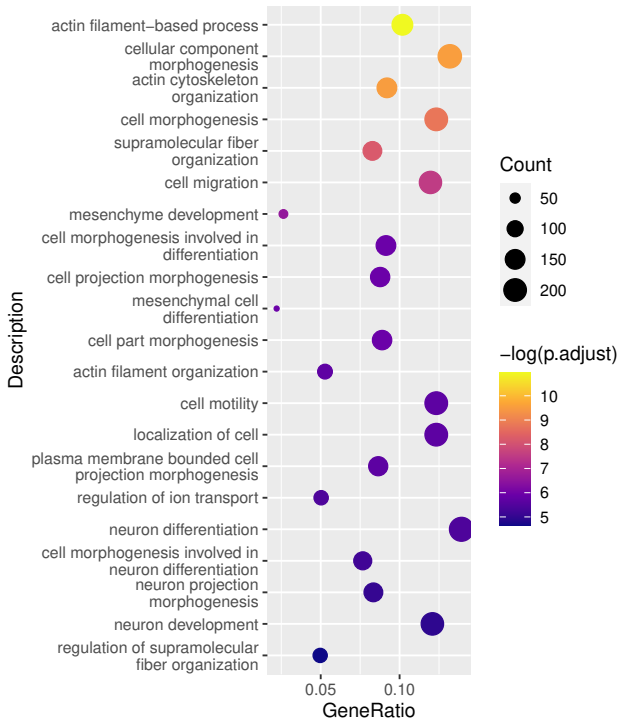

(a) Any

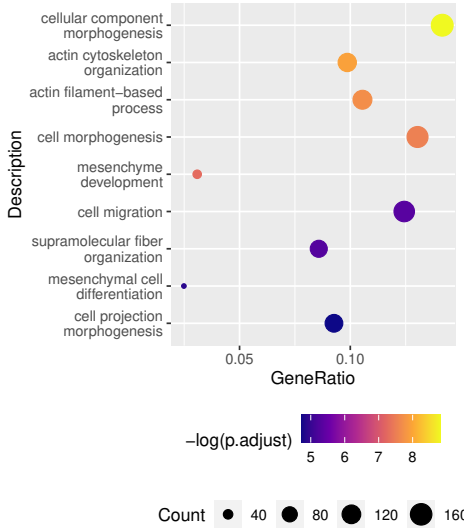

(b) E30.2

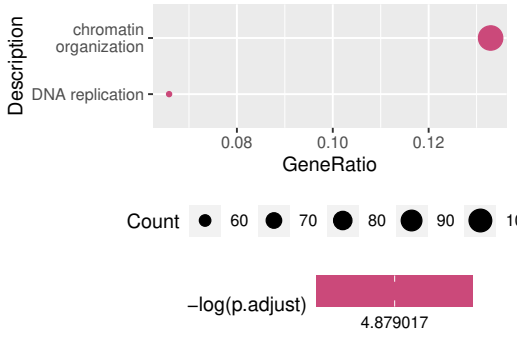

(c) E1.2

Figure Appendix.29: GO Biological Process enrichment for the genes corresponding to the differentially expressed phosphopeptides in (a) both E1.2 and E30.2, (b) E1.2 and (c) E30.2 compared to the parental cell lines. FDR $<$ 0.05, enrichment p-value cutoff 0.01.

D.8 Limits of kinase-substrate coverage

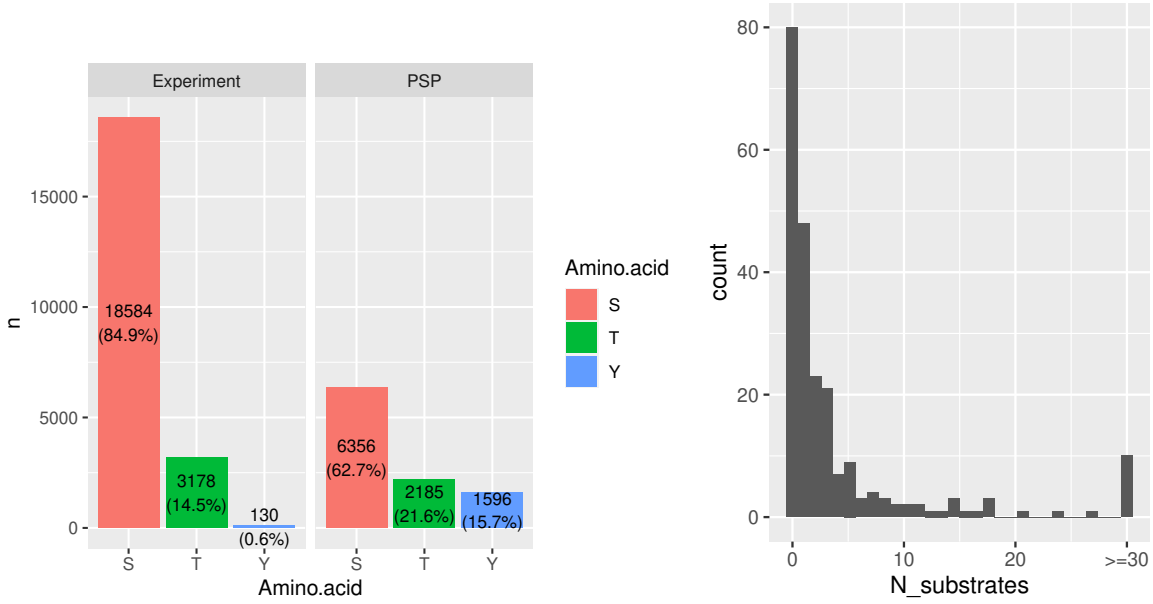

(a) (b)

Set	Matched substrates	Annotated substrates
PSP_RAF1	4	12
PSP_MEK1/MAP2K1	1	11
PSP_ERK2/MAPK1	61	367
PSP_ERK1/MAPK3	50	284
PSP_BRAF	4	16
PSP_ARAF	3	6
PSP_ALK	2	9
PSP_Akt2/AKT2	5	28
PSP_Akt1/AKT1	46	249

(c)

Figure Appendix.30: (a) Distribution of amino acid residues detected among measured phosphosites in the NF1-KO phophoproteomics. (b) Distribution of the number of substrates detected per kinase and (c) specific number of substrates detected and annotated for kinases of interest.

Most of the kinase activity computed only relied on a limited number of readouts detected in our dataset. This is expected for some kinases with few targets, such as MAP2K1 for which the only documented substrates are pERK1$^{T202/Y204}$ and pERK2$^{T185/Y197}$ which are not distinguishable in trypsin digested peptides. However it is not the case for most kinases, with AKT isoforms having dozens of annotated substrates and ALK expected to phosphorylate multiple adaptors but only a handful being detected. Out of 227 kinase annotated in the PhosphositePlus annotation no substrate phosphopeptides can be found in the data for 80 of them and only one substrate for 48 (Figure Appendix.30b). This is mostly due to the low detection of phospho-tyrosine (Figure Appendix.30a), which are less numerous in a cell and can only be detected if specifically enriched (Ding et al., 2007). Those activity data must

thus be interpreted carefully for those kinases, mostly tyrosine receptors.

Abbreviations

ALK	Neural receptor tyrosine kinase
AKT	Protein kinase B isoforms 1, 2 and 3
ASK1	MAP3K5 (Apoptosis Signal-regulating Kinase 1)
AURKA	Aurora kinase A serine/threonine-protein kinase
BET	Bromo- and Extra-Terminal domain protein family
$BRAF^{V600E}$	Natively active mutated version of B-RAF with the valine (V) at position 600 substituted by a glutamate (E)
cJUN	AP-1 transcription factor subunit
EGF	Epidermal Growth Factor
EGFR	Epidermal Growth Factor Receptor
EMA	European Medicines Agency
ERK	MAPK3 and MAPK1 (Dual specificity mitogen-activated protein kinases 1 and 2)
FBXW7	E3 ubiquitin ligase (F-box/WD repeat-containing protein 7)
FDA	Food and Drug Administration
GAP	GTPase activating protein
GO	Gene Ontology
GSK3	Glycogen synthase kinase 3
IGFR	IGF1R (Insulin Growth Factor Receptor 1)
JNK	JNK1/2/3 isoforms (cJUN N-terminal kinases)
KSEA	Kinase-Substrate Enrichment Analysis
MAPK	Mitogen-Activated Protein Kinase
MAX	Transcription regulator of NMYC
ML MRA	Maximum Likelihood Modular Response Analysis
MRA	Modular Response Analysis
MEK	MAP2K1 and MAP2K2 (ERK kinases 1 and 2)
mTORC1	mTOR complex 1 composed of mTOR (Mammalian Target Of Rapamycin), RAPTOR, MLST8, PRAS40 and DEPTOR
MYCN	N-myc proto-oncogene protein
NF1	Neurofibromin 1, RAS-GAP
NF1-KO	NF1 knock out
p38	MAPK11/12/13/14 (p38 mitogen-activated protein kinases)
PI3K	Complex of phosphatidylinositol 3-kinase comprising a catalytic subunit PIK3CA/B/G/D and a regulatory subunit PIK3R1/2/3/4/5/6
r	Local response matrix/Jacobian of differential equation systems implied by an MRA network.
R	Global response matrix/Inverted jacobian

RAF	Wild type isoforms A-RAF, B-RAF and C-RAF (serine/threonine kinase)
RAS	HRAS, KRAS and NRAS isoforms
RTK	Receptor Tyrosine Kinase
S6K/p70S6K	S6K1 (Ribosomal protein S6 kinase beta 1)
s.e.m	Standard Error of the Mean
STASNet	STeady STate Analysis of Signalling Networks, R package

Thesis Acknowledgments

First and foremost I would like to express my sincere gratitude to my supervisor Prof. Dr. Nils Blüthgen for the opportunity to work on this project, for his guidance and suggestions that kept the thesis always going forward, and for the amazing atmosphere of the Group of Computational Modelling in Medicine.

Of course I also want to thank all the colleagues old and new with whom I worked, discussed science or other nerdy subjects, sometimes partied, sometimes bouldered and always enjoyed being around during those years: Franziska Witzel, Bertram Klinger, Anja Sieber, Johannes Meisig, Florian Uhlitz, Manuela Benary, Mattias Rydenfelt, Evrim Besray Ünal, Tincy Simon, Ismail El-Shimy, Thomas Sell. Matthias Fischer, Rosario Astaburuaga, Jennifer Wiederspahn, Stefan Peidli and Anna Welter. Those were great years. A special scientific thank you to Anja for the great help in the lab, to Manuela for the useful analysis suggestion, to Bertram for the support with getting those papers to the finish line and to Tincy and Jenny for their thorough proof-reading. I also want to thank people from the Group of Molecular Tumor Pathology, especially Nathalie and Mareen for their support for my emergency Incucyte runs, as well as Sulafa, Markus and Christine for our very interesting discussions about science and life experience.

I would also like to thank my new boss, Dr. Marie-Laure Yaspo, for giving me the extra time I needed to finish this thesis and for the new exciting opportunities.

I am grateful for my friends in Berlin, who inspired and entertained me, particularly Lili for keeping our board game nights alive all this time. Special thanks to Franziska Schumann for being there for me after long evenings at work, it meant the world to me. I would also like to thank Sophie Reichardt, for being such an enthusiastic and supportive friend on the final stretch.

Lastly my parents, Stéphane Dorel and Nathalie Nys, deserve the greatest share of gratitude, for their support, for always pushing just as much as needed, for believing in my ambitions, and for making it so easy to move to Germany.

Bibliography

S. Ackermann, M. Cartolano, B. Hero, A. Welte, Y. Kahlert, A. Roderwieser, C. Bartenhagen, E. Walter, J. Gecht, L. Kerschke, R. Volland, R. Menon, J. M. Heuckmann, M. Gartlgruber, S. Hartlieb, K.-O. Henrich, K. Okonechnikov, J. Altmüller, P. Nürnberg, S. Lefever, B. de Wilde, F. Sand, F. Ikram, C. Rosswog, J. Fischer, J. Theissen, F. Hertwig, A. D. Singhi, T. Simon, W. Vogel, S. Perner, B. Krug, M. Schmidt, S. Rahmann, V. Achter, U. Lang, C. Vokuhl, M. Ortmann, R. Büttner, A. Eggert, F. Speleman, R. J. O'Sullivan, R. K. Thomas, F. Berthold, J. Vandesompele, A. Schramm, F. Westermann, J. H. Schulte, M. Peifer, and M. Fischer. A mechanistic classification of clinical phenotypes in neuroblastoma. *Science*, 362(6419):1165–1170, dec 2018. ISSN 0036-8075. doi: 10.1126/science.aat6768. URL `http://www.ncbi.nlm.nih.gov/pubmed/30523111http://www.sciencemag.org/lookup/doi/10.1126/science.aat6768`.

E. Aksamitiene, A. Kiyatkin, and B. Kholodenko. Cross-talk between mitogenic Ras/MAPK and survival PI3K/Akt pathways: a fine balance. *Biochemical Society Transactions*, 40(1):139–146, feb 2012. ISSN 0300-5127. doi: 10.1042/BST20110609. URL `https://portlandpress.com/biochemsoctrans/article/40/1/139/66427/Crosstalk-between-mitogenic-RasMAPK-and-survival`.

M. W. Alam, M. Borenäs, D. E. Lind, D. Cervantes-Madrid, G. Umapathy, R. H. Palmer, and B. Hallberg. Alectinib, an Anaplastic Lymphoma Kinase Inhibitor, Abolishes ALK Activity and Growth in ALK-Positive Neuroblastoma Cells. *Frontiers in Oncology*, 9:579, jul 2019. ISSN 2234943X. doi: 10.3389/fonc.2019.00579. URL `https://www.frontiersin.org/article/10.3389/fonc.2019.00579/full`.

R. C. Allsopp, H. Vaziri, C. Patterson, S. Goldstein, E. V. Younglai, A. B. Futcher, C. W. Greider, and C. B. Harley. Telomere length predicts replicative capacity of human fibroblasts. *Proceedings of the National Academy of Sciences of the United States of America*, 89(21):10114–8, nov 1992. ISSN 0027-8424. doi: 10.1073/pnas.89.21.10114. URL `http://www.ncbi.nlm.nih.gov/pubmed/1438199http://www.pubmedcentral.nih.gov/articlerender.fcgi?artid=PMC50288`.

J. C. Alwine, D. J. Kemp, and G. R. Stark. Method for detection of specific RNAs in agarose gels by transfer to diazobenzyloxymethyl-paper and hybridization with DNA probes. *Proceedings of the National Academy of Sciences of the United States of America*, 74(12):5350–5354, 1977. ISSN 00278424. doi: 10.1073/pnas.74.12.5350. URL /pmc/articles/PMC431715/?report=abstracthttps://www.ncbi.nlm.nih.gov/pmc/articles/PMC431715/.

L. Amiri-Kordestani, G. M. Blumenthal, Q. Casey Xu, L. Zhang, S. W. Tang, L. Ha, W. C. Weinberg, B. Chi, R. Candau-Chacon, P. Hughes, A. M. Russell, S. Pope Miksinski, X. Hong Chen, W. David McGuinn, T. Palmby, S. J. Schrieber, Q. Liu, J. Wang, P. Song, N. Mehrotra, L. Skarupa, K. Clouse, A. Al-Hakim, R. Sridhara, A. Ibrahim, R. Justice, R. Pazdur, and P. Cortazar. CCR Perspectives in Drug Approval FDA Approval: Ado-Trastuzumab Emtansine for the Treatment of Patients with HER2-Positive Metastatic Breast Cancer. *Clin Cancer Res*, 20(17), 2014. doi: 10.1158/1078-0432.CCR-14-0012. URL www.aacrjournals.org.

M. Andrec, B. N. Kholodenko, R. M. Levy, and E. Sontag. Inference of signaling and gene regulatory networks by steady-state perturbation experiments: structure and accuracy. *Journal of theoretical biology*, 232(3):427–41, feb 2005. ISSN 0022-5193. doi: 10.1016/j.jtbi.2004.08.022. URL http://www.sciencedirect.com/science/article/pii/S0022519304004047.

M. Artico, G. M. De Caro, B. Fraioli, and R. Giuffrè. 1897 - celebrating the centennial - Hermann Moritz Gocht and radiation therapy in the treatment of trigeminal neuralgia. *Acta Neurochirurgica*, 139(8):761–763, 1997. ISSN 00016268. doi: 10.1007/BF01420050. URL https://link.springer.com/article/10.1007/BF01420050.

M. Ashburner, C. A. Ball, J. A. Blake, D. Botstein, H. Butler, J. M. Cherry, A. P. Davis, K. Dolinski, S. S. Dwight, J. T. Eppig, M. A. Harris, D. P. Hill, L. Issel-Tarver, A. Kasarskis, S. Lewis, J. C. Matese, J. E. Richardson, M. Ringwald, G. M. Rubin, and G. Sherlock. Gene ontology: Tool for the unification of biology, may 2000. ISSN 10614036. URL http://www.ncbi.nlm.nih.gov/pubmed/10802651http://www.pubmedcentral.nih.gov/articlerender.fcgi?artid=PMC3037419.

A. Auton, G. R. Abecasis, D. M. Altshuler, R. M. Durbin, D. R. Bentley, A. Chakravarti, A. G. Clark, P. Donnelly, E. E. Eichler, P. Flicek, S. B. Gabriel, R. A. Gibbs, E. D. Green, M. E. Hurles, B. M. Knoppers, J. O. Korbel, E. S. Lander, C. Lee, H. Lehrach, E. R. Mardis, G. T. Marth, G. A. McVean, D. A. Nickerson, J. P. Schmidt, S. T. Sherry, J. Wang, R. K. Wilson, E. Boerwinkle, H. Doddapaneni, Y. Han, V. Korchina, C. Kovar, S. Lee, D. Muzny, J. G. Reid, Y. Zhu, Y. Chang, Q. Feng, X. Fang, X. Guo, M. Jian, H. Jiang, X. Jin, T. Lan, G. Li, J. Li, Y. Li, S. Liu, X. Liu, Y. Lu, X. Ma, M. Tang, B. Wang, G. Wang,

H. Wu, R. Wu, X. Xu, Y. Yin, D. Zhang, W. Zhang, J. Zhao, M. Zhao, X. Zheng, N. Gupta, N. Gharani, L. H. Toji, N. P. Gerry, A. M. Resch, J. Barker, L. Clarke, L. Gil, S. E. Hunt, G. Kelman, E. Kulesha, R. Leinonen, W. M. McLaren, R. Radhakrishnan, A. Roa, D. Smirnov, R. E. Smith, I. Streeter, A. Thormann, I. Toneva, B. Vaughan, X. Zheng-Bradley, R. Grocock, S. Humphray, T. James, Z. Kingsbury, R. Sudbrak, M. W. Albrecht, V. S. Amstislavskiy, T. A. Borodina, M. Lienhard, F. Mertes, M. Sultan, B. Timmermann, M. L. Yaspo, L. Fulton, V. Ananiev, Z. Belaia, D. Beloslyudtsev, N. Bouk, C. Chen, D. Church, R. Cohen, C. Cook, J. Garner, T. Hefferon, M. Kimelman, C. Liu, J. Lopez, P. Meric, C. O'Sullivan, Y. Ostapchuk, L. Phan, S. Ponomarov, V. Schneider, E. Shekhtman, K. Sirotkin, D. Slotta, H. Zhang, S. Balasubramaniam, J. Burton, P. Danecek, T. M. Keane, A. Kolb-Kokocinski, S. McCarthy, J. Stalker, M. Quail, C. J. Davies, J. Gollub, T. Webster, B. Wong, Y. Zhan, C. L. Campbell, Y. Kong, A. Marcketta, F. Yu, L. Antunes, M. Bainbridge, A. Sabo, Z. Huang, L. J. Coin, L. Fang, Q. Li, Z. Li, H. Lin, B. Liu, R. Luo, H. Shao, Y. Xie, C. Ye, C. Yu, F. Zhang, H. Zheng, H. Zhu, C. Alkan, E. Dal, F. Kahveci, E. P. Garrison, D. Kural, W. P. Lee, W. F. Leong, M. Stromberg, A. N. Ward, J. Wu, M. Zhang, M. J. Daly, M. A. DePristo, R. E. Handsaker, E. Banks, G. Bhatia, G. Del Angel, G. Genovese, H. Li, S. Kashin, S. A. McCarroll, J. C. Nemesh, R. E. Poplin, S. C. Yoon, J. Lihm, V. Makarov, S. Gottipati, A. Keinan, J. L. Rodriguez-Flores, T. Rausch, M. H. Fritz, A. M. Stütz, K. Beal, A. Datta, J. Herrero, G. R. Ritchie, D. Zerbino, P. C. Sabeti, I. Shlyakhter, S. F. Schaffner, J. Vitti, D. N. Cooper, E. V. Ball, P. D. Stenson, B. Barnes, M. Bauer, R. K. Cheetham, A. Cox, M. Eberle, S. Kahn, L. Murray, J. Peden, R. Shaw, E. E. Kenny, M. A. Batzer, M. K. Konkel, J. A. Walker, D. G. MacArthur, M. Lek, R. Herwig, L. Ding, D. C. Koboldt, D. Larson, K. Ye, S. Gravel, A. Swaroop, E. Chew, T. Lappalainen, Y. Erlich, M. Gymrek, T. F. Willems, J. T. Simpson, M. D. Shriver, J. A. Rosenfeld, C. D. Bustamante, S. B. Montgomery, F. M. De La Vega, J. K. Byrnes, A. W. Carroll, M. K. DeGorter, P. Lacroute, B. K. Maples, A. R. Martin, A. Moreno-Estrada, S. S. Shringarpure, F. Zakharia, E. Halperin, Y. Baran, E. Cerveira, J. Hwang, A. Malhotra, D. Plewczynski, K. Radew, M. Romanovitch, C. Zhang, F. C. Hyland, D. W. Craig, A. Christoforides, N. Homer, T. Izatt, A. A. Kurdoglu, S. A. Sinari, K. Squire, C. Xiao, J. Sebat, D. Antaki, M. Gujral, A. Noor, K. Ye, E. G. Burchard, R. D. Hernandez, C. R. Gignoux, D. Haussler, S. J. Katzman, W. J. Kent, B. Howie, A. Ruiz-Linares, E. T. Dermitzakis, S. E. Devine, H. M. Kang, J. M. Kidd, T. Blackwell, S. Caron, W. Chen, S. Emery, L. Fritsche, C. Fuchsberger, G. Jun, B. Li, R. Lyons, C. Scheller, C. Sidore, S. Song, E. Sliwerska, D. Taliun, A. Tan, R. Welch, M. K. Wing, X. Zhan, P. Awadalla, A. Hodgkinson, Y. Li, X. Shi, A. Quitadamo, G. Lunter, J. L. Marchini, S. Myers, C. Churchhouse, O. Delaneau, A. Gupta-Hinch, W. Kretzschmar, Z. Iqbal, I. Mathieson, A. Menelaou, A. Rimmer, D. K. Xifara, T. K. Oleksyk, Y. Fu, X. Liu, M. Xiong,

L. Jorde, D. Witherspoon, J. Xing, B. L. Browning, S. R. Browning, F. Hormozdiari, P. H. Sudmant, E. Khurana, C. Tyler-Smith, C. A. Albers, Q. Ayub, Y. Chen, V. Colonna, L. Jostins, K. Walter, Y. Xue, M. B. Gerstein, A. Abyzov, S. Balasubramanian, J. Chen, D. Clarke, Y. Fu, A. O. Harmanci, M. Jin, D. Lee, J. Liu, X. J. Mu, J. Zhang, Y. Zhang, C. Hartl, K. Shakir, J. Degenhardt, S. Meiers, B. Raeder, F. P. Casale, O. Stegle, E. W. Lameijer, I. Hall, V. Bafna, J. Michaelson, E. J. Gardner, R. E. Mills, G. Dayama, K. Chen, X. Fan, Z. Chong, T. Chen, M. J. Chaisson, J. Huddleston, M. Malig, B. J. Nelson, N. F. Parrish, B. Blackburne, S. J. Lindsay, Z. Ning, Y. Zhang, H. Lam, C. Sisu, D. Challis, U. S. Evani, J. Lu, U. Nagaswamy, J. Yu, W. Li, L. Habegger, H. Yu, F. Cunningham, I. Dunham, K. Lage, J. B. Jespersen, H. Horn, D. Kim, R. Desalle, A. Narechania, M. A. Sayres, F. L. Mendez, G. D. Poznik, P. A. Underhill, D. Mittelman, R. Banerjee, M. Cerezo, T. W. Fitzgerald, S. Louzada, A. Massaia, F. Yang, D. Kalra, W. Hale, X. Dan, K. C. Barnes, C. Beiswanger, H. Cai, H. Cao, B. Henn, D. Jones, J. S. Kaye, A. Kent, A. Kerasidou, R. Mathias, P. N. Ossorio, M. Parker, C. N. Rotimi, C. D. Royal, K. Sandoval, Y. Su, Z. Tian, S. Tishkoff, M. Via, Y. Wang, H. Yang, L. Yang, J. Zhu, W. Bodmer, G. Bedoya, Z. Cai, Y. Gao, J. Chu, L. Peltonen, A. Garcia-Montero, A. Orfao, J. Dutil, J. C. Martinez-Cruzado, R. A. Mathias, A. Hennis, H. Watson, C. McKenzie, F. Qadri, R. LaRocque, X. Deng, D. Asogun, O. Folarin, C. Happi, O. Omoniwa, M. Stremlau, R. Tariyal, M. Jallow, F. S. Joof, T. Corrah, K. Rockett, D. Kwiatkowski, J. Kooner, T. T. Hien, S. J. Dunstan, N. ThuyHang, R. Fonnie, R. Garry, L. Kanneh, L. Moses, J. Schieffelin, D. S. Grant, C. Gallo, G. Poletti, D. Saleheen, A. Rasheed, L. D. Brooks, A. L. Felsenfeld, J. E. McEwen, Y. Vaydylevich, A. Duncanson, M. Dunn, and J. A. Schloss. A global reference for human genetic variation, oct 2015. ISSN 14764687. URL `http://www.nature.com/articles/nature15393`.

O. Bagci, S. Tumer, N. Olgun, and O. Altungoz. Copy number status and mutation analyses of anaplastic lymphoma kinase (ALK) gene in 90 sporadic neuroblastoma tumors. *Cancer Letters*, 317(1):72–77, apr 2012. ISSN 0304-3835. doi: 10.1016/J.CANLET.2011.11.013. URL `https://www.sciencedirect.com/science/article/pii/S0304383511006914`.

G. Barone, J. Anderson, A. D. J. Pearson, K. Petrie, and L. Chesler. New strategies in neuroblastoma: Therapeutic targeting of MYCN and ALK. *Clinical cancer research : an official journal of the American Association for Cancer Research*, 19(21):5814–21, nov 2013. ISSN 1078-0432. doi: 10.1158/1078-0432. CCR-13-0680. URL `http://www.ncbi.nlm.nih.gov/pubmed/23965898http://www.pubmedcentral.nih.gov/articlerender.fcgi?artid=PMC3818140`.

T. S. Batth, C. Francavilla, and J. V. Olsen. Off-line high-pH reversed-phase fractionation for in-depth phosphoproteomics. *Journal of Proteome Research*, 13(12):

6176–6186, dec 2014. ISSN 15353907. doi: 10.1021/pr500893m. URL https://pubs.acs.org/doi/10.1021/pr500893m.

M. Baum, R. Demicheli, W. Hrushesky, and M. Retsky. Does surgery unfavourably perturb the "natural history" of early breast cancer by accelerating the appearance of distant metastases? *European Journal of Cancer*, 41(4):508–515, mar 2005. ISSN 09598049. doi: 10.1016/j.ejca.2004.09.031. URL https://www.sciencedirect.com/science/article/pii/S0959804904009803.

E. Bell, L. Chen, T. Liu, G. M. Marshall, J. Lunec, and D. A. Tweddle. MYCN oncoprotein targets and their therapeutic potential. *Cancer Letters*, 293(2):144–157, jul 2010. ISSN 03043835. doi: 10.1016/j.canlet.2010.01.015. URL https://www.sciencedirect.com/science/article/pii/S0304383510000418?via%3Dihub.

A. Bellini, V. Bernard, Q. Leroy, T. Rio Frio, G. Pierron, V. Combaret, E. Lapouble, N. Clement, H. Rubie, E. Thebaud, P. Chastagner, A. S. Defachelles, C. Bergeron, N. Buchbinder, S. Taque, A. Auvrignon, D. Valteau-Couanet, J. Michon, I. Janoueix-Lerosey, O. Delattre, and G. Schleiermacher. Deep Sequencing Reveals Occurrence of Subclonal ¡i¿ALK¡/i¿ Mutations in Neuroblastoma at Diagnosis. *Clinical Cancer Research*, 21(21):4913–4921, nov 2015. ISSN 1078-0432. doi: 10.1158/1078-0432.CCR-15-0423. URL http://www.ncbi.nlm.nih.gov/pubmed/26059187http://clincancerres.aacrjournals.org/lookup/doi/10.1158/1078-0432.CCR-15-0423.

S. C. Bendall, E. F. Simonds, P. Qiu, E.-a. D. Amir, P. O. Krutzik, R. Finck, R. V. Bruggner, R. Melamed, A. Trejo, O. I. Ornatsky, R. S. Balderas, S. K. Plevritis, K. Sachs, D. Pe'er, S. D. Tanner, and G. P. Nolan. Single-Cell Mass Cytometry of Differential Immune and Drug Responses Across a Human Hematopoietic Continuum. *Science*, 332(6030):687–696, may 2011. ISSN 0036-8075. doi: 10.1126/science.1198704. URL https://www.sciencemag.org/lookup/doi/10.1126/science.1198704.

F. Berthold, C. Spix, P. Kaatsch, and F. Lampert. Incidence, Survival, and Treatment of Localized and Metastatic Neuroblastoma in Germany 1979–2015. *Pediatric Drugs*, 19(6):577–593, dec 2017. ISSN 11792019. doi: 10.1007/s40272-017-0251-3. URL https://link.springer.com/article/10.1007/s40272-017-0251-3.

S. Birkenhake and R. Sauer. Historical essentials influencing the development of radiooncology in the past 100 years. *Experientia*, 51(7):681–685, jul 1995. ISSN 00144754. doi: 10.1007/BF01941265. URL https://link.springer.com/article/10.1007/BF01941265.

K. Bister. Discovery of oncogenes: The advent of molecular cancer research, dec 2015. ISSN 10916490. URL www.pnas.org/cgi/doi/10.1073/pnas.1521145112.

V. M. Bolanos-Garcia. MET meet adaptors: Functional and structural implications in downstream signalling mediated by the Met receptor. *Molecular and Cellular Biochemistry*, 276(1-2):149–157, 2005. ISSN 03008177. doi: 10.1007/s11010-005-3696-6. URL https://link.springer.com/article/10.1007/PL00022009.

G. Bollag, D. W. Clapp, S. Shih, F. Adler, Y. Y. Zhang, P. Thompson, B. J. Lange, M. H. Freedman, F. McCormick, T. Jacks, and K. Shannon. Loss of NF1 results in activation of the Ras signaling pathway and leads to aberrant growth in haematopoietic cells. *Nature Genetics*, 12(2):144–148, feb 1996. ISSN 1061-4036. doi: 10.1038/ng0296-144. URL http://www.nature.com/articles/ng0296-144.

G. Bollag, P. Hirth, J. Tsai, J. Zhang, P. N. Ibrahim, H. Cho, W. Spevak, C. Zhang, Y. Zhang, G. Habets, E. A. Burton, B. Wong, G. Tsang, B. L. West, B. Powell, R. Shellooe, A. Marimuthu, H. Nguyen, K. Y. J. Zhang, D. R. Artis, J. Schlessinger, F. Su, B. Higgins, R. Iyer, K. D'Andrea, A. Koehler, M. Stumm, P. S. Lin, R. J. Lee, J. Grippo, I. Puzanov, K. B. Kim, A. Ribas, G. A. McArthur, J. A. Sosman, P. B. Chapman, K. T. Flaherty, X. Xu, K. L. Nathanson, and K. Nolop. Clinical efficacy of a RAF inhibitor needs broad target blockade in BRAF-mutant melanoma. *Nature*, 467(7315):596–9, sep 2010. ISSN 1476-4687. doi: 10.1038/nature09454. URL http://www.ncbi.nlm.nih.gov/pubmed/20823850http://www.pubmedcentral.nih.gov/articlerender.fcgi?artid=2948082&tool=pmcentrez&rendertype=abstract.

R. Brandt, T. Sell, M. Lüthen, F. Uhlitz, B. Klinger, P. Riemer, C. Giesecke-Thiel, S. Schulze, I. A. El-Shimy, D. Kunkel, B. Fauler, T. Mielke, N. Mages, B. G. Herrmann, C. Sers, N. Blüthgen, and M. Morkel. Cell type-dependent differential activation of ERK by oncogenic KRAS in colon cancer and intestinal epithelium. *Nature Communications*, 10(1): 2919, 2019. ISSN 20411723. doi: 10.1038/s41467-019-10954-y. URL http://www.ncbi.nlm.nih.gov/pubmed/31266962http://www.pubmedcentral.nih.gov/articlerender.fcgi?artid=PMC6606648.

S. C. Bresler, D. A. Weiser, P. J. Huwe, J. H. Park, K. Krytska, H. Ryles, M. Laudenslager, E. F. Rappaport, A. C. Wood, P. W. McGrady, M. D. Hogarty, W. B. London, R. Radhakrishnan, M. A. Lemmon, and Y. P. Mossé. ALK Mutations Confer Differential Oncogenic Activation and Sensitivity to ALK Inhibition Therapy in Neuroblastoma. *Cancer Cell*, 26(5):682–694, nov 2014. ISSN 18783686. doi: 10.1016/j.ccell.2014.09.019. URL https://www.sciencedirect.com/science/article/pii/S1535610814003936.

S. Cabodi, M. del Pilar Camacho-Leal, P. Di Stefano, and P. Defilippi. Integrin signalling adaptors: not only figurants in the cancer story. *Nature Reviews Cancer*,

10(12):858–870, dec 2010. ISSN 1474-175X. doi: 10.1038/nrc2967. URL http://www.nature.com/articles/nrc2967.

T. A. Cage, Y. Chanthery, L. Chesler, M. Grimmer, Z. Knight, K. Shokat, W. A. Weiss, and W. C. Gustafson. Downregulation of MYCN through PI3K Inhibition in Mouse Models of Pediatric Neural Cancer. *Frontiers in oncology*, 5:111, 2015. ISSN 2234-943X (Electronic). doi: 10.3389/fonc.2015.00111. URL http://www.ncbi.nlm.nih.gov/pubmed/26029667http://www.pubmedcentral.nih.gov/articlerender.fcgi?artid=PMC4429235.

M. A. Cahill, R. Janknecht, and A. Nordheim. Signalling pathways: Jack of all cascades. *Current Biology*, 6(1):16–19, jan 1996. ISSN 09609822. doi: 10.1016/S0960-9822(02)00410-4. URL https://www.sciencedirect.com/science/article/pii/S0960982202004104.

R. Carnell. Latin Hypercube Samples [R package lhs version 0.1.0], 2012. URL https://cran.r-project.org/package=lhs.

E. Caron, S. Ghosh, Y. Matsuoka, D. Ashton-Beaucage, M. Therrien, S. Lemieux, C. Perreault, P. P. Roux, and H. Kitano. A comprehensive map of the mTOR signaling network. *Molecular systems biology*, 6:453, dec 2010. ISSN 1744-4292. doi: 10.1038/msb.2010.108. URL http://www.pubmedcentral.nih.gov/articlerender.fcgi?artid=3018167&tool=pmcentrez&rendertype=abstract.

A. Carrel. ON THE PERMANENT LIFE OF TISSUES OUTSIDE OF THE ORGANISM. *The Journal of experimental medicine*, 15(5):516–28, may 1912. ISSN 0022-1007. doi: 10.1084/jem.15.5.516. URL http://www.ncbi.nlm.nih.gov/pubmed/19867545http://www.pubmedcentral.nih.gov/articlerender.fcgi?artid=PMC2124948.

A. Carrel and A. H. Ebeling. AGE AND MULTIPLICATION OF FIBROBLASTS. *Journal of Experimental Medicine*, 34(6):599–623, dec 1921. ISSN 1540-9538. doi: 10.1084/jem.34.6.599. URL https://rupress.org/jem/article/34/6/599/8166/AGE-AND-MULTIPLICATION-OF-FIBROBLASTS.

P. Casado, J. C. Rodriguez-Prados, S. C. Cosulich, S. Guichard, B. Vanhaesebroeck, S. Joel, and P. R. Cutillas. Kinase-substrate enrichment analysis provides insights into the heterogeneity of signaling pathway activation in leukemia cells, mar 2013. ISSN 19450877. URL http://www.ncbi.nlm.nih.gov/pubmed/23532336.

A. F. Castro, T. Campos, J. T. Babcock, M. E. Armijo, A. Martínez-Conde, R. Pincheira, and L. A. Quilliam. M-Ras induces Ral and JNK activation to regulate MEK/ERK-independent gene expression in MCF-7 breast cancer cells. *Journal of Cellular Biochemistry*, 113(4):1253–1264, apr 2012. ISSN 07302312. doi: 10.1002/jcb.23458. URL http://doi.wiley.com/10.1002/jcb.23458.

A. Cerezo, M. C. Guadamillas, J. G. Goetz, S. Sánchez-Perales, E. Klein, R. K. Assoian, and M. A. del Pozo. The Absence of Caveolin-1 Increases Proliferation and Anchorage- Independent Growth by a Rac-Dependent, Erk-Independent Mechanism. *Molecular and Cellular Biology*, 29(18):5046–5059, sep 2009. ISSN 0270-7306. doi: 10.1128/mcb.00315-09. URL http://mcb.asm.org/.

G. Chan, D. Kalaitzidis, and B. G. Neel. The tyrosine phosphatase Shp2 (PTPN11) in cancer, jun 2008. ISSN 01677659. URL http://link.springer.com/10.1007/s10555-008-9126-y.

P. B. Chapman, A. Hauschild, C. Robert, J. B. Haanen, P. Ascierto, J. Larkin, R. Dummer, C. Garbe, A. Testori, M. Maio, D. Hogg, P. Lorigan, C. Lebbe, T. Jouary, D. Schadendorf, A. Ribas, S. J. O'Day, J. A. Sosman, J. M. Kirkwood, A. M. Eggermont, B. Dreno, K. Nolop, J. Li, B. Nelson, J. Hou, R. J. Lee, K. T. Flaherty, and G. A. McArthur. Improved Survival with Vemurafenib in Melanoma with BRAF V600E Mutation. *New England Journal of Medicine*, 364 (26):2507–2516, jun 2011. ISSN 0028-4793. doi: 10.1056/nejmoa1103782. URL http://www.nejm.org/doi/abs/10.1056/NEJMoa1103782.

L. Chesler, C. Schlieve, D. D. Goldenberg, A. Kenney, G. Kim, A. McMillan, K. K. Matthay, D. Rowitch, and W. A. Weiss. Inhibition of phosphatidylinositol 3-kinase destabilizes Mycn protein and blocks malignant progression in neuroblastoma. *Cancer Research*, 66(16):8139–8146, 2006. ISSN 00085472. doi: 10.1158/0008-5472.CAN-05-2769. URL http://cancerres.aacrjournals.org/content/66/16/8139?ijkey=0cc60697ce004837fcad95f07abbe5e65a62297c&keytype2=tf_ipsecsha.

N. K. V. Cheung, I. Y. Cheung, B. H. Kushner, I. Ostrovnaya, E. Chamberlain, K. Kramer, and S. Modak. Murine anti-GD2 monoclonal antibody 3F8 combined with granulocyte- macrophage colony-stimulating factor and 13-cis-retinoic acid in high-risk patients with stage 4 neuroblastoma in first remission. *Journal of Clinical Oncology*, 30(26):3264–3270, sep 2012. ISSN 0732183X. doi: 10.1200/JCO.2011.41.3807. URL /pmc/articles/PMC3434986/?report=abstracthttps://www.ncbi.nlm.nih.gov/pmc/articles/PMC3434986/.

K. Cichowski and T. Jacks. NF1 tumor suppressor gene function: Narrowing the GAP, feb 2001. ISSN 00928674. URL http://www.ncbi.nlm.nih.gov/pubmed/11239415.

S. Claeys, G. Denecker, K. Durinck, B. Decaesteker, L. M. Mus, S. Loontiens, S. Vanhauwaert, K. Althoff, C. Wigerup, D. Bexell, E. Dolman, K. O. Henrich, L. Wehrmann, E. M. Westerhout, J. B. Demoulin, C. Kumps, T. Van Maerken, G. Laureys, C. Van Neste, B. De Wilde, O. De Wever, F. Westermann, R. Versteeg,

J. J. Molenaar, S. Påhlman, J. H. Schulte, K. De Preter, and F. Speleman. ALK positively regulates MYCN activity through repression of HBP1 expression. *Oncogene*, 38(15):2690–2705, apr 2019. ISSN 14765594. doi: 10.1038/s41388-018-0595-3. URL http://www.nature.com/articles/s41388-018-0595-3.

M. A. Cobleigh, M. Najor, S. Brar, S. Turturro, L. Portt, T. Yung, and A. M. Abukhdeir. Abstract PS18-30: Loss of NF1 leads to rho GTPase activation and sensitivity to multiple agents in breast cancer. In *Poster Session Abstracts*, volume 81, pages PS18–30–PS18–30. American Association for Cancer Research, feb 2021. doi: 10.1158/1538-7445.sabcs20-ps18-30. URL http://cancerres.aacrjournals.org/lookup/doi/10.1158/1538-7445.SABCS20-PS18-30.

J. W. Cook and E. L. Kennaway. Chemical compounds as carcinogenic agents: Second supplementary report: Literature of 1938 and 1939. *American Journal of Cancer*, 39(4):521–582, aug 1940. ISSN 15387445. doi: 10.1158/ajc.1940.521. URL https://cancerres.aacrjournals.org/content/39/4/521https://cancerres.aacrjournals.org/content/39/4/521.abstract.

R. B. Corcoran, H. Ebi, A. B. Turke, E. M. Coffee, M. Nishino, A. P. Cogdill, R. D. Brown, P. D. Pelle, D. Dias-Santagata, K. E. Hung, K. T. Flaherty, A. Piris, J. A. Wargo, J. Settleman, M. Mino-Kenudson, and J. A. Engelman. EGFR-mediated reactivation of MAPK signaling contributes to insensitivity of BRAF-mutant colorectal cancers to RAF inhibition with vemurafenib. *Cancer Discovery*, 2(3):227–235, mar 2012. ISSN 21598274. doi: 10.1158/2159-8290.CD-11-0341. URL http://www.ncbi.nlm.nih.gov/pubmed/22448344http://www.pubmedcentral.nih.gov/articlerender.fcgi?artid=PMC3308191http://cancerdiscovery.aacrjournals.org/lookup/doi/10.1158/2159-8290.CD-11-0341.

R. B. Corcoran, T. André, C. E. Atreya, J. H. Schellens, T. Yoshino, J. C. Bendell, A. Hollebecque, A. J. McRee, S. Siena, G. Middleton, K. Muro, M. S. Gordon, J. Tabernero, R. Yaeger, P. J. O'Dwyer, Y. Humblet, F. De Vos, A. S. Jung, J. C. Brase, S. Jaeger, S. Bettinger, B. Mookerjee, F. Rangwala, and E. Van Cutsem. Combined BRAF, EGFR, and MEK Inhibition in Patients with ¡i¿BRAF¡/i¿ ¡sup¿V600E¡/sup¿ -Mutant Colorectal Cancer. *Cancer Discovery*, 8(4):428–443, apr 2018. ISSN 2159-8274. doi: 10.1158/2159-8290.CD-17-1226. URL http://www.ncbi.nlm.nih.gov/pubmed/29431699http://www.pubmedcentral.nih.gov/articlerender.fcgi?artid=PMC5882509http://cancerdiscovery.aacrjournals.org/lookup/doi/10.1158/2159-8290.CD-17-1226.

C. F. Cori, G. Schmidt, and G. T. Cori. The synthesis of a polysaccharide from glucose-1-phosphate in muscle extract. *Science*, 89(2316):464–465, may 1939. ISSN 00368075. doi: 10.1126/science.89.2316.464. URL http://science.sciencemag.org/content/89/2316/464.

D. W. Coulter, J. Blatt, A. J. D'Ercole, and B. M. Moats-Staats. IGF-I receptor inhibition combined with rapamycin or temsirolimus inhibits neuroblastoma cell growth. *Anticancer Research*, 28(3 A):1509–1516, 2008. ISSN 02507005. doi: 10.17615/r8pv-9v41. URL http://ar.iiarjournals.org/content/28/3A/1509.full.pdf.

P. Crespo and J. León. Ras proteins in the control of the cell cycle and cell differentiation. *Cellular and Molecular Life Sciences*, 57(11):1613–1636, oct 2000. ISSN 1420-682X. doi: 10.1007/PL00000645. URL http://link.springer.com/10.1007/PL00000645.

B. Cseh, E. Doma, and M. Baccarini. "RAF" neighborhood: Protein-protein interaction in the Raf/Mek/Erk pathway, aug 2014. ISSN 18733468.

P. Cuatrecasas. Membrane receptors. *Annual Review of Biochemistry*, Vol 43:169–214, 1974. ISSN 00664154. doi: 10.1146/annurev.bi.43.070174.001125.

A. M. Czarnecka, E. Bartnik, M. Fiedorowicz, and P. Rutkowski. Targeted therapy in melanoma and mechanisms of resistance, jun 2020. ISSN 14220067. URL https://www.mdpi.com/1422-0067/21/13/4576.

P. Datlinger, A. F. Rendeiro, C. Schmidl, T. Krausgruber, P. Traxler, J. Klughammer, L. C. Schuster, A. Kuchler, D. Alpar, and C. Bock. Pooled CRISPR screening with single-cell transcriptome readout. *Nature Methods*, 14(3):297–301, mar 2017. ISSN 15487105. doi: 10.1038/nmeth.4177. URL http://www.nature.com/articles/nmeth.4177.

H. Davies, G. R. Bignell, C. Cox, P. Stephens, S. Edkins, S. Clegg, J. Teague, H. Woffendin, M. J. Garnett, W. Bottomley, N. Davis, E. Dicks, R. Ewing, Y. Floyd, K. Gray, S. Hall, R. Hawes, J. Hughes, V. Kosmidou, A. Menzies, C. Mould, A. Parker, C. Stevens, S. Watt, S. Hooper, R. Wilson, H. Jayatilake, B. A. Gusterson, C. Cooper, J. Shipley, D. Hargrave, K. Pritchard-Jones, N. Maitland, G. Chenevix-Trench, G. J. Riggins, D. D. Bigner, G. Palmieri, A. Cossu, A. Flanagan, A. Nicholson, J. W. C. Ho, S. Y. Leung, S. T. Yuen, B. L. Weber, H. F. Seigler, T. L. Darrow, H. Paterson, R. Marais, C. J. Marshall, R. Wooster, M. R. Stratton, and P. A. Futreal. Mutations of the BRAF gene in human cancer. *Nature*, 417(6892):949–54, jun 2002. ISSN 0028-0836. doi: 10.1038/nature00766. URL http://dx.doi.org/10.1038/nature00766.

B. De Bernardi, B. Nicolas, L. Boni, P. Indolfi, M. Carli, L. C. Di Montezemolo, A. Donfrancesco, A. Pession, M. Provenzi, A. Di Cataldo, A. Rizzo, G. P. Tonini, S. Dallorso, M. Conte, C. Gambini, A. Garaventa, F. Bonetti, A. Zanazzo, P. D'Angelo, and P. Bruzzi. Disseminated neuroblastoma in children older than one year at diagnosis: Comparable results with three consecutive high-dose protocols adopted by the Italian Co-Operatiye Group for Neuroblastoma. *Journal of*

Clinical Oncology, 21(8):1592–1601, apr 2003. ISSN 0732183X. doi: 10.1200/JCO.2003.05.191. URL http://ascopubs.org/doi/10.1200/JCO.2003.05.191http://www.ncbi.nlm.nih.gov/pubmed/12697885.

E. de Klerk and P. A. 't Hoen. Alternative mRNA transcription, processing, and translation: Insights from RNA sequencing, mar 2015. ISSN 13624555. URL http://www.cell.com/article/S0168952515000025/fulltexthttp://www.cell.com/article/S0168952515000025/abstracthttps://www.cell.com/trends/genetics/abstract/S0168-9525(15)00002-5.

D. N. Debruyne, R. Dries, S. Sengupta, D. Seruggia, Y. Gao, B. Sharma, H. Huang, L. Moreau, M. McLane, D. S. Day, E. Marco, T. Chen, N. S. Gray, K.-K. Wong, S. H. Orkin, G.-C. Yuan, R. A. Young, and R. E. George. BORIS promotes chromatin regulatory interactions in treatment-resistant cancer cells. *Nature*, 572(7771):676–680, aug 2019. ISSN 0028-0836. doi: 10.1038/s41586-019-1472-0. URL http://www.nature.com/articles/s41586-019-1472-0.

R. Demicheli, M. W. Retsky, W. J. Hrushesky, M. Baum, and I. D. Gukas. The effects of surgery on tumor growth: A century of investigations, nov 2008. ISSN 15698041. URL https://www.sciencedirect.com/science/article/pii/S0923753419401403.

S. J. Ding, W. J. Qian, and R. D. Smith. Quantitative proteomic approaches for studying phosphotyrosine signaling, feb 2007. ISSN 14789450. URL http://www.tandfonline.com/doi/full/10.1586/14789450.4.1.13.

A. Dixit, O. Parnas, B. Li, J. Chen, C. P. Fulco, L. Jerby-Arnon, N. D. Marjanovic, D. Dionne, T. Burks, R. Raychowdhury, B. Adamson, T. M. Norman, E. S. Lander, J. S. Weissman, N. Friedman, and A. Regev. Perturb-Seq: Dissecting Molecular Circuits with Scalable Single-Cell RNA Profiling of Pooled Genetic Screens. *Cell*, 167(7):1853–1866.e17, dec 2016. ISSN 10974172. doi: 10.1016/j.cell.2016.11.038. URL https://www.sciencedirect.com/science/article/pii/S0092867416316105.

A. Dobin, C. A. Davis, F. Schlesinger, J. Drenkow, C. Zaleski, S. Jha, P. Batut, M. Chaisson, and T. R. Gingeras. STAR: Ultrafast universal RNA-seq aligner. *Bioinformatics*, 29(1):15–21, jan 2013. ISSN 13674803. doi: 10.1093/bioinformatics/bts635. URL http://code.google.com/p/rna-star/.

M. Dorel, B. Klinger, T. Gross, A. Sieber, A. Prahallad, E. Bosdriesz, L. F. Wessels, and N. Blüthgen. Modelling signalling networks from perturbation data. *Bioinformatics*, 34(23):4079–4086, dec 2018. ISSN 14602059. doi: 10.1093/bioinformatics/bty473. URL https://academic.oup.com/bioinformatics/article/34/23/4079/5040310.

M. Dorel, B. Klinger, T. Mari, J. Toedling, E. Blanc, C. Messerschmidt, M. Nadler-Holly, M. Ziehm, A. Sieber, F. Hertwig, D. Beule, A. Eggert, J. H. Schulte, M. Selbach, and N. Blüthgen. Neuroblastoma signalling models unveil combination therapies targeting feedback-mediated resistance. *PLoS computational biology*, 17(11):e1009515, jun 2021. ISSN 1553-7358. doi: 10.1101/2021.06.14.448322. URL https://www.biorxiv.org/content/10.1101/2021.06.14.448322v1.

V. G. Dovì, O. Paladino, and A. P. Reverberi. Some remarks on the use of the inverse hessian matrix of the likelihood function in the estimation of statistical properties of parameters. *Applied Mathematics Letters*, 4(1):87–90, jan 1991. ISSN 08939659. doi: 10.1016/0893-9659(91)90129-J. URL https://www.sciencedirect.com/science/article/pii/089396599190129J.

E. Driehuis, K. Kretzschmar, and H. Clevers. Establishment of patient-derived cancer organoids for drug-screening applications. *Nature Protocols*, 15(10):3380–3409, oct 2020. ISSN 1754-2189. doi: 10.1038/s41596-020-0379-4. URL https://www.nature.com/articles/s41596-020-0379-4.

B. J. Druker, M. Talpaz, D. J. Resta, B. Peng, E. Buchdunger, J. M. Ford, N. B. Lydon, H. Kantarjian, R. Capdeville, S. Ohno-Jones, and C. L. Sawyers. Efficacy and Safety of a Specific Inhibitor of the BCR-ABL Tyrosine Kinase in Chronic Myeloid Leukemia. *New England Journal of Medicine*, 344(14):1031–1037, apr 2001. ISSN 0028-4793. doi: 10.1056/nejm200104053441401. URL http://www.nejm.org/doi/abs/10.1056/NEJM200104053441401.

P. H. Duesberg and P. K. Vogt. Differences between the ribonucleic acids of transforming and nontransforming avian tumor viruses. *Proceedings of the National Academy of Sciences of the United States of America*, 67(4):1673–1680, dec 1970. ISSN 00278424. doi: 10.1073/pnas.67.4.1673. URL https://www.pnas.org/content/67/4/1673https://www.pnas.org/content/67/4/1673.abstract.

T. Ebendal. Function and evolution in the NGF family and its receptors, aug 1992. ISSN 10974547. URL https://onlinelibrary.wiley.com/doi/10.1002/jnr.490320402.

O. M. El-Badry, J. A. Romanus, L. J. Helman, M. J. Cooper, M. M. Rechler, and M. A. Israel. Autonomous growth of a human neuroblastoma cell line is mediated by insulin-like growth factor II. *Journal of Clinical Investigation*, 84(3):829–839, sep 1989. ISSN 00219738. doi: 10.1172/JCI114243. URL http://www.ncbi.nlm.nih.gov/pubmed/2547840http://www.pubmedcentral.nih.gov/articlerender.fcgi?artid=PMC329726.

T. F. Eleveld, D. A. Oldridge, V. Bernard, J. Koster, L. C. Daage, S. J. Diskin, L. Schild, N. B. Bentahar, A. Bellini, M. Chicard, E. Lapouble, V. Combaret,

P. Legoix-Né, J. Michon, T. J. Pugh, L. S. Hart, J. Rader, E. F. Attiyeh, J. S. Wei, S. Zhang, A. Naranjo, J. M. Gastier-Foster, M. D. Hogarty, S. Asgharzadeh, M. A. Smith, J. M. Guidry Auvil, T. B. K. Watkins, D. A. Zwijnenburg, M. E. Ebus, P. van Sluis, A. Hakkert, E. van Wezel, C. E. van der Schoot, E. M. Westerhout, J. H. Schulte, G. A. Tytgat, M. E. M. Dolman, I. Janoueix-Lerosey, D. S. Gerhard, H. N. Caron, O. Delattre, J. Khan, R. Versteeg, G. Schleiermacher, J. J. Molenaar, and J. M. Maris. Relapsed neuroblastomas show frequent RAS-MAPK pathway mutations. *Nature genetics*, 47(8):864–71, aug 2015. ISSN 1546-1718. doi: 10.1038/ng.3333. URL http://www.ncbi.nlm.nih.gov/pubmed/26121087http://www.pubmedcentral.nih.gov/articlerender.fcgi?artid=PMC4775079.

L. Ellis and D. J. Hicklin. Pathways mediating resistance to vascular endothelial growth factor-targeted therapy, oct 2008. ISSN 10780432. URL http://www.ncbi.nlm.nih.gov/pubmed/18927275http://clincancerres.aacrjournals.org/lookup/doi/10.1158/1078-0432.CCR-07-5287.

K. B. Emdal, A. K. Pedersen, D. B. Bekker-Jensen, A. Lundby, S. Claeys, K. De Preter, F. Speleman, C. Francavilla, and J. V. Olsen. Integrated proximal proteomics reveals IRS2 as a determinant of cell survival in ALK-driven neuroblastoma. *Science Signaling*, 11(557), nov 2018. ISSN 19379145. doi: 10.1126/scisignal.aap9752. URL http://www.ncbi.nlm.nih.gov/pubmed/30459283.

Eurostat. Still 1 in 4 deaths caused by cancer in the EU. *Eurostat Newsrelease*, 2016(February):1–5, 2016. URL https://ec.europa.eu/eurostat/documents/2995521/7149996/3-03022016-BP-EN.pdf/0bbc3389-8c0d-44a0-9b0c-2a0bff49f466http://ec.europa.eu/eurostat/documents/2995521/7149996/3-03022016-BP-EN.pdf/0bbc3389-8c0d-44a0-9b0c-2a0bff49f466%0Ahttp://ec.europa.eu/eurost.

A. Fabregat, S. Jupe, L. Matthews, K. Sidiropoulos, M. Gillespie, P. Garapati, R. Haw, B. Jassal, F. Korninger, B. May, M. Milacic, C. D. Roca, K. Rothfels, C. Sevilla, V. Shamovsky, S. Shorser, T. Varusai, G. Viteri, J. Weiser, G. Wu, L. Stein, H. Hermjakob, and P. D'Eustachio. The Reactome Pathway Knowledgebase. *Nucleic Acids Research*, 46(D1):D649–D655, jan 2018. ISSN 0305-1048. doi: 10.1093/nar/gkx1132. URL http://academic.oup.com/nar/article/46/D1/D649/4626770.

S. Farber. Chemotherapy in the Treatment of Leukemia and Wilms' Tumor. *JAMA: The Journal of the American Medical Association*, 198(8):826–836, nov 1966. ISSN 15383598. doi: 10.1001/jama.1966.03110210076025. URL http://jama.jamanetwork.com/article.aspx?doi=10.1001/jama.1966.03110210076025.

S. Farber, L. K. Diamond, R. D. Mercer, R. F. Sylvester, and J. A. Wolff. Temporary Remissions in Acute Leukemia in Children Produced by Folic Acid Antagonist, 4-Aminopteroyl-Glutamic Acid (Aminopterin). *New England Journal of Medicine*,

238(23):787–793, jun 1948. ISSN 0028-4793. doi: 10.1056/nejm194806032382301. URL http://www.nejm.org/doi/abs/10.1056/NEJM194806032382301.

S. Farber, R. Toch, E. M. Sears, and D. Pinkel. Advances in Chemotherapy of Cancer in Man. *Advances in Cancer Research*, 4(C):1–71, jan 1956. ISSN 0065230X. doi: 10.1016/S0065-230X(08)60721-6. URL https://www.sciencedirect.com/science/article/pii/S0065230X08607216.

G. G. Faust and I. M. Hall. SAMBLASTER: fast duplicate marking and structural variant read extraction. *Bioinformatics*, 30(17):2503–2505, sep 2014. ISSN 1367-4803. doi: 10.1093/bioinformatics/btu314. URL https://academic.oup.com/bioinformatics/article-lookup/doi/10.1093/bioinformatics/btu314.

A. R. Finch, C. J. Caunt, R. M. Perrett, K. Tsaneva-Atanasova, and C. A. McArdle. Dual specificity phosphatases 10 and 16 are positive regulators of EGF-stimulated ERK activity: Indirect regulation of ERK signals by JNK/p38 selective MAPK phosphatases. *Cellular Signalling*, 24(5):1002–1011, may 2012. ISSN 08986568. doi: 10.1016/j.cellsig.2011.12.021. URL https://www.sciencedirect.com/science/article/pii/S089865681100413X.

E. H. Fischer and E. G. Krebs. Regulation of phosphorylase b to a conversion in muscle, 1955. ISSN 00243205. URL http://www.jbc.org/.

B. B. Friday, C. Yu, G. K. Dy, P. D. Smith, L. Wang, S. N. Thibodeau, and A. A. Adjei. BRAF V600E disrupts AZD6244-induced abrogation of negative feedback pathways between extracellular signal-regulated kinase and Raf proteins. *Cancer Research*, 68 (15):6145–6153, aug 2008. ISSN 00085472. doi: 10.1158/0008-5472.CAN-08-1430. URL https://cancerres.aacrjournals.org/content/68/15/6145.short.

R. Fritsche-Guenther, F. Witzel, A. Sieber, R. Herr, N. Schmidt, S. Braun, T. Brummer, C. Sers, and N. Blüthgen. Strong negative feedback from Erk to Raf confers robustness to MAPK signalling. *Molecular Systems Biology*, 7(1):489–489, apr 2011. ISSN 17444292. doi: 10.1038/msb.2011.27. URL http://msb.embopress.org/cgi/doi/10.1038/msb.2011.27.

W. Fu, T. D. O'Connor, G. Jun, H. M. Kang, G. Abecasis, S. M. Leal, S. Gabriel, M. J. Rieder, D. Altshuler, J. Shendure, D. A. Nickerson, M. J. Bamshad, N. E. S. NHLBI Exome Sequencing Project, and J. M. Akey. Analysis of 6,515 exomes reveals the recent origin of most human protein-coding variants. *Nature*, 493(7431):216–220, jan 2013. ISSN 0028-0836. doi: 10.1038/nature11690. URL http://www.nature.com/articles/nature11690.

M. J. Garnett and R. Marais. Guilty as charged: B-RAF is a human oncogene. *Cancer Cell*, 6(4):313–319, oct 2004. ISSN 1535-6108. doi: 10.1016/

J.CCR.2004.09.022. URL https://www.sciencedirect.com/science/article/pii/S153561080400279X.

G. Gey. Tissue culture studies of the proliferative capacity of cervical carcinoma and normal epithelium. *Cancer Res.*, 12:264–265, 1952. URL https://ci.nii.ac.jp/naid/10006432514/.

P. Ghosh, N. M. Dahms, and S. Kornfeld. Mannose 6-phosphate receptors: new twists in the tale. *Nature Reviews Molecular Cell Biology*, 4(3):202–213, mar 2003. ISSN 1471-0072. doi: 10.1038/nrm1050. URL http://www.nature.com/articles/nrm1050.

J. Gill and G. King. What to do when your Hessian is not invertible: Alternatives to model respecification in nonlinear estimation, aug 2004. ISSN 00491241. URL http://journals.sagepub.com/doi/10.1177/0049124103262681.

R. M. Goldberg, A. P. Venook, and R. L. Schilsky. Cetuximab in the treatment of colorectal cancer. *Clinical advances in hematology and oncology*, 2(11):2040–2048, nov 2004. ISSN 15430790. doi: 10.1056/nejmoa071834. URL http://www.nejm.org/doi/abs/10.1056/NEJMoa071834.

L. S. Goodman, M. M. Wintrobe, W. Dameshek, M. J. Goodman, A. Gilman, and M. T. Mclennan. Nitrogen mustard therapy: Use of Methyl-Bis(Beta-Chloroethyl)amine Hydrochloride and Tris(Beta-Chloroethyl)amine Hydrochloride for Hodgkin's Disease, Lymphosarcoma, Leukemia and Certain Allied and Miscellaneous Disorders. *Journal of the American Medical Association*, 132(3):126–132, sep 1946. ISSN 23768118. doi: 10.1001/jama.1946.02870380008004. URL https://jamanetwork.com/journals/jama/fullarticle/288442.

C. W. Greider. Telomere length regulation, jun 1996. ISSN 00664154. URL https://www.annualreviews.org/doi/10.1146/annurev.bi.65.070196.002005.

L. Grieco, L. Calzone, I. Bernard-Pierrot, F. Radvanyi, B. Kahn-Perlès, and D. Thieffry. Integrative Modelling of the Influence of MAPK Network on Cancer Cell Fate Decision. *PLoS Computational Biology*, 9 (10):e1003286, oct 2013. ISSN 1553734X. doi: 10.1371/journal.pcbi.1003286. URL http://www.ncbi.nlm.nih.gov/pubmed/24250280http://www.pubmedcentral.nih.gov/articlerender.fcgi?artid=PMC3821540.

S. Gupta, D. A. Silveira, and J. C. M. Mombach. Towards DNA-damage induced autophagy: A Boolean model of p53-induced cell fate mechanisms. *DNA Repair*, 96:102971, dec 2020. ISSN 1568-7864. doi: 10.1016/J.DNAREP.2020.102971. URL https://www.sciencedirect.com/science/article/abs/pii/S1568786420302202?casa_token=zTErPs1seBgAAAAA:5rllRmqqp7Fd_w8saYqHnNfAiwhizCEgop5HNp54I9QrMdwLpHYv6ptJ1eCRHsMa17Hz65pEHQ.

S. P. Gygi, B. Rist, S. A. Gerber, F. Turecek, M. H. Gelb, and R. Aebersold. Quantitative analysis of complex protein mixtures using isotope-coded affinity tags. *Nature Biotechnology*, 17(10):994–999, oct 1999. ISSN 10870156. doi: 10.1038/13690. URL http://www.nature.com/articles/nbt1099_994.

E. J. Hahn, M. K. Rayens, A. T. Wiggins, W. Gan, H. M. Brown, and T. W. Mullett. Lung cancer incidence and the strength of municipal smoke-free ordinances. *Cancer*, 124(2):374–380, jan 2018. ISSN 10970142. doi: 10.1002/cncr.31142. URL http://doi.wiley.com/10.1002/cncr.31142.

S. I. Hajdu. A note from history: Landmarks in history of cancer, part 3, feb 2012. ISSN 10970142. URL http://doi.wiley.com/10.1002/cncr.26320.

D. Hanahan and R. a. Weinberg. Hallmarks of cancer: The next generation. *Cell*, 144(5):646–674, 2011. ISSN 00928674. doi: 10.1016/j.cell.2011.02.013. URL http://dx.doi.org/10.1016/j.cell.2011.02.013.

C. B. Harley, A. B. Futcher, and C. W. Greider. Telomeres shorten during ageing of human fibroblasts. *Nature*, 345(6274):458–460, may 1990. ISSN 0028-0836. doi: 10.1038/345458a0. URL http://www.nature.com/articles/345458a0.

L. H. Hartwell and T. A. Weinert. Checkpoints: Controls that ensure the order of cell cycle events. *Science*, 246(4930):629–634, nov 1989. ISSN 00368075. doi: 10.1126/science.2683079. URL https://science.sciencemag.org/content/246/4930/629https://science.sciencemag.org/content/246/4930/629.abstract.

C. H. Heldin, B. Lu, R. Evans, and J. S. Gutkind. Signals and receptors. *Cold Spring Harbor Perspectives in Biology*, 8(4):a005900, apr 2016. ISSN 19430264. doi: 10.1101/cshperspect.a005900. URL http://cshperspectives.cshlp.org/.

B. A. Hemmings and D. F. Restuccia. PI3K-PKB/Akt pathway. *Cold Spring Harbor Perspectives in Biology*, 4(9), 2012. ISSN 19430264. doi: 10.1101/cshperspect.a011189. URL http://cshperspectives.cshlp.org/content/4/9/a011189.full.pdf.

H. Hirai, H. Sootome, Y. Nakatsuru, K. Miyama, S. Taguchi, K. Tsujioka, Y. Ueno, H. Hatch, P. K. Majumder, B. S. Pan, and H. Kotani. MK-2206, an allosteric akt inhibitor, enhances antitumor efficacy by standard chemotherapeutic agents or molecular targeted drugs in vitro and in vivo. *Molecular Cancer Therapeutics*, 9(7):1956–1967, jul 2010. ISSN 15357163. doi: 10.1158/1535-7163.MCT-09-1012.

M. Hölzel, S. Huang, J. Koster, I. Øra, A. Lakeman, H. Caron, W. Nijkamp, J. Xie, T. Callens, S. Asgharzadeh, R. C. Seeger, L. Messiaen, R. Versteeg, and R. Bernards. NF1 Is a Tumor Suppressor in Neuroblastoma that Determines Retinoic Acid Response and Disease Outcome.

Cell, 142(2):218–229, jul 2010. ISSN 00928674. doi: 10.1016/j.cell.2010.06.004. URL http://www.ncbi.nlm.nih.gov/pubmed/20655465http://www.pubmedcentral.nih.gov/articlerender.fcgi?artid=PMC2913027.

F. E. Hood, B. Klinger, A. U. Newlaczyl, A. Sieber, M. Dorel, S. P. Oliver, J. M. Coulson, N. Blüthgen, and I. A. Prior. Isoform-specific Ras signaling is growth factor dependent. *Molecular Biology of the Cell*, 30(9):1108–1117, apr 2019. ISSN 19394586. doi: 10.1091/mbc.E18-10-0676. URL https://www.molbiolcell.org/doi/10.1091/mbc.E18-10-0676.

R. Hooke, J. Martyn, and J. Allestry. The Project Gutenberg eBook, Micrographia, by Robert Hooke Title: Micrographia Some Physiological Descriptions of Minute Bodies Made by Magnifying Glasses with Observations and Inquiries Thereupon Character set encoding: ISO-8859-1 ***START OF THE PROJECT. Technical report, The Royal Society of London for Improving Natural Knowledge, 2005. URL http://www.gutenberg.org/files/15491/15491-h/15491-h.htm.

Hopp, Grüter, and Hottiger. Regulation of Glucose Metabolism by NAD+ and ADP-Ribosylation. *Cells*, 8(8):890, aug 2019. ISSN 2073-4409. doi: 10.3390/cells8080890. URL www.mdpi.com/journal/cells.

P. V. Hornbeck, B. Zhang, B. Murray, J. M. Kornhauser, V. Latham, and E. Skrzypek. PhosphoSitePlus, 2014: Mutations, PTMs and recalibrations. *Nucleic Acids Research*, 43(D1):D512–D520, jan 2015. ISSN 13624962. doi: 10.1093/nar/gku1267. URL http://academic.oup.com/nar/article/43/D1/D512/2439467/PhosphoSitePlus-2014-mutations-PTMs-and.

N. Howlader, A. Noone, M. Krapcho, D. Miller, K. Bishop, S. Altekruse, C. Kosary, M. Yu, J. Ruhl, Z. Tatalovich, A. Mariotto, D. Lewis, H. Chen, E. Feuer, and K. Cronin. SEER Cancer Statistics Review. *National Cancer Institute*, 2015. URL https://seer.cancer.gov/csr/1975_2016/results_merged/sect_29_childhood_cancer_iccc.pdfhttps://seer.cancer.gov/csr/1975_2016/.

C.-L. Hsu, H.-Y. Chang, J.-Y. Chang, W.-M. Hsu, H.-C. Huang, H.-F. Juan, C.-L. Hsu, H.-Y. Chang, J.-Y. Chang, W.-M. Hsu, H.-C. Huang, H.-F. Juan, and H.-F. J. Chia-Lang Hsu, Hsin-Yi Chang, Jen-Yun Chang, Wen-Ming Hsu, Hsuan-Cheng Huang. Unveiling MYCN regulatory networks in neuroblastoma via integrative analysis of heterogeneous genomics data. *Oncotarget*, 7(24):36293–36310, jun 2016. ISSN 1949-2553. doi: 10.18632/oncotarget.9202. URL http://www.ncbi.nlm.nih.gov/pubmed/27167114http://www.pubmedcentral.nih.gov/articlerender.fcgi?artid=PMC5095001.

D. J. Hudson. Interval Estimation from the Likelihood Function. *Journal of the Royal Statistical Society: Series B (Methodological)*, 33(2):256–262, jul

1971. ISSN 00359246. doi: 10.1111/j.2517-6161.1971.tb00877.x. URL https://onlinelibrary.wiley.com/doi/10.1111/j.2517-6161.1971.tb00877.x.

C. S. Hughes, S. Moggridge, T. Müller, P. H. Sorensen, G. B. Morin, and J. Krijgsveld. Single-pot, solid-phase-enhanced sample preparation for proteomics experiments. *Nature Protocols*, 14(1):68–85, jan 2019. ISSN 17502799. doi: 10.1038/s41596-018-0082-x. URL http://www.nature.com/articles/s41596-018-0082-x.

T. Ideker, T. Galitski, and L. Hood. A new approach to decoding life: Systems biology, nov 2001. ISSN 15278204. URL www.annualreviews.org.

L. O. Jacobson, C. L. Spurr, E. S. Barron, T. Smith, C. Lushbaugh, and G. F. Dick. Nitrogen mustard therapy: Studies on the effect of methyl-bis (beta-chloroethyl) amine hydrochloride on neoplastic diseases and allied disorders of the hemopoietic system. *Journal of the American Medical Association*, 132(5):263–271, oct 1946. ISSN 23768118. doi: 10.1001/jama.1946.02870400011003. URL https://jamanetwork.com/journals/jama/fullarticle/288767.

P. Jeggo and M. Löbrich. How cancer cells hijack DNA double-strand break repair pathways to gain genomic instability. *Biochemical Journal*, 471(1):1–11, oct 2015. ISSN 0264-6021. doi: 10.1042/BJ20150582. URL https://portlandpress.com/biochemj/article/471/1/1/48612/How-cancer-cells-hijack-DNA-doublestrand-break.

J. I. Johnsen, C. Dyberg, S. Fransson, and M. Wickström. Molecular mechanisms and therapeutic targets in neuroblastoma. *Pharmacological Research*, 131:164–176, may 2018. ISSN 10961186. doi: 10.1016/j.phrs.2018.02.023.

M. C. Jongmans, I. Van Der Burgt, P. M. Hoogerbrugge, K. Noordam, H. G. Yntema, W. M. Nillesen, R. P. Kuiper, M. J. Ligtenberg, A. G. Van Kessel, J. H. J. Van Krieken, L. A. Kiemeney, and N. Hoogerbrugge. Cancer risk in patients with Noonan syndrome carrying a PTPN11 mutation. *European Journal of Human Genetics*, 19 (8):870–874, aug 2011. ISSN 10184813. doi: 10.1038/ejhg.2011.37. URL http://www.nature.com/articles/ejhg201137.

P. Kaatsch, C. Spix, A. Katalanic, S. Hentschel, and S. Luttmann. *Cancer in Germany in 2013/2014. 11th.* Robert Koch Institute, Berlin, 2018. ISBN 978-3-89606-289-5. doi: 10.17886/rkipubl-2017-008. URL https://www.krebsdaten.de/Krebs/EN/Content/Publications/Cancer_in_Germany/cancer_chapters_2013_2014/cancer_germany_2013_2014.pdf;jsessionid=046D40131922E8968A320CE094894231.2_cid290?__blob=publicationFile.

M. Kanehisa and S. Goto. KEGG: Kyoto Encyclopedia of Genes and Genomes. *Nucleic Acids Research*, 28(1):27–30, jan 2000. ISSN 13624962. doi: 10.1093/nar/28.1.

27. URL https://academic.oup.com/nar/article-lookup/doi/10.1093/nar/28.1.27.

K. Kapeli and P. J. Hurlin. Differential Regulation of N-Myc and c-Myc Synthesis, Degradation, and Transcriptional Activity by the Ras/Mitogen-activated Protein Kinase Pathway. *Journal of Biological Chemistry*, 286(44):38498–38508, nov 2011. ISSN 0021-9258. doi: 10.1074/jbc.M111.276675. URL http://www.ncbi.nlm.nih.gov/pubmed/21908617http://www.pubmedcentral.nih.gov/articlerender.fcgi?artid=PMC3207449http://www.jbc.org/lookup/doi/10.1074/jbc.M111.276675.

D. R. Kaplan, K. Matsumoto, E. Lucarelli, and C. J. Thielet. Induction of TrkB by retinoic acid mediates biologic responsiveness to BDNF and differentiation of human neuroblastoma cells. *Neuron*, 11(2):321–331, aug 1993. ISSN 08966273. doi: 10.1016/0896-6273(93)90187-V. URL https://www.sciencedirect.com/science/article/pii/089662739390187V.

A. M. Kenney, H. R. Widlund, and D. H. Rowitch. Hedgehog and PI-3 kinase signaling converge on Nmyc1 to promote cell cycle progression in cerebellar neuronal precursors, jan 2004. ISSN 09501991. URL https://dev.biologists.org/content/131/1/217https://dev.biologists.org/content/131/1/217.abstract.

K. Keyomarsi and A. B. Pardee. Redundant cyclin overexpression and gene amplification in breast cancer cells. *Proceedings of the National Academy of Sciences of the United States of America*, 90(3):1112–1116, feb 1993. ISSN 00278424. doi: 10.1073/pnas.90.3.1112. URL https://www.pnas.org/content/90/3/1112https://www.pnas.org/content/90/3/1112.abstract.

B. N. Kholodenko, A. Kiyatkin, F. J. Bruggeman, E. Sontag, H. V. Westerhoff, and J. B. Hoek. Untangling the wires: a strategy to trace functional interactions in signaling and gene networks. *Proceedings of the National Academy of Sciences of the United States of America*, 99(20):12841–6, oct 2002. ISSN 0027-8424. doi: 10.1073/pnas.192442699. URL http://www.ncbi.nlm.nih.gov/pubmed/12242336http://www.pubmedcentral.nih.gov/articlerender.fcgi?artid=PMC130547http://www.pubmedcentral.nih.gov/articlerender.fcgi?artid=130547&tool=pmcentrez&rendertype=abstract.

M. K. Kiessling, A. Curioni-Fontecedro, P. Samaras, S. Lang, M. Scharl, A. Aguzzi, D. A. Oldrige, J. M. Maris, and G. Rogler. Targeting the mTOR complex by everolimus in NRAS mutant neuroblastoma. *PLoS ONE*, 11(1):e0170851–undefined, jan 2016. ISSN 19326203. doi: 10.1371/journal.pone.0147682. URL https://journals.plos.org/plosone/article/file?id=10.1371/journal.pone.0147682&type=printable.

S. Kim, K. Scheffler, A. L. Halpern, M. A. Bekritsky, E. Noh, M. Källberg, X. Chen, Y. Kim, D. Beyter, P. Krusche, and C. T. Saunders. Strelka2: fast and accurate calling of germline and somatic variants. *Nature Methods*, 15(8):591–594, aug 2018. ISSN 15487105. doi: 10.1038/s41592-018-0051-x. URL http://www.nature.com/articles/s41592-018-0051-x.

M. Kjær. Role of Extracellular Matrix in Adaptation of Tendon and Skeletal Muscle to Mechanical Loading, apr 2004. ISSN 00319333. URL www.prv.org.

B. Klinger and N. Blüthgen. Consequences of feedback in signal transduction for targeted therapies. *Biochemical Society Transactions*, 42(4): 770–775, aug 2014. ISSN 0300-5127. doi: 10.1042/BST20140130. URL https://portlandpress.com/biochemsoctrans/article/42/4/770/68707/Consequences-of-feedback-in-signal-transduction.

B. Klinger and N. Blüthgen. Reverse engineering gene regulatory networks by modular response analysis – a benchmark. *Essays in Biochemistry*, 62(4):535–547, oct 2018. ISSN 0071-1365. doi: 10.1042/EBC20180012. URL https://portlandpress.com/essaysbiochem/article/62/4/535/78543/Reverse-engineering-gene-regulatory-networks-by.

B. Klinger, A. Sieber, R. Fritsche-Guenther, F. Witzel, L. Berry, D. Schumacher, Y. Yan, P. Durek, M. Merchant, R. Schäfer, C. Sers, and N. Blüthgen. Network quantification of EGFR signaling unveils potential for targeted combination therapy. *Molecular Systems Biology*, 9(1):673, jan 2013. ISSN 17444292. doi: 10.1038/msb.2013.29. URL http://www.pubmedcentral.nih.gov/articlerender.fcgi?artid=3964313&tool=pmcentrez&rendertype=abstract.

A. Korkut, W. Wang, E. Demir, B. A. Aksoy, X. Jing, E. J. Molinelli, Ö. Babur, D. L. Bemis, S. Onur Sumer, D. B. Solit, C. A. Pratilas, and C. Sander. Perturbation biology nominates upstream-downstream drug combinations in RAF inhibitor resistant melanoma cells. *eLife*, 4:e04640, jan 2015. ISSN 2050-084X. doi: 10.7554/eLife.04640. URL https://elifesciences.org/content/4/e04640.

I. Kuperstein, E. Bonnet, H. A. Nguyen, D. Cohen, E. Viara, L. Grieco, S. Fourquet, L. Calzone, C. Russo, M. Kondratova, M. Dutreix, E. Barillot, and A. Zinovyev. Atlas of Cancer Signalling Network: A systems biology resource for integrative analysis of cancer data with Google Maps. *Oncogenesis*, 4(7):e160–e160, jul 2015. ISSN 21579024. doi: 10.1038/oncsis.2015.19. URL http://www.nature.com/articles/oncsis201519.

Y. Kyo, T. Tanaka, K. Hayashi, T. Iehara, M. Kaneko, H. Hosoi, T. Sugimoto, M. Hamasaki, M. Kobayashi, and T. Sawada. Identification of therapy-sensitive and

therapy-resistant neuroblastoma subtypes in stages III, IVs and IV. *Cancer Letters*, 306(1):27–33, jul 2011. ISSN 03043835. doi: 10.1016/j.canlet.2011.02.016. URL https://www.sciencedirect.com/science/article/pii/S0304383511000899.

D. Lake, S. A. Corrêa, and J. Müller. Negative feedback regulation of the ERK1/2 MAPK pathway, dec 2016. ISSN 14209071. URL http://link.springer.com/10.1007/s00018-016-2297-8.

H. Lavoie, J. Gagnon, and M. Therrien. ERK signalling: a master regulator of cell behaviour, life and fate, jun 2020. ISSN 14710080. URL http://www.nature.com/articles/s41580-020-0255-7.

E. Le Rhun, M. Preusser, P. Roth, D. A. Reardon, M. van den Bent, P. Wen, G. Reifenberger, and M. Weller. Molecular targeted therapy of glioblastoma, nov 2019. ISSN 15321967. URL https://www.sciencedirect.com/science/article/abs/pii/S0305737219301124.

S. Legewie, H. Herzel, H. V. Westerhoff, and N. Blüthgen. Recurrent design patterns in the feedback regulation of the mammalian signalling network. *Molecular Systems Biology*, 4(1):190, jan 2008. ISSN 17444292. doi: 10.1038/msb.2008.29. URL https://onlinelibrary.wiley.com/doi/10.1038/msb.2008.29.

K. Levenberg and F. Arsenal. A Method for the Solution of Certain Non-Linear Problems in Least Squares. *Quarterly of Applied Mathematics*, 1 (278):536–538, 1943. URL https://www.ams.org/journals/qam/1944-02-02/S0033-569X-1944-10666-0/S0033-569X-1944-10666-0.pdf.

H. Li. Aligning sequence reads, clone sequences and assembly contigs with BWA-MEM. *arXiv.org*, mar 2013. URL http://arxiv.org/abs/1303.3997.

J. Li, J. G. Van Vranken, L. Pontano Vaites, D. K. Schweppe, E. L. Huttlin, C. Etienne, P. Nandhikonda, R. Viner, A. M. Robitaille, A. H. Thompson, K. Kuhn, I. Pike, R. D. Bomgarden, J. C. Rogers, S. P. Gygi, and J. A. Paulo. TMTpro reagents: a set of isobaric labeling mass tags enables simultaneous proteome-wide measurements across 16 samples. *Nature Methods*, 17(4):399–404, apr 2020. ISSN 15487105. doi: 10.1038/s41592-020-0781-4. URL http://www.nature.com/articles/s41592-020-0781-4.

Y. Liao, G. K. Smyth, and W. Shi. FeatureCounts: An efficient general purpose program for assigning sequence reads to genomic features. *Bioinformatics*, 30(7):923–930, apr 2014. ISSN 14602059. doi: 10.1093/bioinformatics/btt656. URL https://academic.oup.com/bioinformatics/article-lookup/doi/10.1093/bioinformatics/btt656.

A. Liberzon, A. Subramanian, R. Pinchback, H. Thorvaldsdottir, P. Tamayo, and J. P. Mesirov. Molecular signatures database (MSigDB) 3.0. *Bioinformatics*, 27(12):1739–1740, jun 2011. ISSN 1367-4803. doi: 10.1093/bioinformatics/btr260. URL https://academic.oup.com/bioinformatics/article-lookup/doi/10.1093/bioinformatics/btr260.

P. Lito, C. A. Pratilas, E. W. Joseph, M. Tadi, E. Halilovic, M. Zubrowski, A. Huang, W. L. Wong, M. K. Callahan, T. Merghoub, J. D. Wolchok, E. de Stanchina, S. Chandarlapaty, P. I. Poulikakos, J. A. Fagin, and N. Rosen. Relief of Profound Feedback Inhibition of Mitogenic Signaling by RAF Inhibitors Attenuates Their Activity in BRAFV600E Melanomas. *Cancer Cell*, 22(5):668–682, nov 2012. ISSN 15356108. doi: 10.1016/j.ccr.2012.10.009.

X. Liu, T. Turbyville, A. Fritz, and L. Whitesell. Inhibition of insulin-like growth factor I receptor expression in neuroblastoma cells induces the regression of established tumors in mice. *Cancer research*, 58(23):5432–8, dec 1998. ISSN 0008-5472. URL http://www.ncbi.nlm.nih.gov/pubmed/9850076.

L. Ljung and T. Glad. On global identifiability for arbitrary model parametrizations. *Automatica*, 30(2):265–276, feb 1994. ISSN 00051098. doi: 10.1016/0005-1098(94)90029-9. URL https://www.sciencedirect.com/science/article/pii/0005109894900299.

M. I. A. Lourakis. A Brief Description of the Levenberg-Marquardt Algorithm Implemented by levmar. *Computer*, 2005: 1–2, 2005. URL https://www.semanticscholar.org/paper/A-Brief-Description-of-the-Levenberg-Marquardt-by-Lourakis/a92844ea0726e0ebb3fdf99b070d1e8e289eb97f.

S. M. Mac, C. A. D'Cunha, and P. J. Farnham. Direct recruitment of N-myc to target gene promoters. *Molecular Carcinogenesis*, 29(2):76–86, oct 2000. ISSN 0899-1987. doi: 10.1002/1098-2744(200010)29:2⟨76::AID-MC4⟩3.0.CO;2-Y. URL https://onlinelibrary.wiley.com/doi/10.1002/1098-2744(200010)29:2%3C76::AID-MC4%3E3.0.CO;2-Y.

K. Manjang, S. Tripathi, O. Yli-Harja, M. Dehmer, and F. Emmert-Streib. Graph-based exploitation of gene ontology using GOxploreR for scrutinizing biological significance. *Scientific Reports*, 10(1):16672, dec 2020. ISSN 2045-2322. doi: 10.1038/s41598-020-73326-3. URL https://www.nature.com/articles/s41598-020-73326-3.

J. M. Maris, M. D. Hogarty, R. Bagatell, and S. L. Cohn. Neuroblastoma. *Lancet*, 369(9579):2106–2120, jun 2007. ISSN 01406736. doi: 10.

1016/S0140-6736(07)60983-0. URL https://www.sciencedirect.com/science/article/pii/S0140673607609830?via%3Dihub.

T. Martinsson, T. Eriksson, J. Abrahamsson, H. Caren, M. Hansson, P. Kogner, S. Kamaraj, C. Schönherr, J. Weinmar, K. Ruuth, R. H. Palmer, and B. Hallberg. Appearance of the Novel Activating F1174S ALK Mutation in Neuroblastoma Correlates with Aggressive Tumor Progression and Unresponsiveness to Therapy. *Cancer Research*, 71(1):98–105, jan 2011. ISSN 0008-5472. doi: 10.1158/0008-5472.CAN-10-2366. URL http://www.ncbi.nlm.nih.gov/pubmed/21059859http://cancerres.aacrjournals.org/lookup/doi/10.1158/0008-5472.CAN-10-2366.

P. Mertins, L. C. Tang, K. Krug, D. J. Clark, M. A. Gritsenko, L. Chen, K. R. Clauser, T. R. Clauss, P. Shah, M. A. Gillette, V. A. Petyuk, S. N. Thomas, D. R. Mani, F. Mundt, R. J. Moore, Y. Hu, R. Zhao, M. Schnaubelt, H. Keshishian, M. E. Monroe, Z. Zhang, N. D. Udeshi, S. R. Davies, R. R. Townsend, D. W. Chan, R. D. Smith, H. Zhang, T. Liu, and S. A. Carr. Reproducible workflow for multiplexed deep-scale proteome and phosphoproteome analysis of tumor tissues by liquid chromatography-mass spectrometry. *Nature Protocols*, 13(7):1632–1661, jul 2018. ISSN 17502799. doi: 10.1038/s41596-018-0006-9. URL http://www.nature.com/articles/s41596-018-0006-9.

D. R. Miller. A tribute to Sidney Farber - The father of modern chemotherapy, jul 2006. ISSN 00071048. URL http://doi.wiley.com/10.1111/j.1365-2141.2006.06119.x.

M. K. Morris, J. Saez-Rodriguez, P. K. Sorger, and D. A. Lauffenburger. Logic-based models for the analysis of cell signaling networks, apr 2010. ISSN 00062960. URL http://pubs.acs.org/doi/abs/10.1021/bi902202q.

M. K. Morris, J. Saez-Rodriguez, D. C. Clarke, P. K. Sorger, and D. A. Lauffenburger. Training Signaling Pathway Maps to Biochemical Data with Constrained Fuzzy Logic: Quantitative Analysis of Liver Cell Responses to Inflammatory Stimuli. *PLoS Computational Biology*, 7(3):e1001099, mar 2011. ISSN 1553-7358. doi: 10.1371/journal.pcbi.1001099. URL https://dx.plos.org/10.1371/journal.pcbi.1001099.

Y. P. Mossé, M. Laudenslager, L. Longo, K. A. Cole, A. Wood, E. F. Attiyeh, M. J. Laquaglia, R. Sennett, J. E. Lynch, P. Perri, G. Laureys, F. Speleman, C. Kim, C. Hou, H. Hakonarson, A. Torkamani, N. J. Schork, G. M. Brodeur, G. P. Tonini, E. Rappaport, M. Devoto, and J. M. Maris. Identification of ALK as a major familial neuroblastoma predisposition gene. *Nature*, 455(7215):930–935, oct 2008. ISSN 00280836. doi: 10.1038/nature07261. URL http://www.sanger.ac.uk/.

D. M. Murphy, P. G. Buckley, K. Bryan, K. M. Watters, J. Koster, P. van Sluis, J. Molenaar, R. Versteeg, and R. L. Stallings. Dissection of the oncogenic MYCN transcriptional network reveals a large set of clinically relevant cell cycle genes as drivers of neuroblastoma tumorigenesis. *Molecular Carcinogenesis*, 50(6):403–411, jun 2011. ISSN 08991987. doi: 10.1002/mc.20722. URL http://doi.wiley.com/10.1002/mc.20722.

R. Nahta, D. Yu, M. C. Hung, G. N. Hortobagyi, and F. J. Esteva. Mechanisms of disease: Understanding resistance to HER2-targeted therapy in human breast cancer, may 2006. ISSN 17434254. URL http://www.nature.com/articles/ncponc0509.

B. G. Neel, H. Gu, and L. Pao. The 'Shp'ing news: SH2 domain-containing tyrosine phosphatases in cell signaling. *Trends in Biochemical Sciences*, 28(6):284–293, jun 2003. ISSN 0968-0004. doi: 10.1016/S0968-0004(03)00091-4. URL https://www.sciencedirect.com/science/article/pii/S0968000403000914?casa_token=3plRVlL4l20AAAAA:gIqHCuZnbWNNPW2spkkzzyOw7zUW728Kun3saZl224w80CPrnSTQ7CDl8bWnzd_NC51CCgBsDw.

S. Nelander, W. Wang, B. Nilsson, Q. She, C. Pratilas, N. Rosen, P. Gennemark, and C. Sander. Models from experiments: combinatorial drug perturbations of cancer cells. *Molecular Systems Biology*, 4(1):216, jan 2008. ISSN 1744-4292. doi: 10.1038/msb.2008.53. URL https://onlinelibrary.wiley.com/doi/10.1038/msb.2008.53.

L. K. Nguyen and B. N. Kholodenko. Feedback regulation in cell signalling: Lessons for cancer therapeutics, feb 2016. ISSN 10963634. URL https://www.sciencedirect.com/science/article/pii/S1084952115001846.

B. Niederdorfer, V. Touré, M. Vazquez, L. Thommesen, M. Kuiper, A. Lægreid, and Å. Flobak. Strategies to Enhance Logic Modeling-Based Cell Line-Specific Drug Synergy Prediction. *Frontiers in Physiology*, 11:862, jul 2020. ISSN 1664042X. doi: 10.3389/fphys.2020.00862. URL https://www.frontiersin.org/article/10.3389/fphys.2020.00862/full.

M. H. Nissan, C. A. Pratilas, A. M. Jones, R. Ramirez, H. Won, C. Liu, S. Tiwari, L. Kong, A. J. Hanrahan, Z. Yao, T. Merghoub, A. Ribas, P. B. Chapman, R. Yaeger, B. S. Taylor, N. Schultz, M. F. Berger, N. Rosen, and D. B. Solit. Loss of NF1 in cutaneous melanoma is associated with RAS activation and MEK dependence. *Cancer Research*, 74(8):2340–2350, jul 2014. ISSN 15387445. doi: 10.1158/0008-5472.CAN-13-2625. URL http://www.ncbi.nlm.nih.gov/pubmed/12873990.

A. J. Oates, L. M. Schumaker, S. B. Jenkins, A. A. Pearce, S. A. DaCosta, B. Arun, and M. J. Ellis. The mannose 6-phosphate/insulin-like growth factor 2 receptor (M6P/IGF2R), a putative breast tumor suppressor gene. *Breast Cancer Research and Treatment*, 47(3):269–281, feb 1998. ISSN 0167-6806. doi: 10.1023/A:1005959218524. URL http://link.springer.com/10.1023/A:1005959218524.

C. J. Oates, B. T. Hennessy, Y. Lu, G. B. Mills, and S. Mukherjee. Network inference using steady-state data and goldbeter-koshland kinetics. *Bioinformatics*, 28(18):2342–2348, sep 2012. ISSN 13674803. doi: 10.1093/bioinformatics/bts459. URL https://academic.oup.com/bioinformatics/article/28/18/2342/253991.

C. L. O'Bryant, S. D. Wenger, M. Kim, and L. A. Thompson. crizotinib: Una nueva opción de tratamiento para cáncer pulmonar de célula no pequeña ALK positivo, feb 2013. ISSN 10600280. URL http://journals.sagepub.com/doi/10.1345/aph.1R002http://www.ncbi.nlm.nih.gov/pubmed/23386065.

L. O'Connell and D. C. Winter. Organoids: Past learning and future directions, mar 2020. ISSN 15578534. URL https://www.liebertpub.com/doi/10.1089/scd.2019.0227.

S. D. O'Dell and I. N. Day. Insulin-like growth factor II (IGF-II). *International Journal of Biochemistry and Cell Biology*, 30(7):767–771, jul 1998. ISSN 13572725. doi: 10.1016/S1357-2725(98)00048-X. URL https://www.sciencedirect.com/science/article/pii/S135727259800048X?via%3Dihub#BIB6.

T. Okuzumi, D. Fiedler, C. Zhang, D. C. Gray, B. Aizenstein, R. Hoffman, and K. M. Shokat. Inhibitor hijacking of Akt activation. *Nature Chemical Biology*, 5(7):484–493, jul 2009. ISSN 15524469. doi: 10.1038/nchembio.183. URL http://www.nature.com/articles/nchembio.183.

R. J. Orton, O. E. Sturm, V. Vyshemirsky, M. Calder, D. R. Gilbert, and W. Kolch. Computational modelling of the receptor-tyrosine-kinase-activated MAPK pathway. *The Biochemical journal*, 392(Pt 2):249–61, dec 2005. ISSN 1470-8728. doi: 10.1042/BJ20050908. URL http://www.ncbi.nlm.nih.gov/pubmed/16293107http://www.pubmedcentral.nih.gov/articlerender.fcgi?artid=PMC1316260http://www.pubmedcentral.nih.gov/articlerender.fcgi?artid=1316260&tool=pmcentrez&rendertype=abstract.

N. Osinalde, K. Aloria, M. J. Omaetxebarria, and I. Kratchmarova. Targeted mass spectrometry: An emerging powerful approach to unblock the bottleneck in phosphoproteomics. *Journal of Chromatography B*, 1055-1056:29–38, jun 2017. ISSN 1570-0232. doi: 10.1016/J.JCHROMB.2017.04.026. URL https://www.sciencedirect.com/science/article/pii/S1570023217306682?

casa_token=Aw4XXQ3KbgkAAAAA:I68TVOcnzGvLIMo46u9q3zPqPh-p_
-6DrDP9R8jjAizmosH7XTEDmrqCjQ-dDBPc8B6jXP49lA.

M. Ottaviano, E. F. Giunta, M. Tortora, M. Curvietto, L. Attademo, D. Bosso, C. Cardalesi, M. Rosanova, P. De Placido, E. Pietroluongo, V. Riccio, B. Mucci, S. Parola, M. G. Vitale, G. Palmieri, B. Daniele, and E. Simeone. BRAF gene and melanoma: Back to the future, mar 2021. ISSN 14220067. URL https://www.mdpi.com/1422-0067/22/7/3474.

T. Otto, S. Horn, M. Brockmann, U. Eilers, L. Schüttrumpf, N. Popov, A. M. Kenney, J. H. Schulte, R. Beijersbergen, H. Christiansen, B. Berwanger, and M. Eilers. Stabilization of N-Myc Is a Critical Function of Aurora A in Human Neuroblastoma. *Cancer Cell*, 15(1):67–78, jan 2009. ISSN 15356108. doi: 10.1016/j.ccr.2008.12.005. URL http://linkinghub.elsevier.com/retrieve/pii/S153561080800408X.

J. R. Park, S. G. Kreissman, W. B. London, A. Naranjo, S. L. Cohn, M. D. Hogarty, S. C. Tenney, D. Haas-Kogan, P. J. Shaw, J. D. Geiger, J. J. Doski, S. W. Gorges, G. Khanna, S. D. Voss, J. M. Maris, S. A. Grupp, and L. Diller. A phase III randomized clinical trial (RCT) of tandem myeloablative autologous stem cell transplant (ASCT) using peripheral blood stem cell (PBSC) as consolidation therapy for high-risk neuroblastoma (HR-NB): A Children's Oncology Group (COG) study. *Journal of Clinical Oncology*, 34(suppl18):LBA3–LBA3, jun 2016. ISSN 0732-183X. doi: 10.1200/jco.2016.34.18_suppl.lba3.

M. Pasparakis, T. Luedde, and M. Schmidt-Supprian. Dissection of the NF-κB signalling cascade in transgenic and knockout mice, may 2006. ISSN 13509047. URL http://www.nature.com/articles/4401870.

M. Peifer, F. Hertwig, F. Roels, D. Dreidax, M. Gartlgruber, R. Menon, A. Krämer, J. L. Roncaioli, F. Sand, J. M. Heuckmann, F. Ikram, R. Schmidt, S. Ackermann, A. Engesser, Y. Kahlert, W. Vogel, J. Altmüller, P. Nürnberg, J. Thierry-Mieg, D. Thierry-Mieg, A. Mariappan, S. Heynck, E. Mariotti, K. O. Henrich, C. Gloeckner, G. Bosco, I. Leuschner, M. R. Schweiger, L. Savelyeva, S. C. Watkins, C. Shao, E. Bell, T. Höfer, V. Achter, U. Lang, J. Theissen, R. Volland, M. Saadati, A. Eggert, B. De Wilde, F. Berthold, Z. Peng, C. Zhao, L. Shi, M. Ortmann, R. Büttner, S. Perner, B. Hero, A. Schramm, J. H. Schulte, C. Herrmann, R. J. O'Sullivan, F. Westermann, R. K. Thomas, and M. Fischer. Telomerase activation by genomic rearrangements in high-risk neuroblastoma. *Nature*, 526(7575):700–704, oct 2015. ISSN 14764687. doi: 10.1038/nature14980. URL http://www.ncbi.nlm.nih.gov/pubmed/26466568http://www.pubmedcentral.nih.gov/articlerender.fcgi?artid=PMC4881306.

H. A. Pickett and R. R. Reddel. Molecular mechanisms of activity and derepression of alternative lengthening of telomeres. *Nature Structural and Molecular Biology*,

22(11):875–880, nov 2015. ISSN 15459985. doi: 10.1038/nsmb.3106. URL http://www.nature.com/articles/nsmb.3106.

M. Pomaznoy, B. Ha, and B. Peters. GOnet: A tool for interactive Gene Ontology analysis. *BMC Bioinformatics*, 19(1):470, dec 2018. ISSN 14712105. doi: 10.1186/s12859-018-2533-3. URL https://bmcbioinformatics.biomedcentral.com/articles/10.1186/s12859-018-2533-3.

F. Porter. Interval estimation using the likelihood function. *Nuclear Instruments and Methods in Physics Research Section A: Accelerators, Spectrometers, Detectors and Associated Equipment*, 368(3):793–803, jan 1996. ISSN 0168-9002. doi: 10.1016/0168-9002(95)00792-X. URL https://www.sciencedirect.com/science/article/pii/016890029500792X.

P. I. Poulikakos, C. Zhang, G. Bollag, K. M. Shokat, and N. Rosen. RAF inhibitors transactivate RAF dimers and ERK signalling in cells with wild-type BRAF. *Nature*, 464(7287):427–430, mar 2010. ISSN 00280836. doi: 10.1038/nature08902. URL http://www.nature.com/articles/nature08902.

A. Prahallad, C. Sun, S. Huang, F. Di Nicolantonio, R. Salazar, D. Zecchin, R. L. Beijersbergen, A. Bardelli, and R. Bernards. Unresponsiveness of colon cancer to BRAF(V600E) inhibition through feedback activation of EGFR. *Nature*, 483(7387):100–104, mar 2012. ISSN 00280836. doi: 10.1038/nature10868. URL https://pubmed.ncbi.nlm.nih.gov/22281684/.

A. Prahallad, G. J. J. E. Heynen, G. Germano, S. M. Willems, B. Evers, L. Vecchione, V. Gambino, C. Lieftink, R. L. Beijersbergen, F. Di Nicolantonio, A. Bardelli, and R. Bernards. PTPN11 Is a Central Node in Intrinsic and Acquired Resistance to Targeted Cancer Drugs. *Cell Reports*, 12(12):1978–1985, sep 2015. ISSN 22111247. doi: 10.1016/j.celrep.2015.08.037. URL http://www.ncbi.nlm.nih.gov/pubmed/26365186http://linkinghub.elsevier.com/retrieve/pii/S2211124715009225.

T. J. Pugh, O. Morozova, E. F. Attiyeh, S. Asgharzadeh, J. S. Wei, D. Auclair, S. L. Carter, K. Cibulskis, M. Hanna, A. Kiezun, J. Kim, M. S. Lawrence, L. Lichenstein, A. McKenna, C. S. Pedamallu, A. H. Ramos, E. Shefler, A. Sivachenko, C. Sougnez, C. Stewart, A. Ally, I. Birol, R. Chiu, R. D. Corbett, M. Hirst, S. D. Jackman, B. Kamoh, A. H. Khodabakshi, M. Krzywinski, A. Lo, R. A. Moore, K. L. Mungall, J. Qian, A. Tam, N. Thiessen, Y. Zhao, K. A. Cole, M. Diamond, S. J. Diskin, Y. P. Mosse, A. C. Wood, L. Ji, R. Sposto, T. Badgett, W. B. London, Y. Moyer, J. M. Gastier-Foster, M. A. Smith, J. M. Guidry Auvil, D. S. Gerhard, M. D. Hogarty, S. J. Jones, E. S. Lander, S. B. Gabriel, G. Getz, R. C. Seeger, J. Khan, M. A. Marra, M. Meyerson, and J. M. Maris. The genetic landscape of high-risk

neuroblastoma. *Nature Genetics*, 45(3):279–284, jan 2013. ISSN 1546-1718. doi: 10.1038/ng.2529. URL http://www.nature.com/doifinder/10.1038/ng.2529http://www.nature.com/ng/journal/v45/n3/pdf/ng.2529.pdf.

K. Rahmouni, D. A. Morgan, G. M. Morgan, X. Liu, C. D. Sigmund, A. L. Mark, and W. G. Haynes. Hypothalamic PI3K and MAPK differentially mediate regional sympathetic activation to insulin. *The Journal of clinical investigation*, 114(5):652–8, sep 2004. ISSN 0021-9738. doi: 10.1172/JCI21737. URL http://www.ncbi.nlm.nih.gov/pubmed/15343383http://www.pubmedcentral.nih.gov/articlerender.fcgi?artid=PMC514588.

A. Raue, C. Kreutz, T. Maiwald, J. Bachmann, M. Schilling, U. Klingmüller, and J. Timmer. Structural and practical identifiability analysis of partially observed dynamical models by exploiting the profile likelihood. *Bioinformatics*, 25(15):1923–1929, aug 2009. ISSN 13674803. doi: 10.1093/bioinformatics/btp358. URL https://academic.oup.com/bioinformatics/article-lookup/doi/10.1093/bioinformatics/btp358.

A. Raue, V. Becker, U. Klingmüller, and J. Timmer. Identifiability and observability analysis for experimental design in nonlinear dynamical models. *Chaos: An Interdisciplinary Journal of Nonlinear Science*, 20(4):045105, dec 2010. ISSN 1054-1500. doi: 10.1063/1.3528102. URL http://aip.scitation.org/doi/10.1063/1.3528102.

A. Raue, B. Steiert, M. Schelker, C. Kreutz, T. Maiwald, H. Hass, J. Vanlier, C. Tönsing, L. Adlung, R. Engesser, W. Mader, T. Heinemann, J. Hasenauer, M. Schilling, T. Höfer, E. Klipp, F. Theis, U. Klingmüller, B. Schöberl, and J. Timmer. Data2Dynamics: A modeling environment tailored to parameter estimation in dynamical systems. *Bioinformatics*, 31(21):3558–3560, nov 2015. ISSN 14602059. doi: 10.1093/bioinformatics/btv405. URL https://academic.oup.com/bioinformatics/article-lookup/doi/10.1093/bioinformatics/btv405.

V. W. Rebecca, G. M. Alicea, K. H. Paraiso, H. Lawrence, G. T. Gibney, and K. S. Smalley. Vertical inhibition of the MAPK pathway enhances therapeutic responses in NRAS-mutant melanoma. *Pigment Cell and Melanoma Research*, 27(6):1154–1158, nov 2014. ISSN 1755148X. doi: 10.1111/pcmr.12303. URL https://onlinelibrary.wiley.com/doi/10.1111/pcmr.12303.

J. G. Reiter, I. Bozic, B. Allen, K. Chatterjee, and M. A. Nowak. The effect of one additional driver mutation on tumor progression. *Evolutionary Applications*, 6(1):34–45, jan 2013. ISSN 17524563. doi: 10.1111/eva.12020. URL https://onlinelibrary.wiley.com/doi/10.1111/eva.12020.

M. R. Ricciardi, M. C. Scerpa, P. Bergamo, L. Ciuffreda, M. T. Petrucci, S. Chiaretti, S. Tavolaro, M. G. Mascolo, S. L. Abrams, L. S. Steelman, T. Tsao, A. Marchetti, M. Konopleva, D. Del Bufalo, F. Cognetti, R. Foà, M. Andreeff, J. A. McCubrey, A. Tafuri, and M. Milella. Therapeutic potential of MEK inhibition in acute myelogenous leukemia: Rationale for "vertical" and "lateral" combination strategies. *Journal of Molecular Medicine*, 90(10):1133–1144, oct 2012. ISSN 09462716. doi: 10.1007/s00109-012-0886-z. URL www.affymetrix.com.

M. W. Richards, S. G. Burgess, E. Poon, A. Carstensen, M. Eilers, L. Chesler, and R. Bayliss. Structural basis of N-Myc binding by Aurora-A and its destabilization by kinase inhibitors. *Proceedings of the National Academy of Sciences of the United States of America*, 113(48):13726–13731, nov 2016. ISSN 10916490. doi: 10.1073/pnas.1610626113. URL https://www.pnas.org/content/113/48/13726https://www.pnas.org/content/113/48/13726.abstract.

B. I. Rini and M. B. Atkins. Resistance to targeted therapy in renal-cell carcinoma, oct 2009. ISSN 14702045. URL https://www.sciencedirect.com/science/article/pii/S1470204509702402.

M. E. Ritchie, B. Phipson, D. Wu, Y. Hu, C. W. Law, W. Shi, and G. K. Smyth. Limma powers differential expression analyses for RNA-sequencing and microarray studies. *Nucleic Acids Research*, 43(7):e47, apr 2015. ISSN 13624962. doi: 10.1093/nar/gkv007. URL http://academic.oup.com/nar/article/43/7/e47/2414268/limma-powers-differential-expression-analyses-for.

T. Robin, A. Capes-Davis, and A. Bairoch. CLASTR: The Cellosaurus STR similarity search tool - A precious help for cell line authentication. *International Journal of Cancer*, 146(5):1299–1306, oct 2019. ISSN 10970215. doi: 10.1002/ijc.32639. URL https://onlinelibrary.wiley.com/doi/abs/10.1002/ijc.32639.

M. Rolfe, L. E. McLeod, P. F. Pratt, and C. G. Proud. Activation of protein synthesis in cardiomyocytes by the hypertrophic agent phenylephrine requires the activation of ERK and involves phosphorylation of tuberous sclerosis complex 2 (TSC2). *The Biochemical journal*, 388(Pt 3):973–84, jun 2005. ISSN 1470-8728. doi: 10.1042/BJ20041888. URL http://www.ncbi.nlm.nih.gov/pubmed/15757502http://www.pubmedcentral.nih.gov/articlerender.fcgi?artid=PMC1183479.

G. Rosen, N. Wollner, C. Tan, S. J. Wu, S. I. Hajdu, W. Cham, G. J. D'Angio, and M. L. Murphy. Disease-free survival in children with Ewing's sarcoma treated with radiation therapy and adjuvant four-drug sequential chemotherapy. *Cancer*, 33(2):384–393, feb 1974. ISSN 10970142. doi: 10.1002/1097-0142(197402)33:2⟨384::AID-CNCR2820330213⟩3.0.CO;2-T. URL http://doi.wiley.com/10.1002/1097-0142%28197402%2933%3A2%3C384%3A%3AAID-CNCR2820330213%3E3.0.CO%3B2-T.

W. Roux. Beitrage zur Morphologie der funktionnellen Anspassung. *Arch Anat Physiol Anat Abt*, 9:120–158, 1885. URL https://ci.nii.ac.jp/naid/10003529123/.

E. Rozengurt, H. P. Soares, and J. Sinnet-Smith. Suppression of feedback loops mediated by pi3k/mtor induces multiple overactivation of compensatory pathways: An unintended consequence leading to drug resistance. *Molecular Cancer Therapeutics*, 13(11):2477–2488, nov 2014. ISSN 15388514. doi: 10.1158/1535-7163.MCT-14-0330. URL http://www.ncbi.nlm.nih.gov/pubmed/25323681http://www.pubmedcentral.nih.gov/articlerender.fcgi?artid=PMC4222988.

D. A. Ruess, G. J. Heynen, K. J. Ciecielski, J. Ai, A. Berninger, D. Kabacaoglu, K. Görgülü, Z. Dantes, S. M. Wörmann, K. N. Diakopoulos, A. F. Karpathaki, M. Kowalska, E. Kaya-Aksoy, L. Song, E. A. Z. van der Laan, M. P. López-Alberca, M. Nazaré, M. Reichert, D. Saur, M. M. Erkan, U. T. Hopt, B. Sainz, W. Birchmeier, R. M. Schmid, M. Lesina, and H. Algül. Mutant KRAS-driven cancers depend on PTPN11/SHP2 phosphatase. *Nature Medicine*, 24(7):954–960, jul 2018. ISSN 1078-8956. doi: 10.1038/s41591-018-0024-8. URL http://www.nature.com/articles/s41591-018-0024-8.

M. B. Ryan, F. F. de la Cruz, S. Phat, D. T. Myers, E. Wong, H. A. Shahzade, C. B. Hong, and R. B. Corcoran. Vertical pathway inhibition overcomes adaptive feedback resistance to KrasG12C inhibition. *Clinical Cancer Research*, 26(7):1617–1643, apr 2020. ISSN 15573265. doi: 10.1158/1078-0432.CCR-19-3523. URL http://www.ncbi.nlm.nih.gov/pubmed/31776128http://www.pubmedcentral.nih.gov/articlerender.fcgi?artid=PMC7124991http://clincancerres.aacrjournals.org/lookup/doi/10.1158/1078-0432.CCR-19-3523.

M. Rydenfelt, B. Klinger, M. Klünemann, and N. Blüthgen. SPEED2: inferring upstream pathway activity from differential gene expression. *Nucleic Acids Research*, 48(W1):W307–W312, jul 2020. ISSN 0305-1048. doi: 10.1093/nar/gkaa236. URL https://academic.oup.com/nar/article/48/W1/W307/5822960.

J. Saez-Rodriguez and N. Blüthgen. Personalized signaling models for personalized treatments. *Molecular Systems Biology*, 16(1):e9042–undefined, jan 2020. ISSN 1744-4292. doi: 10.15252/msb.20199042. URL https://onlinelibrary.wiley.com/doi/abs/10.15252/msb.20199042.

J. Saez-Rodriguez, L. G. Alexopoulos, J. Epperlein, R. Samaga, D. A. Lauffenburger, S. Klamt, and P. K. Sorger. Discrete logic modelling as a means to link protein signalling networks with functional analysis of mammalian signal transduction. *Molecular Systems Biology*, 5(1):331, jan 2009. ISSN 1744-4292. doi: 10.1038/msb.2009.87. URL https://onlinelibrary.wiley.com/doi/10.1038/msb.2009.87.

R. Salama, M. Sadaie, M. Hoare, and M. Narita. Cellular senescence and its effector programs, jan 2014. ISSN 08909369. URL http://www.genesdev.org/cgi/doi/10.1101/gad.235184.113.

T. Santra, W. Kolch, and B. N. Kholodenko. Integrating Bayesian variable selection with Modular Response Analysis to infer biochemical network topology. *BMC systems biology*, 7:57, jan 2013. ISSN 1752-0509. doi: 10.1186/1752-0509-7-57. URL http://www.pubmedcentral.nih.gov/articlerender.fcgi?artid=3726398&tool=pmcentrez&rendertype=abstract.

R. Schlatter, K. Schmich, I. Avalos Vizcarra, P. Scheurich, T. Sauter, C. Borner, M. Ederer, I. Merfort, and O. Sawodny. ON/OFF and Beyond - A Boolean Model of Apoptosis. *PLoS Computational Biology*, 5(12):e1000595, dec 2009. ISSN 1553-7358. doi: 10.1371/journal.pcbi.1000595. URL https://dx.plos.org/10.1371/journal.pcbi.1000595.

G. Schleiermacher, N. Javanmardi, V. Bernard, Q. Leroy, J. Cappo, T. Rio Frio, G. Pierron, E. Lapouble, V. Combaret, F. Speleman, B. de Wilde, A. Djos, I. Øra, F. Hedborg, C. Träger, B.-M. Holmqvist, J. Abrahamsson, M. Peuchmaur, J. Michon, I. Janoueix-Lerosey, P. Kogner, O. Delattre, and T. Martinsson. Emergence of New ¡i¿ALK¡/i¿ Mutations at Relapse of Neuroblastoma. *Journal of Clinical Oncology*, 32(25):2727–2734, sep 2014. ISSN 0732-183X. doi: 10.1200/JCO.2013.54.0674. URL http://ascopubs.org/doi/10.1200/JCO.2013.54.0674.

B. Schoeberl, C. Eichler-Jonsson, E. D. Gilles, and G. Muüller. Computational modeling of the dynamics of the MAP kinase cascade activated by surface and internalized EGF receptors. *Nature Biotechnology*, 20(4):370–375, apr 2002. ISSN 10870156. doi: 10.1038/nbt0402-370. URL http://www.nature.com/doifinder/10.1038/nbt0402-370.

C. Schönherr, K. Ruuth, S. Kamaraj, C. L. Wang, H. L. Yang, V. Combaret, A. Djos, T. Martinsson, J. G. Christensen, R. H. Palmer, and B. Hallberg. Anaplastic Lymphoma Kinase (ALK) regulates initiation of transcription of MYCN in neuroblastoma cells. *Oncogene*, 31(50):5193–5200, dec 2012. ISSN 09509232. doi: 10.1038/onc.2012.12. URL http://www.nature.com/articles/onc201212.

J. Schüz, C. Espina, P. Villain, R. Herrero, M. E. Leon, S. Minozzi, I. Romieu, N. Segnan, J. Wardle, M. Wiseman, F. Belardelli, D. Bettcher, F. Cavalli, G. Galea, G. Lenoir, J. M. Martin-Moreno, F. A. Nicula, J. H. Olsen, J. Patnick, M. Primic-Zakelj, P. Puska, F. E. Van Leeuwen, O. Wiestler, W. Zatonski, N. Guha, E. Kralikova, A. McNeill, A. Peruga, A. Anderson, F. Berrino, M. C. Boutron-Ruault, M. Cecchini, T. J. Key, M. Leitzmann, T. Norat, H. J. Powers, C. Scoccianti, A. Auvinen, E. de Vries, F. Erdmann, R. Greinert, J. Harrison, A. Kesminiene,

N. McColl, S. Friis, M. Kogevinas, R. Saracci, K. Straif, H. Vainio, M. Almonte, A. Anttila, H. De Vuyst, J. Dillner, S. Franceschi, P. Gonzalez, A. Hall, J. Y. Park, P. Armaroli, W. Atkin, P. B. Dean, H. de Koning, L. Dillner, E. Kuipers, I. Lansdorp-Vogelaar, E. Paci, J. Regula, E. Suonio, S. Törnberg, L. F. Wood, N. Gaudin, K. G. Frie, V. Terrasse, K. Winstanley, C. Bellisario, E. Biagioli, M. Cinquini, S. Gianola, M. G. Lorenzo, L. von Karsa, and T. Lignini. European code against cancer 4th edition: 12 ways to reduce your cancer risk. *Cancer Epidemiology*, 39:S1–S10, dec 2015. ISSN 1877783X. doi: 10.1016/j.canep.2015.05.009. URL https://www.sciencedirect.com/science/article/pii/S1877782115001277.

T. F. Schwann. Pathologie und Therapie der Whytt'schen Gehirnkrankheit der Kinder, 1838. URL https://books.google.de/books?hl=en&lr=&id=RMM_AAAAcAAJ&oi=fnd&pg=PR5&dq=schwann+1839&ots=Nb798tXn4k&sig=AMX1s-PyV6pHQAdbadLwlCJHcu4&redir_esc=y#v=onepage&q=schwann1839&f=false.

L. Seamer, C. Bagwell, L. Barden, D. Redelman, G. Salzman, J. Wood, and R. Murphy. Proposed new data file standard for flow cytometry, version FCS 3.0. *Cytometry*, 28(2):118–122, jun 1997. ISSN 0196-4763. doi: 10.1002/(SICI)1097-0320(19970601)28:2⟨118::AID-CYTO3⟩3.0.CO;2-B. URL https://onlinelibrary.wiley.com/doi/10.1002/(SICI)1097-0320(19970601)28:2%3C118::AID-CYTO3%3E3.0.CO;2-B.

J. R. Sierra, V. Cepero, and S. Giordano. Molecular mechanisms of acquired resistance to tyrosine kinase targeted therapy, apr 2010. ISSN 14764598. URL http://molecular-cancer.biomedcentral.com/articles/10.1186/1476-4598-9-75.

M. Simian and M. J. Bissell. Organoids: A historical perspective of thinking in three dimensions. *Journal of Cell Biology*, 216(1):31–40, jan 2017. ISSN 0021-9525. doi: 10.1083/jcb.201610056. URL https://rupress.org/jcb/article/216/1/31/46144/Organoids-A-historical-perspective-of-thinking-in.

J. R. Singleton, A. E. Randolph, and E. L. Feldman. Insulin-like growth factor I receptor prevents apoptosis and enhances neuroblastoma tumorigenesis. *Cancer research*, 56(19):4522–9, oct 1996. ISSN 0008-5472. URL http://www.ncbi.nlm.nih.gov/pubmed/8813151.

S. K. Sjostrom, G. Finn, W. C. Hahn, D. H. Rowitch, and A. M. Kenney. The Cdk1 complex plays a prime role in regulating N-myc phosphorylation and turnover in neural precursors. *Developmental Cell*, 9(3):327–338, sep 2005. ISSN 15345807. doi: 10.1016/j.devcel.2005.07.014.

A. Slupianek, M. Nieborowska-Skorska, G. Hoser, A. Morrione, M. Majewski, L. Xue, S. W. Morris, M. A. Wasik, and T. Skorski. Role of phosphatidylinositol 3-kinase-

Akt pathway in nucleophosmin/anaplastic lymphoma kinase-mediated lymphomagenesis. *Cancer Research*, 61(5):2194–2199, mar 2001. ISSN 00085472. URL http://www.ncbi.nlm.nih.gov/pubmed/11280786.

R. L. Smith, M. R. Soeters, R. C. Wüst, and R. H. Houtkooper. Metabolic flexibility as an adaptation to energy resources and requirements in health and disease, aug 2018. ISSN 0163769X. URL https://academic.oup.com/edrv489.

M. L. Sos, S. Fischer, R. Ullrich, M. Peifer, J. M. Heuckmann, M. Koker, S. Heynck, I. Stückrath, J. Weiss, F. Fischer, K. Michel, A. Goel, L. Regales, K. A. Politi, S. Perera, M. Getlik, L. C. Heukamp, S. Ansén, T. Zander, R. Beroukhim, H. Kashkar, K. M. Shokat, W. R. Sellers, D. Rauh, C. Orr, K. P. Hoeflich, L. Friedman, K.-K. Wong, W. Pao, and R. K. Thomas. Identifying genotype-dependent efficacy of single and combined PI3K- and MAPK-pathway inhibition in cancer. *Proceedings of the National Academy of Sciences of the United States of America*, 106(43):18351–6, oct 2009. ISSN 1091-6490. doi: 10.1073/pnas.0907325106. URL http://www.ncbi.nlm.nih.gov/pubmed/19805051http://www.pubmedcentral.nih.gov/articlerender.fcgi?artid=PMC2757399.

L. Soucek, J. Whitfield, C. P. Martins, A. J. Finch, D. J. Murphy, N. M. Sodir, A. N. Karnezis, L. B. Swigart, S. Nasi, and G. I. Evan. Modelling Myc inhibition as a cancer therapy. *Nature*, 455(7213):679–683, oct 2008. ISSN 0028-0836. doi: 10.1038/nature07260. URL http://www.nature.com/articles/nature07260.

E. Southern. Detection of specific sequences among DNA fragments separated by gel electrophoresis. *Journal of Molecular Biology*, 98(3):503–517, nov 1975. ISSN 0022-2836. doi: 10.1016/S0022-2836(75)80083-0. URL https://www.sciencedirect.com/science/article/pii/S0022283675800830?via%3Dihub.

Statistisches Bundesamt. Causes of death by chapters of the ICD-10 and gender, 2020. URL https://www.destatis.de/EN/Themes/Society-Environment/Health/Causes-Death/Tables/number-of-death.html;jsessionid=B361134AE713837CE9F9A5817C5EF47D.live722.

E. Steliarova-Foucher, M. Colombet, L. A. Ries, F. Moreno, A. Dolya, F. Bray, P. Hesseling, H. Y. Shin, C. A. Stiller, S. Bouzbid, M. Hamdi-Cherif, A. Hablas, E. Chirpaz, N. Buziba, G. C. Chesumbai, S. S. Manraj, D. Reynders, H. R. Wabinga, E. Chokunonga, C. A. Lima, C. Asturian Laporte, J. C. de Oliveira, J. P. de Aquino, S. V. Gallagher, C. J. Uribe, L. E. Bravo, M. C. Yepez Chamorro, G. Torres Alvarado, Y. H. Galán Alvarez, F. C. Martinez Reyes, J. C. Castillo Calvas, M. Mendoza Alava, P. Cueva Ayala, B. Hanchard, A. Fajardo-Gutiérrez, D. E. Zavala Zegarra, E. Barrios, C. Nikiforuk, R. Woods, D. Turner, M. MacIntyre, A. Corriveau, T. Navaneelan, C. Bertrand, H. Stuart-Panko, R. J. Wilson, C. Kosary,

X. Shen, J. Brockhouse, G. A. Yee, T. C. Mitchell, K. Snipes, D. West, C. Rao, S. Bolick, R. K. Rycroft, L. Mueller, Y. Zheng, K. Dosch, H. Brown, A. Vargas, G. M. Levin, R. Bayakly, C. Johnson, T. Shen, L. Ruppert, C. F. Lynch, S. M. Lai, T. C. Tucker, X. C. Wu, M. Schwenn, K. Stern, S. Gershman, G. Copeland, S. Bushhouse, D. B. Rogers, J. Jackson Thompson, D. Lemons, S. Frederick, J. A. Harris, B. Riddle, A. Stroup, C. Wiggins, M. J. Schymura, L. K. Giljahn, A. Sheikh, S. Schubert, W. Aldinger, J. P. Fulton, M. Whiteside, L. Nogueira, C. Sweeney, A. Johnson, J. Martin, S. Farley, D. Harrelson, R. Malicki, J. R. Espinoza, B. Y. Hernandez, N. Abulfateh, N. Wang, R. K. Ngan, K. B. Lingegowda, R. Swaminathan, S. S. Koyande, B. Silverman, K. Ozasa, S. Kanemura, M. Soda, I. Miyashiro, A. Shibata, O. Nimri, Y. J. Won, C. H. Kim, N. S. Hong, H. S. Nam, S. Kweon, W. C. Kim, J. S. Huh, K. W. Jung, C. I. Yoo, A. Elbasmy, A. V. Laudico, M. R. Lumague, H. AlMutlag, R. Buasom, S. Srisukho, J. Tanabodee, S. Wiangnon, D. Pongnikorn, H. Sriplung, O. Dirican, S. Eser, M. Le Hoang, M. Hackl, A. Zborovskaya, N. Dimitrova, Z. Valerianova, M. Sekerija, P. Pavlou, M. Dušek, M. Mägi, J. Clavel, B. Lacour, A. V. Guizard, V. Bouvier, X. Troussard, A. S. Woronoff, B. Tretarre, M. Colonna, F. Molinié, S. Bara, M. Velten, E. Marrer, O. Ganry, P. Grosclaude, P. Kaatsch, S. R. Zeissig, B. Holleczek, A. Katalinic, Z. Jakab, H. Birgisson, P. M. Walsh, L. Mangone, F. Merletti, M. Magoni, S. Ferretti, D. Serraino, G. Spagnoli, M. Fusco, M. Michiara, R. Tumino, F. Falcini, F. Sensi, F. Tisano, S. Piffer, F. Stracci, G. Tagliabue, G. Smailyte, D. Agius, O. Visser, G. Ursin, J. Didkowska, M. Trojanowski, U. Wojciechowska, G. Forjaz de Lacerda, M. A. Silva, J. Laranja Pontes, A. da Costa Miranda, E. Kaiserova, M. Primic Žakelj, R. Peris-Bonet, M. L. Vicente Raneda, E. Almar Marqués, J. R. Quirós Garcia, M. Ramos Monserrat, M. Errezola Saizar, A. Alemán Herrera, J. M. Díaz García, R. Marcos-Gragera, M. J. Sanchez-Perez, E. Ardanaz Aicua, J. Galceran, A. Klint, C. E. Kuehni, C. Bouchardy, F. Levi, A. Bordoni, I. Konzelmann, S. Rohrmann, A. T. Gavin, D. H. Brewster, H. Phung, S. Rushton, S. Guthridge, J. Aitken, K. D'Onise, A. Venn, H. Farrugian, T. J. Threlfall, S. Laumond, L. Yen Kai Sun, J. Hendrix, K. Ballantine, and E. Masuyer. International incidence of childhood cancer, 2001–10: a population-based registry study. *The Lancet Oncology*, 18(6):719–731, jun 2017. ISSN 14745488. doi: 10.1016/S1470-2045(17)30186-9. URL `http://www.ncbi.nlm.nih.gov/pubmed/28410997http://www.pubmedcentral.nih.gov/articlerender.fcgi?artid=PMC5461370`.

I. Stelniec-Klotz, S. Legewie, O. Tchernitsa, F. Witzel, B. Klinger, C. Sers, H. Herzel, N. Blüthgen, and R. Schäfer. Reverse engineering a hierarchical regulatory network downstream of oncogenic KRAS. *Molecular systems biology*, 8:601, jan 2012. ISSN 1744-4292. doi: 10.1038/msb.2012.32. URL `http://www.pubmedcentral.nih.gov/articlerender.fcgi?artid=3421447&tool=pmcentrez&rendertype=abstract`.

N. Sugiyama, H. Imamura, and Y. Ishihama. Large-scale Discovery of Substrates of the Human Kinome. *Scientific Reports*, 9(1):1–12, dec 2019. ISSN 20452322. doi: 10.1038/s41598-019-46385-4. URL https://doi.org/10.1038/s41598-019-46385-4.

C. Sun, L. Wang, S. Huang, G. J. J. E. Heynen, A. Prahallad, C. Robert, J. Haanen, C. Blank, J. Wesseling, S. M. Willems, D. Zecchin, S. Hobor, P. K. Bajpe, C. Lieftink, C. Mateus, S. Vagner, W. Grernrum, I. Hofland, A. Schlicker, L. F. A. Wessels, R. L. Beijersbergen, A. Bardelli, F. Di Nicolantonio, A. M. M. Eggermont, and R. Bernards. Reversible and adaptive resistance to BRAF(V600E) inhibition in melanoma. *Nature*, 508(7494):118–122, 2014. ISSN 0028-0836. doi: 10.1038/nature13121. URL http://www.nature.com/nature/journal/v508/n7494/pdf/nature13121.pdfhttp://www.nature.com/doifinder/10.1038/nature13121.

P. Sun, H. Watanabe, K. Takano, T. Yokoyama, J. I. Fujisawa, and T. Endo. Sustained activation of M-Ras induced by nerve growth factor is essential for neuronal differentiation of PC12 cells. *Genes to Cells*, 11(9):1097–1113, sep 2006. ISSN 13569597. doi: 10.1111/j.1365-2443.2006.01002.x. URL https://onlinelibrary.wiley.com/doi/10.1111/j.1365-2443.2006.01002.x.

P. Sundaramurthy and S. Gakkhar. Dynamic modeling and simulation of JNK and P38 kinase cascades with feedbacks and crosstalks. *IEEE Transactions on Nanobioscience*, 9(4):225–231, dec 2010. ISSN 15361241. doi: 10.1109/TNB.2010.2061863. URL http://ieeexplore.ieee.org/document/5551211/.

W. W. Sung, Y. M. Lin, P. R. Wu, H. H. Yen, H. W. Lai, T. C. Su, R. H. Huang, C. K. Wen, C. Y. Chen, C. J. Chen, and K. T. Yeh. High nuclear/cytoplasmic ratio of cdk1 expression predicts poor prognosis in colorectal cancer patients. *BMC Cancer*, 14(1):951, dec 2014. ISSN 14712407. doi: 10.1186/1471-2407-14-951. URL http://bmccancer.biomedcentral.com/articles/10.1186/1471-2407-14-951.

E. Talevich, A. H. Shain, T. Botton, and B. C. Bastian. CNVkit: Genome-Wide Copy Number Detection and Visualization from Targeted DNA Sequencing. *PLOS Computational Biology*, 12(4):e1004873, apr 2016. ISSN 1553-7358. doi: 10.1371/journal.pcbi.1004873. URL https://dx.plos.org/10.1371/journal.pcbi.1004873.

F. Tatin, C. Varon, E. Genot, and V. Moreau. A signalling cascade involving PKC, Src and Cdc42 regulates podosome assembly in cultured endothelial cells in response to phorbol ester. *Journal of Cell Science*, 119(4):769–781, feb 2006. ISSN 00219533. doi: 10.1242/jcs.02787. URL https://journals.biologists.com/jcs/article/119/4/769/29305/A-signalling-cascade-involving-PKC-Src-and-Cdc42.

C. Terfve, T. Cokelaer, D. Henriques, A. MacNamara, E. Goncalves, M. K. Morris, M. van Iersel, D. A. Lauffenburger, and J. Saez-Rodriguez. CellNOptR:

a flexible toolkit to train protein signaling networks to data using multiple logic formalisms. *BMC systems biology*, 6(1):133, oct 2012. ISSN 1752-0509. doi: 10.1186/1752-0509-6-133. URL http://www.ncbi.nlm.nih.gov/pubmed/23079107http://www.pubmedcentral.nih.gov/articlerender.fcgi?artid=PMC3605281http://www.biomedcentral.com/1752-0509/6/133.

C. D. Terfve, E. H. Wilkes, P. Casado, P. R. Cutillas, and J. Saez-Rodriguez. Large-scale models of signal propagation in human cells derived from discovery phosphoproteomic data. *Nature Communications*, 6(1):1–11, sep 2015. ISSN 20411723. doi: 10.1038/ncomms9033. URL www.nature.com/naturecommunications.

H. Towbin, T. Staehelin, and J. Gordon. Electrophoretic transfer of proteins from polyacrylamide gels to nitrocellulose sheets: Procedure and some applications. *Proceedings of the National Academy of Sciences of the United States of America*, 76(9):4350–4354, 1979. ISSN 00278424. doi: 10.1073/pnas.76.9.4350. URL /pmc/articles/PMC411572/?report=abstracthttps://www.ncbi.nlm.nih.gov/pmc/articles/PMC411572/.

M. T. Tracy. The 1869 controversy of cellular theory: Goodsir versus Virchow. *Journal of Medical Biography*, page 096777202094273, aug 2020. ISSN 0967-7720. doi: 10.1177/0967772020942735. URL http://journals.sagepub.com/doi/10.1177/0967772020942735.

R. M. Trigg and S. D. Turner. ALK in neuroblastoma: Biological and therapeutic implications, apr 2018. ISSN 20726694. URL http://www.mdpi.com/2072-6694/10/4/113.

R. M. Trigg, L. C. Lee, N. Prokoph, L. Jahangiri, C. P. Reynolds, G. A. Amos Burke, N. A. Probst, M. Han, J. D. Matthews, H. K. Lim, E. Manners, S. Martinez, J. Pastor, C. Blanco-Aparicio, O. Merkel, I. G. de los Fayos Alonso, P. Kodajova, S. Tangermann, S. Högler, J. Luo, L. Kenner, and S. D. Turner. The targetable kinase PIM1 drives ALK inhibitor resistance in high-risk neuroblastoma independent of MYCN status. *Nature Communications*, 10(1):5428, dec 2019. ISSN 2041-1723. doi: 10.1038/s41467-019-13315-x. URL http://www.nature.com/articles/s41467-019-13315-x.

E. R. Tucker, E. Poon, and L. Chesler. Targeting MYCN and ALK in resistant and relapsing neuroblastoma, sep 2019. ISSN 2578532X. URL https://cdrjournal.com/article/view/3137.

K. Turner, V. Vasu, and D. Griffin. Telomere Biology and Human Phenotype. *Cells*, 8(1):73, jan 2019. ISSN 2073-4409. doi: 10.3390/cells8010073. URL https://www.mdpi.com/2073-4409/8/1/73.

S. Tyanova, T. Temu, and J. Cox. The MaxQuant computational platform for mass spectrometry-based shotgun proteomics. *Nature Protocols*, 11(12):2301–2319, 2016. ISSN 17502799. doi: 10.1038/nprot.2016.136. URL https://www.nature.com/articles/nprot.2016.136.pdf?origin=ppub.

E. E. Tyzzer. Factors in the Production and Growth of tumor Metastases. *The Journal of medical research*, 28(2):309–332.1, jul 1913. ISSN 0097-3599. URL http://www.ncbi.nlm.nih.gov/pubmed/19972114http://www.pubmedcentral.nih.gov/articlerender.fcgi?artid=PMC2099742http://www.ncbi.nlm.nih.gov/pubmed/19972114%0Ahttp://www.pubmedcentral.nih.gov/articlerender.fcgi?artid=PMC2099742.

G. Umapathy, A. E. Wakil, B. Witek, L. Chesler, L. Danielson, X. Deng, N. S. Gray, M. Johansson, S. Kvarnbrink, K. Ruuth, C. Schönherr, R. H. Palmer, and B. Hallberg. The kinase ALK stimulates the kinase ERK5 to promote the expression of the oncogene MYCN in neuroblastoma. *Science Signaling*, 7(349): ra102, oct 2014. ISSN 19379145. doi: 10.1126/scisignal.2005470. URL http://www.ncbi.nlm.nih.gov/pubmed/25351247.

G. Umapathy, J. Guan, D. E. Gustafsson, N. Javanmardi, D. Cervantes-Madrid, A. Djos, T. Martinsson, R. H. Palmer, and B. Hallberg. MEK inhibitor trametinib does not prevent the growth of anaplastic lymphoma kinase (ALK)-addicted neuroblastomas. *Science Signaling*, 10(507), nov 2017. ISSN 19379145. doi: 10.1126/scisignal.aam7550. URL http://www.ncbi.nlm.nih.gov/pubmed/29184034.

B. Vallée, M. Doudeau, F. Godin, A. Gombault, A. Tchalikian, M.-L. de Tauzia, and H. Bénédetti. Nf1 RasGAP Inhibition of LIMK2 Mediates a New Cross-Talk between Ras and Rho Pathways. *PLoS ONE*, 7(10):e47283, oct 2012. ISSN 1932-6203. doi: 10.1371/journal.pone.0047283. URL https://dx.plos.org/10.1371/journal.pone.0047283.

J. Van Den Eynden, G. Umapathy, A. Ashouri, D. Cervantes-Madrid, J. Szydzik, K. Ruuth, J. Koster, E. Larsson, J. Guan, R. H. Palmer, and B. Hallberg. Phosphoproteome and gene expression profiling of ALK inhibition in neuroblastoma cell lines reveals conserved oncogenic pathways. *Science Signaling*, 11(557), nov 2018. ISSN 19379145. doi: 10.1126/scisignal.aar5680. URL http://www.ncbi.nlm.nih.gov/pubmed/30459281.

D. J. Venzon and S. H. Moolgavkar. A Method for Computing Profile-Likelihood-Based Confidence Intervals. *Applied Statistics*, 37(1):87, mar 1988. ISSN 00359254. doi: 10.2307/2347496. URL https://www.jstor.org/stable/10.2307/2347496?origin=crossref.

R. Virchow. Die Cellularpathologie in ihrer Begrundung auf physiologische pathologische Gewebelehre, 1871. URL https://books.google.de/books?hl=en&lr=&id=13ASAAAAYAAJ&oi=fnd&pg=PA27&dq=+Die+Cellularpathologie+in+ihrer+Begrundung+auf+physiologische+pathologische+Gewebelehre&ots=5ZebipAiTa&sig=Zz2SBveNNTX0tRDoxpViw_OMWdg&redir_esc=y#v=onepage&q=Omnis&f=false.

B. A. Walker, K. Mavrommatis, C. P. Wardell, T. Cody Ashby, M. Bauer, F. E. Davies, A. Rosenthal, H. Wang, P. Qu, A. Hoering, M. Samur, F. Towfic, M. Ortiz, E. Flynt, Z. Yu, Z. Yang, D. Rozelle, J. Obenauer, M. Trotter, D. Auclair, J. Keats, N. Bolli, M. Fulciniti, R. Szalat, P. Moreau, B. Durie, A. Keith Stewart, H. Goldschmidt, M. S. Raab, H. Einsele, P. Sonneveld, J. S. Miguel, S. Lonial, G. H. Jackson, K. C. Anderson, H. Avet-Loiseau, N. Munshi, A. Thakurta, and G. J. Morgan. Identification of novel mutational drivers reveals oncogene dependencies in multiple myeloma. *Blood*, 132(6):587–597, aug 2018. ISSN 15280020. doi: 10.1182/blood-2018-03-840132. URL https://ashpublications.org/blood/article/132/6/587/39419/Identification-of-novel-mutational-drivers-reveals.

M. Welcker, A. Orian, J. Jin, J. E. Grim, J. A. Grim, J. W. Harper, R. N. Eisenman, and B. E. Clurman. The Fbw7 tumor suppressor regulates glycogen synthase kinase 3 phosphorylation-dependent c-Myc protein degradation. *Proceedings of the National Academy of Sciences of the United States of America*, 101(24):9085–90, jun 2004. ISSN 0027-8424. doi: 10.1073/pnas.0402770101. URL http://www.ncbi.nlm.nih.gov/pubmed/15150404http://www.pubmedcentral.nih.gov/articlerender.fcgi?artid=PMC428477.

C. P. Wild, C. Espina, L. Bauld, B. Bonanni, H. Brenner, K. Brown, J. Dillner, D. Forman, E. Kampman, M. Nilbert, K. Steindorf, H. Storm, P. Vineis, M. Baumann, and J. Schüz. Cancer Prevention Europe, mar 2019. ISSN 18780261. URL https://onlinelibrary.wiley.com/doi/abs/10.1002/1878-0261.12455.

S. M. Wilhelm, C. Carter, L. Tang, D. Wilkie, A. McNabola, H. Rong, C. Chen, X. Zhang, P. Vincent, M. Mchugh, Y. Cao, J. Shujath, S. Gawlak, D. Eveleigh, B. Rowley, L. Liu, L. Adnane, M. Lynch, D. Auclair, I. Taylor, R. Gedrich, A. Voznesensky, B. Riedl, L. E. Post, G. Bollag, and P. A. Trail. BAY 43-9006 Exhibits Broad Spectrum Oral Antitumor Activity and Targets the RAF / MEK / ERK Pathway and Receptor Tyrosine Kinases Involved in Tumor Progression and Angiogenesis BAY 43-9006 Exhibits Broad Spectrum Oral Antitumor Activity and Targets the Pr. *Cancer Res*, 64(19):7099–7109, 2004. ISSN 00085472. doi: 10.1158/0008-5472.CAN-04-1443. URL http://cancerres.aacrjournals.org/content/64/19/7099.long#T1http://www.ncbi.nlm.nih.gov/pubmed/15466206.

B. Winckler. Fast LXB File Reader [R package lxb version 1.5], mar 2016. URL https://cran.r-project.org/web/packages/lxb/index.html.

D. J. Wong and A. Ribas. Targeted therapy for melanoma. In *Cancer Treatment and Research*, volume 167, pages 251–262. Springer, Cham, 2016. doi: 10.1007/978-3-319-22539-5_10. URL http://link.springer.com/10.1007/978-3-319-22539-5_10.

S.-U. Woo, T. Sangai, A. Akcakanat, H. Chen, C. Wei, and F. Meric-Bernstam. Vertical inhibition of the PI3K/Akt/mTOR pathway is synergistic in breast cancer. *Oncogenesis*, 6(10):e385–e385, oct 2017. ISSN 2157-9024. doi: 10.1038/oncsis.2017.86. URL http://www.nature.com/articles/oncsis201786.

S. E. Woodfield, L. Zhang, K. A. Scorsone, Y. Liu, and P. E. Zage. Binimetinib inhibits MEK and is effective against neuroblastoma tumor cells with low NF1 expression. *BMC cancer*, 16:172, mar 2016. ISSN 1471-2407. doi: 10.1186/s12885-016-2199-z. URL http://www.ncbi.nlm.nih.gov/pubmed/26925841http://www.pubmedcentral.nih.gov/articlerender.fcgi?artid=PMC4772351.

S. Wu, S. Powers, W. Zhu, and Y. A. Hannun. Substantial contribution of extrinsic risk factors to cancer development. *Nature*, 529(7584):43–47, dec 2015. ISSN 0028-0836. doi: 10.1038/nature16166. URL http://dx.doi.org/10.1038/nature16166.

H. W. Yang, M.-G. Shin, S. Lee, J.-R. Kim, W. S. Park, K.-H. Cho, T. Meyer, and W. Do Heo. Cooperative Activation of PI3K by Ras and Rho Family Small GTPases. *Molecular Cell*, 47(2):281–290, jul 2012. ISSN 1097-2765. doi: 10.1016/J.MOLCEL.2012.05.007. URL https://www.sciencedirect.com/science/article/pii/S1097276512003905.

F. E. Yates. Systems Biology as a Concept**Certain portions of this chapter are based on an article that appeared in Physiologist. 11, 115–133 (1968). In *Engineering Principles in Physiology*, pages 3–12. Elsevier, jan 1973. doi: 10.1016/b978-0-12-136201-0.50008-8.

N. Yosef, A. Kaufman, and E. Ruppin. Inferring Functional Pathways from Multi-Perturbation Data. *Bioinformatics*, 22(14):e539–e546, jul 2006. ISSN 1367-4803. doi: 10.1093/bioinformatics/btl204. URL https://academic.oup.com/bioinformatics/article-lookup/doi/10.1093/bioinformatics/btl204.

M. You, D. H. Yu, and G. S. Feng. Shp-2 tyrosine phosphatase functions as a negative regulator of the interferon-stimulated Jak/STAT pathway. *Molecular and cellular biology*, 19(3):2416–24, mar 1999. ISSN 0270-7306. doi: 10.1128/mcb.19.3.2416. URL http://www.ncbi.nlm.nih.gov/pubmed/10022928http://www.pubmedcentral.nih.gov/articlerender.fcgi?artid=PMC84034.

G. Yu, L. G. Wang, Y. Han, and Q. Y. He. ClusterProfiler: An R package for comparing biological themes among gene clusters. *OMICS A Journal of Integrative Biology*, 16(5):284–287, may 2012. ISSN 15362310. doi: 10.1089/omi.2011.0118. URL http://www.liebertpub.com/doi/10.1089/omi.2011.0118.

S. Q. Zhang, W. G. Tsiaras, T. Araki, G. Wen, L. Minichiello, R. Klein, and B. G. Neel. Receptor-specific regulation of phosphatidylinositol 3'-kinase activation by the protein tyrosine phosphatase Shp2. *Molecular and cellular biology*, 22(12):4062–72, jun 2002. ISSN 0270-7306. doi: 10.1128/mcb.22.12.4062-4072.2002. URL http://www.ncbi.nlm.nih.gov/pubmed/12024020http://www.pubmedcentral.nih.gov/articlerender.fcgi?artid=PMC133866.

W. Zhang and L. E. Samelson. The role of membrane-associated adaptors in T cell receptor signalling. *Seminars in Immunology*, 12(1):35–41, feb 2000. ISSN 1044-5323. doi: 10.1006/SMIM.2000.0205. URL https://www.sciencedirect.com/science/article/pii/S1044532300902057.

Y. Zhang, J. L. Liu, and J. Wang. KRAS gene silencing inhibits the activation of PI3K-Akt-mTOR signaling pathway to regulate breast cancer cell epithelial-mesenchymal transition, proliferation and apoptosis. *European Review for Medical and Pharmacological Sciences*, 24(6):3085–3096, 2020. ISSN 22840729. doi: 10.26355/eurrev_202003_20673. URL http://www.ncbi.nlm.nih.gov/pubmed/32271426.